Applications of magnetic particles for oligodendrocyte precursor cell transplantation strategies

Stuart Iain Jenkins

A thesis submitted for the degree of Doctor of Philosophy

June 2013

Keele University

Keele University

SUBMISSION OF THESIS FOR A RESEARCH DEGREE

Degree for which thesis being submitted Doctor of Philosophy

Title of thesis **Applications of magnetic particles for oligodendrocyte precursor cell transplantation strategies**

This thesis contains confidential information and is subject to the protocol set down for the submission and examination of such a thesis? NO

Date of submission 04 February 2013

Original registration date 12 January 2009

Name of candidate Stuart Iain Jenkins

Research Institute Institute for Science and Technology in Medicine

Name of Lead Supervisor Dr Divya Maitreyi Chari

I certify that:

i. The thesis being submitted for examination is my own account of my own research
ii. My research has been conducted ethically. Where relevant a letter from the approving body confirming that ethical approval has been given has been bound in the thesis as an Annex
iii. The data and results presented are the genuine data and results actually obtained by me during the conduct of the research
iv. Where I have drawn on the work, ideas and results of others this has been appropriately acknowledged in the thesis
v. Where any collaboration has taken place with one or more other researchers, I have included within an 'Acknowledgments' section in the thesis a clear statement of their contributions, in line with the relevant statement in the Code of Practice (see Note overleaf).
vi. The greater portion of the work described in the thesis has been undertaken subsequent to my registration for the higher degree for which I am submitting for examination
vii. Where part of the work described in the thesis has previously been incorporated in another thesis submitted by me for a higher degree (if any), this has been identified and acknowledged in the thesis
viii. The thesis submitted is within the required word limit as specified in the Regulations

Total words in submitted thesis (including text and footnotes, but excluding references and appendices) …… 48,988

Signature of candidate …… Date ……

Abstract:

Oligodendrocyte precursor cells (OPCs) are a major transplant population to promote myelin repair and central nervous system (CNS) regeneration in conditions such as Multiple Sclerosis and spinal cord injury. Magnetic particles (MPs) can offer a multifunctional platform for cell therapies, facilitating labelling for cell tracking (*e.g.* by MRI and histopathology); biomolecule delivery (including nonviral gene delivery, enhanceable by novel 'magnetofection' strategies); and magnetic cell targeting of transplant populations. However, MP-based applications for neural tissue engineering have received limited attention to date.

This thesis demonstrates that ~60% of OPCs (derived from a primary source) can be safely labelled using two well-characterised MP formulations, including a novel multimodal MP with transfection plus cell labelling capabilities. A rapid, technically simple, high-throughput ultrastructural imaging technique, OTOTO SEM, has been developed to study the surface interactions of MPs with precursor cells. Safe MP-mediated transfection of OPCs was demonstrated, including with multiple and therapeutic genes. Transfection efficiency was enhanced by static/oscillating 'magnetofection' techniques (~21%; competitive with nonviral alternatives). Organotypic cerebellar slice cultures were developed as a model of 'host' neural tissue, and 'magnetofected' OPCs exhibited normal migration, proliferation and differentiation profiles following transplantation onto such slices.

Safe labelling (~45%) and transfection (enhanced by static/oscillating magnetofection strategies: ~6%) of oligodendrocytes was achieved utilising identical protocols to those developed for OPCs. A comparative intralineage analysis demonstrated that MP-uptake and amenability to transfection were significantly lower in

oligodendrocytes compared to OPCs. Inter-cellular comparisons of MP-handling by the four major CNS glial subtypes (viz. OPCs, oligodendrocytes, astrocytes, microglia; derived from the same primary source) revealed major differences in the rate/extent of MP uptake, amenability to transfection, optimal magnetofection frequency, and MP-associated toxicity. Finally, a stoichiometrically-defined glial co-culture model was developed and utilised to test the hypothesis that microglia represent an 'extracellular barrier' to MP uptake by other glia.

Contents

List of tables and figures

Abbreviations

AAV	Adeno-associated virus
ANOVA	Analysis of variance
ATR	Attenuated total reflection
BBB	Blood brain barrier
BDNF	Brain-derived neurotrophic factor
CNS	Central nervous system
CNTF	Ciliary neurotrophic factor
CT	Computed tomography
D10	Mixed glial culture medium
D10-CM	D10 with 20% conditioned D10
D15A	Multineurotrophin with BDNF and NT3 activity
DAPI	4',6-diamidino-2-phenylindole
DCN	Deep cerebellar nuclei
DIV	Days *in vitro*
DLS	Dynamic light scattering
DMEM	Dulbecco's modified Eagle's medium
DMSA	Dimercaptosuccinic acid
EBSS	Earle's balanced salt solution
EGF	Epidermal growth factor
EGFP	Enhanced green fluorescent protein
ESC	Embryonic stem cell
F	Frequency, of oscillating magnetic field
FGF2	Fibroblast growth factor 2; basic fibroblast growth factor
FITC	Fluorescein isothiocyanate
FTIR	Fourier transform infra-red spectroscopy
GalC	Galactosylceramide
GFAP	Glial fibrillary acidic protein
GFP	Green fluorescent protein
hBOEC	Human blood outgrowth endothelial cells
HBSS	Hank's balanced salt solution
HeLa	Henrietta Lacks, human cervical cancer cell line
HEPES	4-(2-hydroxyethyl)-1-piperazineethanesulfonic acid
HSV	Herpes simplex virus
IGF-1	Insulin-like growth factor-1
ITC	Isothiocyanate
LDH	Lactate dehydrogenase
MAG	Myelin associated glycoprotein
MBP	Myelin basic protein
MEM	Modified Eagle's medium
MOG	Myelin oligodendrocyte protein
MoMuLV	Moloney murine leukaemia virus
MP	Magnetic particle
MRI	Magnetic resonance imaging
mRNA	Messenger ribonucleic acid

MS	Multiple Sclerosis
MTS	3-(4,5-dimethylthiazol-2-yl)-2,5-diphenyltetrazolium bromide
MTT	2-(4,5-dimethyl-2-thiazolyl)-3,5-diphenyl-2H-tetrazolium bromide
NG2	Neuron-glial antigen 2; chondroitin sulphate proteoglycan 4
NLS	Nuclear localisation signal
NSC	Neural stem cell
NT3	Neurotrophic factor 3
OPC	Oligodendrocyte precursor cell
OPC-MM	Oligodendrocyte precursor cell maintenance medium
OTO	Osmium tetroxide-thiocarbohydrazide-osmium tetroxide
OTOTO	Osmium tetroxide-thiocarbohydrazide-osmium tetroxide-thiocarbohydrazide-osmium tetroxide
P#	Postnatal day #
pAN-GFP	Plasmid AN-GFP (control plasmid for pFGF2-GFP)
PBS	Phosphate buffered saline
PDGF-A/AA	Platelet-derived growth factor (single chain: A; dimer: AA)
PDGFRα	Platelet-derived growth factor receptor alpha
PDL	Poly-D-lysine
pDsRed	Plasmid pCMV-DsRed-Express2
PEG	Polyethylene glycol
PEI	Polyethyleneimine
PET	Positron emission tomography
pFGF2-GFP	Plasmid pCMV6-FGF2-GFP
PGA	Polyglycolic acid
PLA	Poly-L-lactic acid
PLL	Poly-L-lysine
PLP/PLP-DM20	Proteolipid protein (PLP-DM20 is a splice variant)
pmaxGFP	Plasmid pmaxGFP
POA	Pro-oligodendroblast antigen, recognised by O4 antibody
PSA-NCAM	Polysialylated neuronal cell adhesion molecule
RFP	Red fluorescent protein
RITC	Rhodamine isothiocyanate
ROS	Reactive oxygen species
RT	Room temperature
Sato	Medium that promotes OPC differentiation (section 2.2)
SCB	Sodium cacodylate buffer
SCI	Spinal cord injury
SD	Standard deviation
SEM	Scanning electron microscopy; standard error of the mean
Shh	Sonic hedgehog
Sphero	Magnetic particles manufactured by Spherotech, Inc. (section 2.2)
SV	Simian virus
TEM	Transmission electron microscopy
TGF-β1	Transforming growth factor-β1
WM	White matter
XRD	X-ray diffraction

Acknowledgments

Dr Divya Chari and Dr Mark Pickard have provided extensive feedback on the writing of this thesis, for which I am extremely grateful. Divya and Mark have spent almost four years supervising and training me, and it has been a privilege to have supervisors with such considerable expertise, imagination, insight and uncompromising standards of scientific rigour. Spare a thought for them, dear reader, as they have suffered many early drafts so that you might be able to read this thesis without much wailing and gnashing of teeth. One day, I hope to repay them.

Dr David Furness has been a highly valued member of my supervisory team, providing excellent insights and advice, and demonstrating great patience during my electron microscopy training. I offer my thanks for this, and for proof-reading the electron microscopy-related sections of this thesis.

I offer my gratitude to Professor Matt Rosseinsky and Dr Humphrey Yiu for providing the Fe_3O_4-PEI-RITC particles used in this thesis, and granting permission for the inclusion of the data. Further to this, Humphrey performed a number of chemical analyses on the Sphero particles used here (credited in section 2.2), provided schematics of the Sphero and Fe_3O_4-PEI-RITC particles (section 2.2), and the Fe_3O_4-PEI-RITC calculations in Appendix 2. I am particularly grateful to Humphrey for extensive discussions about the physics/chemistry of these and other particles, and for commenting on drafts of Chapters 1 and 2.

I have had numerous helpful discussions with Professor Jon Dobson, Dr Neil Telling and Dr Neil Farrow about the oscillating magnetofection technology including the potential mechanisms of action. They have been generous and supportive towards me, and for this I am grateful.

Thanks are due to Professor Chris Exley and Dr James Beardmore for providing access to, and training to operate, the Zetasizer for DLS and zeta potential measurements.

Many people have been generous with their time and resources to help me during my research, and I would like to extend my thanks to Dr Richard Emes, Dr Sarah Hart, Dr Rowan Orme, Professor Gwynn Williams, Dr Mirna Mourtada-Maarabouni, Professor Paul

Egglestone, Dr Rosemary Fricker, Dr Paul Horrocks, Dr Peter Chevins and Jayne Bromley. Dr Paul Roach has been very supportive of me, and I am particularly grateful for his encouragement to apply for an EPSRC fellowship, which I have now been awarded.

Electron microscopy is a harsh mistress, and many of my specimens would have been useless without the assistance/rescue missions provided by Mrs Karen Walker.

Keele medical school provided my PhD stipend, and have been exceptionally supportive of me even beyond this, for which I am grateful.

The following staff at Keele University School of Life Sciences particularly deserve my thanks: Chris Bain, Ron Knapper, Nigel Bowers, Dave Bosworth, Zoe Bosworth, Debbie Adams and Ian Wright. They have all been extremely helpful to me. As have Phil and Chris, who kept our lab clean and kept me up to date with football news.

Dr Dave Mazzocchi-Jones has regaled me with tales of people actually passing their viva and getting a PhD. You gave me hope when I needed it, Dave, so thank you.

I would like to extend my gratitude to the following people for their friendship, scientific help, and regular doses of sanity/insanity as required: Amy Judd, Dr Andrew Morris, Dr Alberto Falco, Chris Adams, Dr Joanna Miest, Lynsey Wheeldon, Alan Weightman, Dr Dan Bray, Dr Doug Paton, Matt Mold and Síle Fada Griffin.

Thank you to my long-suffering wife, Susan, to my mum, Trish, and to Reno, for putting up with a seemingly-eternal student for a husband/son. Finally, thank you to Alexander Darwin for getting me up in the mornings. Now, I believe I have to attend to a list of ‘things Stuart will do after his PhD’...

Epilogue:

The most important of which turned out to be the arrival of Elizabeth Rosalind (Lily).

Chapter 1: General introduction

1.1 Myelin loss is common to Multiple Sclerosis and spinal cord injury

The adult mammalian central nervous system (CNS; the brain and spinal cord) has a limited capacity for regeneration. As a result, disease or injury is often associated with permanent neurological deficits, with poor clinical prognoses and potentially severe personal and socioeconomic costs. Two of the most common neurological conditions in young adults are Multiple Sclerosis (MS) and spinal cord injury (SCI).[1–3] MS is the most prevalent progressive neurological condition in young adults, with onset typically occurring at 20 – 40 years of age, and it is the second most common cause of disability in young people in the Western world, after trauma;[4] SCI can occur at any age, but is most frequent at 16 – 30 years of age, often leading to life-long disability.[5] Consequently, there is a major need for repair-promoting therapies, as current treatments for such conditions attempt to alleviate symptoms and limit progression of the condition, rather than instigate significant regeneration.

In both MS and SCI, impairment or loss of neurological function is due to the loss of nerve fibres and/or the loss of myelin (the fatty insulating sheath around nerve fibres).[6] Myelin is produced and maintained by oligodendrocytes, which are the myelinating cells of the CNS. These cells produce vast quantities of specialised membrane which forms highly compacted myelin sheaths around axons and, as there is very limited water content, myelin functions as an excellent insulating material.[7,8] Approximately 70% (dry weight) of myelin is composed of lipids, predominantly cholesterol and glycosphingolipids [notably galactosylceramide (GalC)], with ~30% protein, and the majority of these components are unique to myelin.[9,10] Myelin sheaths are separated by exposed regions of axon known as nodes of Ranvier, at which ion channels are clustered, and this facilitates rapid and efficient saltatory conduction of electrical impulses (action potentials); this conduction is

diminished or even abolished as a consequence of myelin damage/loss.[11–13] Further, myelin has been shown to be essential for the long-term survival and normal function of axons, including the provision of metabolic support.[14–18]

1.2 Remyelination is a rare example of CNS regeneration

Although the CNS has a poor intrinsic capacity for regeneration, a notable exception to this is the phenomenon of *'remyelination'*: a regenerative event that involves the production of new myelin sheaths that can restore saltatory conduction to demyelinated axons.[1,6] The concept of remyelination in the CNS had been proposed in the 1950s, and was shown by Bunge *et al.* (1960, 1961) to occur following experimental demyelination of the spinal cord.[19,20] Although these and subsequent reports showed that remyelination of CNS axons was possible, it was characterised by thinner sheaths and shorter internodes than normal, leading to doubts about whether this could support impulse conduction.[21,22] It was not until a seminal 1979 report that remyelination was shown to restore axonal conduction and neurological function in the CNS.[23,24] It is now known that following most insults, including SCI[25] and MS,[1] CNS lesions exhibit some evidence of remyelination, which can facilitate functional recovery. Importantly in the context of disease progression, myelin is neuroprotective, and demyelinated axons are vulnerable to environmental stressors, which can lead to axonal atrophy and degeneration, with concomitant loss of neurological function.[14–18] Therefore, **strategies to activate and enhance remyelination are currently a key goal of experimental neurology**.

The development of remyelination enhancing strategies is critically dependent upon a clear understanding of the biology of myelin genesis; valuable insights into this process

have been gained from an understanding of the process of *developmental* myelination in mammals. During this process, a population of highly proliferative and migratory precursor/stem cells called oligodendrocyte precursor cells (or OPCs, which as their name suggests are the parent cells of the oligodendrocytes) arise in defined CNS regions, and in several waves, populating the brain and spinal cord separately.[26] An OPC population arises in the ventral ventricular zone of the spinal cord involving sonic hedgehog (*Shh*) signalling, and these cells start to populate the entire spinal cord, before a second wave arises in the dorsal spinal cord from radial glia, which competes largely unsuccessfully with the first wave, eventually generating ~10 – 15% of spinal cord oligodendrocytes.[26] In the brain, OPCs first arise in the medial ganglionic eminence and the anterior entopeduncular area of the ventral forebrain, populating the entire telencephalon and cortex. However, a second wave of OPCs arises in the lateral and/or caudal ganglionic eminences, almost completely replacing the first wave. Finally a third wave arises in the cortex (postnatal in rodents), which competes with the second wave.[27] Experimental ablation of each of these waves in mice has shown that each alone can populate the entire brain with oligodendrocytes and result in normal myelination.[27] Eventually, OPCs receive temporally- and spatially-controlled signals that halt migration and stimulate most (but not all) OPCs to differentiate into oligodendrocytes (an OPC subpopulation persists into adulthood hence both cell types are present in the adult CNS, with the OPCs representing 5 – 8% of CNS cells).[28]

In the next stage of the process, the OPCs lose their characteristic bipolar morphology (becoming multipolar), lose their migratory capacity, and undergo a sequence of antigenic shifts as they progress through several developmental stages, eventually becoming mature myelinating oligodendrocytes **(Figure 1)**.[9,29] Early oligodendrocytes extend membrane processes to make contact with numerous axons (reports vary, with 10 to

60 axons per oligodendrocyte being suggested) within ~30 μm of the cell body.[9,10] As they mature, oligodendrocytes form myelin sheaths, in a tightly temporally-regulated event that appears to occur within an 18 h window; such regulation depends on several factors, including electrical activity in neurons, and the expression of complementary cell adhesion molecules by oligodendrocyte processes and axons.[7,30]

The leading edge of the oligodendrocyte process then wraps once around the axon, and forms a spiral by growing between the continuously extending process and the axon. After approximately three wraps/layers are formed, the process of lamellar compaction begins, aided by myelin basic protein (MBP), which links the layers (lamellae) in tight apposition forming what are known as the major dense lines, and extruding the cytoplasm to the less tightly compacted lamellae at the paranodes abutting the nodes of Ranvier.[31] Oligodendrocytes and axons engage in extensive cross-talk during myelination, which mutually influences their development. For example, the number of wraps determines the myelin thickness, which in turn is proportional to the axon diameter; this is likely controlled by axonal signalling, as individual oligodendrocytes can myelinate axons of differing diameters, resulting in differing numbers of lamellae.[10] In turn, the presence of myelin prevents the aberrant sprouting of new branches from axons during development.[31] This cross-talk illustrates that highly coordinated events are necessary for the generation of functional myelin sheaths, and this is followed by continuous turnover of myelin components,[32,33] a process which is critical to neuronal survival and function.

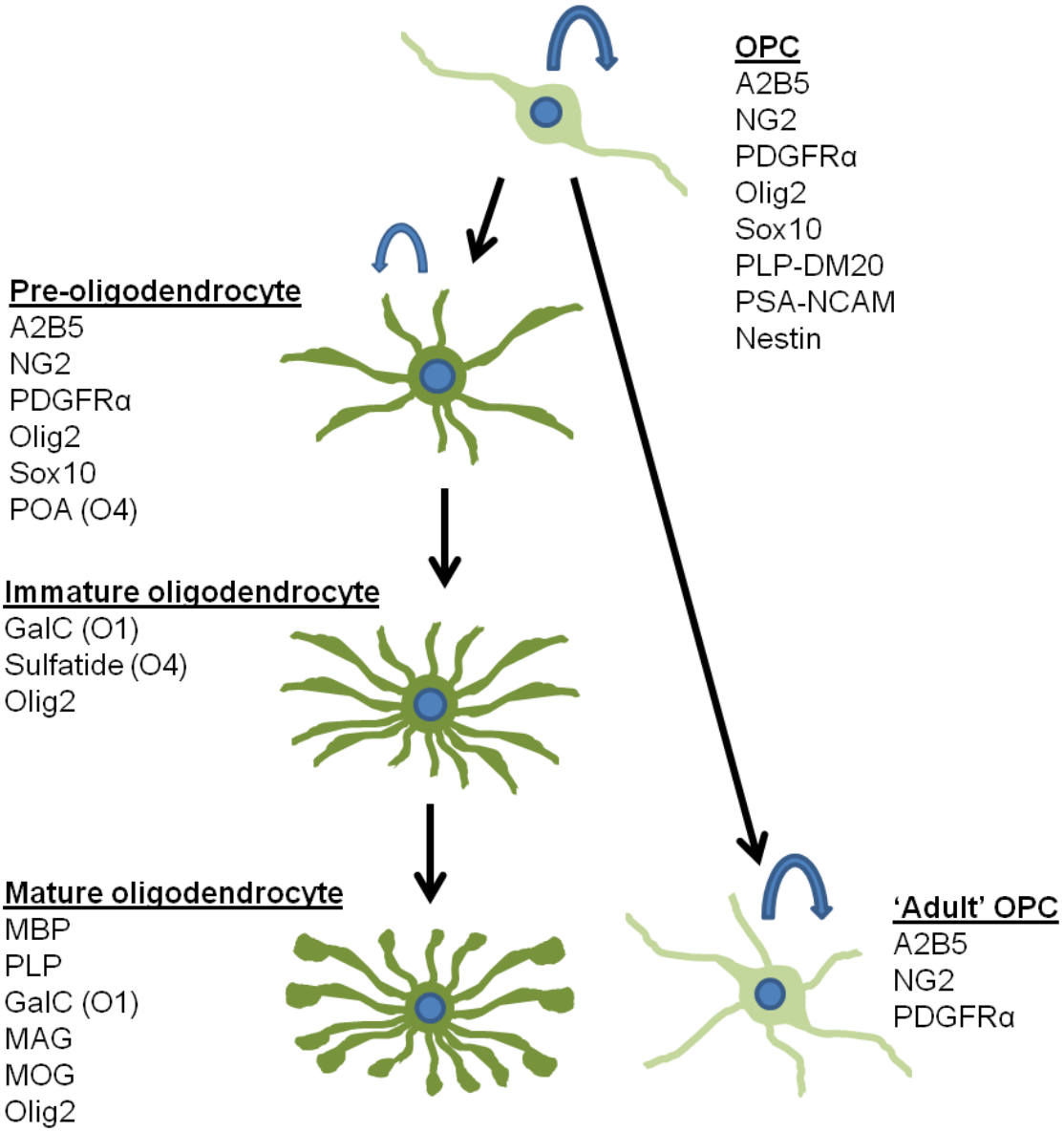

Figure 1: Schematic illustrating the developmental stages of the oligodendroglial lineage. *OPCs are proliferative cells, which generate oligodendrocytes during developmental myelination (through the stages indicated), and also leave a residual population of 'adult' OPCs. Following activation, adult OPCs engage in proliferation. Antigenic profiles are indicated for each stage.*[9,34,35] *Blue arrows indicate proliferating cell types.*

The vast majority of what is known about the oligodendroglial lineage and developmental myelination of the CNS has been derived from rodent models, but what is known from equivalent human biology is largely in agreement, including the sequence of events in myelination, the broad rostro-caudal sequence in which CNS regions are myelinated **(Table 1)**, and the antigenic markers of the oligodendroglia.[34,36,37] Various therapeutic molecules (*e.g.* fingolimod, FTY720)[38] that enhance survival or promote differentiation in rodent oligodendroglia produce the same effects in human oligodendroglia, further suggesting that rodent models of myelination serve as good models of human myelination, of relevance to basic research studies that aim to develop myelin repair strategies.

Table 1: Age at which myelination begins in various brain regions for human and rat.

Brain Region	**Human age (Postnatal months; GM = Gestational month)**	**Rat age (Postnatal days)**
Cerebellar peduncles	GM 7	7
Lateral lemniscus	GM 6	9
Medial lemniscus	GM 6	10
Brachium, superior colliculus	GM 8	10
Internal capsule	1	10
Stria medullaris	4	10
Habenula-peduncular	GM 6	12
Brachium, inferior colliculus	GM 7	12
Fornix	6	12
Corpus callosum & corticospinal tract	GM 7	14
Olfactory tract	2	14
Anterior commissure	3	17
50% of adult myelination complete	18	25
100% of adult myelination complete	20-30 years	90-100

Adapted from Yakovlev *et al.*[11]

1.3 Remyelination recapitulates developmental myelination

It is important to note here that the process of remyelination broadly recapitulates the process of developmental myelination. As in CNS development, the OPCs play critical roles in generating new oligodendrocytes that subsequently mediate the remyelination process; the appearance of remyelinating oligodendrocytes in lesions is preceded by the appearance of a population of OPCs, which have now been proven by fate-mapping to generate remyelinating oligodendrocytes.[39] Remyelination has been proposed to consist of three stages:[28] (i) activation of OPCs, with subsequent proliferation and colonisation of lesion sites, (ii) differentiation of these OPCs to generate oligodendrocytes which associate with demyelinated axons, and (iii) the formation of functional myelin sheaths by these oligodendrocytes. Each of these stages is associated with temporally-specific growth factor expression, and the expression (and downregulation) of each factor must occur in an appropriate sequence in order to orchestrate the relevant stages of remyelination (for example, see **Figure 2**).[40,41]

Remyelination failure: Remyelination in rodent models can be extensive, however, human remyelination frequently does not proceed to completion and ultimately fails in the majority of patients and lesions.[28,42,43] The reasons for remyelination failure are still unclear, and a detailed discussion is beyond the scope of this introduction, but in brief, the prevailing theories suggest: (i) depletion of the repair mediating OPC population, (ii) the limited migratory capacity of adult OPCs, and 'temporal mismatches' between the presence of a repair-promoting environment and lesion colonisation by OPCs, (iii) the failure of quiescent OPCs to generate myelinating oligodendrocytes, and (iv) the unreceptive nature of mature axons for (re)myelination.[1,28]

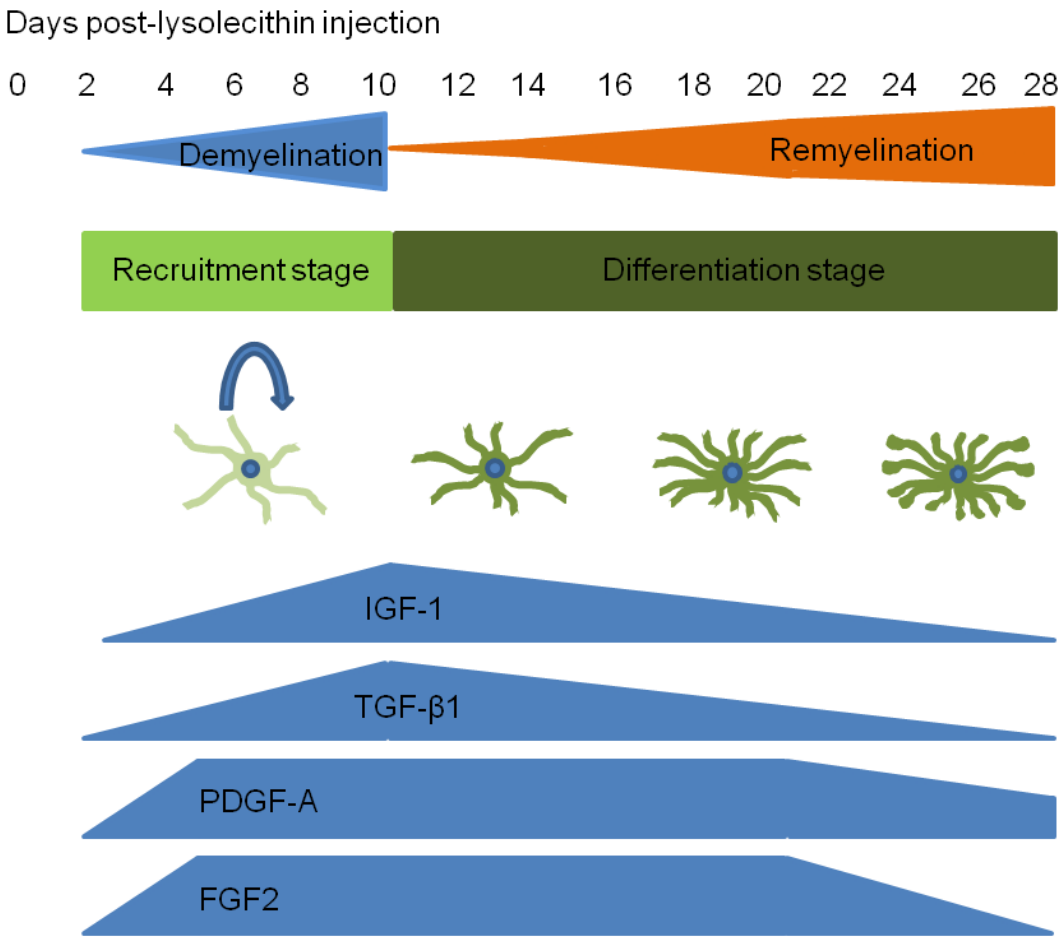

Figure 2: Stages of remyelination and associated growth factor expression. *Focal demyelination was induced by lysolecithin injection into the spinal cord of adult rats (day 0). By 2 days post-lesion, demyelinated fibres were apparent, by 5 days demyelination was widespread, peaking at 10 days. Remyelinated fibres were apparent from day 10, the peak rate of remyelination was from days 14 – 21, and remyelination was complete by day 28. Shapes labelled IGF-1 (insulin-like growth factor-I), TGF-β1 (transforming growth factor-β1), PDGF-A and FGF2 indicate increased mRNA expression of these growth factors. The recruitment phase is associated with upregulation of PDGF-A and FGF2, whereas peak IGF-1 and TGF-β1 expression coincides with the onset of remyelination, suggesting their involvement in the differentiation phase, which may also require downregulation of FGF2. Adapted from published data.*[40,41]

1.4 OPCs are a major transplant population to promote myelin repair

Given our knowledge of the remyelination process, it is clear that OPCs play a pivotal role in myelin repair and that one of two strategies can be adopted to enhance this important regenerative event: (i) activate and enhance intrinsic repair mechanisms, or (ii) bypass intrinsic repair by cell transplantation. The latter is likely to be the more feasible strategy from a practical and clinical (translational) perspective,[28] and will be considered in more detail in this thesis. The potential for transplanted OPCs (derived from a variety of sources) to enhance myelin repair has been demonstrated by their transplantation into animal models.[44–46] These reports can be broadly divided into (a) developmental studies, involving myelination of previously unmyelinated axons, and (b) injury studies, involving remyelination of demyelinated axons.

As examples of the former, transplantation of OPCs into dysmyelinating/ hypomyelinating mutant rodents has resulted in myelination throughout the CNS, and rescue of individuals from typically lethal conditions. A widely used example is the hypomyelinated *shiverer* mouse, which is MBP-deficient, allowing the identification of the transplant-derived oligodendrocytes as MBP^+.[47] For example, Windrem *et al.* transplanted human OPCs into newborn *shiverer* mice, demonstrating extensive myelination, neurological improvement and enhanced survival in ~26% of the mice receiving transplants (with the suggestion of complete rescue of several animals), whereas all control mice died at an early timepoint.[48] Of greater relevance to promoting remyelination, OPC transplant populations have also been successfully tested in demyelination models.[46,49] Givogri *et al.* transplanted primary OPCs into the ventricle of a neonatal mouse model of metachromatic leukodystrophy, a genetic disorder leading to demyelination and extensive loss of oligodendrocytes.[50] These OPCs generated myelinating oligodendrocytes, which

were identifiable one year post-transplantation, and motor function was significantly improved compared to animals without transplants. Keirstead *et al.* transplanted human embryonic stem cell (ESC)-derived OPCs into adult rodent models of SCI, demonstrating remyelination and associated improvement in motor function.[51] The developing CNS is a far more favourable environment for regeneration and for the survival of transplanted cells, and therefore the latter study is significant in that functional improvements were shown after cells were transplanted into the *adult* CNS. OPCs do not survive when transplanted into the normal adult (myelinated) CNS, but do survive when transplanted in the vicinity of demyelinated lesions in the adult CNS.[52,53] All of these studies support the concept that OPCs represent a major transplant population for promoting remyelination.

OPC transplant populations can be derived from a variety of sources [including foetal tissue, adult tissue, neural stem cells (NSCs) and ESCs], and ESC, NSC and OPC populations can all be expanded *in vitro*, suggesting the potential for clinical translation.[11,34,54,55] Indeed, a phase I clinical trial has been approved for transplantation of human ESC-derived OPCs into SCI.[56] This trial has stopped enrolling new patients, a decision taken on financial grounds, but the current subjects will continue to be monitored, and no adverse effects of the transplants have been reported.[57,58] Further evidence of the safety of OPC transplantation was provided by a recent review of preclinical OPC transplant studies for SCI models, which noted that across 24 separate studies there were no recorded instances of teratomas, systemic toxicity, allodynia (pain resulting from aberrant integration of the transplant cells), increased mortality or allogeneic immune responses.[56]

1.5 'Combinatorial' approaches are required for CNS regeneration

Despite the positive outcomes from the above studies and the enhanced remyelination seen following OPC transplantation, it seems likely that the repair capability of transplant populations will require augmentation in order to further enhance CNS regeneration, for example by introducing growth factors or other therapeutic molecules into the lesion site, typically achieved by intravenous or intrathecal injection, or implantation of an osmotic pump.[45,59,60] *'Combinatorial therapies'* that combine multiple strategies, particularly when in an appropriate sequence for appropriate periods of time, have produced more promising results than singular therapies, and are widely considered to be necessary for CNS repair in general.[43,59] Studies using a variety of cell types and disease/injury models lend support to this notion, including the demonstration of synergistic effects of multiple treatments.[45,59,60] For example, Karimi-Abdolrezaee *et al.* produced a rodent SCI model, then compared the functional recovery due to a variety of therapies [intrathecal chondroitinase ABC; intrathecal PDGF-AA, FGF2 and epidermal growth factor (EGF); NSC transplantation] delivered individually and in combination.[59] Both the chondroitinase- and growth factor-treated groups (with cell transplantation) showed significantly greater transplant cell survival and migration distance, and a greater proportion of NSCs underwent oligodendroglial differentiation compared to control animals, which received cell transplants without supplementary treatments. Importantly, the authors report that significant locomotor recovery (13 – 15 weeks post-injury; 6 – 8 weeks post-treatment) occurred only when all three treatments were combined.

With respect to combinatorial therapies involving OPCs, Milward *et al.* transplanted CG4 cells (an oligodendroglial cell line originally derived from neonatal rat cortex), along with a neuroblastoma cell line (B104) intended to provide growth factors for

the CG4 cells, into the spinal cord of hypomyelinated mutant rats.[61] The authors concluded that this stimulated more proliferation of the CG4 cells than transplantation of CG4 cells alone.[61] However, the transplantation of tumour cells is not a suitable strategy for translation to the clinic. By applying gene therapy approaches to cells prior to transplantation, for so-called '*ex vivo* gene delivery', transplanted cells can serve as delivery vehicles for therapeutic biomolecules. This technique can overcome many of the problems inherent to other drug delivery methods, including the short half-life of proteins, which necessitates costly production and repeated applications.[62] These combinatorial approaches could be harnessed to manipulate multiple aspects of the remyelination process to promote more effective regeneration.[43,59] Magy *et al.* made the first report of genetically modified OPCs showing a functional effect, by transfecting CG4 cells to express FGF2 and selecting stably transfected clones.[63] The transgenic cells were shown to enhance the production of myelin-associated proteins and myelin sheaths when co-cultured with dissociated cortical tissue containing neurons. Two studies by Cao *et al.* have gone further, and investigated the transplantation (into *in vivo* models of SCI) of primary OPCs genetically modified to express neurotrophic factors [ciliary neurotrophic factor (CNTF) in one study,[60] and a multineurotrophin (D15A, with both brain-derived neurotrophin factor, BDNF, and neurotrophin-3, NT3, activity) in the other[64]]. In both cases, transplanted cells were shown to generate remyelinating oligodendrocytes within the lesions, which were associated with restored impulse conduction and functional improvements. It is critical to note that these improvements were significantly greater than were observed following transplantation of unmodified OPCs, transplantation of fibroblasts secreting the same neurotrophin, or *in vivo* gene therapy with the same neurotrophin (adenoviral delivery of D15A; D15A experiment only). This demonstrates the effectiveness of genetically

engineering an *appropriate* transplant population as a combinatorial approach to remyelination-promoting therapy.

1.6 Testing the therapeutic potential of cell therapies: Organotypic neural slice models for transplantation biology

Cell transplantation studies such as those detailed above are necessary to facilitate translation to the clinic, but progress in transplant biology is hampered by a heavy reliance on live animal experimentation for such studies, which require large numbers of animals (for sufficient statistical power, and for sham surgical controls), surgical expertise, considerable time and financial costs, and raise ethical concerns, especially with respect to injury/disease models. These factors have fuelled a major international drive to develop alternatives to live animal experimentation. To address these issues and with reference to the reduction element of the 3Rs principle (the Replacement, Reduction and Refinement of the use of animal models),[65] there is significant interest in developing high-throughput *in vitro* models of the CNS (including injury/disease models) in order to test therapeutic interventions. [66–68]

One promising approach in this regard is the use of organotypic slice cultures, which can be prepared from various regions of the CNS through a simple slicing technique, and then maintained in culture on a piece of membrane for up to seven months. [69–72] These slice cultures offer major advantages which may serve to bridge the gap between isolated cell and pre-clinical animal experimentation, including low costs,[73,74] technical simplicity,[69,70,75] the potential for high throughput assays,[73] reduced experimental variability due to the ability to use slices from the same animal for both treatment and

control assays, preservation of neural cytoarchitecture,[70,75,76] and the ability to produce injury[74,77] and disease[38,78–80] models in slices. The most appropriate CNS regions for the establishment of slice cultures are those with lamellar structure, with the main axonal tracts in a single plane (*e.g.* spinal cord and cerebellum).[73] Such regions can be sectioned parallel to these tracts, preserving the cytoarchitecture of particular neural circuits.[73] The distribution of oligodendrocytes[81] and the expression of MBP[82] in neural slice cultures has been reported to closely mimic *in vivo* observations. In particular, rodent cerebellar slice cultures offer an appropriate environment for the study of transplanted OPCs, as large tracts of Purkinje nerve fibres descending from the cerebellar folia to the deep cerebellar nuclei (DCN) are preserved, with these tracts undergoing myelination *in vitro*,[83] mimicking *in vivo* myelination of the cerebellum, which occurs postnatally in rodents.[84]

Synaptic connections are preserved in slice cultures, as evidenced by spontaneous electrical activity,[71] and electrophysiological recordings can be obtained from nerve fibre tracts.[85] Rodent cerebellar slices have been used as *in vitro* models of alcohol-related disorders,[86] tumour invasion,[87] and cerebellar ataxia,[80] in order to screen therapies such as drug delivery.[73] These neural slices can also be used as models of demyelination/remyelination, and the ability to culture them for several months enables 'transplant' studies to be performed, with the slice as 'host' tissue.[78,88] When neonatal neural tissue is placed in contact with cerebellar slices (from hypomyelinated mutants, or pretreated with cytosine arabinoside to prevent oligodendrocyte differentiation), OPCs will migrate from this tissue into the cerebellar slice, resulting in cerebellar myelination.[89] Purified, dissociated OPCs have also been transplanted onto cerebellar slice cultures (cytosine arabinoside treated), resulting in remyelination.[90] Recently, Zhang *et al.* transplanted OPCs (lentivirally transduced to express green fluorescent protein, GFP) onto mouse cerebellar slices and found that they produced GFP^+ myelin sheaths.[4] These

experiments demonstrate the utility of organotypic cerebellar slice cultures as a high throughput screening system for testing the effects of OPC transplantation on remyelination without the use of a live animal injury/disease model, before proceeding to pre-clinical animal testing.

1.7 Technical challenges in cell transplant studies and translational considerations

A variety of cell transplantation therapies (both neural and non-neural) are currently the subject of active research globally, and they face many of the same technical challenges with respect to the testing of their efficacy and suitability for translation to the clinic: (i) Cells must be non-invasively tracked post-transplantation, (ii) transplanted cells must be identifiable by histology, post-mortem, (iii) for the development of combinatorial therapies, the need to genetically engineer a transplant population must be met, (iv) cells must be delivered/targeted to lesions, and (v) all of these processes must be demonstrably safe for both the transplant population and the host. These will now be considered in turn.

1.7.1 Non-invasive imaging of transplanted cells

A non-invasive imaging technique to track transplanted cells is essential to accurately correlate functional neurological recovery with the biodistribution of transplant cells in particular lesion sites in real-time.[91,92] Non-invasive imaging would enable long-term studies to be performed, and such a technique could be employed clinically.[93,94] . Magnetic resonance imaging (MRI) is a major candidate technique for this purpose, and is being extensively tested in cell transplant studies, including with OPC cell lines.[95–98] This

technique requires that the transplant population is labelled with a suitable contrast agent, such as a compound including a heavy metal (*e.g.* iron, gadolinium). MRI has a resolution of ~500 µm in current clinical scanners, but high magnetic field (up to 9 T) research scanners have demonstrated a resolution of ~10 µm,[99] with recent refinements allowing the identification of individual cells.[100] Although MRI is currently the most widely used non-invasive imaging technique, optoacoustic, computed tomography (CT) and fluorescence imaging have been developed, which can be used to track gold particle-labelled cells (optoacoustic and CT imaging) and fluorophore-labelled cells (fluorescence imaging).[99] Optoacoustic imaging is achieved by causing expansion of gold nanoparticles through infra-red irradiation and detecting the resulting soundwaves.[99] Non-invasive fluorescence imaging involves changing the electron energy levels in fluorophores through illumination, and detecting the emitted light as the fluorophore returns to its original activation state.[99] Positron emission tomography (PET) has been employed for tracking radionuclide-labelled cells, but this technique is unlikely to be applied to cell transplant imaging due to the short half-life of such radio-isotopes,[99] and PET has poor spatial resolution, of approximately 1 – 3 mm.[92,101] Although MRI has lower sensitivity than optoacoustic and fluorescence imaging, it has the advantages: (i) of providing detailed anatomical imaging (*e.g.* allowing identification of inflammation and assessment of lesion size) in parallel to the detection of the labelled cells;[92,99] (ii) of not using potentially harmful radiation (in contrast to CT and PET scanners);[92] and (iii) significant infrastructure and expertise is in place at clinics worldwide.

1.7.2 Histopathological detection of transplanted cells

Post-mortem histological analyses are required to assess transplant cell survival, rejection, differentiation profiles and integration, including for example the extent of remyelination.[91,94,102] A diverse range of approaches have been utilised to address the problem of graft detection. Identifying the transplant population may rely on the selection of a distinguishable donor and host (*e.g.* different gender or species,[103] GFP^+ cells from a mutant donor;[104] these approaches may require immune suppression of the host,[105] and can be predicted to have limited translational potential), or will require effective labelling of the cells pre-transplantation.[97] The labelling of a cell transplant population for histological detection can be achieved by staining cells with a dye (*e.g.* carbocyanine),[106] incorporation of a contrast agent,[93,107] incorporation of a fluorophore,[106] or transduction/transfection with a transgene that will render the cells identifiable.[97] A common gene delivery technique involves transduction with the *lacZ* gene, which encodes the *β*-galactosidase enzyme. Successfully modified cells ($LacZ^+$) are then histochemically-detected post-transplantation by incubation with the X-gal enzyme substrate (5-bromo-4-chloro-3-indolyl-β-D-galactopyranoside), resulting in an intense blue product.[108] There are a range of drawbacks associated with these labelling approaches. For example, labelling cells with a dye is generally unreliable, as the dye can leach from the transplanted cells and stain endogenous cells, post-transplantation.[95] Delivery of a reporter gene, such as *lacZ*, is not ideal for tracking transplant populations in the CNS since microglia exhibit high endogenous levels of *β*-galactosidase, increasing the risk of obtaining false-positive results.[108] Finally, the gene delivery technique used, for example viral delivery, can have unwanted toxic effects (section 1.7.3 will discuss viral toxicity).

1.7.3 Gene delivery to cell transplant populations

Free nucleic acids are not readily taken up by cells, as their size and negative charge hinder membrane interactions.[109] Although this can be overcome by direct microinjection into cells, electroporation, or gene gun (ballistic) delivery,[110,111] these techniques have limited clinical potential, with the latter two techniques being associated with adverse effects including membrane damage, abnormal cell physiology and substantial cell death (up to 80% cell loss in OPCs),[110,111] necessitating the use of viral or nonviral vectors to facilitate nucleic acid transport into cells.[109] Gene delivery to neural cells is largely achieved using viral vectors (a process termed 'transduction'), which include adenovirus, adeno-associated virus (AAV), an amplicon based on the herpes simplex virus (HSV), and various retroviruses **(Table 2)**.[60,64,112,113] Whilst viral methods can mediate gene delivery to a significant proportion of a cell population (up to 90% has been shown with OPCs,[50] although results are highly variable), and have yielded valuable information in experimental studies on myelin repair, they are associated with significant drawbacks, primarily safety concerns including direct toxicity, inflammatory responses, nonspecific cellular uptake and oncogenic effects leading to abnormal cellular growth.[110,112,114–117] For example, adenoviral vectors are typically highly efficient for gene delivery, but are also highly immunogenic, prompting adaptive immune responses against the viral capsid proteins, which possibly leads to the suppression of transgene expression.[118] Adenoviruses can trigger cellular immune responses which cause viral clearance and humoral immune responses which make re-administration of the vectors ineffective.[118] There is also evidence that viral vectors are directly toxic to oligodendroglial cells, altering OPC proliferation and differentiation, causing oligodendrocyte death, and damaging myelin.[114,119] There are major limitations with viral transduction in terms of limited plasmid insert size, and the infrastructure necessary to achieve large scale

production for clinical applications (which includes biological safety cabinets), and it should be noted that the safest viral option (AAV) is also the least efficient,[120] leading to a major international drive to develop nonviral alternatives for gene delivery.[116,117] A number of nonviral transfection methods have been tested with OPCs, including calcium phosphate precipitation and liposomes, but these also have significant disadvantages, including typically lower levels of transfection efficiency than viral methods, and toxicity, with calcium phosphate precipitation in particular resulting in a 10% viability rate.[108,111] As a consequence, physical gene delivery techniques have been applied, such as biolistic transfection (gene gun)[111] and electroporation,[108] with adverse consequences as mentioned at the outset of this section.

Table 2: Comparison of viral vectors for gene delivery, with associated drawbacks.

Viral vector	Genome	vector size (nm)	Insert size (kb)	Transduction efficiency	Large scale production	Pathogenicity	Stable insertion/ Insertional mutagenesis
Adeno-associated virus (AAV)	ssDNA	~20	~4.5	Low	Yes	Low	Low
			~2.2	Low, but greater than 4.5 kb AAV			
			~8*	Low*			
Retrovirus (*e.g.* MoMuLV, lentivirus)	ssDNA	~100	~8	High, but requires mitosis[121]	Yes, but only of moderately-pure vector	Initial exposure can be toxic	Yes; vectors typically modified to limit this
Adenovirus	dsDNA	70-100	~36	High	Yes, but with helper virus contamination	Yes, immune response to adenovirus and helper virus	Low
Amplicon (HSV-based plasmid in HSV coat)	dsDNA	~186	~150	No data available; can infect non-dividing cells	No	Cytotoxicity and immune response to helper HSV contamination	Low

All data refers to replication-deficient, modified viruses. ssDNA = single stranded DNA; dsDNA = double-stranded DNA; MoMuLV = Moloney murine leukaemia virus; HSV = herpes simplex virus. Details from Lentz *et al.*[120] and Neve & Carlezon.[122] *Requires co-transduction with two inserts which are then joined within the cell.

1.7.4 Targeting of transplant cells to lesion sites

In order to be effective, transplant populations must be delivered or targeted to lesions. However, direct injection into a lesion, or the CNS parenchyma, will likely cause secondary physical damage including disruption of the blood brain barrier (BBB) risking inflammation, haemorrhage and embolism formation.[1] Alternatively, cells can be introduced intravenously, intraventricularly or intrathecally, methods which are more likely to be used clinically than parenchymal injection.[95] However, it is probable that these approaches will result in many cells diffusing away from the target site, and it would be beneficial to develop strategies to localise or target the transplant cells to the desired area to facilitate attachment and integration, particularly to minimise cell loss in situations where a limited cell source exists. One possibility is the implantation of a synthetic scaffold pre-seeded with cells,[123,124] with such technology being the subject of extensive preclinical testing, which has demonstrated functional improvements in a rat model of SCI.[125] However, delivery of a scaffold would likely involve highly invasive surgery to expose the CNS for implantation.

1.7.5 Safety of cellular engineering and transplant procedures

The requirement that transplantation of a genetically modified cell population is safe, encompasses a wide variety of factors. The transplant cells must be pathogen-free,[1] and the cell type chosen must not be tumourigenic (as ESCs have been shown to be) or immunogenic.[126,127] In this context, human ESC-derived OPCs have been shown to retain some of the immunological properties of ESCs which confer immunological privileges, preventing adverse immune responses, and hence graft rejection, but do not demonstrate

the tumourigenic potential of ESCs.[128] The risk of introducing pathogens (bacterial, viral, or simply xenogeneic material from culture or engineering procedures)[55] into the transplant population increases with multi-step manipulations, for example separate labelling and gene delivery procedures. Multiple manipulations also increase the risk of unintended alterations to the cells, and immune cells can mount responses to cells that they determine to be abnormal.[129] It is important to ensure a high rate of survival of labelled cells, as dying cells will release their labelling agent, which is then likely to be taken up by host cells, as has been shown following rejection of cell grafts, leading to a false detection rate of transplanted cells.[130] The techniques employed to engineer the transplant cells, including labelling and gene delivery, must not cause unwanted side effects, such as prolonged cell cycle[131] or oncogenesis.[132]

1.8 Magnetic particles can satisfy many technical requirements of cell transplantation

It is clear from the above section that the development and testing of cell therapies is associated with a range of technical issues that can hamper the rate of discovery in this field. In this context, magnetic particles (MPs) can serve as a multifunctional engineering platform, which can be harnessed to meet the technical requirements detailed in section 1.7 **(Figure 3)**. The term MP encompasses a variety of synthetic particles, of various physico-chemical properties, with the common element being the incorporation of a magnetic component. The following section will briefly outline the synthesis of iron oxide MPs. There are numerous ways to synthesise these particles, allowing the design to be tailored to specific applications.

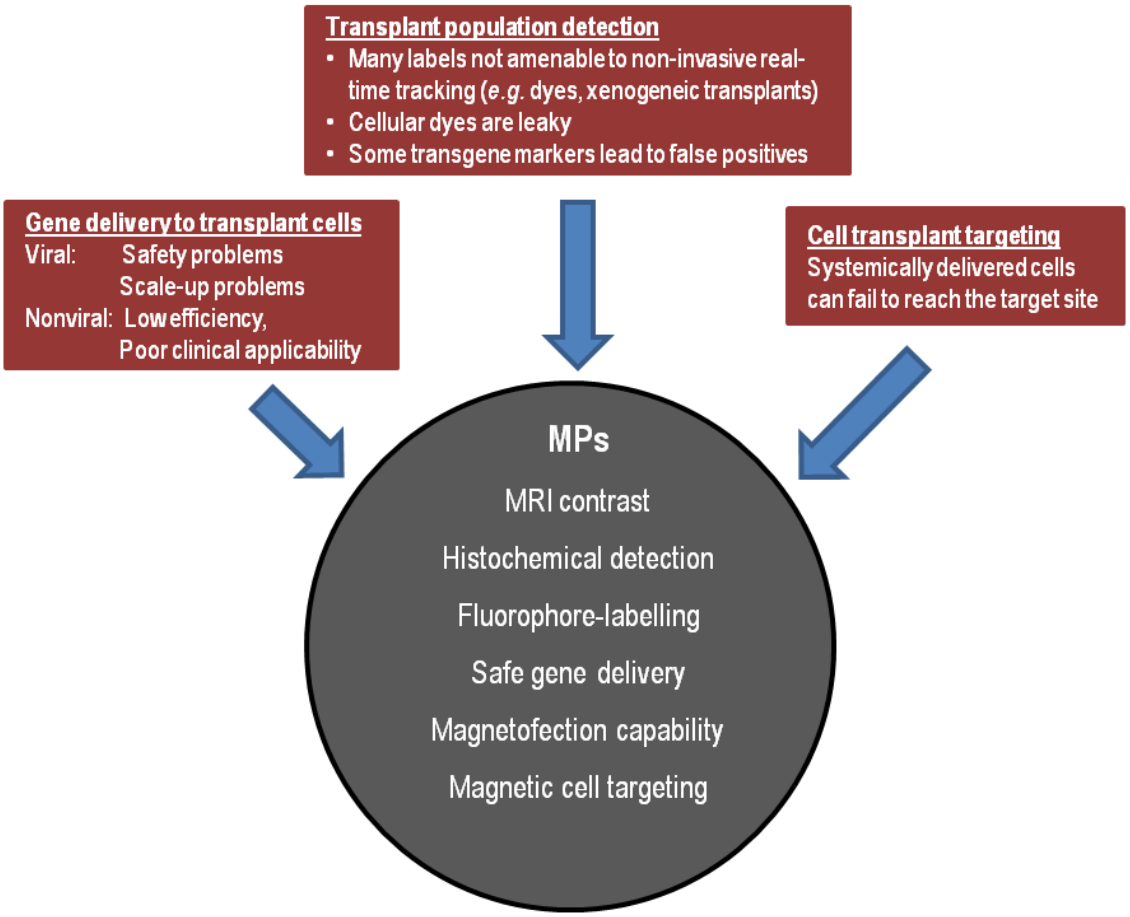

Figure 3: Schematic illustrating various technical issues in transplant biology, and the properties of MPs that can address these issues. *See section 1.7 for details of the technical problems faced by transplant biologists, and see section 1.8 for details of how MPs can provide solutions to these problems.*

Although other materials can be used as the core (*e.g.* polystyrene), with iron oxide crystals incorporated as a layer, the iron oxide component is typically synthesised first and used as the core of the particle. Iron oxide particles (5 – 100 nm core) can be prepared by precipitation from iron salt solutions through the use of a base, and this procedure can be tailored to produce the particular size and consistency required.[133] When iron oxide

crystals form certain structures (*e.g.* magnetite, Fe_3O_4, or maghemite, γ-Fe_2O_3), and remain smaller than approximately 30 nm, they exhibit superparamagnetism, which is desirable as such particles become magnetised only in the presence of a magnetic field, losing this magnetism once the field is removed.[134] This allow the particles to be manipulated by external fields (including MRI), but prevents aggregation due to permanent magnetisation of the particles.

As iron oxide does not readily attach to organic molecules and as iron ions (Fe^{2+}) can cause oxidative stress through free radical production,[135–137] a biocompatible coating is applied to protect the core and facilitate either further coating or functionalisation. Typically, a natural biocompatible polymer is employed for this layer, for example dextran, starch or chitosan.[138] As these cannot be covalently bound to the iron oxide core, they are cross-linked in a network, surrounding the core with cages of polymers.[133] These polymers help to prevent aggregation, and have active groups [*e.g.* dextran presents hydroxyl groups (-OH); chitosan presents hydroxyl and amine groups (-NH2)] which facilitate biomolecule attachment.[138] Alternative coatings include synthetic polymers, such as poly-L-lactic acid (PLA), polyethylene glycol (PEG) and polyglycolic acid (PGA), which are all considered biocompatible. However, these polymers are not readily functionalised as they lack active groups, and introducing active groups requires that the polymer skeleton is broken and hence shortened.[133] All of the synthetic and natural polymers mentioned can leach, which means that particles constructed in this manner can degrade. Therefore, an alternative method of coating the core has been developed, which involves silanisation: using alkoxysilanes to covalently attach a stable layer of silica (-Fe-O-Si-), offering the core some protection from corrosion by physiological electrolytes, and providing a surface composed of readily functionalised organic groups.[133]

Unifunctional MPs are simple to synthesise by sequential layering over the core material, resulting in an outer layer of functional molecules. However, as more sophisticated particles are required for multimodal applications, the synthesis process requires that consideration be given to the coexistence of functional groups.[133] For example, it is possible to exploit the inefficiency of certain organic chemical reactions when performed at a solid/liquid interface. The incomplete transformation of primary amine groups at the particle surface to imines (aldehyde end groups) when reacted with glutaraldehyde means that both groups will be present after the reaction, to which different functional molecules can then be attached.[139] This principle has been demonstrated by the transformation of ~30% of amine groups at the particle surface into carboxyl groups, allowing the particles to be functionalised with both a fluorophore and an antibody.[139] **The development of such multifunctional particles is especially desirable in the context of cell transplantation**, as although MPs have been shown to facilitate each of the applications listed in section 1.7, no single particle is available which can mediate all of them. Such a particle would be of great value for research, as current transplant studies either neglect certain aspects (*e.g.* gene delivery without real-time imaging) or require cells to undergo multiple manipulations (*e.g.* separate gene delivery and cell labelling procedures).

MPs have been exploited for a variety of biomedical applications so far, in a number of physiological systems,[135,140–142] raising interest in their potential utility for neural engineering, but this has received limited attention. There is significant interest in using MPs as contrast agents to track neural transplant populations using MRI,[92,143] and a small number of studies have investigated the potential for magnetic targeting of MP-labelled transplant populations, using external/implanted magnets.[144,145] The applications

of MPs relevant to cell transplantation in general will now be detailed, with reference to OPC applications where such data is available.

1.8.1 Intracellular MPs serve as contrast agents for non-invasive imaging

MPs may be synthesised using elements such as gadolinium, cobalt, iron or nickel, with gadolinium being the most widely used as a contrast agent.[146,147] These materials provide contrast for MRI through high magnetic moments,[148] which disturb local magnetic field homogeneities.[146] This results in short proton relaxivity times in water protons in the immediate vicinity of the particles, leading to loss of signal in T2*-weighted MRI, which is beneficial for imaging purposes.[149,150] The relaxation rate of these protons (*i.e.* the contrast generated) is proportional to the quantity of metal, and is inversely proportional to the distance between the metal and the water protons.[99] Therefore, particles designed with large quantities of iron and/or iron near their surface are likely to provide enhanced contrast, which may be achieved by synthesis of a small particle with high iron content, or a particle with a layer of iron immediately beneath the outer (ideally hydrophilic) layer.[99] Iron-based MPs have been used as systemically delivered MRI contrast agents, as well as cell-labelling agents for tracking individual cells.[151]

For example, Ben-Hur *et al.* have demonstrated *in vivo* MRI tracking (for one month) of MP-labelled [poly-L-lysine (PLL)-coated Feridex] mouse NSCs following transplantation into a mouse MS model.[152] Lepore *et al.* labelled co-cultures of NSCs and glial precursor cells (from mutant rats expressing human alkaline phosphatase) with Feridex MPs and transplanted these cells into adult rat spinal cord.[95] After 5 weeks, the spinal cord was extracted and *ex vivo* MRI showed coincidence of MP contrast with both Perls' iron staining (for MPs) and with alkaline phosphatase staining (for transplant cells).

Feridex-labelled human NSCs have been transplanted into monkey brain and human brain, without neurological effects or seizures, and successfully detected *in vivo* by MRI.[153] Focke *et al.* labelled human embryonic NSCs with iron oxide MPs (8 nm) and transplanted these cells into rat striatum, before successfully tracking them *in vivo* with a clinical (1.5 T) scanner.[154] Several studies have used MRI to track MP-labelled OPCs (CG4 cell line) post-transplantation,[94,143,155] and these will be discussed in detail in section 2.1.

1.8.2 Histological detection of MP-labelled cells

Many MPs can be readily detected due to their metal content, for example by simple histochemical staining to detect iron,[102,155] and this has been demonstrated post-mortem with NSCs[153,154] and OPCs.[94,143] For particles not amenable to metal-based detection (*e.g.* due to low iron content), fluorophores can be incorporated,[92,102,156] either internally or attached to the surface, to facilitate post-mortem detection by fluorescence microscopy. This has been demonstrated using gadolinium-based MPs incorporating a red fluorophore, which were used to label a hippocampal cell line, before transplantation into a rat model of global ischaemia.[157] Following *in vivo* MRI imaging, cells labelled with these fluorescent MPs were identified in post-mortem brain tissue by fluorescence microscopy. Kircher *et al.* have demonstrated detection of a cyanine dye (Cy5.5)-tagged dextran-coated iron oxide MP through fluorescence microscopy of post-mortem tissue, although this particle was delivered intravenously to delineate a brain tumour, rather than being used to label a cell transplant population.[158] By these methods, MP-labelled cells can be detected post-mortem, and iron staining has been shown to correlate well with MRI observations, including studies with OPC cell lines.[95,143,159]

1.8.3 MP-mediated gene delivery: The use of novel *'magnetofection'* strategies

MPs can be functionalised to facilitate the addition of nucleic acids to their surface, and can then serve as gene delivery vectors. This can be achieved using nonviral transfection agents [*e.g.* polyethyleneimine (PEI), PLL] with subsequent nucleic acid binding, but MPs can also be conjugated with viral vectors, typically by biotinylating the viral particles and conjugating (strept)avidin to the MPs, or *vice versa*.[160,161] Alternatively, viral vectors or nucleic acids can be bound to cationic MPs by electrostatic interactions, or MPs with hydrophobic surface regions can associate with viral particles/nucleic acids through hydrophobic interactions.[161]

Nonviral MP-mediated gene delivery has been demonstrated in a wide range of cell lines, and primary cells including neurons,[162] NSCs,[163] and astrocytes.[164] Such vector-mediated delivery of DNA to cells in culture must overcome a number of obstacles: (1) vector-cell contact; (2) transport across the cell membrane; (3) endosomal escape, if the vectors are internalised within vesicles; (4) transport to the nucleus; and (5) delivery of DNA into the nucleus.[165,166] With respect to the first barrier (1), cell contact is largely diffusion-limited for nanoscale vectors (viruses and most synthetic alternatives, including MPs), and a number of attempts have been made to facilitate more rapid vector-cell contact, rather than relying on Brownian motion. For example, Luo and Saltzman exploited gravitational effects on high density particles to cause sedimentation of DNA onto adherent cells, increasing transfection efficiency.[167] When the same technique was used with cells cultured on an elevated membrane with 3 μm pores (allowing sedimenting particles to pass through), the enhanced transfection effect was abolished. Centrifugal force has also been successfully used to increase vector-cell contact.[168] The fact that heavier nucleic acid

vectors are more likely to sediment onto adherent cells may explain why some large vectors have proven more efficient than smaller particles.[169]

For MPs with a sufficient magnetic component, the rate and extent of vector-cell interactions can be enhanced by employing the *'magnetofection'* technique, with the first reports in the literature of such magnet-assisted gene delivery being those of Mah *et al.*[170] (using polystyrene magnetite microspheres complexed with AAV vectors) and Plank *et al.*[171] In a recent review, Plank *et al.* defined magnetofection as "...nucleic acid delivery under the influence of a magnetic field acting on nucleic acid vectors that are associated with magnetic (nano)particles."[161] In such protocols, a magnetic field is placed beneath a culture plate, increasing the rate of MP-nucleic acid complex sedimentation, and thereby enhancing transfection efficiency by exploiting the magnetic properties of these particles.[161] For the rest of this thesis, the term magnetofection will refer only to *nonviral* gene delivery.

Although originally developed to employ a static magnetic field, the magnetofection concept has been refined by several groups, notably by Professor Jon Dobson's group, which introduced lateral motion to the particles in addition to the sedimentation effect, through horizontal oscillation of the array of magnets beneath the culture plate, while the plate remains stationary.[172] The Dobson group has demonstrated enhanced transfection efficiency for oscillating field conditions compared to static field conditions in various cell lines, and published a number of reports addressing the optimisation of the system, for example through varying the oscillation frequency and amplitude,[172] or by altering the arrangement of the magnetic fields in relation to the cells (*e.g.* vertical separation).[173] The mechanisms of enhanced transfection efficiency through magnetofection techniques will be discussed further in section 3.4.

With respect to the second barrier (2), crossing the plasma membrane, this is typically achieved through endocytosis, such that the vectors are contained within endosomes, which may be subject to acidification, and trafficking to lysosomes for enzymatic digestion of the contents, preventing gene delivery. Endocytosis will be discussed in more detail in section 1.9. The third barrier (3), endosomal escape can reportedly be achieved through the 'proton sponge effect',[174] made possible by functionalising particles with highly cationic molecules. For PEI, this is proposed to occur due to the secondary and tertiary amine groups of PEI buffering the acidification process in the endosome. This acidification process occurs as endosomal membrane pumps import protons into the endosome. The endosomal proton pumps continue to import protons, resulting in osmotic swelling and rupture of the endosome, releasing the vectors into the cytosol. Alternative approaches include the incorporation of chloroquine into the vector, which raises the pH of lysosomes, deactivating the lysosomal degradative enzymes and potentially rupturing the lysosome,[116] or the inclusion of membrane-destabilising peptides (*e.g.* synthetic N-terminal peptides of Rhinovirus VP-1).[109] The fourth barrier (4), transport to the nucleus, is poorly understood for nonviral vectors, but trafficking of PEI has been shown to be mediated by microtubule transport (which is exploited by some viruses).[116] However, it is not known whether this transport involved PEI within vesicles, and therefore may not apply to free PEI or PEI-coated MPs.[175] The final barrier (5) is the nuclear envelope, as DNA must enter the nucleus for transgene expression to occur.[176] In non-dividing cells, nuclear entry is regulated by nuclear pore complexes, and nuclear uptake is dependent on the size and sequence of the DNA, with smaller DNA molecules more efficiently gaining entry. The size is not only dependent on the length of the sequence, but also the conformation, as DNA has a smaller diameter when supercoiled than when open/circular, with the additional advantage that supercoiled DNA is more

transcriptionally active.[176] Also, some DNA sequences demonstrate enhanced nuclear entry due to having binding sites for transcription factors [*e.g.* a region of simian virus (SV) 40], some of which may be cell type-dependent.[176] Dividing cells undergo nuclear membrane breakdown,[176] during which nucleic acids can potentially gain entry, and proliferative populations are frequently reported to be more amenable to transfection.[177–179] Enhanced nuclear entry can be achieved using nuclear localisation signals (NLS; *e.g.* by conjugating importin β to either vector or DNA), which molecules larger than ~40 kDa require for active transport into the nucleus.[109,176,180] The intracellular mechanisms that affect gene delivery are under intensive study, and various molecules are being tested to enhance gene delivery at each of the steps outlined here.[109,176]

1.8.4 Magnetic cell targeting approaches

Manipulation of MP-labelled cells following transplantation has been demonstrated,[144,145,181,182] a technique that could facilitate the retention of transplant cells at a target site, and raises the possibility of magnetic 'capture' of transplanted cells from the circulation, following intravenous/intrathecal delivery at a distant site. For example, an implanted magnet has been employed to localise (limit dispersion of) MP-labelled cells at a rat spinal cord lesion following intrathecal delivery,[144,145] and Kyrtatos *et al.* demonstrated localisation of intravenously delivered endothelial progenitor cells to the rat common carotid arteries using an externally applied magnetic field.[181] The common carotid arteries are ~5 mm beneath the skin of the neck and subject to considerable hydrodynamic forces (systolic blood flow is up to 10 ml/min), which significantly reduced the number of transplanted cells remaining in this region in control animals, without the application of an external magnetic field. These magnetic targeting approaches may facilitate the

concentration of transplanted cells at lesion sites, of high relevance in situations where the cell source may be limited.

1.8.5 Safety of iron oxide-based MPs for biomedical applications

Of the MPs reported in the literature, those incorporating iron oxide (typically either magnetite or maghemite) have a good safety profile, and some formulations have been approved for clinical applications [*e.g.* Endorem™, Resovist® and Sinerem™, as MRI contrast agents;[150,183] NanoTherm® for hyperthermic tumour therapy;[99] ferumoxytol (Feraheme®) for iron-deficiency anaemia[184]], suggesting that iron oxide-based MPs may be suitable as non-toxic agents for the engineering of neural cells.[92,146] The static magnetofection technology has been safely used by a large number of laboratories, and although fewer groups are exploiting the oscillating magnetofection technology, reports show that safe protocols can be developed.[140,172,185–188] No adverse effects of magnetic targeting of MP-labelled cells have been noted.[144,145,181,182] As they have received approval for clinical use, are widely available commercially, and can be readily synthesised, this thesis will focus on iron oxide-based MPs, formulations of which (typically unimodal MRI contrast agents) have been used successfully with neural transplant populations.[92,97,154]

It should be noted here, that despite the demonstrable potential of MPs for cell transplant applications, there is a critical lack of neurocompatible *multimodal* MPs designed for these purposes, representing a major scientific and commercial gap. The development of such particles is hindered by the lack of data relating to MP handling by neural cells, data that is particularly lacking with respect to OPCs. Although a number of reports have shown MP uptake by neural cells, each of these studies typically employs a

physico-chemically different particle, which is rarely characterised in detail, barring an effective assessment of which parameters are desirable in a neurocompatible MP. An understanding of how various *permutations* of these physico-chemical characteristics affect cellular interactions will be essential for the development of multimodal MPs, which will likely possess heterogeneous surface properties due to the presence of multiple functional molecules (*e.g.* fluorophores, transfection agents and targeting molecules).

1.9 Uptake of MPs is typically by endocytosis, but the relationship between physico-chemical properties and cell uptake is poorly understood in neural cells

In general, mammalian cells appear to take up MPs by endocytosis,[156] which encompasses a number of mechanisms, which vary in the specificity and size of their cargo **(Figure 4)**.[189,190] Phagocytosis is a form of endocytosis usually employed for the removal of pathogens, debris and apoptotic cells, and in the CNS is exhibited by microglia and astrocytes, with some controversy about whether oligodendrocytes have this capability.[191–194] Professional phagocytic cells (*e.g.* macrophages) readily take up most formulations of MPs, but 'non-phagocytic cells' are often reported to display little, or inefficient, MP uptake.[195,196] Phagocytosis has the greatest payload capacity of any uptake mechanism, and macrophages have demonstrated phagocytosis of latex beads >20 μm in diameter.[197] Other forms of endocytosis are referred to as pinocytosis ('cell drinking'),[198,199] which may be subdivided into macropinocytosis, and a collection of pit-based uptake mechanisms, together described as micropinocytotic uptake.[200] After phagocytosis, macropinocytosis has the potential to internalise the largest payload, as the process involves forming ruffles (lamellipodia-like or circular) or 'blebs' in the membrane which extend from the cell

before collapsing back to the membrane and forming intracellular vesicles known as macropinosomes which may be 5 μm in diameter **(Figure 4)**.[200] This is a non-specific mechanism, and therefore extracellular molecules are internalised at the same concentration as found extracellularly (fluid-phase uptake), although it should be noted that membrane-bound particles are more likely to be endocytosed than unattached particles.[201] The other pinocytotic mechanisms [described as caveolae-dependent clathrin-dependent, or caveolae- and clathrin-independent (which includes at least four mechanisms; see **Figure 4**)] involve the formation of pits in the membrane, which mediate uptake of molecules smaller than ~500 nm,[202] giving rise to vesicles. Some of these micropinocytotic mechanisms are receptor-mediated (selectively internalising specific growth factors, for example), but others act non-specifically. Therefore, for non-phagocytic cells, any particle that can associate with the cell membrane can potentially be taken up by macropinocytosis, whereas micropinocytosis is limited to smaller particles (possibly <300 nm, although there are suggestions that multiple-pit complexes may facilitate uptake of larger entities)[198] and may require specific receptor-binding for uptake.

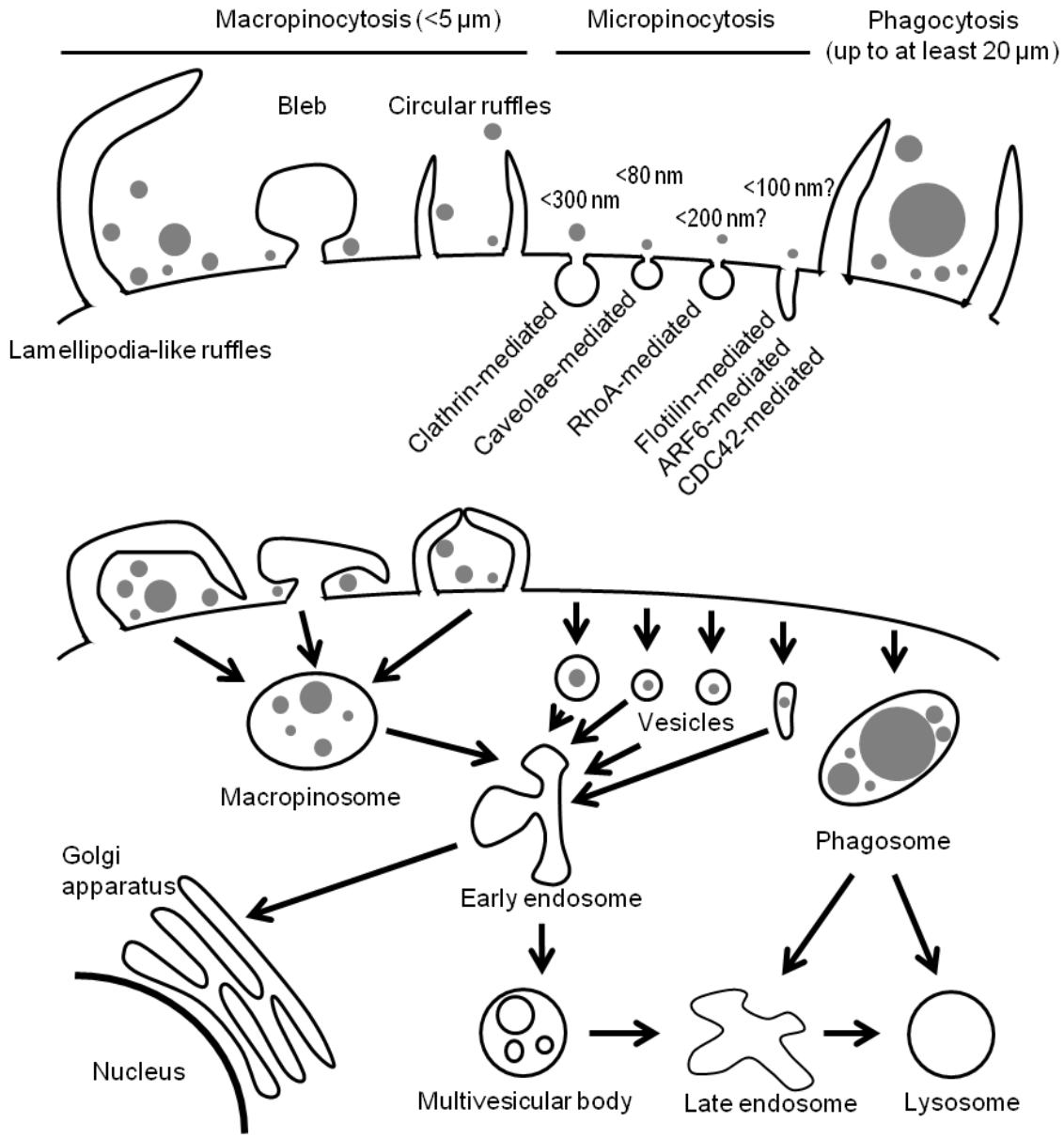

Figure 4: Endocytotic mechanisms of MP uptake. *The cell membrane is shown with endocytotic membrane extensions and pits, and uptake of various sizes of particle is illustrated. Uptake may result in transport to the nucleus, degradation in a lysosome, or exocytosis (not shown). Four clathrin- and caveolae-independent micropinocytotic uptake mechanisms are known: RhoA-. flotilin-, ARF6- and CDC42-dependent uptake. The cargo size limit for each mechanism is indicated, but these are largely unconfirmed. Some evidence suggests that multiple pits can cooperate to internalise larger molecules than a single pit can accommodate.*[198] *Schematic adapted from Canton & Battaglia.*[198]

The uptake of MPs is not only dependent upon cell-intrinsic factors, such as the particular endocytotic mechanisms employed by that cell type and their rates of activity, but is also dependent upon the physico-chemical characteristics of the MPs, including the size, shape and charge, which can significantly affect the uptake and processing of the particles.[203,204] However, there are no studies in the literature systematically comparing OPC (or other neural cell) uptake of particles of differing sizes. One report has compared uptake of dextran-coated iron oxide nanoparticles in a non-phagocytic cell line, with particle sizes ranging from 33 nm to 1.5 μm, with identical surface properties.[204] They report efficient uptake of all MPs (up to 300 nm), except for the 1.5 μm MPs, with a 107 nm (highly cationic) particle producing the most effective cellular labelling for MRI purposes.[204] Uptake of large MPs has been reported in various cell types, including cells that may not be expected to exhibit phagocytosis, for example, ~50% of a rat neuronal precursor cell population has been labelled with a 5.8 μm MP (magnetite core, carboxylated divinyl benzene/styrene polymer coating).[156] In general, uptake of non-targeted vector-nucleic acid complexes is reportedly size-dependent, with a recent review suggesting that 70 – 90 nm is the optimal size for transfection across various cell lines.[109] However, there are considerable inconsistencies in the literature, due in part to the sheer variety of particles and cell types tested, which hampers efforts to compare and contrast the available data.

No data is available for OPC interactions with *non-spherical* MPs, but particle shape may be an important factor for engineering, as it can affect cellular uptake and even cellular responses, on a cell type-dependent basis. This has been shown for some neural cells by Hutter *et al.* who examined the uptake of gold nanoparticles (spheres, rods and 'urchins': spheres with protrusions; respective dimensions: ~23 nm, ~43 x 12 nm, ~77 nm) by microglia and neurons.[205] Neurons only showed uptake of rods, but microglia not only

internalised all three shapes, with a preference for the spiky urchins, but responded differently to each particle with respect to cytokine production.[205] Cylindrical gold nanoparticles were less efficiently internalised by HeLa cells than were spherical particles and efficiency and rate of uptake decreased with increasing aspect ratio of the particles.[203] However, when studying the effect of aspect ratio on the uptake of gold nanorods, another group concluded that surface chemistry was more influential than shape.[206] In a study by Gratton *et al.*, cylinders demonstrated more efficient uptake by HeLa cells than did cubes,[196] although it is not clear how best to perform a reasonable comparison between such differing morphologies. Influencing cellular uptake or behaviour through particle morphology may be possible, yet little is known about how shape affects cellular interactions, particularly with regard to iron oxide MPs.

In general, it is not clear whether uptake is favoured by a positive (cationic), negative (anionic) or neutral surface charge, in part because it is difficult to manufacture particles that differ only in their surface charge, without confounding alterations in the surface chemistry. The plasma membrane is negatively charged, and therefore positively charged particles have a high affinity for the cell membrane, with this interaction being exploited for cellular delivery of therapeutic agents.[207] However, the strong non-specific interactions of cationic particles with cell membranes and negatively charged proteins can lead to aggregation of the particles, and this has been associated with toxic effects.[208] Cytotoxic effects of positively charged iron oxide-based particles have also been suggested to be related to extensive, 'uncontrolled' uptake.[204,209] In reviews of the subject, the general view has been stated that positively charged particles are more readily taken up by cells than neutral or negatively charged particles.[198,210] However, negatively-charged particles have been reported to exhibit high levels of cellular uptake, sometimes to a greater extent than seen with similar-sized positively-charged particles.[146,211,212] **These contradictory**

observations illustrate the need for a systematic review of particle handling by neural cells, which should be performed on a cell-by-cell basis. There is a requirement for cationic MPs, as transfection-grade MPs often utilise cationic surface groups in order to electrostatically bind nucleic acids. In these cases, the surface charge of the functionalised particle is likely to depend on the extent to which these cationic groups are occupied by nucleic acids, but complexes such as PEI-DNA and PLL-DNA can retain their overall cationic charge after nucleic acid binding.[109] However, the influence of surface charge on uptake is clouded by the fact that once added to culture medium the MPs will typically develop a corona of proteins and other molecules, affecting the size, and potentially the shape and charge of the particles.[213,214] In addition to these factors, the particular molecules that constitute the corona can be expected to influence interactions of the particles with the cell membrane, as coronal molecules (*e.g.* albumin, growth factors) may interact with cell surface receptors, facilitating attachment to the membrane, and possibly uptake.[214,215]

The literature does not contain any reports of MP uptake by OPCs derived from primary sources, but does contain some reports of MP-labelling of OPC cell lines. However, the uptake demonstrated by these cell lines may not be a reliable indicator of the amenability of primary cells to MP-labelling, for reasons to be discussed in the next section, and therefore the question of whether OPCs from a primary source will take up MPs remains unresolved.

1.10 Are cell lines biologically relevant models for MP testing?

Much of the research conducted so far investigating the cellular uptake and handling of MPs has used cell lines.[216–221] Whilst such research has yielded valuable data, a number of studies have shown that cell line behaviour can differ markedly from the behaviour of primary cells, limiting its predictive value. For example, Pinkernelle *et al.* compared uptake of iron oxide MPs by primary neurons and the 'neuron-like' cell line (PC12).[222] PC12 cells were originally derived from a pheochromocytoma of the rat adrenal medulla, and possess only 40 chromosomes,[223] but are commonly used as a model of neurons,[219,224] including for particle uptake studies.[131,219,225] Uptake in the cell line (76.9 ± 11.8% standard deviation, SD) was six-fold greater than in the primary cells (12.8 ± 13.2% SD),[222] illustrating the fact that cell lines can be poor models of primary cell behaviour.[222]

More generally, warnings about cell line identity have been made since the 1950s, and many instances of published work have been shown to have been carried out in misidentified cell lines.[226,227] Despite articles highlighting this, a 2004 survey of 483 cell culture workers by Buehring *et al.* indicated that 9% were inadvertently using HeLa contaminants, 33% never verified their cell lines, and 35% had acquired their cells from other laboratories, rather than through a cell line repository.[228] The risk of cross-contamination cannot be overstated, and is not a problem exclusive to laboratories handling multiple cell lines.[229–231] Even if the provenance of a cell line has been established, other potential problems exist. The creation of cell lines involves either the selection of a naturally immortal cell (*e.g.* a cancer cell), or the transformation of a cell population to create immortal cells.[232–234] In either situation, the cells possess an altered physiology compared with the corresponding primary cells - such alterations are not readily characterized in many situations. Once established, cell lines are subjected to

selection pressures, such that progeny with the highest proliferative potential numerically dominate subsequent passages.[235] Therefore, cell lines behave in a relatively homogenous clonal manner being derived from a relatively small precursor cell population, and their properties may not be representative of the natural biological variations that exist *in vivo*. Such variations reflect factors such as the existence of cellular subtypes, ongoing cell proliferation and differentiation, presence of cells at different developmental stages and states of biological activation (of particular relevance in regions of neurological injury/disease), all of which will impact the outcomes of MP use. A further aspect common to many cell lines is their relatively high survival and proliferation rates and resistance to adverse stimuli, such as cell death signals. This robust culture growth also plays a role in cryptic (undetectable) contamination, often by mycoplasma.[232] Such contamination may not be detected for several passages, but can result in alterations in cell structure, metabolism and growth characteristics.[232–234] These considerations, in combination with the risk of cellular aneuploidy, can make cell lines a relatively poor model for toxicity testing.[232,235] This is an issue of high relevance in the field of nanotechnology, where the neurotoxicity of a range of nano- and micro-sized particles is currently an issue of major public and scientific concern.[236]

In terms of gathering clinically relevant data, a viable therapeutic cell transplant therapy is unlikely to utilise an immortalised cell line, as such cells are prone to tumour formation.[237] The most likely sources of cells for transplantation are aborted human tissue or OPCs derived from either human ESCs or NSCs.[34] Primary OPC populations, such as would be obtained from abortion tissue, have been shown to consist of various subclasses of cells,[238] a characteristic which will not be adequately represented within a cell line, further limiting the relevance of data obtained from cell lines.[29,239]

1.11 Aims and objectives of the experimental chapters

The development of cell transplantation and gene therapy strategies for promoting remyelination in the CNS offer the hope of recovery from debilitating conditions, in contrast to the majority of current CNS therapies, which are directed at managing symptoms. The first aim of this thesis is to address the utility of MPs as a tool for engineering OPC transplant populations. To this end, different formulations of MPs were tested as labelling and gene delivery agents for OPCs. These formulations were iron oxide-based, for the reasons given in section 1.8.5. The efficiency and safety of these protocols were assessed, including the effectiveness of magnetofection protocols for enhancing MP-mediated gene delivery; an organotypic cerebellar slice culture model was developed to test the behaviour of transplanted OPCs, serving as an assay of the safety of the genetic engineering procedures (the rationale for employing slice models is given in section 1.6). As a second aim, the amenability of oligodendrocytes to MP labelling and transfection was assessed, and contrasted with the amenability of OPCs, constituting an intralineage comparison of MP handling. Finally, the interesting results of the intralineage comparison prompted a cross-cellular comparison of MP handling by all of the major neuroglia. This was performed by collating the novel OPC and oligodendrocyte data with previously published data for astrocytes[164,240] and microglia,[241] the other major neuroglial cell types. All the experimental studies in this thesis utilised cells derived from a primary source, an approach I consider to be of higher relevance to future clinical transplantation than cell lines, for the reasons outlined in section 1.10. More detailed descriptions of the chapter objectives follow:

Chapter 2: Magnetic particle (MP) uptake in oligodendrocyte precursor cell (OPC) transplant populations

The potential for MP-labelling of OPCs derived from a primary source was investigated in this chapter. The uptake dynamics of two physico-chemically different MPs were assessed, including a novel multimodal particle with cell labelling and gene delivery capabilities. An ultrastructural imaging technique was developed for future rapid, technically simple, high-throughput analysis of particle-cell surface interactions.

Chapter 3: MP-mediated transfection of OPC transplant populations: effects of novel 'magnetofection' techniques

The potential for MP-mediated gene delivery to OPCs, and the effects of magnetofection protocols employing static and oscillating magnetic fields, were investigated in this chapter. The safety of the gene delivery procedures was tested by transplanting modified cells onto an organotypic cerebellar slice culture model. MP-mediated delivery of multiple genes and a therapeutic gene were also tested.

Chapter 4: Labelling and gene delivery applications of MPs in oligodendrocytes: An intralineage comparison with OPCs

The amenability of oligodendrocytes to MP labelling and MP-mediated transfection, and the safety of these procedures, were investigated in this chapter. These data were then collated with the OPC data obtained in chapters 2 and 3, in order to perform an intralineage analysis of oligodendroglial MP-handling. Differences in particle uptake and amenability to MP-mediated transfection were discussed in terms of biological differences between the OPC and oligodendrocyte cell types.

Chapter 5: Differences in MP-handling by CNS glial subclasses: Competitive MP uptake in glial co-cultures

This chapter first collated MP-handling data reported in chapters 2 – 4, for oligodendroglial cells, with data previously published by the host laboratory (pertaining to the other major CNS glial cell types: astrocytes and microglia) in order to perform a systematic cross-cellular comparison of particle uptake and processing, including amenability to MP-labelling and MP-mediated gene delivery, and presence of MP-related toxicity. Based on observations made during this comparison, a hypothesis was proposed that competitive microglial MP uptake will limit MP uptake by other glial cell types in mixed glial cultures. A glial co-culture model with defined cell stoichiometry was developed for the purpose of testing this hypothesis.

Chapter 2: Magnetic particle (MP) uptake in oligodendrocyte precursor cell (OPC) transplant populations

2.1 Introduction

As discussed in section 1.3, endogenous OPCs mediate myelin repair following injury/disease, but the remyelination process is often incomplete.[1,6,42] In attempts to address this problem through cell transplantation therapies, a range of studies prove that transplanted OPCs derived from a variety of sources can promote myelin repair.[45,242,243] In parallel with the growth of the field of neural cell therapies, there is a significant and growing biomedical demand for technological methods and adjunct tools to facilitate research into the development of cell transplantation therapies in the CNS.[91,117] This demand includes techniques to track cells post-transplantation, both non-invasively (especially for clinical studies) and histologically, to assess the safety and efficacy of the cell replacement procedures. Sections 1.7.1 and 1.7.2 discuss current labelling approaches, including associated drawbacks, and sections 1.8.1 and 1.8.2 detail how these may be addressed by the use of MPs as cellular labels. MPs have been shown to be broadly suitable for both non-invasive and histological imaging, serving as contrast agents for MRI and being readily detectable in post-mortem tissue.[96,97,101,240]

This chapter will address a series of issues related to MP-labelling of OPCs derived from primary cultures. Previous studies have assessed the cellular labelling potential of iron oxide MPs by employing the oligodendroglial cell lines CG4 (considered an OPC line due to the behavioural and morphological similarities between these cells and primary OPCs)[53] and OLN-93 (described as a "*primary oligodendrocyte*" line; these cells morphologically resemble bipolar OPCs and proliferate in culture, but stain $A2B5^-/MBP^+$ and produce constituent molecules of myelin, which are characteristics of mature oligodendrocytes).[94,143,155,244] Following reports that dextran-coated MPs do not efficiently label mammalian cells (other than professional phagocytes),[143] Bulte *et al.* attempted to

label CG4 cells with dextran-coated MPs of 8 – 20 nm diameter.[155] They report that no CG4 cells were labelled following 48 h incubation of MPs with cells. However, CG4 cells possess a high number of transferrin receptors, and by conjugating anti-transferrin-receptor antibodies to these MPs "*significant*" uptake by CG4 cells was achieved, though the percentage of cells labelled was not reported. Based on transmission electron microscope (TEM) analysis, the authors suggest that uptake was by receptor-mediated endocytosis. No MP-related toxicity data were provided, but a trypan blue exclusion assay showed "*similar viability*" to control cultures at all doses tested. Labelled cells were then transplanted into the spinal cord of postnatal day (P)7 myelin deficient (*md*) rats and normal littermates. Post-transplantation, fixed spinal cords were removed for *ex vivo* MRI analysis, which showed that transplanted cells had migrated from the injection site (up to 10 mm) and retained their MP label for up to 14 days post-transplantation.

In contrast to the prior report, Franklin *et al.* successfully labelled CG4 cells with iron oxide MPs without the need to employ specific cell targeting strategies, and transplanted these labelled cells into adult rat ventricles.[94] MP-labelled cells were detected by *ex vivo* MRI in tissue fixed at seven days post-transplantation. The particles were synthesised by the authors, based on a patent which reports the iron oxide core diameter as 10 – 50 nm, and were coated with dextran. However, the overall particle size is not reported. Measurements of EM images in the article suggest that the particles are ~400 nm in diameter, although this figure could be based on agglomerations of particles. The authors report that >60% of cells contained at least one intracellular MP inclusion, but no safety/toxicity data is reported.

A later report by Bulte *et al.* studied uptake of magnetodendrimers across a range of cell lines, including CG4, and also with OPCs derived from rat NSCs (it is not stated

whether these were derived from primary NSCs or a cell line).[93] These magnetodendrimers were formed by attaching 7 – 8 nm iron oxide crystals to dendrimers (~100 iron oxide crystals per dendrimer; overall size not reported), and the resulting particles were used as transfection agents.[93,97] The authors report comparable levels of uptake in these and other cell types, concluding that uptake is non-specific and not dependent on cell type.[93] The extent of labelling was described as "*remarkably high*", but the percentage of cells labelled was unreported. Unlabelled cells were determined to contain ~1 pg endogenous Fe, and following 48 h exposure to magnetodendrimers (at a concentration of 25 μg Fe/ml), labelled cells contained an average of 10 pg Fe/cell. There was no obvious decrease in labelling after one week *in vitro*, and proliferation capacity and viability "*appeared unaffected*", although numerical data are not provided in this regard.[93] In this and a related publication,[96] reporting part of the same study, rat NSC-derived OPCs were labelled with the same magnetodendrimers (simultaneously transfecting the cells with *lacZ*) and transplanted into the ventricles of neonatal Long Evans shaker (*les*) rats. It was reported that these transplanted OPCs could be detected by *in vivo* MRI for up to six weeks post-transplantation (the latest time-point assessed).[96] Good anatomical correlation was reported between the MRI detection of particle contrast and the histological detection of $LacZ^+$ cells.[93,96]

Frank *et al.* incubated CG4 cells with Feridex (also known as ferumoxides; dextran-coated iron oxide particles, 5 nm iron core diameter, 50 – 180 nm hydrodynamic diameter, zeta potential -31.3 mV in water)[150,245,246] with and without a complexed transfection agent (Lipofectamine or PLL).[143] In the absence of a transfection agent, Feridex labelling was reportedly "*low*" or not detectable using Perls' Prussian blue iron stain. CG4 cells were successfully labelled when Feridex was combined with each of the transfection agents, and the average iron content per cell was reported to be significantly

greater than the iron content in control cultures, following 48 h exposure to the single concentration of each MP-transfection agent complex tested (in picograms per cell, control: 1.9 ± 0.9; Feridex-PLL: 3.8 ± 1.2; Feridex-Lipofectamine: 14.7 ± 1.7). However, the percentage of cells labelled was not reported, and no toxicity data were provided.

2.1.1 Knowledge gap: Which MP characteristics are relevant for labelling primary OPC transplant populations?

The literature pertaining to MP-OPC interactions is limited, and contains contradictory information regarding the ability of OPC cell lines to take up MPs without conjugation of cell targeting molecules or transfection agents (*e.g.* data of Bulte[143,155] versus Franklin[94]). From the review presented here, a number of substantial gaps in the literature are apparent: (i) only one report provides even an approximation of the percentage of cells which can be labelled, and none report the extent to which the cells can be loaded with particles, beyond an average iron content per cell measurement,[93,143] which may mask heterogeneity of particle accumulation within a cell population;[240,247–249] (ii) although two of these four studies report a lack of MP-associated cytotoxicity, no numerical viability/safety data have been presented, which is a significant shortcoming as these data will be vital to the development of safe particles and related protocols and in order to assess the clinical potential of MPs; and (iii) the MPs employed by these studies, as with many synthetic materials used with other cell types, are typically not fully characterised by the authors, yet these details are essential to the development and optimisation of MP-based cell engineering. For example, most studies of iron oxide MP interactions with mammalian cells report that particle uptake does not require specific targeting, but the reasons behind the exceptions to this (*e.g.* Bulte *et al.*,[155] *Frank et al.*[143])

are not clear, and are difficult to address in the absence of detailed particle characterisation. There has been little attempt so far to systematically determine which specific physico-chemical properties of MPs are associated with greater or lesser particle uptake by OPCs, a matter of high relevance from a cell labelling perspective. Indeed, no previous studies have systematically compared how the physico-chemical properties of MPs affect their interactions with OPCs in any context; knowledge that will aid the development of MPs for specific applications in OPCs.

A further point to note here is that to the best of my knowledge, the literature does not contain any studies of MP interactions with OPCs derived from primary cultures, an approach that will be of greater biological and translational relevance than the widely employed cell lines (discussed in detail in section 1.10).

2.1.2 Knowledge gap: How do MPs interact with the OPC membrane?

In the context of studying cellular interactions with sub-micron sized particles, ultrastructural analyses are inevitably required for a high resolution analysis of particle-membrane associations and to obtain evidence of endocytosis of particles. From a technical perspective, TEM analysis is a commonly used method for studying cell-particle interactions,[131,219,250] but requires considerable expertise, time and expense to analyse a large number of cells. Therefore there is a significant need to develop alternative, cost effective and rapid methods to study the interactions of neural precursor cells and nanomaterials, to optimise the use of such platforms for transplant therapies. One such possibility is the use of scanning electron microscopy (SEM) techniques, which are frequently employed to study particles in the absence of cells.[251] Ultrastructural analyses

can be performed using electron or ion beams to produce high resolution images, but electrically non-conductive samples (typical of biological specimens) are not readily visualised by such techniques, as they become charged. Therefore, biological samples are commonly post-fixed with osmium tetroxide (OsO_4) to preserve the sample and enable conductivity in the sample, allowing electron microscopical analysis.[252] However, this single osmium treatment often results in poor osmium penetration, leading to suboptimal sample preservation and inferior conductivity.[253] Overcoating the osmicated sample with thiocarbohydrazide allows further overcoating with OsO_4, and this OTO technique improves sample conductivity and secondary electron generation by completely and evenly coating the sample with metal.[252,253] By coating a sample with further alternating layers of thiocarbohydrazide and OsO_4 (the OTOTO technique) specimen charging can be eliminated, reducing artefacts.[252,254,255] As a 'non-coating' technique (not employing relatively thick, 12 – 25 nm, layers of metal), OTOTO results in optimal internal and external fixation and an even conductive layer, ensuring that fine structures can be visualised at comparably high resolution to TEM.[256] Some neuroscientists have exploited the OTOTO method, particularly as the affinity of osmium for unsaturated lipids provides enhanced mass-density in myelin,[254,257] and the technique has been employed for analysis of the structures of the inner ear.[256,258,259] Although SEM in general has been used to visualise particles in non-neural cell cultures,[251,260–262] identification of endocytotic activity has rarely been reported.[260,262] These studies did not utilise an OTOTO protocol, which may allow more detailed analysis at high magnification, with improved definition of particles and endocytotic processes, which would facilitate the study of membrane surface interactions of neural precursor cells with biomaterials; to the best of my knowledge, this technique has not previously been used for this purpose. The OTOTO SEM technique is rarely utilised for the study of neural cells or for studying the interactions of synthetic

materials with cells, yet it may offer a simple, high-throughput alternative to conventional TEM studies of particle-cell interactions.

2.1.3 Objectives

The principle aim of this chapter is to assess how OPCs derived from primary cultures interact with MPs, and determine whether OPCs can be efficiently labelled with such particles. The second aim of this chapter is to develop a high throughput ultrastructural imaging technique, OTOTO SEM, for the analysis of MP-OPC membrane interactions.

In the first part of this chapter, the main 'test' MP (termed Sphero^{TM}) will be characterised and the following questions addressed: (i) Do OPCs exhibit uptake of these MPs? (ii) Is the rate and extent of MP uptake by OPCs time- and/or concentration-dependent? (iii) Does exposure to these MPs result in acute cytotoxicity in OPCs? (iv) Do the differentiated progeny of MP-labelled OPCs safely inherit the particles? (v) Over what period of time are particles retained in daughter cells?

In the second part of this chapter, OPC labelling will be tested using a novel multimodal MP, which has significantly different physico-chemical properties to the 'test' particle above, including notable differences in size, iron content and the layering of its constituent parts (*e.g.* surface rather than core-bound fluorophores, an iron oxide core rather than a polystyrene core). The following questions will then be addressed in OPC cultures: (i) Are OPC populations amenable to labelling with these particles? (ii) Is labelling of OPCs with these MPs concentration-dependent? (iii) Does exposure to these MPs result in acute cytotoxicity in OPCs?

The final part of this chapter will explore the potential for studying MP-OPC interactions using the SEM technique known as OTOTO, developing the technique and applying it to OPCs incubated with MPs. The ability to detect MPs and identify endocytotic processes in OPC cultures will be assessed.

2.2 Methods and materials

The care and use of animals was in accordance with the Animals (Scientific Procedures) Act of 1986 (United Kingdom) with approval by the local ethics committee.

Reagents and equipment: Tissue culture-grade plastics, media, and media supplements were from Fisher Scientific (Loughborough, UK) and Sigma-Aldrich (Poole, UK). Recombinant human platelet-derived growth factor (PDGF-AA) and basic fibroblast growth factor (FGF2) were from Peprotech (London, UK). Monoclonal rat anti-MBP was from Serotech (Kidlington, UK), monoclonal mouse anti-A2B5 was from Sigma-Aldrich (Poole, UK), and secondary antibodies [Fluorescein isothiocyanate (FITC)-conjugated] were from Jackson ImmunoResearch Laboratories Inc. (West Grove, PA, USA). Mounting medium (with and without DAPI, 4',6-diamidino-2-phenylindole) was from Vector Laboratories (Peterborough, UK). Chemicals for Perls' staining (potassium hexacyanoferrate and HCl) were from Sigma-Aldrich (Poole, UK).

OPC cultures: Primary mixed glial cultures were prepared from cerebral cortices of Sprague-Dawley rats at P1 – 3, based on an established protocol.[263] Cultures were maintained in D10 medium [Dulbecco's modified Eagle's medium (DMEM) supplemented with 10% fetal bovine serum, 2 mM glutaMAX-I, 1 mM sodium pyruvate, 50 U/ml penicillin, and 50 µg/ml streptomycin] at 37°C in 5% CO_2/95% humidified air for 8 – 10 days, then shaken for 2 h on a rotary shaker at 200 rpm. This medium (containing largely microglia) was discarded, fresh D10 medium was added and allowed to re-gas, then the flasks were shaken overnight at 200 rpm. The resulting medium, containing largely OPCs, was transferred to non-tissue-culture grade petri dishes, to which microglia readily attach, reducing residual microglial contamination. After 30 min, unattached cells were resuspended in OPC maintenance medium (OPC-MM: DMEM supplemented with 2 mM

glutaMAX-I, 1 mM sodium pyruvate, 10 nM biotin, 10 nM hydrocortisone, 30 nM sodium selenite, 50 µg/ml transferrin, 5 µg/ml insulin, 0.1% bovine serum albumin, 50 U/ml penicillin, 50 µg/ml streptomycin, 10 ng/ml PDGF-AA, and 10 ng/ml FGF2) then plated onto poly-D-lysine (PDL) coated glass coverslips in 24-well plates (0.3 ml/well, at 3 x 10^4 cells/cm^2). OPC cultures were maintained for 24 h before incubation with MPs, to allow cell adherence and re-growth of processes.

Sphero MPs: Sphero^{TM} MPs (diameter 200 – 390 nm, iron content 15 – 20% w/v) were obtained from Spherotech Inc. (Lake Forest, Illinois, USA). These particles are prepared by the manufacturer as described in the results and comprise a polystyrene core (stained with the fluorophore nile red) surrounded by a layer of polystyrene and magnetite, over which carboxyl groups have been bound using an undisclosed monomer linker. Although these particles have been previously analysed in this laboratory by scanning electron microscopy (SEM),[241] batch-to-batch variability can occur during MP synthesis, and particle size and shape are important factors in cellular uptake and processing.[212,264] Therefore, Sphero MPs were analysed by SEM for size and shape assessments. We have observed that their fluorophore does not leach, and their emission spectra remain stable following long periods of storage.[240,241] The stability of the fluorophore (due to its incorporation into the polystyrene core, as opposed to conjugation at the particle surface where it would be more prone to oxidation, quenching or detachment) was a significant factor in selecting these MPs, as pilot experiments (involving MP-labelling of neuroblastoma cells and astrocytes) employed transfection grade MPs with surface-bound fluorophores (FluoMag, OZ Biosciences) demonstrating dye-related toxicity (unpublished observations, Dr Divya Chari, Dr Mark Pickard, Keele University, UK). Sphero MPs can be readily visualised by MRI, with the higher concentrations used here (20 and 50 µg/ml) demonstrating concentration-dependent contrast in agar gel when visualised using a 1.5 T

clinical MRI scanner,[240] and Sphero-labelled mouse NSCs transplanted into rodent spinal cord could be detected using a 7 T scanner (unpublished data, this laboratory). Although the Sphero particles are relatively large, it should be noted that particles up to 1 μm diameter have been employed to image transplanted cells in the CNS without demonstrable effects on even complex biological functions such as myelination,[98] and other particles, including functionalised transfection grade particles, are of comparable diameter,[100,265] justifying their use here.

Fe_3O_4-PEI-RITC MPs: In collaboration with Professor M J Rosseinsky, novel multimodal MPs were synthesised at the University of Liverpool by Dr H H P Yiu (now at Heriot-Watt University, Edinburgh, UK).[102] These Fe_3O_4-PEI-RITC particles comprise a magnetite core, surrounded by a covalently attached PEI layer, onto which a red fluorophore (rhodamine isothiocyanate, RITC) is bound. These particles have previously been characterised in detail, with TEM analyses indicating a uniform spherical shape and a core diameter of 24.3 ± 5.7 nm.[102] These particles have been formulated with a higher iron content than typically found in commercial particles (~58%, compared to <30% in typical commercial particles; uncoated magnetite is ~72.4% iron) in order to provide superior MRI contrast at lower particle doses.[102] The number of particles in 1 μg of the prepared MP suspension is calculated to be approximately 19.2 billion (Dr H H P Yiu, personal communication; calculation included in Appendix 1). **Table 1** compares the characteristics of these particles with the Sphero MPs, and **Figure 1** provides a schematic comparison of the components and layers.

Table 1. Comparison of physico-chemical characteristics of Sphero and Fe_3O_4-PEI-RITC MPs		
Physico-chemical property	**Sphero MPs**	**Fe_3O_4-PEI-RITC MPs**[102]
Iron oxide crystal size	~18.5 nm (layer of crystals around polystyrene core)†	24.3 ± 5.7 nm (core, TEM) 25.5 nm (core, XRD)
Magnetisation	Not evaluated	80 emu/g
Coating material	1.63×10^6 carboxyl groups per particle*	PEI (MW = 1800)
Fe content (w/v)	15 – 20%*	~58%
Zeta potential (mV)	-23.13*	+18.6
r2 relaxivity values (7T MRI scanner)	Not evaluated	199 $mM^{-1}s^{-1}$
Particles per µg	25.9×10^6*	19.2×10^9†
*Data provided by manufacturer, Spherotech Inc.; †Data gathered by Dr H H P Yiu (Heriot-Watt University, Edinburgh, UK). All Fe_3O_4-PEI-RITC data taken from Yiu *et al.*[102]		

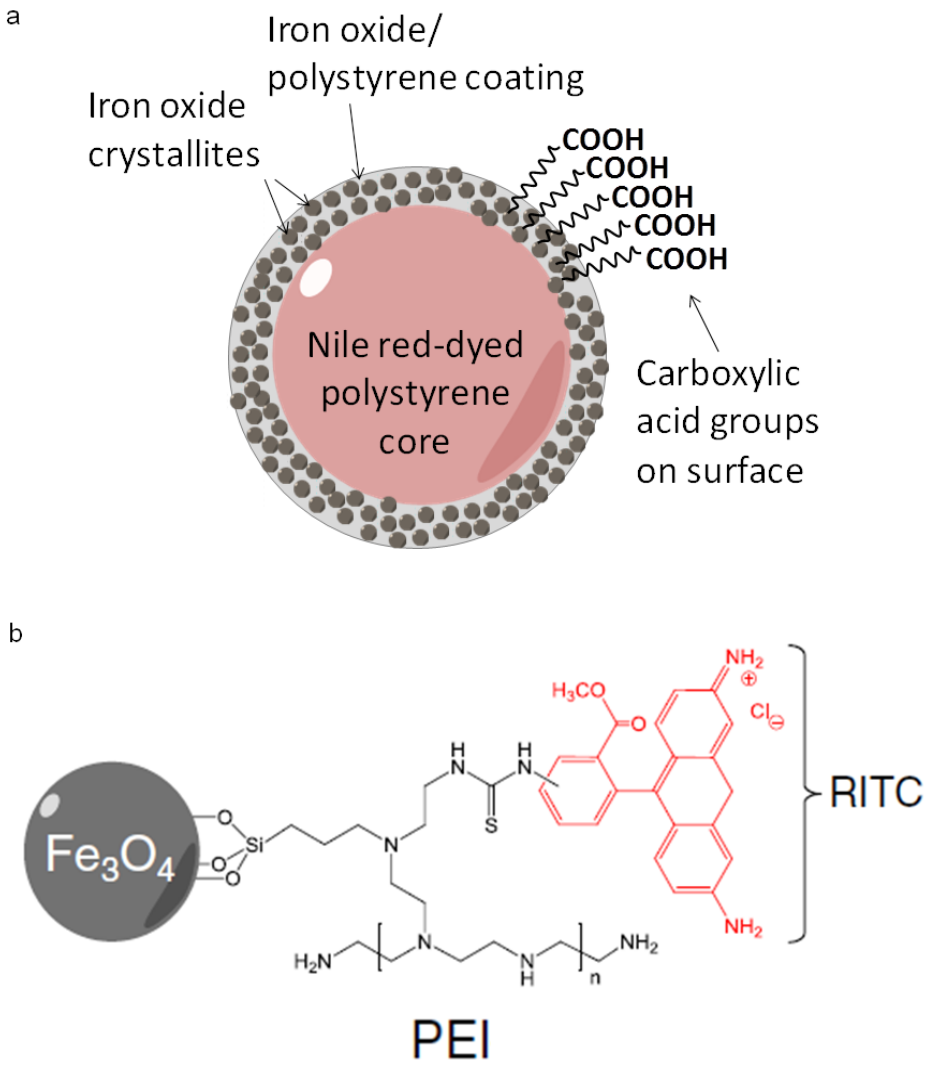

Figure 1: Schematic diagrams of idealised Sphero and Fe_3O_4-PEI-RITC particles. *(a) Idealised Sphero MP. Illustrates the polystyrene core stained with nile red fluorophores, surrounded by a layer of magnetite (Fe_3O_4) and polystyrene to which carboxyl groups have been attached using an undisclosed monomer linker. (b) Idealised Fe_3O_4-PEI-RITC MP. Illustrates the magnetite core (Fe_3O_4) within a silica shell (achieved through silanisation). The shell is functionalised with short chain polyethyleneimine (PEI; to which nucleic acids can be electrostatically bound),*[188] *which is in turn functionalised with a RITC fluorophore. Schematic (a) was produced by Dr H H P Yiu, and (b) is adapted from Yiu et al.;*[102] *particles and layers not drawn to scale.*

Fourier transform infrared (FTIR) spectroscopic analysis of Sphero MPs: FTIR was carried out by Dr H H P Yiu (Heriot-Watt University, Edinburgh) using a Perkin Elmer Spectrum 100 spectrometer fitted with an attenuated total reflection (ATR) sampling unit. For the sample measurement, 32 scans in the region from 650 to 4000 cm^{-1} were accumulated with a resolution of 4 cm^{-1}. This technique was used to identify the chemical groups at the particle surface.

Powder XRD (X-ray diffraction) analysis of Sphero MPs: XRD analysis of the iron oxide component of the particles was carried out Dr H H P Yiu (Heriot-Watt University, Edinburgh, UK) using a Bruker D8 Advance diffractometer with Cu $K\alpha_1$ radiation (λ = 1.542 Å). This technique allows the identification of the structure of crystalline components.[266] The diffraction pattern was collected from 2θ = 5° to 80°, at a step size of 0.009° and a step time of 120 s. The particle size of iron oxide was estimated using Scherrer analysis on the most intense peak (311). This calculation estimates the mean domain size rather than the physical size of the particle, and is used as a complementary technique to TEM size analysis.[266]

Sphero uptake experiments: At 24 h after plating, OPCs were incubated with 2 – 50 µg/ml MPs for 1 – 24 h. Control cultures were treated with equal volumes of fresh medium, without MPs. Samples were washed with phosphate buffered saline (PBS), then fixed and either immunostained, or processed for Perl's Prussian blue histochemical staining. OPC cultures are not strongly adherent to PDL-coated coverslips and this presented a methodological problem for particle uptake experiments with regard to the removal of extracellular particles when terminating incubations. In previous work with astrocytes[240] and microglia,[241] extensive washing with PBS was necessary to reduce non-specific binding of MPs to minimal levels, and this was well tolerated by microglial and

astrocyte cultures, resulting in minimal cell detachment. In the present study a similar washing protocol resulted in the loss of many OPCs, even without the prior addition of MPs (*i.e.* control cultures). Consequently, to minimize the loss of cells, several washes were performed by gently applying PBS to the walls of culture wells.

Differentiation potential of MP-labelled OPCs: OPCs (plated in OPC-MM 24 h previously) were pulse-labelled with Sphero MPs for 24 h (20 µg/ml) then washed with PBS and the medium replaced with Sato medium [DMEM supplemented with 2 mM glutaMAX-I, 1 mM sodium pyruvate, 1x N2 supplement (insulin, human transferrin, progesterone, putrescin, selenite),[267] 30 nM thyroxine, 30 nM triiodothyronine, 50 U/ml penicillin, and 50 µg/ml streptomycin] to induce differentiation. Cultures were maintained for 30 days (medium changes every 2 – 3 days) then either immunostained for MBP or subjected to Perls' staining.

Fe_3O_4-PEI-RITC uptake experiments: At 24 h after plating, OPCs were incubated with 5 or 20 µg/ml MPs for 24 h. Control cultures were treated with equal volumes of fresh medium, without MPs. Samples were washed with PBS, then fixed and either immunostained, or processed for Perl's Prussian blue histochemical staining.

Immunocytochemistry: In all cases, washed cells were fixed with 4% paraformaldehyde [PFA; room temperature (RT); 25 min] then washed again (PBS). For staining, cells were incubated with blocking solution (5% serum in PBS, with 0.3% Triton X-100 for MBP; RT; 30 min), then with primary antibody in blocking solution (A2B5 1:200; MBP 1:200; 4°C; overnight). Cells were then washed with PBS, incubated with blocking solution (RT; 30 min), and incubated with the appropriate FITC-conjugated secondary antibody in blocking solution (1:200; RT; 2 h). Finally, coverslips were washed with PBS and mounted with the nuclear stain DAPI.

Perls' Prussian blue iron staining: Fixed OPCs were incubated with 2% potassium ferricyanide in 2% HCl for 10 min, washed three times with distilled water and then mounted in glycerol-based mounting medium without DAPI.

Fluorescence microscopy: Samples were imaged using fixed exposure settings on an Axio Scope A1 fluorescence microscope (Carl Zeiss MicroImaging GmbH, Goettingen, Germany), and the images merged using Adobe Photoshop CS3 (version 10.0.1).

Z-stack fluorescence microscopy: Z-stack fluorescence images of samples were created using fixed exposure settings on a Nikon Eclipse 80i microscope fitted with a CA742-95 camera (Hamamatsu Photonics, Hamamatsu, Japan), with manual focus stepping at 0.5 or 1.0 µm, and the image manipulations performed using Nikon NIS Elements (version 3.00).

Confocal fluorescence microscopy: Confocal fluorescence images of samples were taken using a BioRad MRC1024 confocal laser scanning microscope. This employed a krypton-argon laser with excitation at 488 nm and emission filters of 522/535 nm.

Scanning electron microscopy (SEM; Sphero MPs): For analysis of MPs without cells, Sphero particles in OPC-MM were air-dried onto aluminium stubs and visualised uncoated using a high resolution field emission SEM (Hitachi S4500) operated at an accelerating voltage of 5 kV.

SEM (OTOTO): For analysis of MP-OPC interactions, OPCs in OPC-MM were plated onto PDL-coated glass coverslips (13 mm), then incubated with 20 µg/ml Sphero MPs for 24 h before OTOTO processing as follows (RT): Samples were fixed in 2.5% glutaraldehyde [in 0.1 M sodium cacodylate buffer containing 2 mM $CaCl_2$, pH 7.4 (SCB; 2 h)], washed with SCB, post-fixed with 1% OsO_4 in SCB (1 h), and washed with SCB

again. Samples were washed thoroughly with distilled water after each of the following incubations: thiocarbohydrazide (in water, saturated solution; 20 min), 1% OsO_4 (2 h), thiocarbohydrazide (20 min), 1% OsO_4 (2 h). Samples were then dehydrated through a graded series of ethanol, before critical point drying (2 h). Coverslips were finally mounted on aluminium stubs using carbon pads, and visualised using a high resolution field emission SEM (Hitachi S4500) operated at an accelerating voltage of 5kV. To determine OPC shrinkage due to sample processing, the longest axis of the cell body was measured in OTOTO samples and compared to the longest axis of the cell body in samples prepared for fluorescence microscopy. Bipolar OPCs were identified for these measurements (12 cells for each microscopic technique) and the longest axis was the distance across the cell body between the two processes.

Transmission electron microscopy (TEM): OPC cultures were established for 24 h on polyornithine-coated aclar sheet, previously cut to fit a 24-well plate (0.3 ml/well, at 6 x 10^4 cells/cm^2), then incubated with 20 µg/ml MPs for 24 h. Samples were fixed with 2.5% glutaraldehyde (in SCB; RT; 2 h), then washed with SCB. Samples were postfixed with 1% OsO_4 in SCB for 1 h, washed with SCB, dehydrated in a graded series of ethanol, then infiltrated with Spurr resin, before polymerization at 60°C for 16 h. To obtain sections, the block was trimmed to expose the aclar sheet which was peeled off, leaving the cells in the resin. Ultrathin sections were then cut parallel to the original plane of the sheet on a Reichert Ultracut E ultramicrotome, mounted on 200 mesh thin bar copper grids, and stained with 2% uranyl acetate in 70% ethanol (RT; 20 min) and 2% Reynolds lead citrate (RT; <5 min). Sections were examined using a JEOL 100-CX transmission electron microscope operated at 100 kV. Images were acquired using a SIS systems Megaview III digital camera (Olympus).

Culture purity analysis: The purity of each culture was determined by scoring at least 100 DAPI-stained nuclei for coincidence with A2B5 staining in fluorescence micrographs.

Sphero uptake/toxicity analysis: For uptake studies, fluorescence micrographs were used to assess the proportion of $A2B5^+$ OPCs with coincident nile red fluorescence, scoring the extent of uptake in each cell as 'low', 'medium' or 'high' (see: *semi-quantitative assessment of MP uptake*), and recording whether each MP-labelled cell exhibiting any perinuclear MPs (minimum 100 DAPI-stained nuclei for each concentration and time point). Initial experiments used a 3-[4,5-dimethylthiazol-2-yl]-2,5-diphenyltetrazolium bromide (MTS) assay to assess MP toxicity in OPCs, by comparing cellular metabolic activity, a technique previously used with astrocytes[240] and microglia.[241] However, typically low levels of MTS reduction to formazan were consistently found in both control and MP-treated OPC cultures, which was not deemed sufficiently sensitive to accurately assess toxicity. Therefore, fluorescence micrographs were used to count the pyknotic and total (healthy plus pyknotic) nuclei per microscopic field, as measures of MP-related toxicity (minimum five microscopic fields for each concentration and time point).

Fe_3O_4-PEI-RITC uptake/toxicity analysis: OPCs were identified in Perls' stained cultures by phase contrast microscopy, and judged to be labelled if intracellular Perls' staining was apparent (minimum 100 DAPI-stained nuclei for each concentration and time point). The extent of uptake by each cell was judged as 'low', 'medium' or 'high' (see: *semi-quantitative assessment of MP uptake*). Duplicate coverslips (plated and treated identically) were immunostained for A2B5 and mounted with DAPI. Toxicity was determined by assessing the percentage of pyknotic nuclei, as judged by DAPI-staining

(shrunken, fragmenting nuclei were classed as pyknotic). Minimum five microscopic fields for each concentration and time point.

Semi-quantitative assessment of MP uptake: The level of MP uptake in individual cells was assessed in a semi-quantitative manner by comparison with the average cross-sectional area of an OPC nucleus, and scored as either 'low' (<10% of the area of an average nucleus), 'medium' (10 – 50%), or 'high' (>50%). It was deemed unsuitable to assess levels of uptake by means of a fluorescence plate reader, or in terms of incorporated iron per cell, as these techniques quantify the total fluorescence or iron present in a culture, and therefore assume an even distribution between cells. Such techniques would not enable the determination of uptake heterogeneity within the cell population, as observed in these cultures. A flow cytometry approach was also considered and rejected, as it is likely that extracellular MPs adherent to the plasma membrane would lead to a number of 'false positives' and this technique cannot distinguish cytoplasmic versus nuclear accumulations of particles within cells. Microscopic cell counting analysis was therefore considered the most appropriate method to assess whether MPs were intracellular, or merely extracellularly attached to plasma membrane, and detailed microscopic assessment of MP uptake was considered to more accurately reflect the heterogeneity that is typically found in primary cell cultures. A minimum of 100 DAPI-stained nuclei were assessed for each concentration and time point.

Statistical analysis: Data were analysed using GraphPad Prism statistical analysis software. All data are expressed as mean ± SEM. The number of experiments (*n*) refers to the number of mixed glial cultures from which OPC cultures were derived, with each primary culture being established from a different rat litter. **Sphero MP analysis**: for (i) the percentage of cells labelled, (ii) percentage of cells exhibiting perinuclear particles,

percentage of labelled cells demonstrating (iii) ‘low’ or (iv) ‘medium’ uptake, (v) total nuclei per microscopic field, and (vi) percentage of pyknotic nuclei per microscopic field, data were analysed by two-way ANOVA for concentration- and time-dependence, with Bonferroni’s post-tests for (i), (ii), (iii) and (iv). **Fe_3O_4-PEI-RITC MP analysis**: for (i) the percentage of cells labelled, (ii) the percentage of cells exhibiting ‘medium’ uptake, and (iii) the percentage of cells exhibiting ‘medium’ uptake plus the percentage of cells exhibiting ‘high’ uptake, data were analysed by unpaired two-tailed *t*-tests; for OPCs per microscopic field and percentage of pyknotic nuclei, data were analysed by one-way ANOVA.

2.3 Results

2.3.1 OPC culture characterisation

Phase contrast microscopy of untreated and MP-treated cultures revealed phase-bright cells with the bipolar morphologies characteristic of OPCs **(Figure 2a)**. Fluorescence microscopy showed that high purity cultures of OPCs were routinely derived from primary mixed glial cultures, as assessed by immunostaining for the OPC marker A2B5 (95.4 ± 0.9%; n = 4), and DAPI-staining showed typical round or oval nuclei **(Figure 2b)**.

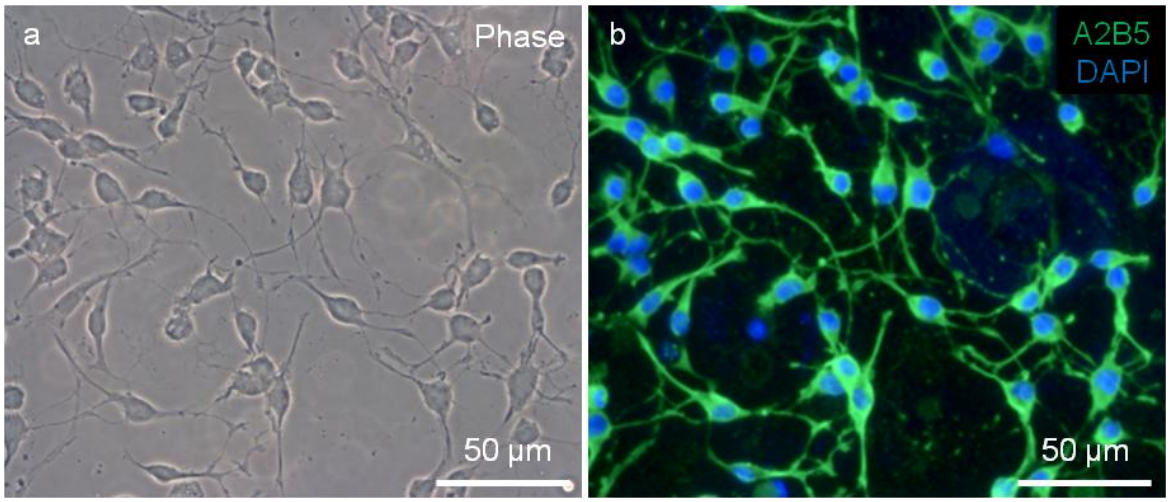

Figure 2: Characterisation of OPC cultures. *(a) Typical phase-contrast micrograph of OPCs. (b) Counterpart fluorescence micrograph of (a) showing A2B5 staining and DAPI-stained nuclei.*

2.3.2 Sphero MP characterisation

SEM data were consistent with previous findings, showing that the particles used were regular in shape, and within the size range reported by the manufacturer **(Figure 3)**. The FTIR spectrum of these particles was dominated by the polystyrene component (**Figure 4a**) with a small number of carboxylic groups, shown as $\nu_{C=O}$ (C=O stretching) at 1707 cm^{-1}. The powder XRD pattern (**Figure 4b**) revealed that the iron oxide crystallites in the particles are of an inverse spinel structure, *e.g.* Fe_3O_4 (magnetite) or γ-Fe_2O_3 (maghemite), consistent with the inclusion of magnetite stated by the manufacturer. However, due to the small crystal size or low crystallinity of the iron oxide, the diffraction peaks are broad and of low intensity. This is also partly due to the predominant amount of polystyrene (*ca.* 80%) present in the particles. The average crystal size was estimated to be approximately 18.5 nm in diameter using Scherrer analysis on the most prominent diffraction peak (311).

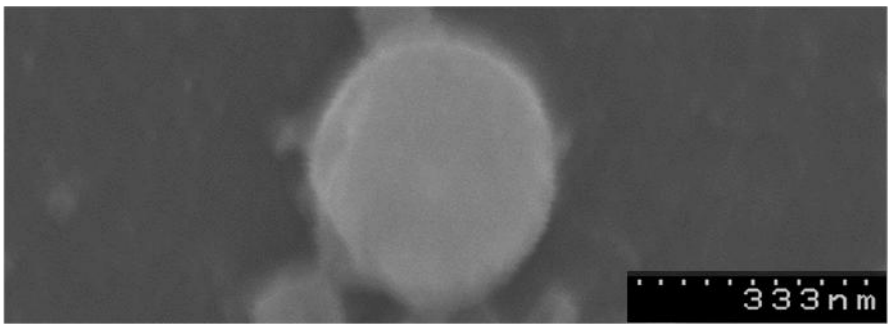

Figure 3: Characterisation of Sphero MPs by SEM. *Scanning electron micrograph of an individual particle, showing typical size and shape.*

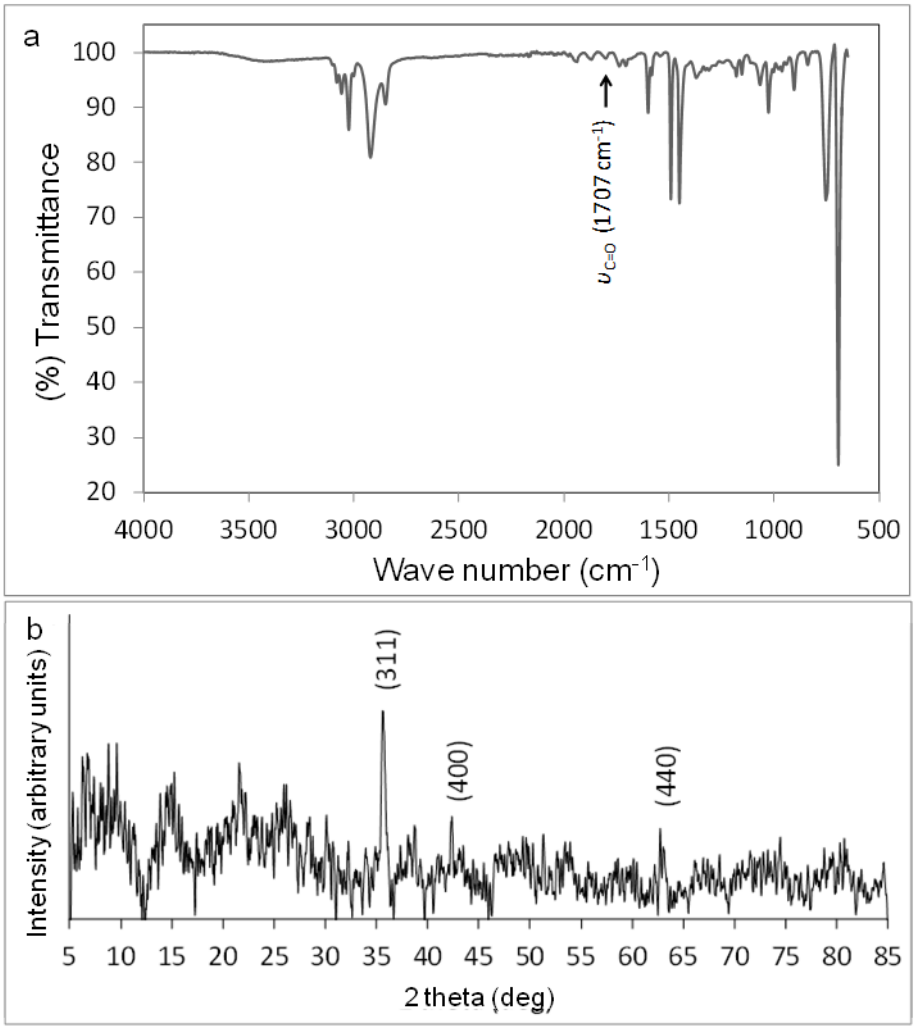

Figure 4: Characterisation of Sphero MPs by FTIR and XRD analyses. *(b) FTIR spectroscopic analysis of Sphero MPs shows a major polystyrene component characterised by peaks in the ranges of 3083 – 3025 cm^{-1} (C-H stretch, aliphatic) and 2923 – 2851 cm^{-1} (C-H stretch, aromatic ring). The peaks within the fingerprint region 1601, 1492 and 1452 cm^{-1} correspond to the C=C stretch in an aromatic system. The strong peaks at 755 and 696 cm^{-1} correspond to the C-H bending mode of the benzene ring. A small number of carboxylic acid groups were detected at 1707 cm^{-1} (C=O stretching; arrow). (c) Powder XRD pattern of particles showing an inverse spinel structure of iron oxide crystallites in particles, consistent with the presence of magnetite. The average diameter of an individual crystal was estimated to be 18.5 nm, based on Scherrer analysis of diffraction peak 311.*

2.3.3 Sphero MPs can be detected within OPCs by both fluorescence and iron staining

Perls' Prussian blue iron staining of cells labelled for 24 h with Sphero MPs revealed the presence of iron coincident with nile red fluorescence **(Figure 5)**. Analyses of cultures which had been pulse-labelled for 24 h then maintained in Sato medium showed that Perls' staining was still coincident with nile red fluorescence after 30 days in culture. This demonstrates the reliability of fluorescence as an indicator of Sphero MP presence, and suggests the stability of MPs in both the culture media and the cells. No blue staining was observed after Perls' staining of control cultures, presumably due to the low levels of endogenous iron.

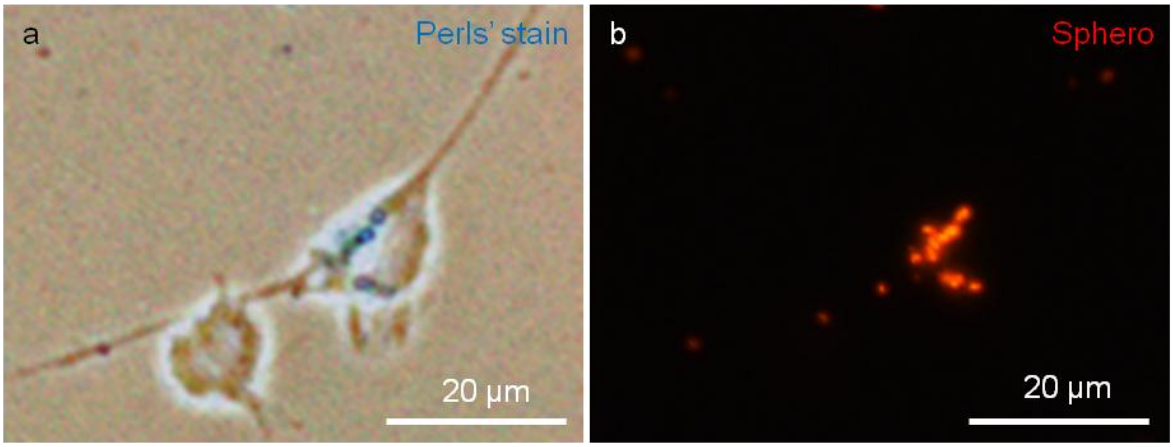

Figure 5: Sphero particle visualisation by fluorescence and histochemical staining. *(a) Phase-contrast micrograph, showing Perls' Prussian blue staining of iron within an OPC (24 h incubation with 20 µg/ml Sphero MPs). (b) Counterpart fluorescence micrograph image to (a) showing nile red fluorescence is coincident with iron accumulations.*

2.3.4 Sphero uptake and perinuclear localisation is concentration- and time-dependent in OPCs

Fluorescence microscopy, including z-stack and confocal analyses, confirmed the intracellular presence of Sphero MPs in OPCs **(Figure 6a-b)**. Both cytoplasmic and perinuclear particle accumulations were observed, with the typical diameter of these accumulations being <2 µm; z-stack analyses revealed accumulations to be typically spherical. MP uptake was time- and concentration-dependent, with the highest dose and longest exposure tested resulting in MP-labelling of *ca.* 60% of A2B5^{+} cells **(Figure 7a)**. Concentrations of 20 and 50 µg/ml resulted in the labelling of a significantly greater percentage of A2B5^{+} cells than 2 µg/ml, at all time points **(Figure 7a)**. Heterogeneity was apparent in the extent of MP-uptake by individual cells. Under all conditions, the majority of MP-labelled OPCs were judged to exhibit a 'low' level of particle accumulation **(Table 2)**. The proportion of labelled OPCs exhibiting 'medium' levels of MP accumulation was both time- ($F_{2,36}$ = 14.2; p < 0.001) and concentration-dependent ($F_{3,36}$ = 15.2; p < 0.001; two-way ANOVA; n = 4). 'High' levels of uptake by OPCs were rarely observed **(Table 2)**. With respect to MP-labelled OPCs, the percentage of cells with perinuclear MPs was found to be time- and concentration-dependent **(Figure 7b)**. Perinuclear, but not intranuclear, particles were observed using confocal and z-stack analyses **(Figure 6)**.

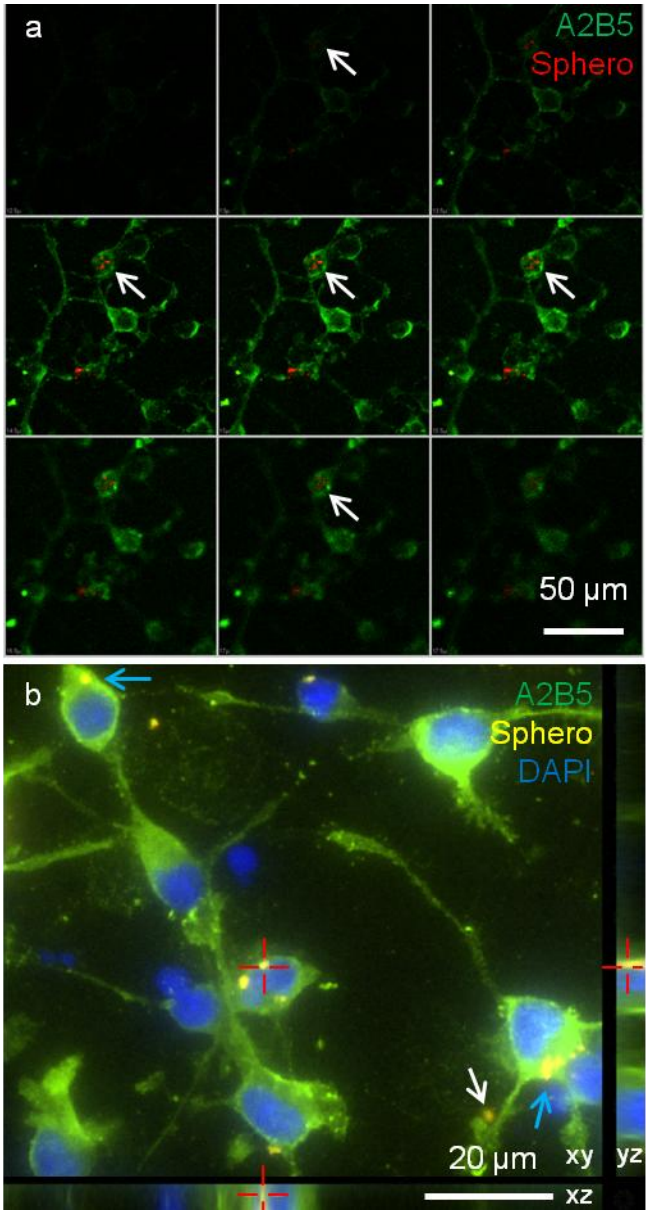

Figure 6: Uptake and perinuclear localisation of Sphero MPs by OPCs was confirmed by confocal and z-stack microscopy. *(a) Series of confocal fluorescence micrographs of cells incubated with 20 µg/ml MPs for 24 h, then stained for A2B5. Arrows indicate nile red fluorescence within a cell. The intracellular nature of particles is inferred by the fact that the cell and particles are in focus within the same planes. (b) Z-stack fluorescence analysis of cells incubated with 5 µg/ml MPs for 4 h, then stained for A2B5. Nile red fluorescence reveals MPs in cytoplasmic accumulations (blue arrow), perinuclear accumulations (crosshairs), and attached to the substratum (white arrow).*

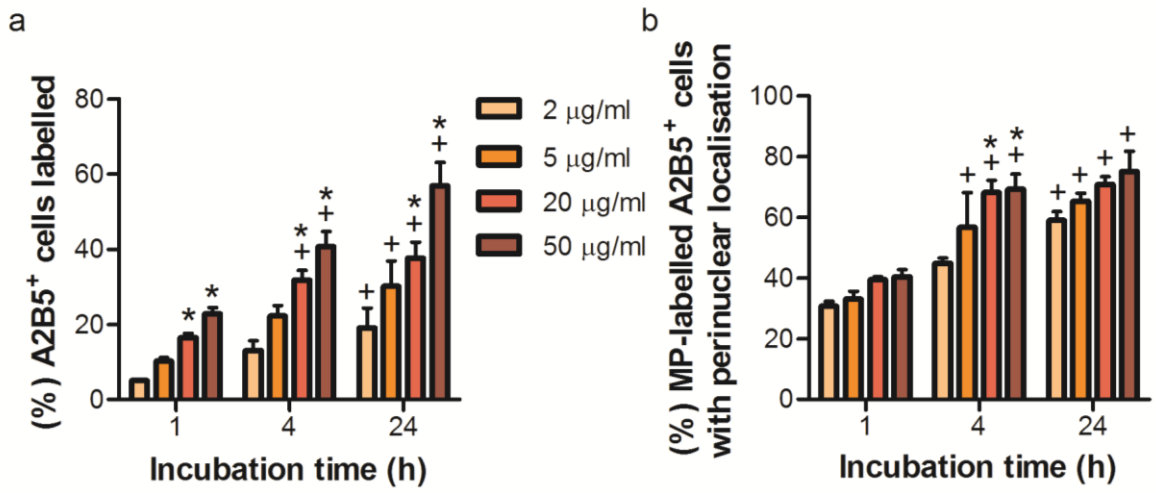

Figure 7: Uptake and perinuclear localisation of Sphero MPs by OPCs is time-and concentration-dependent. *(a) Bar chart showing the percentage of OPCs labelled with MPs. The percentage of MP-labelled cells is related to particle concentration (*$F_{3,36}$ *= 29.2;* $p < 0.001$*) and incubation time (*$F_{2,36}$ *= 35.1;* $p < 0.001$*; two-way ANOVA;* $n = 4$*). (b) Bar chart showing the percentage of MP-labelled OPCs with perinuclear MPs. The percentage of cells exhibiting perinuclear MP localisation was related to both particle concentration (*$F_{3,36}$ *= 8.22;* $p < 0.001$*) and incubation time (*$F_{2,36}$ *= 50.8;* $p < 0.001$*; two-way ANOVA;* $n = 4$*). For (a) and (b),* $^{*}p < 0.05$ *versus 2 µg/ml at the same timepoint;* $^{+}p < 0.05$ *versus the same concentration at 1 h (Bonferroni's post-tests).*

Table 2. Semi-quantitative analysis of the extent of Sphero MP uptake by OPCs.

Incubation time (h)	MP concentration (µg Sphero/ml)	Level of particle accumulation in MP-labelled OPCs (%)		
		'Low'	'Medium'	'High'
1	**2**	100.0	0.0	0.0
	5	100.0	0.0	0.0
	20	100.0	0.0	0.0
	50	95.0 ± 1.0	5.0 ± 1.0	0.0
4	**2**	99.6 ± 0.5	0.4 ± 0.5	0.0
	5	96.7 ± 2.6	3.3 ± 2.6	0.0
	20	88.2 ± 4.1**	11.8 ± 4.1$^{**/††}$	0.0
	50	87.0 ± 3.1†	12.1 ± 2.2††	0.9 ± 1.0
24	**2**	97.3 ± 1.9	2.7 ± 1.9	0.0
	5	95.9 ± 2.2	4.1 ± 2.2	0.0
	20	86.8 ± 4.3$^{**/††}$	12.2 ± 3.6$^{***/†}$	1.1 ± 0.7
	50	85.1 ± 4.3$^{*/†††}$	13.3 ± 3.0††	1.6 ± 1.5

$^{*}p < 0.05$, $^{**}p < 0.01$, $^{***}p < 0.001$ *versus* same concentration at 1 h; $^{†}p < 0.05$, $^{††}p < 0.01$, $^{†††}p < 0.001$ *versus* 2 µg/ml at the same time-point; Bonferroni's post-tests; $n = 4$.

2.3.5 Sphero MPs are not acutely toxic to OPCs

At all concentrations and incubation times tested, no significant effects of Sphero MPs were observed in OPC cultures with respect to (a) cell adherence, as judged by number of DAPI-labelled nuclei (either healthy or pyknotic) per microscopic field (one-way ANOVA at each timepoint; 1 h: $F_{4,15} = 0.314$, ns; 4 h: $F_{4,15} = 0.921$, ns; 24 h: $F_{4,15} = 0.261$, ns; $n = 4$; **Figure 8a**), and (b) cell death, as judged by the percentage of cells exhibiting pyknotic nuclei (*i.e.* shrunken or fragmenting morphologies; one-way ANOVA at each timepoint; 1 h: $F_{4,15} = 0.913$, ns; 4 h: $F_{4,15} = 1.41$, ns; 24 h: $F_{4,15} = 0.0444$, ns; $n = 4$; **Figure 8b**). For all concentrations and incubation times, OPC cultures appeared morphologically similar to controls at 24 h.

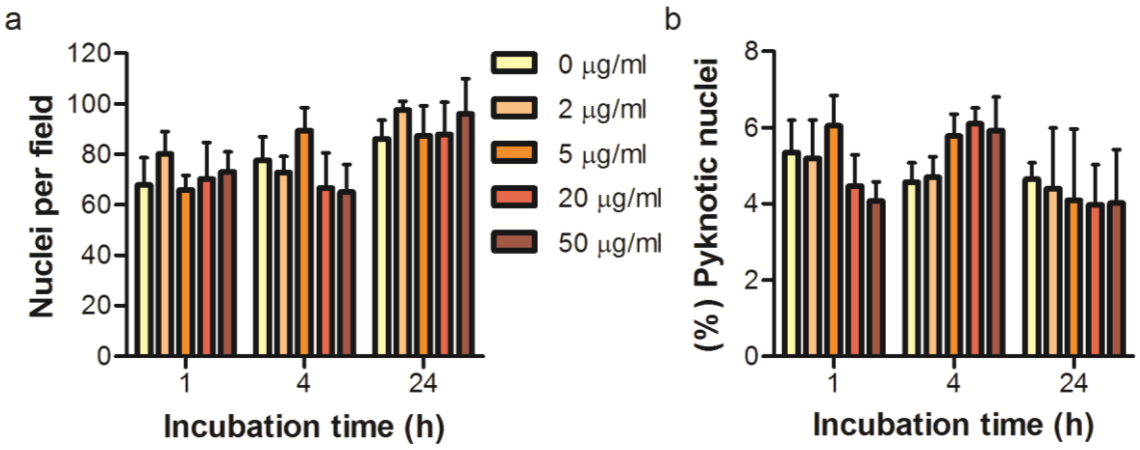

Figure 8: Incubation of OPCs with Sphero MPs at a range of concentrations does not result in acute cytotoxicity. *Bar graphs of OPC time course experiments showing (a) total (healthy plus pyknotic) nuclei per microscopic field, and (b) percentage of nuclei with pyknotic features (n = 4 for both graphs).*

2.3.6 Oligodendrocytes inherit MPs from labelled OPC parent cells without obvious long term toxicity

When OPCs were pulse-labelled with Sphero MPs for 24 h then cultured for 30 days in differentiation medium, no differences were observed in treated versus control cultures with respect to the number of cells, percentage of cells staining for MBP, or morphology. Accumulations of MPs were evident within approximately 60% of oligodendroglial cells **(Figure 9)**. Occasional dense rings of MPs were present within MBP^- cells, which morphologically resembled microglia. Heterogeneity in the extent of cellular MP accumulation was apparent **(Figure 9)**.

2.3.7 Fe_3O_4-PEI-RITC MPs can be detected within OPCs by both fluorescence and iron staining

Whereas the Sphero particles contain a relatively small proportion of iron (15 – 20% w/v), the Fe_3O_4-PEI-RITC particles have a high iron content (~58% w/v), and therefore uptake was assessed by Perls' Prussian blue iron stain which was found to robustly label even small (<1 μm diameter) accumulations of particles **(Figure 10a)**. Red fluorescence attributable to the RITC fluorophore could also be detected within OPCs using confocal and z-stack microscopy, confirming that the particles were intracellular rather than merely adherent to the plasma membrane **(Figure 10b)**. Both cytoplasmic and perinuclear accumulations of particles were observed **(Figure 10b)**.

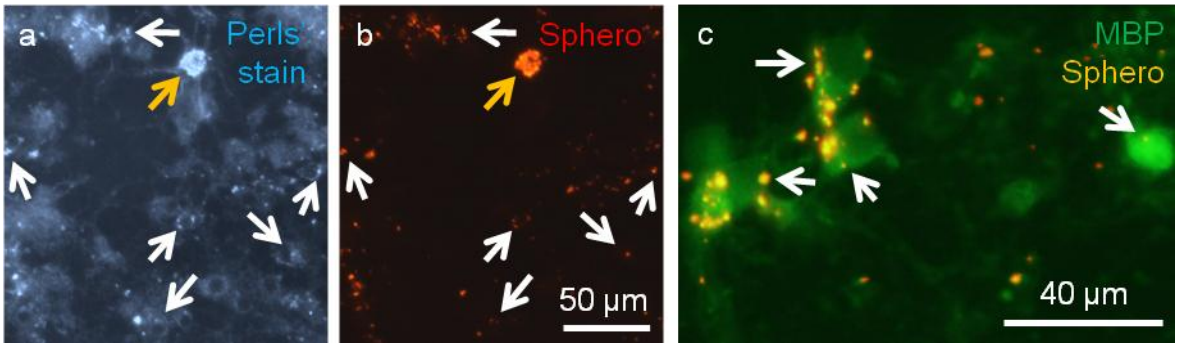

Figure 9: Sphero particles are stably retained within oligodendrocytes generated from labelled OPCs for up to 30 days. *OPCs were pulse-treated with Sphero particles (24 h incubation with 20 µg/ml Sphero MPs) then maintained in differentiation medium for 30 days, generating an enriched oligodendrocyte culture. (a) Dark field micrograph showing Perls' iron stain of Sphero MPs within cells identified morphologically as oligodendrocytes. (b) Counterpart fluorescence micrograph to (a) showing nile red fluorescence of Sphero MPs. Orange arrow indicates the same large accumulation of MPs in both images, located within a multipolar oligodendrocyte. White arrows indicate the same intracellular accumulations of Sphero particles in both images. Note that MPs are frequently located at the edge of the nucleus, which can be identified as a dark circle or oval in the centre of each cell. (c) Fluorescence micrograph of a culture stained with the late-stage oligodendrocyte marker MBP. White arrows indicate example accumulations of Sphero particles within cells. Note the heterogeneity in the extent of particle uptake, and the intense MP fluorescence.*

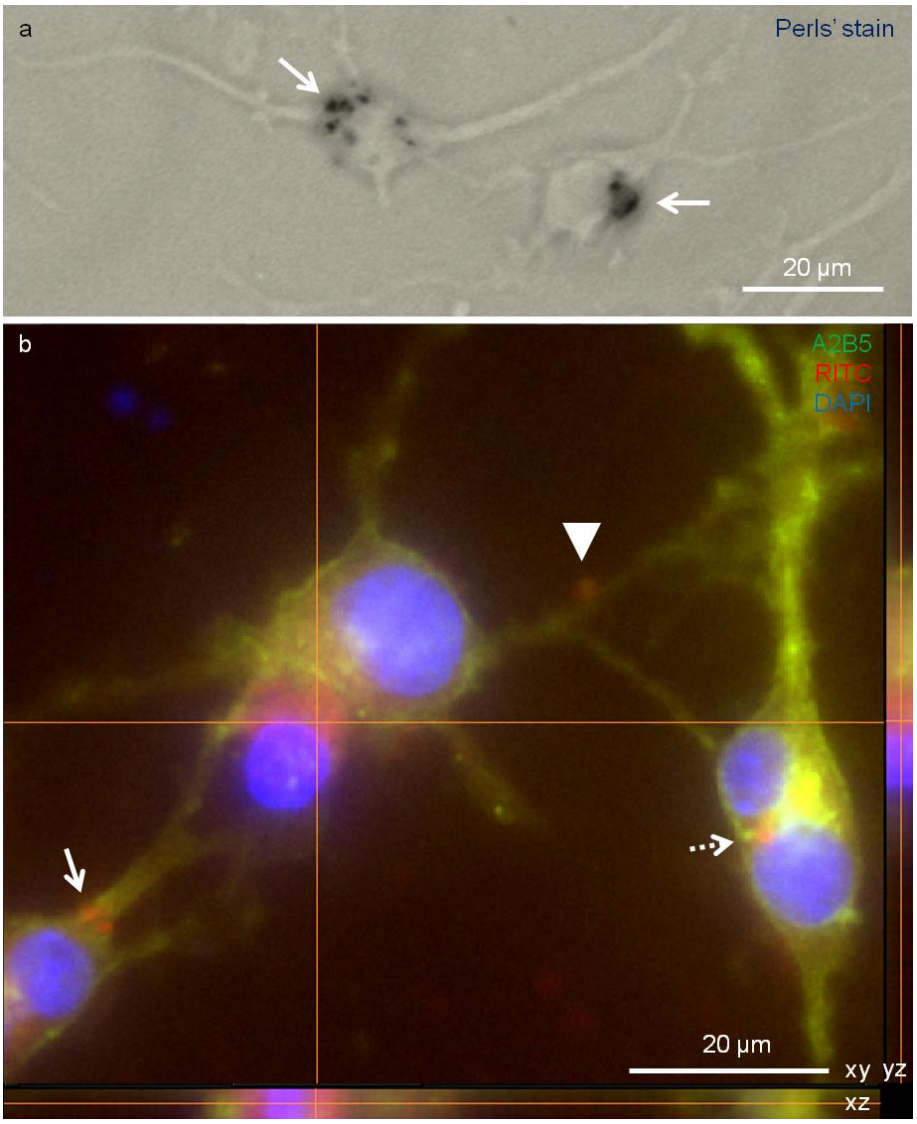

Figure 10: Fe_3O_4-PEI-RITC particle visualisation by histochemical staining and fluorescence microscopy. *(a) Phase-contrast micrograph, showing Perls' Prussian blue staining of iron within OPCs (24 h incubation with 20 µg/ml Fe_3O_4-PEI-RITC MPs). Arrows indicate intracellular particle accumulations. (b) Z-stack fluorescence micrograph of OPCs (identified by the OPC marker A2B5) following 24 h incubation with 20 µg/ml Fe_3O_4-PEI-RITC MPs. RITC fluorescence indicates the intracellular presence of particles, with perinuclear (crosshairs and dashed arrow) and cytoplasmic (white arrow) accumulations apparent. Arrowhead indicates an extracellular particle accumulation.*

2.3.8 Uptake of Fe_3O_4-PEI-RITC particles by OPCs is concentration-dependent

Concentration-dependent labelling of OPCs with Fe_3O_4-PEI-RITC particles was apparent, with >50% of OPCs demonstrating either 'medium' or 'high' levels of particle uptake at 24 h with the highest concentration tested (**Figure 11a**). At both concentrations tested, no significant effects of Fe_3O_4-PEI-RITC MPs were observed in OPC cultures with respect to: (a) cell adherence, as judged by the number of OPCs per microscopic field **(Figure 11b)**, and (b) cytotoxicity, as judged by the percentage of cells exhibiting pyknotic nuclei (*i.e.* shrunken or fragmenting morphologies in duplicate cultures labelled with DAPI and A2B5, but without Perls' staining; **Figure 11c**). For both concentrations, OPC cultures appeared morphologically similar to controls after 24 h incubation. The percentage of OPCs exhibiting perinuclear accumulations was not specifically counted in the Perls' analyses as DAPI-staining is not compatible with Perls' staining. However, perinuclear particle accumulations were frequently observed using fluorescence microscopy, and could be inferred by the characteristic Perls' staining of particles in arcs or curves around the centre of cells (see **Figure 10a** for examples). From these assessments, the approximate percentage of cells exhibiting these perinuclear patterns (~70% for both 5 and 20 µg/ml, 24 h) was comparable to that observed with Sphero MPs.

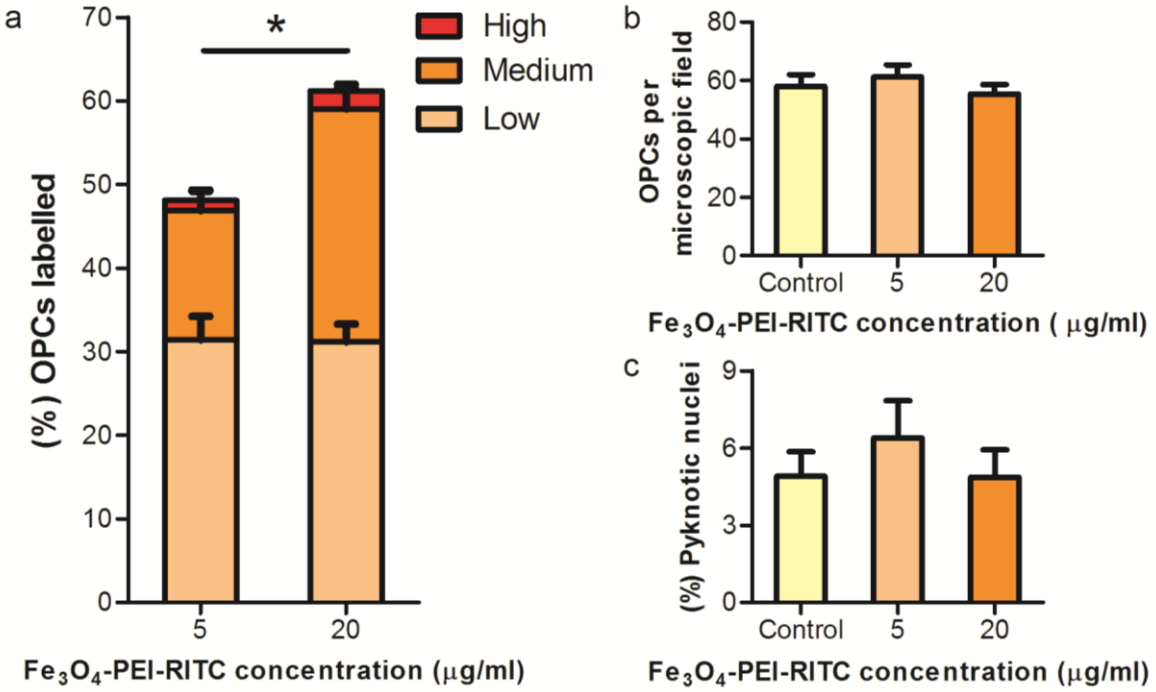

Figure 11: Fe_3O_4-PEI-RITC MPs label OPCs in a concentration-dependent manner and do not exhibit acute toxicity. *(a) Bar graph illustrating the concentration-dependent uptake of Fe_3O_4-PEI-RITC MPs by OPCs following 24 h incubation (*$p < 0.05$). The stacked bars indicate the proportions of labelled OPCs which exhibited 'low', 'medium' or 'high' levels of MP accumulation. The proportion of OPCs exhibiting 'medium' levels of MP accumulation was concentration-dependent ($p < 0.05$). The percentage of OPCs exhibiting 'medium'-to-'high' MP uptake was concentration-dependent ($p < 0.05$). Bar graphs illustrating no differences in (b) the number of OPCs per microscopic field ($F_{2,6} = 0.602$; ns; one-way ANOVA; $n = 3$) and (c) the percentage of pyknotic cells per microscopic field ($F_{2,6} = 0.559$; ns; one-way ANOVA; $n = 3$) following incubation of OPC cultures with or without Fe_3O_4-PEI-RITC MPs for 24 h. For (b) and (c), OPCs and pyknotic nuclei were identified by A2B5 and DAPI staining of identically treated sister cultures, without Perls' staining;* $n = 3$ *for all graphs.*

2.3.9 OTOTO SEM facilitates the identification of MP-cell interactions and endocytotic processes

Samples demonstrated good cell adherence, with few cells exhibiting membrane fractures (<5%). Membrane features could be readily identified in the high resolution images obtained, revealing cellular interactions with MPs **(Figure 12)**. Control cultures showed no evidence of MPs **(Figure 12a)**, and OPCs were readily identifiable by their characteristic bipolar morphologies, with small cell bodies and fine processes **(Figure 12b).** Cells with proliferative morphologies could be observed in MP-treated samples **(Figure 12c)**. Based on the measurement of the longest axis of the cell body, OTOTO-processed OPCs appear to shrink to ~80% of the size of OPCs fixed for fluorescence microscopy, but the lack of obvious fractures in the membrane attributable to shrinkage suggests no cells were damaged by this shrinkage. Sphero MPs could be identified by their regular spherical morphology and size, in agreement with SEM of particles without cells, and the absence of similar structures from control cultures, and these MPs could be found in association with cell membranes **(Figure 12d-f; Figure 13a)**. Small 'blebs' of membrane were observed projecting from the cell surface, of slightly larger diameter than the MPs, although it was not apparent from these analyses whether MPs were inside these 'blebs' **(Figure 12d-e)**. Many cells displayed large numbers of microvilli and/or pits, indicating highly active endocytotic membrane (**Figure 12d-e**; contrast with regions of 'smooth' membrane in **Figure 12a-c**. Some cell-associated MPs were observed to be within membrane depressions, which may indicate the early stages of endocytotic pit formation **(Figure 12f)**, and in close proximity to pit-like structures, suggestive of endocytotic activity **(Figure 13a)**. Macropinocytotic membrane elaborations could also be seen near MPs **(Figure 13a)**, suggesting that OTOTO SEM may allow identification of the same endocytotic activity as was observed using TEM analysis **(Figure 13b)**.

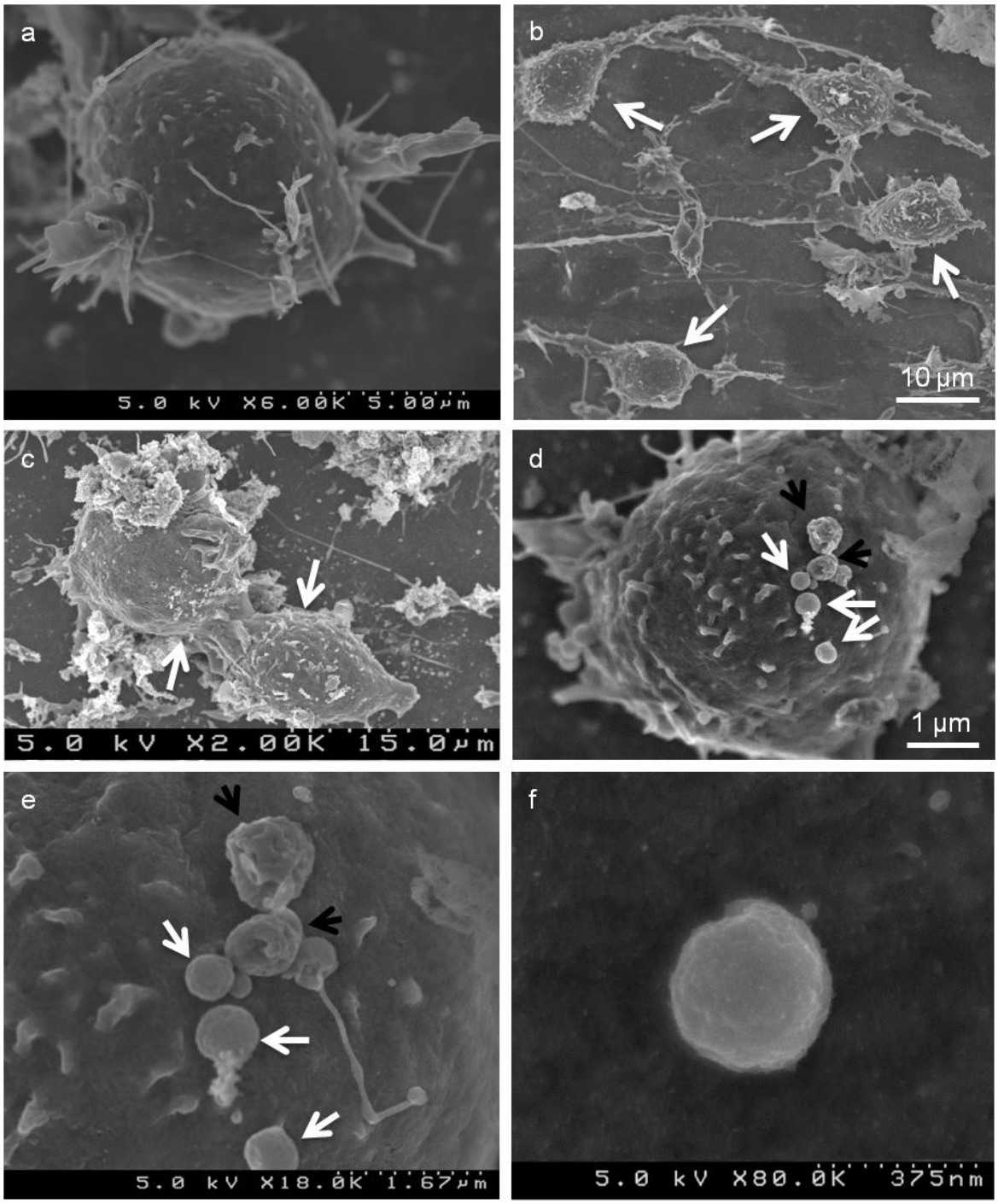

Figure 12: Particle-cell interactions visualised by OTOTO SEM. *Scanning electron micrographs of OPC cultures, incubated without (a) and with (b-f) Sphero MPs (24 h, 20 µg/ml). (a) Cell surface without particles. (b) Cells with the small, bipolar morphologies and fine processes typical of OPCs (arrows). (c) Cells demonstrating a mitotic profile (arrows indicate two daughter cells about to complete mitosis). (d) Sphero MPs associated with a cell surface (white arrows). Black arrows indicate membrane projections, 'blebs', which may be wrapped around individual MPs. Note the numerous microvilli projecting from the cell surface, suggesting a highly active region of membrane. (e) Enlarged image from (d), with arrows indicating the same features. (f) Membrane-associated MP which appears to be situated within a depressed region of membrane, suggestive of endocytotic pit-formation, illustrating that this technique can facilitate the identification of such features.*

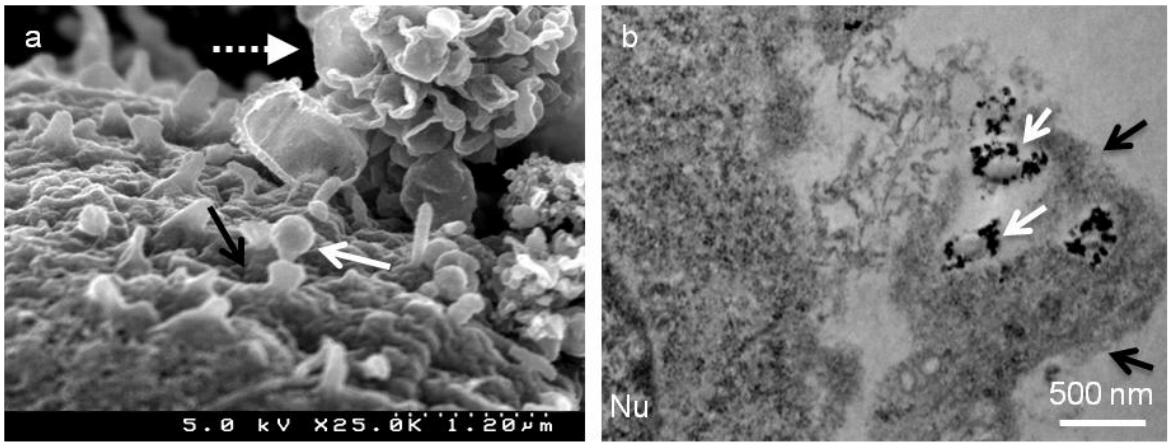

Figure 13: OTOTO SEM and TEM images illustrating the potential to identify the same endocytotic events. *OPC cultures were incubated with Sphero MPs (24 h, 20 µg/ml) (a) SEM image of a Sphero MP (white arrow) associated with OPC membrane. An endocytotic pit (black arrow) may be forming in the vicinity of the particle, and macropinocytotic membrane elaboration is apparent (dashed arrow). (b) TEM image of an OPC. A small cluster of MPs is apparent (white arrows), and they appear to be associated with macropinocytotic membrane (black arrows). This can be compared with the SEM image of macropinocytotic membrane in (a).*

2.4 Discussion

2.4.1 OPCs are amenable to labelling with physico-chemically different MP formulations

This is the first report of MP-labelling of high purity OPC cultures derived from a primary source. As detailed in section 1.10, data from primary cultures will be of greater biological relevance for informing clinical MP-based engineering than will data from cell lines. Labelling was successfully achieved using two MP formulations with very different physico-chemical properties. For the given concentrations used in this study (5 and 20 µg/ml at 24 h), the smaller MP (Fe_3O_4-PEI-RITC) labelled a greater percentage of OPCs, consistent with a number of other reports in different cell types suggesting greater uptake of smaller particles.[204,268–270] At the highest concentrations and incubation times tested, both particles labelled ~60% of OPCs. The time- and concentration-dependence observed with the Sphero particles, and the concentration-dependence observed with the Fe_3O_4-PEI-RITC particles suggest that labelling of a higher percentage of OPCs may be achieved by simply increasing the concentration and/or incubation time, although such an approach would entail further toxicity assessment.

However, it should be noted that the concentrations reported here were based on equal weights of particles (µg/ml) rather than equal numbers of particles (particles/ml). The disparity in particle number is such that the highest Sphero concentration (50 µg/ml) contains 1.3 billion particles/ml, whereas the lowest Fe_3O_4-PEI-RITC concentration (5 µg/ml) contains 96 billion particles/ml, a ratio of 1:74 (Appendix 1). As incubation with this far larger number of particles did not result in labelling of more than 60% of the

population, it is possible that this represents an intrinsic labelling limit in the OPC cultures. This further suggests the presence of an OPC sub-population which is intransigent to MP uptake, and may require specific cell-targeting approaches to achieve labelling. For transplantation applications, labelled cells could be purified using a magnetic cell separation step;[271] it would additionally be of high biological interest to separate the labelled/unlabelled subpopulations and compare their gene expression, or endocytotic profiles. The particles also differ in their coating material and zeta potential, each of which could influence cellular uptake. The Fe_3O_4-PEI-RITC particles have previously been tested in cultures of astrocytes, for labelling purposes (as used here) and also as transfection agents (particles incubated with plasmid DNA to form complexes).[102] The percentage of MP-labelled astrocytes was not found to differ between particles with and without complexed DNA at the three concentrations tested (MPs at 7, 21 and 67 μg/ml, 24 h). As the addition of DNA would alter the surface groups and presumably the charge, this suggests that the coating and charge do not significantly affect cellular uptake of the Fe_3O_4-PEI-RITC particles, although equivalent assays would be required to demonstrate that this is also the case for OPCs. Formation of a particle-plasmid complex will of course also increase the size, and although these complexes are not anticipated to approach the size of the Sphero particles, it will be important to determine the physico-chemical properties of MP-plasmid complexes before conclusions can be drawn regarding the specific factors that may influence cellular uptake of these particles.

Some iron oxide MPs are reported to require specific cellular targeting to result in cellular uptake, for example by conjugation of anti-transferrin-receptor antibodies to the particles.[155] Even for particles that are taken up by cells without targeting, attempts are frequently made to increase the extent of labelling by complexing the particles with transfection agents, such as Lipofectamine 2000.[131] It is of note that cell targeting

techniques such as these were not required for OPC uptake of the Sphero particles tested here, but it remains possible that incorporating such a targeting technique could yield greater levels of OPC labelling, in terms of both percentage of cells and extent of accumulation, and this warrants further investigation. It may also be possible to enhance MP-labelling of OPCs by employing a magnetic field, placed beneath the culture plate, to enhance particle sedimentation and therefore particle-cell interactions.[217]

2.4.2 MP-labelled OPCs retain this label when differentiated into oligodendrocytes

As a transplant population of MP-labelled OPCs is intended to eventually differentiate into mature oligodendrocytes as part of a regeneration-enhancing strategy, it is important to assess whether MPs are retained within the differentiated cells (for imaging applications), and whether any adverse effects become apparent post-differentiation. When pulse-labelled OPCs (24 h, 20 µg/ml Sphero) were cultured in differentiation medium for 30 days, MPs were clearly visible within MBP^+ oligodendrocytes, although it is not apparent whether these particles (i) were present within the same cells for the entire duration of the experiment, (ii) were only endocytosed during the prolonged incubation period (beyond the 24 h pulse-labelling period; cultures were washed after 24 h, but some residual extracellular MPs would be expected), or (iii) were exocytosed and subsequently endocytosed by another cell. Approximately 60% of oligodendroglia were MP-labelled at 30 days, compared to ~38% of OPCs at 24 h exposure to the same concentration. There are several possible explanations for these observations. If cells unlabelled at 24 h did not later become labelled, and assuming equal survival and proliferative capacity of the initial labelled and unlabelled subpopulations, the percentage of labelled cells would be expected to remain steady. If MP-labelled cells experienced impaired survival or proliferative

capacity, then the percentage of labelled cells would be expected to diminish. Therefore, this increase in the percentage of cells labelled supports both option (i), which suggests that proliferation of labelled OPCs resulted in particle inheritance in both daughters and also that MP-labelled OPCs retained at least some of their particles during differentiation into oligodendrocytes, and option (ii) which suggests that cells unlabelled at 24 h exhibited particle uptake at some later time-point, without precluding an effect due to option (iii).

Longer term MP retention studies will be necessary in order to determine the length of time over which oligodendroglial cells retain MPs and to assess their ultimate fate. For example, it will be of value to determine whether an OPC transplant population may exocytose intact MPs, or MP breakdown products, over time. It will also be important to assess how MP-labelling is diluted by mitosis, given that OPCs are a proliferative cell population. The retention study reported here used oligodendrocyte differentiation medium in order to determine whether the labelled cells could produce mature oligodendrocytes and to assess the extent of particle retention in the differentiated progeny of labelled OPCs, but a similar study could be performed with proliferative medium, passaging the OPCs and monitoring the dilution of the MP-label. Proliferation of particle-labelled cells is reported to typically result in random and asymmetric inheritance by daughter cells.[272] Although large-scale culture of OPCs may become part of a future therapeutic procedure, it is unlikely that cells would be labelled prior to a significant expansion of the cultures, as this would be expected to dilute the labelling effect. Rather, it is to be anticipated that an eventual clinical labelling procedure would label cells close to the time of transplantation, limiting dilution due to proliferation.

2.4.3 MP-labelling of OPCs is safe

In order to develop MPs for clinical applications it is of paramount importance to assess potential cytotoxic effects associated with particle uptake and/or breakdown. Oligodendroglial cells contain more iron than any other CNS cell type, but are also the most vulnerable to excess iron, which typically leads to an increase in oxidative stress due to reactive oxygen species (ROS) produced by the Fenton reaction.[273] Oxidative stress is of particular concern in the CNS as it is associated with neurodegenerative disease, and has been associated with oligodendrocyte damage in MS.[274] Therefore, it is important to determine whether it is safe to introduce iron-based particles into oligodendroglial cells. In addition, MPs could impair cellular function through a wide variety of other mechanisms, including physically disrupting the cytoskeleton/cell membrane[131,225] or intracellular trafficking processes,[275] directly damaging intracellular structures/organelles, or by producing toxic substances, potentially by particle degradation releasing iron[219] or fluorophores. Through these or other mechanisms, MP uptake could also perturb cellular behaviour, including capacity for migration or proliferation.[276]

Limited MP-related safety/toxicity data is available for glia, but Soenen *et al.* have shown some cytoskeletal effects of MP accumulation in human blood outgrowth endothelial cells (hBOECs). These effects were only present at high concentrations of MPs [>400 μg Fe/ml for Endorem (4 – 10 nm iron oxide core, dextran coating, 80 – 150 nm hydrodynamic diameter, neutral zeta potential),[150,277] and >300 μg Fe/ml for Resovist (4.2 nm iron oxide core, dextran coating, 60 nm hydrodynamic diameter, neutral zeta potential)[131]], and were typically transient.[131] No morphological perturbations were apparent during the experiments reported here, but more detailed analyses would be

required to exclude the possibility that either MP tested can produce adverse effects in OPCs, or at least to establish a safe dose, which avoids such effects.

The lack of MP-associated toxicity in OPCs reported here is in general agreement with Hohnholt *et al.*, who employed a battery of assays [lactate dehydrogenase (LDH) activity; propidium iodide/nigrosin infiltration; cellular protein content (Lowry assay); counting nuclei per mm^2; MTT reduction assay; intracellular ROS (rhodamine 123)] to test the toxicity of dimercaptosuccinic acid (DMSA)-coated iron oxide MPs (5 – 20 nm iron oxide core, 60 nm hydrodynamic diameter, -26 mV zeta potential) in the OLN-93 cell line.[273] They found no evidence of acute cytotoxicity (up to 72 h exposure), even at high concentrations (1000 μM Fe; 55 μg Fe/ml), although the authors noted a "*trend*" towards a reduction in proliferative capacity at the highest dose, which was not found to be significant. In the current studies, OPC proliferation was unaffected by MP-labelling using either Sphero or Fe_3O_4-PEI-RITC particles, and no intranuclear MPs were observed at any time-point, suggesting no adverse effects on mitosis, including the exclusion of MPs from the nucleus even during nuclear membrane breakdown. Although it has been shown here that Sphero MP-labelling does not impair OPC differentiation into oligodendrocytes, it will be important to determine whether the progeny of MP-labelled OPCs are competent to remyelinate axons. *In vitro* assays could be performed to address this issue in order to compare, for example, the rate of myelin production, the thickness of myelin sheaths, and the internode lengths of sheaths produced by labelled versus unmodified cells.

2.4.4 OTOTO SEM analyses reveal MP-cell interactions and endocytotic processes

The development of MP-based cellular applications will benefit greatly from insights into the cellular uptake mechanisms that result in MP internalisation, and in order to facilitate such future studies a powerful but not widely utilised histological technique has for the first time been brought to the study of neural stem/progenitor cells and the interactions of cells with synthetic materials.

Ultrastructural analyses such as TEM enable direct observation of the uptake process, allowing the identification of specific endocytotic processes by visualisation of endocytotic structures and vesicle formation. However, this is a time- and labour-intensive process,[278] and few uptake events may be observed in an individual sample, consisting as it does of an ultrathin section (typically 30 – 100 nm, rarely exceeding 150 nm, as electrons less readily pass through biological material of this thickness)[279] containing a limited sample of membrane from each cell. Artefacts may be introduced into TEM samples due to damage during the sectioning process, which can be a particular problem for the study of cellular interactions with synthetic materials, as the interface between 'soft' biological material and 'hard' synthetic particles can be altered.[255] An advantage of TEM analyses over SEM analyses is the ability to observe intracellular processing, including vesicular trafficking and association of particles with intracellular structures. However, by employing backscatter detection, it may be possible to detect MPs immediately beneath the cell membrane, including within macropinocytotic membrane.[280] A significant advantage of OTOTO processing for analysis of synthetic particles, including nanoparticles, is that the need for a gold coating of the sample (after critical point drying) is avoided. Gold coating can potentially obscure small diameter MPs, and is not compatible with backscatter electron detection, which can be used to detect iron oxide particles.[279]

OTOTO-preparation of samples for SEM provides a greater number of cells per sample than is possible for TEM samples, and a greater proportion of each cell's membrane is available for study. Following OTOTO processing, a whole coverslip (13 mm diameter) can be placed into a scanning electron microscope allowing an entire culture to be analysed. By comparison, for TEM samples, cells are cultured on a 13 mm diameter aclar disc (which must first be cut from an aclar sheet) and the sample processed in resin, yielding a single ~13 mm disc of resin containing the cells. However, the resin must then be broken into smaller pieces to be amenable to ultrathin sectioning. A single piece of resin must be mounted in the correct orientation, which requires some expertise, and then sections must be taken from this, which also requires significant training in order to generate high quality specimens – sections prepared by inexperienced personnel commonly contain score-lines, and are often torn during the necessary process of mounting the sections on copper grids. Ultrathin sections will contain far fewer cells than an SEM specimen, even if sectioned parallel to the original cell monolayer, which is a more difficult technique than sectioning perpendicular to the monolayer. Many sections would need to be analysed in order to build up a profile of the extent of endocytosis occurring in a single cell, as a single section may be unrepresentative. It is common during TEM resin sectioning to obtain a semi-thin section (typically 0.5 – 2.0 μm) for light microscopy, in order to assess the current position and orientation of the sample, and such a section can constitute a significant proportion of the total sample in a monolayer of cells, which then cannot be analysed by TEM. Each time a new ultrathin section is taken from a sample, there is a risk of damage to, or even loss of, the rest of that sample. Finally, the sections commonly undergo a further, lengthy staining process (*e.g.* uranyl acetate and lead citrate) individually, which when performed by a non-expert commonly results in unwanted artefacts. It should also be noted that only a small number of ultrathin sections can be

studied by TEM at a time, and these will commonly all have been obtained from a single face of a single fragment of the original resin-embedded sample. All of this processing makes TEM analyses more expensive and time-consuming than OTOTO SEM.[257]

Further benefits of the OTOTO SEM method include the ability to combine it with techniques such as backscatter detection of iron oxide particles and stereo image analysis, involving a red/green anaglyph, which produces three-dimensional images and facilitates the measurement of the depth of membrane depressions/pits. Such data can enable the identification of the mechanisms responsible for cellular uptake of particles, and reveal which particular mechanisms a particular cell type is capable of employing. There is the potential to develop a high-throughput assay for counting 'particle uptake events' by cells, by identifying and scoring instances of endocytosis. Bases on these advantages, the OTOTO protocol described here can provide significantly more quantifiable data than is achievable with TEM analyses, given the same resources in terms of time and expense. As such, I consider that development of this method will therefore provide a rapid and simple methodology for use in the field of bio-nanotechnology, to evaluate interactions of neural cells with biomaterials, currently an area of high scientific interest.

Endocytotic pits, macropinocytotic membrane and cell-associated Sphero MPs could be identified in OTOTO-processed samples of OPC cultures. These observations provide proof-of-principle that that such morphological/microstructural data can be further quantified for detailed analysis of the extent of membrane activity and particle association. It can be predicted that this will be of high relevance to investigations into the underlying mechanisms of magnetofection, effects of physico-chemical properties of particles on endocytotic uptake and the specific mechanisms associated with the latter.

2.4.5 Conclusions and future directions

Although MP-labelling of OPCs has been previously reported (for cell lines),[93,94,96,97,143,155] detailed data (relating to uptake dynamics, intracellular particle fate and MP-associated toxicity, all with reference to the properties of the specific particle used) are lacking, representing critical knowledge gaps in the literature, which must be addressed in a systematic manner to allow the development of this field. The OTOTO SEM samples obtained indicate significant potential for the development of a high-throughput screening process for studying and quantifying MP-cell interactions, although early data will need to be compared with parallel TEM studies to verify the efficacy of the OTOTO approach. This will consist of attempts to confirm that each specific endocytotic mechanism (and related particle uptake) observed in one technique is also observed in the other, and with comparable frequency. Measurements should also be made of particles and structures such as nuclei (possible for SEM samples through techniques such as freeze-fracture), to compare the effects of sample shrinkage during processing.

The finding that ~60% of OPCs from a primary culture were safely labelled with two physico-chemically differing MPs (that have demonstrated MRI contrast capability) without the need for a specific cell targeting or purification strategy shows significant potential for the translation of MP-labelling approaches, as these data suggest that the majority of cells from a primary OPC population could be detected both non-invasively and histologically post-transplantation. Further studies will be necessary to confirm that cells labelled with each of these particles can be detected by MRI *in vivo,* including after transplantation into neurological injury sites. It can be predicted that the Fe_3O_4-PEI-RITC prototype particles will have the greater translational potential to serve as a cell labelling agent for transplant studies, as T2 proton relaxivity is predicted to decrease in a linear

fashion with increasing concentration of the contrast agent (iron oxide), providing increasing imaging contrast.[245,281] However, when tested *in vivo*, compartmentalisation of contrast agents within cells/tissues often causes this linear relationship to fail, and the relative MRI contrast capability of these and indeed any MPs must be verified *in vivo*.[281] A further advantage is that the versatile design of these particles enables simple surface modification to functionalise the particles for biological applications. For example, alternative fluorophores can readily replace the RITC tag by attachment to the PEI layer, such as the succinimidyl ester- or isothiocyanate- (ITC) derivatives of common dyes (*e.g.* the Alexa Fluor family). The PEI skeleton can also be further functionalised by, for example, the incorporation of an anti-transferrin receptor antibody to enhance cellular uptake and the extent of cell labelling (as transferrin receptors are recycled to the cell surface within minutes of endocytosis, facilitating rapid uptake)[155] for transplantation applications.

Based on these findings, it is clear that further studies will be required to evaluate interactions of OPCs with MPs possessing a wider range of physico-chemical properties, in order to inform the development of MPs tailored to specific biomedical applications. Such investigations should typically include: (i) ultrastructural analyses of particle-cell interactions, intracellular processing and fate; (ii) endocytotic blocker studies to establish the relative contribution of each endocytotic mechanism to the uptake of differently-configured particles; (iii) microarray and proteomic analyses to detect alterations in gene and protein expression following MP-treatment, providing detailed toxicity analyses; (iv) vesicle tracking analyses to inform the development of MPs with the potential for endosomal escape, or suggest the specific endocytotic mechanism to which MPs should be preferentially targeted; and (v) functional assays of the migratory and myelinating capacity of transplanted labelled cells, for example by 'galvanotaxis' studies of cell migration or co-

culture with unmyelinated/demyelinated axons. The fact that OPCs demonstrate uptake and perinuclear localisation of MPs implies that MPs could be exploited as gene delivery vectors for engineering of OPCs, and this possibility will be explored in the next chapter.[a]

[a] Most of the Sphero-related data in this chapter have now been published. The article is reproduced here as Appendix 3.

Chapter 3: MP-mediated transfection of OPC transplant populations: effects of novel ‘magnetofection’ techniques

3.1 Introduction

In order to treat CNS injury or disease, there is reason to believe that therapeutic benefit can be derived by genetically engineering a cell transplant population to release therapeutic factors.[117,118,282] This may involve delivering growth factors to promote migration, proliferation or differentiation of particular cell types, introducing immunomodulatory molecules, or otherwise manipulating a lesion site, for example by down-regulating molecules that inhibit axonal growth (*e.g.* Nogo).[283] Such modifications can facilitate 'combinatorial' approaches to regeneration (*e.g.* delivery of cells *plus* therapeutic biomolecules to lesions; section 1.5 discusses combinatorial therapies) which are increasingly believed to be necessary to mediate repair in the CNS.[59] With particular reference to promoting remyelination in MS or SCI lesions, these therapeutic factors could be chosen to manipulate the lesion site, making it a more favourable milieu for regeneration, or to stimulate differentiation of endogenous OPCs, which are typically present within or adjacent to injury sites, but in a 'quiescent' state that limits or even prevents the replacement of lost oligodendrocytes/myelin.[284–287]

In this context, genetic engineering of OPC transplant populations to release therapeutic factors post-transplantation may be a suitable combinatorial therapy to promote remyelination following CNS injury/disease. This has been demonstrated in animal models, with two reports of genetically modified OPC transplants demonstrating enhanced remyelination and functional recovery[60,64] (detailed in section 1.5), but in both these studies, as with the majority of genetic manipulations of OPCs, viral gene vectors were used, which are associated with various problems that may prevent translation to the clinic, chiefly safety concerns (detailed in section 1.7.3). However, the nonviral alternatives tested in OPCs so far have also demonstrated drawbacks, including safety concerns, inefficient

gene delivery and lack of potential for clinical translation (section 1.7.3). With respect to transfection of primary rodent OPCs, the most efficient technique reported is electroporation, with ~49%[288] and ~43%[289] of cells being transfected. However, both of these reports are from company websites rather than peer-reviewed publications, and both show significant reductions in cell viability (to ~78% and ~60%, respectively). The only other nonviral techniques tested, lipofection[110,267,290] and calcium phosphate precipitation,[108,110] have reported less than 5% transfection efficiency, and significant toxicity. It should be noted that many reports of OPC transfection do not provide details of transfection efficiency, and there is an even more frequent lack of detail relating to safety/toxicity, hindering efforts to compare gene delivery techniques, and assess their potential for clinical translation.

3.1.1 Knowledge gap: Are OPCs amenable to MP-mediated transfection, including magnetofection strategies?

An alternative nonviral transfection technique which has not been tested with OPCs is the use of MPs as nucleic acid vectors. Several studies have demonstrated successful MP-mediated transfection of neural cell types, mainly neurons and NSCs, but also astrocytes.[102,161–164,291,292] Furthermore, the amenability of MPs to *magnetofection* techniques for enhanced gene delivery highlights one of the additional benefits of this multifunctional engineering platform (see sections 1.8.3 for details of magnetofection, and 1.8 for further benefits of MPs in the context of cell transplantation). Several papers have reported that magnetofection techniques can result in increased transfection efficiency, including a report of enhanced transfection efficiency in astrocytes.[164,172] Despite the potential of this approach, the efficacy of MPs as nucleic acid vectors and the application

of magnetofection techniques have not been assessed to date with OPCs, and addressing this knowledge gap will be the principle aim of this chapter.

A further point to note here is that safety is a primary concern for the development of therapeutic strategies, and represents a major impetus behind the development of nonviral gene delivery technologies. Therefore, the safety of MPs as gene delivery agents for transplant populations must be assessed in detail. However, in order to test the safety and efficacy of cell transplantation, live animal models are typically used as hosts. These *in vivo* cell transplantation studies have significant drawbacks, as they are technically demanding, expensive, time-consuming and raise ethical concerns.[293] As discussed in section 1.6, organotypic cerebellar slice cultures offer major advantages which may serve to bridge the gap between isolated cell studies and pre-clinical animal experimentation.

It should also be noted that while OPCs have previously been transplanted onto cerebellar slices in order to study myelination/remyelination,[90,294,295] only one report exists of genetically engineered OPCs being transplanted onto a slice culture: Zhang *et al.* used a lentivirus to transduce mouse OPCs, resulting in GFP expression (transfection efficiency and toxicity not reported), then pipetted these cells onto demyelinated organotypic neural slices; transplanted cells were shown to generate remyelinating oligodendrocytes.[4] Critically, the same group conducted a comparison of remyelination-enhancing therapies in demyelination models using co-cultures versus slice cultures, showing that **results in slices more closely correlated with findings from lesion models *in vivo***.[4] By contrast, results in co-culture models often contradicted *in vivo* results, suggesting slice cultures represent a superior model of *in vivo* conditions.[4] These data demonstrate the feasibility and utility of organotypic neural slice cultures as 'host' tissue for cell transplantation studies. Therefore, transplantation of modified OPCs onto cerebellar slice cultures will be tested in this

chapter with a view to developing a toxicity assay to monitor the behaviour of MP-engineered OPCs.

3.1.2 Objectives

Having established that two different MP formulations are internalised by OPCs (Chapter 2), the principle aim of this chapter is to assess the potential for MPs to serve as gene delivery vectors for OPCs, by addressing the following questions using a different (transfection grade) MP formulation:

(i) Do MP-nucleic acid complexes and/or magnetic fields have acute toxic effects on OPCs?

(ii) Does the application of a static or oscillating magnetic field (magnetofection) result in enhanced MP-mediated transfection efficiency in OPCs?

(iii) Does MP-mediated transfection of OPCs affect their capacity for proliferation or differentiation?

(iv) Can multiple genes be delivered to an OPC population using MP vectors?

(v) Can therapeutic genes be delivered to an OPC population using MP vectors?

The second aim of this chapter is to establish and characterise organotypic cerebellar slice cultures, and assess their potential to serve as 'host' tissue for transplanted modified OPCs. The survival and behaviour of genetically engineered OPCs will be monitored following transplantation onto these slices, to assess the safety of the transfection procedures. Four key parameters will be evaluated with respect to the transplanted OPCs, namely survival, proliferation, migration and differentiation into oligodendrocytes.

3.2 Methods and materials

Reagents and equipment: The pmaxGFP plasmid (3.5 kb in size; encodes GFP; map shown in **Figure 1**) was from Amaxa Biosciences (Cologne, Germany), pCMV-DsRed-Express2 plasmid [4.6 kb; encodes red fluorescent protein (RFP); herein termed pDsRed] from Clontech (Saint-Germain-en-Laye, France), the pCMV6-FGF2-GFP plasmid (7.4 kb; encodes the open reading frame of human FGF2 with a carboxy-terminal turboGFP tag; herein termed pFGF2-GFP; map shown in **Figure 1**) and the recommended control plasmid, pCMV6-AN-GFP (6.6 kb; herein termed pAN-GFP), were from OriGene Technologies (Rockville, MD, USA), as was the anti-FGF2 antibody (clone 3D9; mouse IgG2b anti-human FGF2). Polyclonal rabbit anti-glial fibrillary acidic protein (GFAP; a marker for astrocytes) was from DakoCytomation (Ely, UK). Anti-calbindin antibody was from Santa Cruz (CA, USA); calbindin is a calcium-binding protein common to many classes of neuron[86] but within cerebellar slices stains only Purkinje cells, the axons of which provide the main myelinating tracts.[80,85] Cy3-conjugated secondary antibodies were from Jackson ImmunoResearch Laboratories Inc. (West Grove, PA, USA). Anti-NG2 antibody, Millicell culture inserts and Omnipore membrane were from Millipore (Watford, UK). Accutase was from Sigma-Aldrich (Poole, UK). DNase I was from Roche Diagnostics Ltd. (Burgess Hill, UK). The McIlwain tissue chopper was from The Mickle Laboratory Engineering Co. (Guildford, UK).

OPC culture: As described in section 2.2, OPCs were derived from mixed glial cultures and plated on coverslips (0.3 ml/well, at 3 x 10^4 cells/cm^2). Once cells had attached, medium was replaced with 225 µl fresh medium, and cultured for 24 – 48 h (to allow cells to recover from plating and extend processes) before transfection.

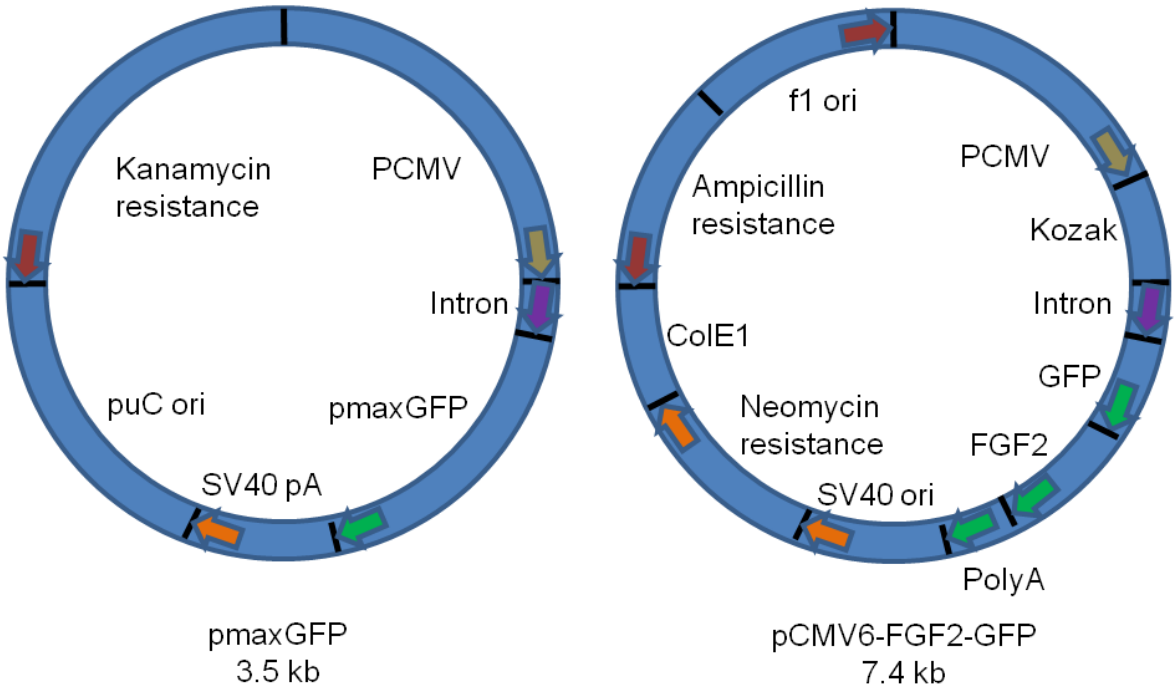

Figure 1: Plasmid maps for pmaxGFP and pFGF2-GFP. *PCMV represents the cytomegalovirus promoter which drives heterologous expression in mammalian cells (although post-transcriptional and regulatory effects may affect the protein expression levels on a cell type-dependent basis). ColE1 is the bacterial origin of replication. SV40 ori is the simian virus 40 origin of replication, which allows for replication in mammalian cells. f1 ori is the filamentous phage origin of replication which allows for the recovery of single stranded plasmids. puC ori: origin of replication for propagation in Escherichia coli. Kanamycin/ampicillin resistance allows the selection of E. coli which contain the plasmid of interest during plasmid production. Neomycin resistance allows the selection of stably transfected mammalian cells by culturing cells in medium containing G418 (geneticin), which will kill cells that have not stably incorporated the transgene into their genome, leaving stably transfected colonies. PolyA is the human growth hormone (hGH) polyadenylation signal, which protects the mRNA from degradation by exonucleases. Kozak: Kozak consensus sequence, facilitates initiation of translation of eukaryotic mRNA.*

Choice of MPs for transfection: A commercially-available transfection-grade MP (Neuromag) was employed for these studies (OZ Biosciences, Marseille, France). These particles have an average diameter of 160 nm (range 140 – 200 nm), contain ~0.5% Fe, and a positive zeta potential (though undisclosed for these commercial particles).[292] They are reported to bind DNA non-covalently through electrostatic and hydrophobic interactions.[292] DNA binding curves showed that these particles bind DNA effectively with pmaxGFP binding increasing the hydrodynamic diameter of the particles by 35%, as assessed using a Malvern Zetasizer 3000.[164] These Neuromag particles were developed for gene delivery to primary neurons, which are typically difficult to transfect, and the particles have demonstrated minimal toxicity with such cells.[291,292,296] These particles have also been used in this laboratory to successfully transfect astrocytes,[164] NSCs,[163] and olfactory ensheathing cells (OECs; unpublished data), generally with greater transfection efficiencies than achieved with other transfection grade MPs, such as various commercial PolyMag formulations (tested in this laboratory, unpublished data). *The magnefect-nano^{TM} magnetofection device:* The magnefect-nano oscillating magnetic array system, used for both static and oscillating magnetofection methods, was from nanoTherics Ltd. (Stoke-on-Trent, UK; commercially available since 2009; **Figure 2**). This system allows 24-well culture plates to be placed over a horizontal array of 24 neodymium (NdFeB) magnets, grade N42, which match the plate configuration. The magnetic array can be programmed to oscillate laterally beneath the culture plate *via* a computerized motor; both the frequency (up to 5 Hz) and the amplitude (10 µm to 1 mm) of oscillation can be varied. The field strength at the face of each magnet is 421 ± 20 mT (nanoTherics Ltd., personal communication). In static mode (frequency, F = 0 Hz), this system has been shown to produce similar transfection efficiencies in astrocytes to commercially available magnetic

plates in routine use for static magnetofection,[164] and it is the only commercially available device for oscillating magnetofection applications.

Figure 2: The magnefect-nano system (nanoTherics Ltd., Stoke-on-Trent, UK). *A laptop with software is pictured above the computerised motor that drives an oscillating magnetic array, situated to the left of this image and configured for a 96-well plate. Image courtesy of nanoTherics Ltd.*

Transfection (magnetofection) protocols: It was necessary to determine the maximum safe dose of Neuromag-plasmid complexes for transfection of OPCs, and to determine whether magnetofection conditions affected toxicity. Neuromag MPs are recommended for use with neurons at a final concentration of 7 µl/ml in medium (referred to here as a 1.0x dose), but lower concentrations have been required for safe use with other neural cells (astrocytes,[164] NSCs[163,297]). The DNA-binding capacity of Neuromag MPs is maximal at a ratio of 3.5 µl Neuromag to 1 µg DNA;[164] this ratio was therefore routinely used in the present study.

In preliminary experiments, transfection complexes were prepared at 1.0x and 0.1x doses. A 1.0x dose was prepared by mixing 600 ng plasmid in 75 µl DMEM base medium, then gently mixing this with 2.1 µl Neuromag. For control wells, plasmid was mixed in DMEM, but no Neuromag was included. After 20 min incubation, the entire complex mix was added dropwise to cells, whilst gently swirling the plate. Complexes (1.0x and 0.1x) were incubated with cells for a total of 1 h (the first 30 min in the presence of a magnetic field, when appropriate) then the medium was replaced, as incubation times >1 h had demonstrated toxicity in astrocytes.[164] However, very limited transgene expression was observed in OPCs with or without application of magnetic fields (typically <1%, cultures monitored for 72 h). Therefore, complexes (1.0x and 0.1x) were applied to cultures and GFP expression was monitored continuously for 72 h without complex removal. This resulted in greater transgene expression, with peak expression occurring at approximately 48 h post-transfection. Plasmid-based transfection is often reported to result in peak expression at approximately 48 h,[111,164,267] and as continuous incubation with particle-plasmid complexes for 48 h was without obvious effects on cell morphology or adherence (0.1x preliminary experiments), complexes were not removed from the cultures in subsequent experiments and transgene expression was routinely assessed at 48 h.

Following these preliminary experiments, it was decided to test 0.1x and 0.5x doses. Control cultures were treated with pmaxGFP plasmid alone, without Neuromag, at the highest concentration of plasmid used as a complex with Neuromag (equivalent to either 0.5x or 0.1x). For magnetofection, immediately following application of complexes to cells, the 24-well plate was placed above a 24-magnet array on the magnefect-nano device, which had been pre-warmed in the incubator. The array either remained static (F = 0 Hz), or was programmed to oscillate at F = 1 or 4 Hz (amplitude 0.2 mm). It has been predicted by modelling that an incubation time of 20 min is sufficient for the accumulation

of 200 nm diameter particles at the surface of a cell monolayer, with larger particles likely to require shorter incubation times, and therefore 30 min was deemed a sufficient incubation time for these experiments.[298] After 30 min, the plate was removed from the magnetic array. For the no field condition, plates were returned to the incubator without application of a magnetic field. Total Neuromag-plasmid incubation time for all conditions was 48 h, at which point cells were either fixed or switched to Sato medium for differentiation experiments. The established safe dose of 0.1x was prepared using 60 ng plasmid in 75 µl DMEM, then mixing this with 0.21 µl Neuromag.

Assessment of toxicity: Several parameters of cytotoxicity were assessed by microscopy, specifically: (i) whether cells were phase bright, adherent and extending processes; (ii) the presence of pyknotic (fragmenting) nuclei, as judged by DAPI staining; (iii) expression of the OPC marker A2B5; and (iv) cell counts per microscopic field. As transfection grade MPs, Neuromag particles have no intended purpose without conjugation of nucleic acids, and the positive surface charge of naked Neuromag particles could result in differing uptake kinetics and/or toxicity compared to Neuromag-plasmid complexes. Therefore, it was not deemed appropriate to systematically assess their effects in the absence of plasmid, but pilot experiments were performed with 0.1x particles alone which showed no effects on OPC proliferation or differentiation (data not shown).

Differentiation potential of transfected OPCs and long-term GFP-expression in oligodendrocyte progeny: At 48 h post-transfection, cells were washed with PBS, then switched to Sato medium to induce oligodendrocyte differentiation. Cells were monitored to assess the extent of cellular expression of GFP and to evaluate potential adverse effects on OPC differentiation for up to 3 weeks. Medium was changed every 2 – 3 days.

Co-transfection protocol: For co-transfection experiments, pmaxGFP and pDsRed plasmids were used at half the dose stated above (*i.e.* 0.05x, 30 ng each plasmid per 75 µl DMEM) producing a total plasmid dose equivalent to 0.1x, with the corresponding safe dose of Neuromag (0.1x, 0.21 µl per well) to maintain the plasmid:Neuromag ratio. Single transfection controls (either pmaxGFP or pDsRed only) were performed in parallel at 0.05x (30 ng plasmid, with 0.105 µl Neuromag per 75 µl DMEM). Plasmid-only controls were treated with both pmaxGFP and pDsRed.

Transfection with plasmid encoding therapeutic fusion protein: Experiments to assess the delivery of the plasmid pFGF2-GFP (which encodes a fusion protein consisting of FGF2 and turboGFP: FGF2-GFP), and the appropriate control plasmid pAN-GFP (which encodes turboGFP alone), were conducted as described for pmaxGFP (0.1x dose), with pFGF2-GFP used as the plasmid-only control. To detect the presence of the fusion protein, fixed cultures were immunostained with an anti-FGF2 antibody.

Organotypic cerebellar slice cultures: This culture technique is based on the interface method described by Stoppini *et al.*[69] Brains were extracted from P8 – 14 rats into ice-cold slicing medium [Earle's balanced salt solution (EBSS) buffered with 25 mM 4-(2-hydroxyethyl)-1-piperazineethanesulfonic acid (HEPES)]. Cerebella were dissected and meninges removed, then 350 – 400 µm parasagittal slices were prepared using a McIlwain tissue chopper. Slices were incubated in ice-cold slicing medium for 30 min, then transferred by wide-bore pipette to pieces of Omnipore membrane ('confetti', cut to be slightly larger than a cerebellar slice) on Millicell culture inserts in six-well plates containing slice culture medium [50% minimum essential medium (MEM), 25% heat-inactivated horse serum, 25% EBSS, supplemented with 36 mM D-glucose, 50 U/ml penicillin and 50 µg/ml streptomycin]. Slices were incubated at 37°C in 5% CO_2/95%

humidified air for at least 8 days before transplantation studies, live/dead staining or fixation and staining for slice characterisation, with medium changes every 2 – 3 days.

Transplantation of transfected OPCs onto slice cultures: At 24 h post-magnetofection (0.1x, F = 4 Hz), OPCs were washed with PBS, then enzymatically detached using accutase-DNase I. Cells were resuspended at 2 x 10^7 cells/ml Sato differentiation medium, and 0.5 µl was pipetted onto cerebellar slice cultures. The passive spread of cells is the area covered by transplanted cells when delivered by pipette or syringe, and is due to the force of delivery. It is important to assess this to gauge whether focal delivery can be achieved; if cells can be reliably delivered to one end of a slice, then attempts can be made to assess the extent of migration. Passive spread due to the pipetting procedure was assessed by transferring cerebellar slices to a small quantity of PBS on a microscope slide, then transplanting cells onto these slices and viewing immediately using fluorescence microscopy. Transplants were performed with 15 slices in total from four animals. At the end of the transplant procedure, remaining cells were also plated at 2 x 10^5 cells/ml Sato medium on PDL-coated chamber slides. Samples were fixed and stained 24 – 48 h post-transplantation to assess the survival and morphology of the transplanted and re-plated cells.

Immunocytochemistry: Cells and slices were incubated with blocking solution [5% serum in PBS with 0.3% Triton X-100; RT; 30 min], then with primary antibody in blocking solution (FGF2 1:100; NG2 1:150; GFAP 1:500; calbindin 1:5000; 4°C; overnight). Cells and slices were then washed with PBS, incubated with blocking solution (RT; 30 min), and incubated with the appropriate FITC- or Cy3-conjugated secondary antibody in blocking solution (1:200; RT; 2 h). Finally, coverslips, chamber slides and slices were washed with PBS and mounted with the nuclear stain DAPI.

Slice culture viability assays: Live slices were transferred to a 24-well plate, washed with PBS then incubated (15 min; 37°C) with ethidium bromide (12 µM) and calcein-AM (acetomethoxy derivate of calcein; 2 µM). Slices were then washed, mounted with DAPI and immediately visualised using fluorescence microscopy. Ethidium homodimer-1 is excluded from viable cells, but permeates dead/dying cells, which have lost membrane integrity, labelling them red; calcein-AM is transported across the plasma membrane and is converted to calcein by intracellular esterases, active only in live cells, labelling the cells green.[299,300]

Fluorescence microscopy and image analysis: Samples were imaged using fixed exposure settings on an Axio Scope A1 fluorescence microscope (Carl Zeiss MicroImaging GmbH, Goettingen, Germany), and the images merged using Adobe Photoshop CS3 (version 10.0.1). For toxicity and transfection experiments, a minimum of 200 nuclei per treatment per culture were scored for association with A2B5 or MBP staining (for OPC culture purity) and GFP expression (for transfection efficiency). For OPC differentiation experiments, a minimum of 100 nuclei per treatment per culture were scored for MBP expression.

Statistical analysis: Data were analysed using GraphPad Prism statistical analysis software. Data are expressed as mean ± SEM. The number of experiments (*n*) refers to the number of OPC cultures used, each from a different rat litter. For toxicity analyses of the 0.1x and 0.5x doses, with magnetic fields, a two-way ANOVA was performed with respect to the number of $A2B5^+$ cells per field, with Bonferroni's post tests. For transfection efficiency, the percentage of $A2B5^+$ cells expressing GFP under each field condition was analysed by one-way ANOVA, with Bonferroni's post tests. To determine whether transfection conditions affected the differentiation of OPCs into MBP^+ oligodendrocytes,

the percentage of MBP^+ cells in cultures without Neuromag and without application of a magnetic field was compared to magnetofected cultures (F = 4 Hz, 0.1x) using a two-tailed unpaired *t*-test. For co-transfection experiments, a two-way ANOVA was performed with respect to transfection efficiency with single and combined plasmids, with Bonferroni's post tests, and a one-way ANOVA was performed with respect to the percentage of transfected cells in co-transfected cultures that expressed either a single transgene or both transgenes, with Bonferroni's post tests. To compare transfection efficiency for different field conditions with pAN-GFP, a one-way ANOVA was performed with Bonferroni's post-tests. An identical analysis was performed for pFGF2-GFP. To compare transfection efficiency achieved with the pmaxGFP, pAN-GFP and pFGF2-GFP plasmids, a two-way ANOVA was performed for the no field and F = 4 Hz conditions, with Bonferroni's post tests. To determine the correlation between plasmid size and transfection efficiency, linear regression analyses were performed for pmaxGFP, pAN-GFP and pFGF2-GFP, for both the no field and F = 4 Hz conditions.

3.3 Results

3.3.1 Establishment of safe MP-plasmid doses and magnetic field conditions

OPC cultures used in these experiments were of high purity as judged by staining for the OPC marker A2B5 (94.3 ± 2.3%; *n* = 5). In preliminary experiments, a 1.0x Neuromag:plasmid dose resulted in transfection of OPCs, with apparently normal bipolar morphologies, but also the obvious loss of processes by many cells, detachment of cells from the substrate, and the presence of cellular debris **(Figure 3)**.

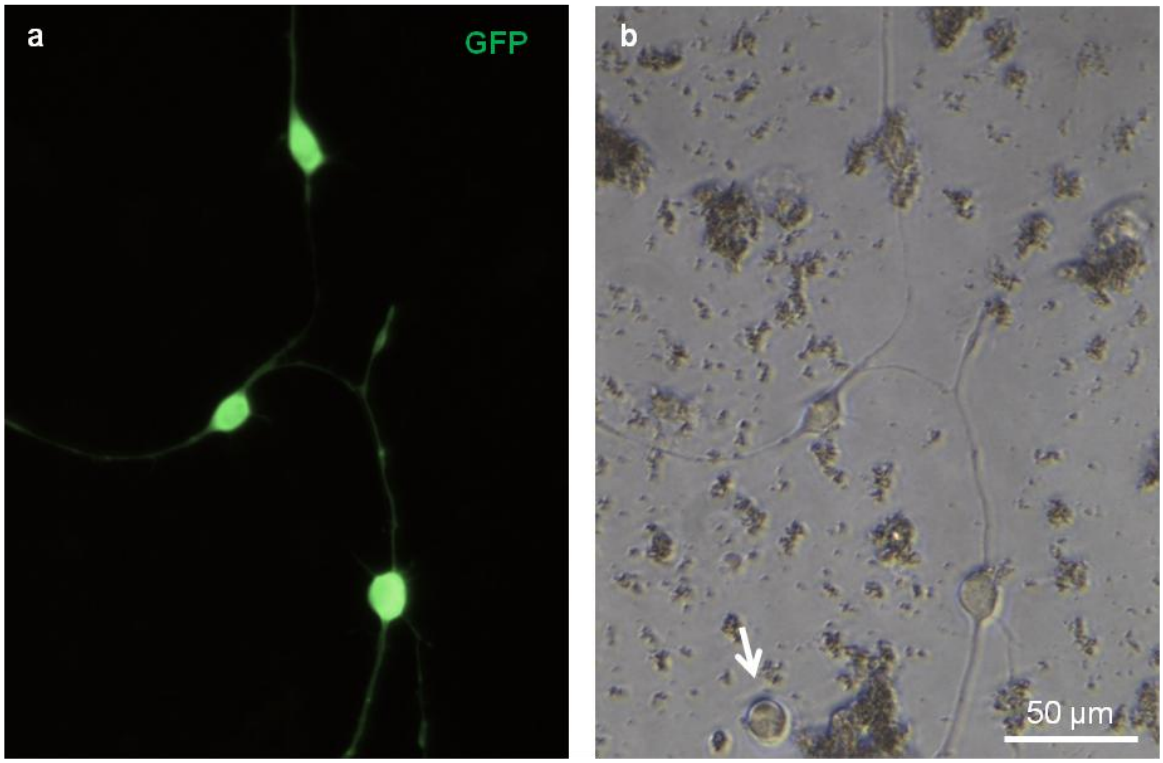

Figure 3: High doses of MP-plasmid complexes mediate gene delivery to OPCs, but with toxic effects on many cells. *(a) Fluorescence micrograph illustrating GFP$^+$ transfected OPCs (1.0x dose, F = 4 Hz, 24 h post-transfection). (b) Counterpart phase contrast micrograph to (a), illustrating rounded cells (arrow) and large quantities of debris, indicative of toxicity.*

With a 0.1x Neuromag:plasmid dose, phase-contrast microscopic observation showed phase-bright morphologically typical OPCs at 48 h post-transfection **(Figure 4)**, but particle-plasmid cytotoxicity was apparent at a 0.5x dose, as judged by the presence of rounded non-adherent cells **(Figure 4, inset)**, pyknotic nuclei, and a reduction in the number of $A2B5^+$ cells per microscopic field **(Figure 5)**. By these same criteria, no significant effects were apparent at a particle-plasmid dose of 0.1x, and no magnetic field-related effects were apparent in either control or treated cultures **(Figure 5)**.

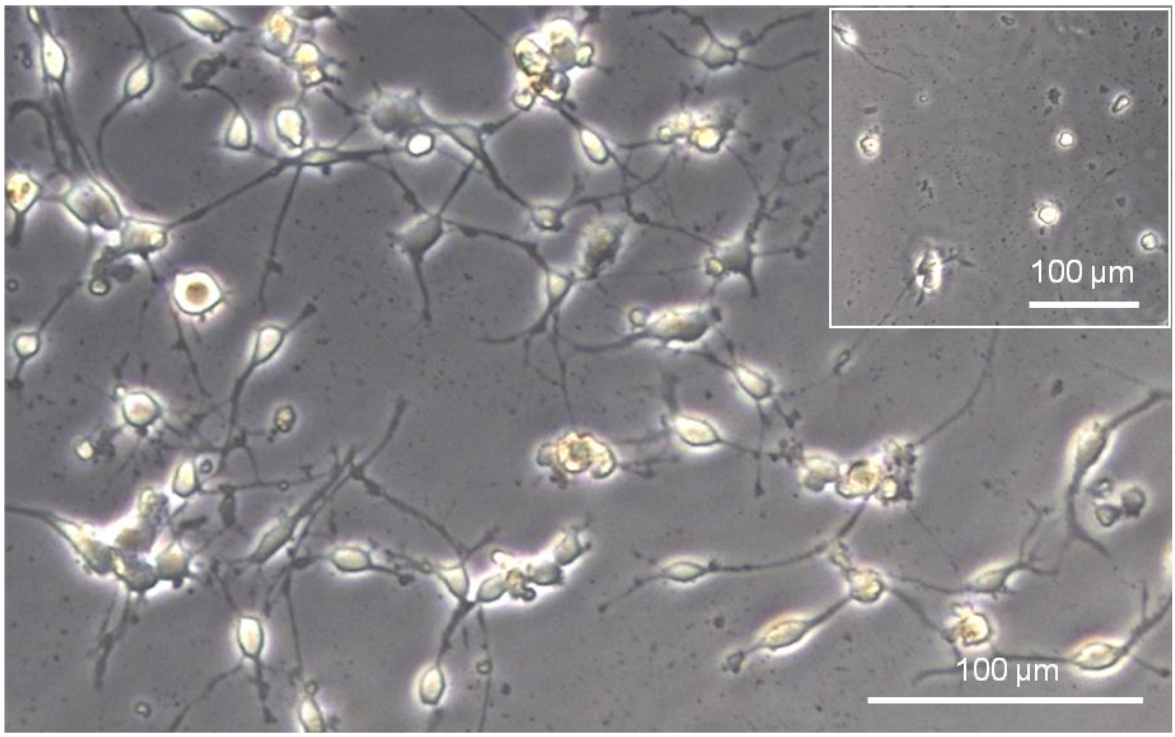

Figure 4: An MP-plasmid dose that does not affect OPC morphology has been established. *Representative phase-contrast micrograph of OPCs, 48 h post-transfection with 0.1x Neuromag-plasmid complexes. Note phase-bright cells with mostly bipolar morphologies. Inset shows OPCs 48 h post-transfection with 0.5x Neuromag-plasmid complexes. Note reduced density of cells and lack of processes.*

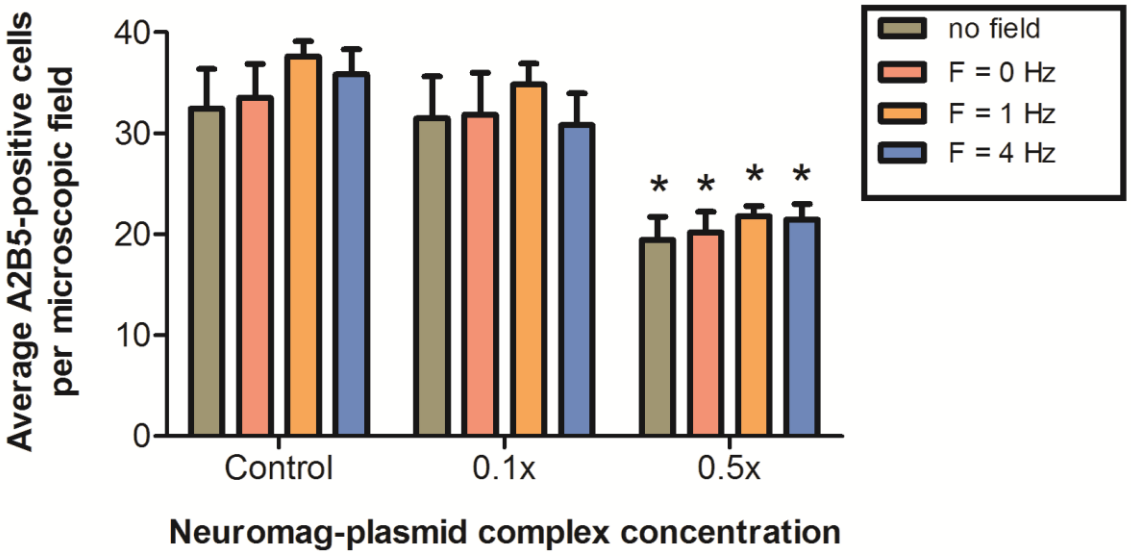

Figure 5: Establishment of safe particle dose and magnetic field conditions for OPC magnetofection. *Bar chart showing average number of cells stained for the OPC marker A2B5 per microscopic field, 48 h post-transfection with Neuromag-plasmid complexes. There was a concentration-dependent effect on the number of A2B5$^+$ cells ($F_{2,72} = 28.1$; $p < 0.001$), but no effect due to the application of a magnetic field ($F_{3,72} = 0.913$; ns; two-way ANOVA; $n = 5$). For all magnetic field conditions tested and the no field condition, the number of A2B5$^+$ cells per field was markedly reduced at 0.5x complex concentration, but not at 0.1x, compared to control cultures exposed to plasmid alone (0.5x equivalent dose).* $*p < 0.05$ *versus control, no field; Bonferroni's post-tests.*

3.3.2 Static and oscillating magnetofection strategies enhance MP-mediated transfection efficiency in OPCs

Having established a safe transfection protocol (0.1x complexes, 48 h incubation), including a lack of magnetic field-related toxicity, the transfection efficiency of these complexes was evaluated in the presence of static and oscillating magnetic field conditions. Expression of GFP was not observed in any control cultures (plasmid only). Basal GFP expression was observed (no magnetic field; mean transfection efficiency: 6.1 ± 1.0%; range: 3.1 – 8.1%; **Figure 6a**). Application of a static magnetic field resulted in significantly enhanced GFP expression, approximately two-fold greater than basal levels (F = 0 Hz; 12.5 ± 1.2%; range: 10.8 – 17%). Application of an oscillating magnetic field also produced enhanced GFP expression, with levels approximately 2.5-fold (F = 1 Hz; 15.5 ± 1.9%; range: 9.3 – 19.9%) and 3.5-fold (F = 4 Hz; 20.6 ± 2.2%; range: 15.9 – 26.3%) greater than basal levels. Importantly, application of a 4 Hz oscillating field resulted in a significantly greater proportion of GFP^+ OPCs than the static field condition **(Figure 6a)**. Under all field conditions, transgene-expressing OPCs were phase bright, adherent and exhibited bipolar morphologies typical of OPCs, with GFP-expression throughout the cells **(Figure 6b; Figure 7a)**. Transfected cells also displayed normal A2B5 staining profiles and DAPI-labelled nuclei were without evidence of increased chromatin condensation or pyknosis **(Figure 7b)**.

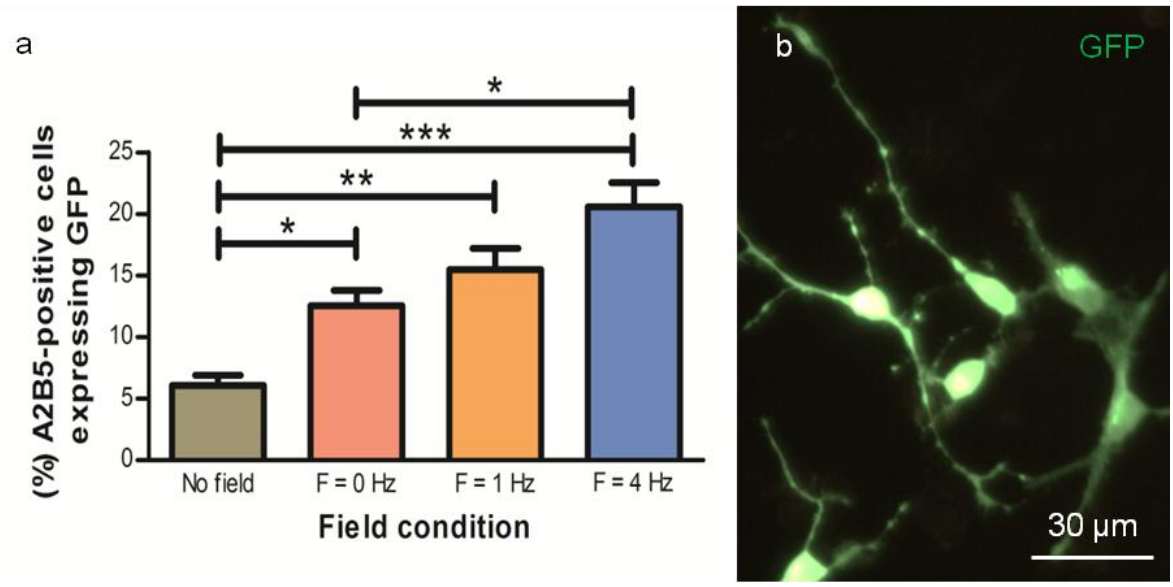

Figure 6: Application of static or oscillating magnetic field conditions (magnetofection) enhances MP-mediated gene delivery to OPCs. *(a) Bar graph indicating transfection efficiencies achieved in OPC cultures 48 h post-transfection using Neuromag-plasmid complexes encoding GFP (0.1x complex concentration), as judged by the percentage of A2B5$^+$ cells expressing GFP. All magnetic field conditions significantly enhanced transfection efficiency compared to the basal (no field) condition (*$F_{3,16} = 16.1$; $p < 0.001$; *one-way ANOVA;* $n = 5$*). Importantly, a 4 Hz oscillating field significantly enhanced transfection efficiency over the static field condition (*$p < 0.05$, **$p < 0.01$, ***$p < 0.001$; Bonferroni's post-tests; $n = 5$*). (b) Representative fluorescence micrograph of transfected OPCs (0.1x, F = 4 Hz) with bipolar morphologies, expressing GFP throughout the cell body and processes.*

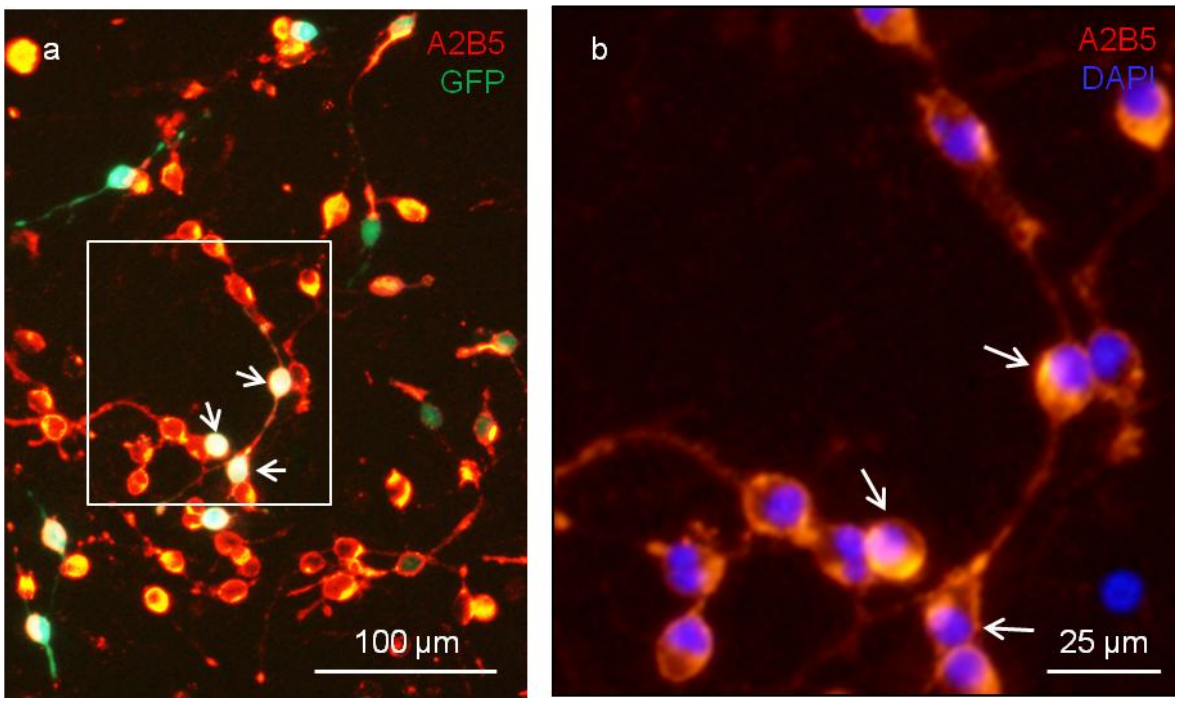

Figure 7: Magnetofection does not affect OPC morphologies or staining profiles. *(a) Representative fluorescence micrograph of transfected OPCs. Note co-localisation of GFP expression with A2B5 staining. (b) Magnified section of (a), indicated by white box, showing morphologically normal DAPI-stained nuclei. Arrows indicate the same transfected cells in (a) and (b).*

3.3.3 Magnetofection does not affect the proliferation or differentiation potential of OPCs

The developed transfection protocols (0.1x Neuromag-plasmid dose) did not affect OPC proliferation under any magnetic field condition, as assessed by comparing OPC densities with controls at 48 h **(Figure 5)**. In addition, when transfected OPC cultures were maintained in Sato differentiation medium to generate oligodendrocytes, the progeny could be observed with closely-apposed daughter nuclei, indicative of recent mitosis **(Figure 8a)**. Furthermore, when monitoring live transfected cultures, the striking observation was made that transfected cells were often in pairs, suggestive of a recent cell division, and providing further evidence that transfection does not adversely affect OPC proliferation potential **(Figure 8b)**. Transfected OPCs produced GFP^+/MBP^+ oligodendrocytes with mature, highly branched morphologies comparable to those observed in control cultures **(Figure 9a)**. No significant difference was observed in the proportion of MBP^+ cells in control cultures compared to transfected cultures (F = 4 Hz; 12 days post-magnetofection; **Figure 9b**). No differences were apparent in the range of oligodendroglial phenotypes present in control and treated cultures, from bipolar OPCs to multipolar, highly branched oligodendrocytes with extensive membrane elaboration (see **Figure 9** for a highly-processed example), providing further evidence that this protocol does not affect the differentiation potential of OPCs. Longer term monitoring of cultures showed persistence of GFP expression for up to 22 days post-transfection (the latest time-point examined), although expression had declined to approximately 5% of peak levels by this time.

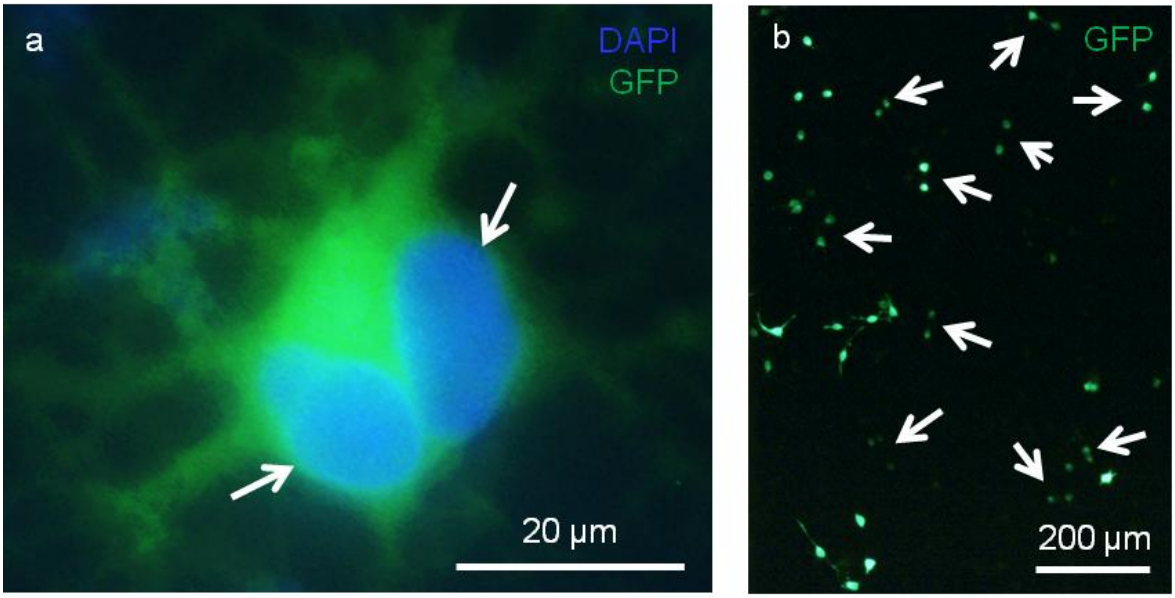

Figure 8: Magnetofection does not affect OPC proliferation potential. *(a) Multipolar morphologies typical of early-stage oligodendrocytes were present in cultures at 48 h post-magnetofection (arrows indicate two nuclei, suggestive of a recent cell division, and therefore normal proliferative activity). (b) In magnetofected cultures (culture shown: 0.1x, F = 4 Hz, 40 h post-transfection), GFP$^+$ cells were frequently observed in pairs (arrows), indicative of a recent cell division, further suggesting normal proliferative activity. Note that indicated pairs are frequently without processes, which is indicative of recent mitosis.*

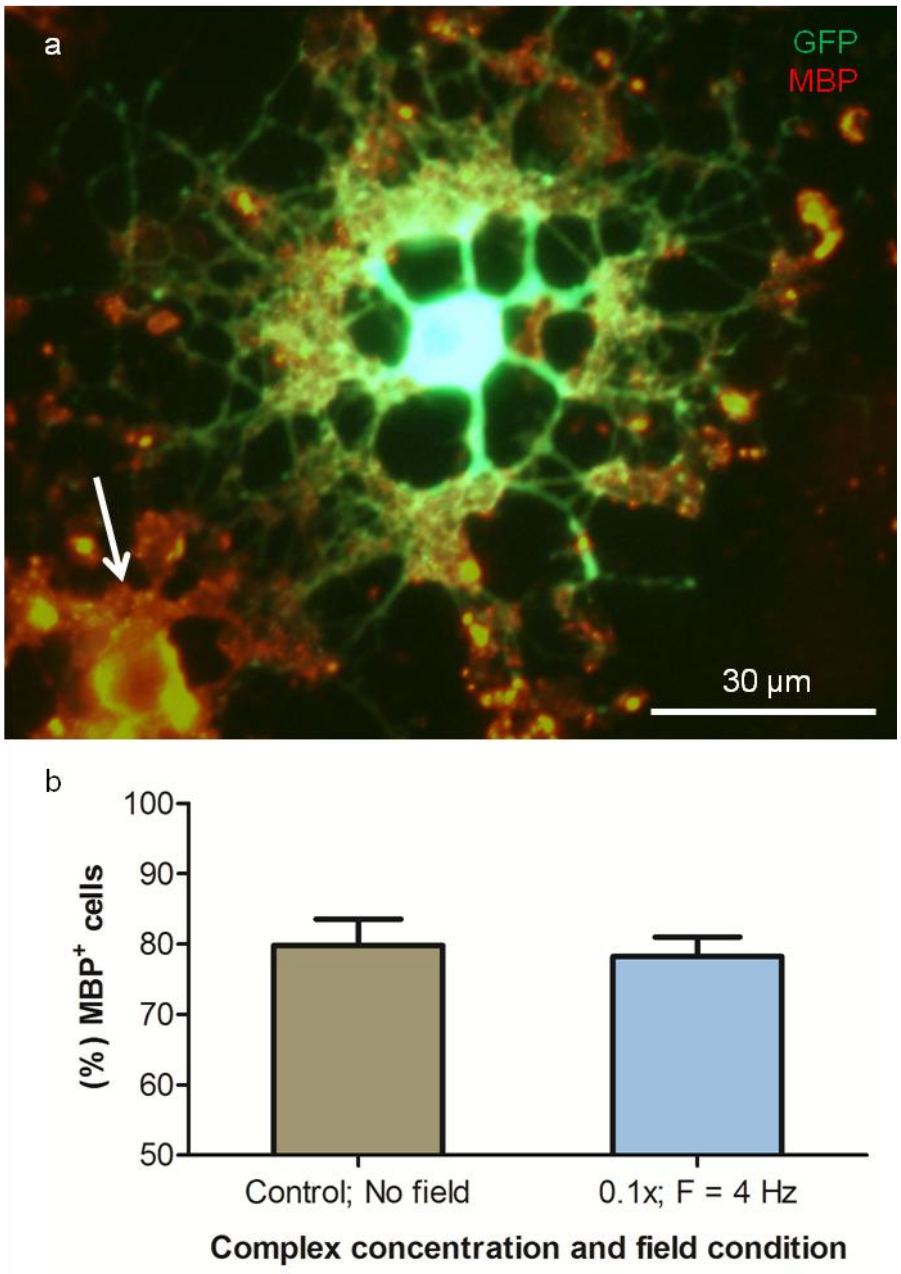

Figure 9: Magnetofection does not affect OPC differentiation potential. *(a) Following culture in Sato differentiation medium, magnetofected OPCs developed morphologies typical of mature oligodendrocytes, with GFP expressed throughout their processes, which stained for MBP (a late-stage oligodendrocyte marker). Arrow indicates a* MBP^+/GFP^- *cell. (b) Bar graph showing percentage of* MBP^+ *cells, 12 days post-transfection. The percentage of* MBP^+ *cells in magnetofected cultures (0.1x complex concentration; F = 4 Hz) was not significantly different from controls (plasmid only, no magnetic field;* n = 4*).*

3.3.4 MPs can mediate delivery of multiple genes to OPCs (co-transfection)

The potential to deliver two genes to an OPC population was assessed, and expression of both transgenes was apparent **(Figure 10)**, with ~75% of transfected cells expressing both GFP and RFP **(Figure 11a)**. In co-transfected cultures the proportion of magnetofected cells expressing RFP only was significantly lower than that expressing GFP only **(Figure 11b)**, and transfection levels in cultures treated with pDsRed only tended to be lower than with pmaxGFP only (with or without application of a magnetic field), although this was not shown to be significant **(Figure 11a)**. These data suggest that transfection using pDsRed is less efficient than with pmaxGFP. For both field conditions, co-transfection with pDsRed and pmaxGFP tended towards greater transfection than with either plasmid alone, although this was only shown to be significant compared to pDsRed in the presence of a 4 Hz oscillating field **(Figure 11a)**.

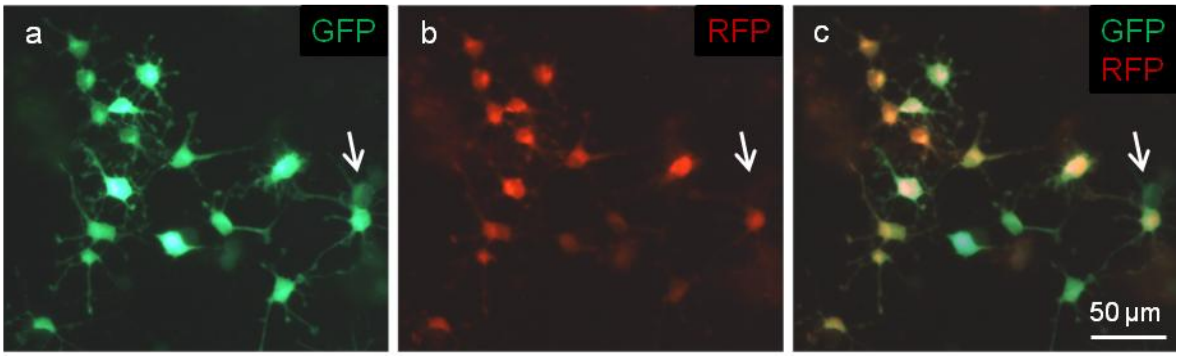

Figure 10: Multiple genes can be delivered to OPCs using MPs. *(a & b) Counterpart representative fluorescence micrographs of an OPC culture 48 h following simultaneous magnetofection (F = 4 Hz) with both GFP and RFP encoding plasmids (0.1x Neuromag, 0.05x pmaxGFP, 0.05x pDsRed). Cells are clearly expressing both GFP (a) and RFP (b), and the majority of cells are both GFP^+ and RFP^+, appearing yellow in the merged image (c). Arrows in (a-c) indicate the same GFP^+/RFP^- cell.*

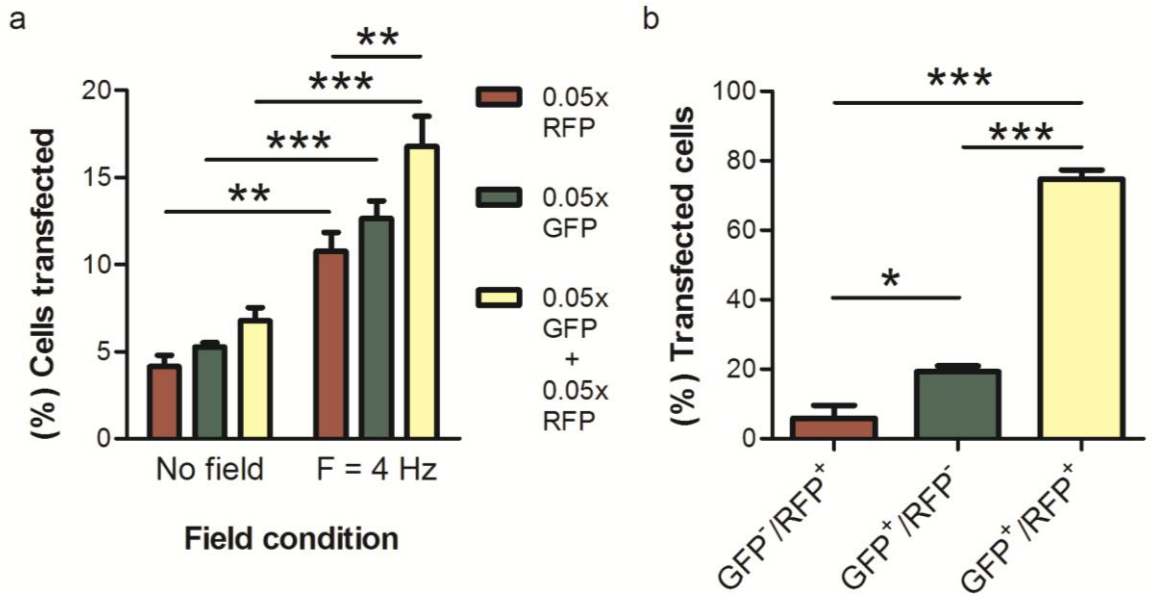

Figure 11: Combinatorial gene delivery typically results in co-expression of both transgenes. *(a) Bar chart indicating the total percentage of transfected OPCs (identified morphologically) 48 h post-transfection (either no field or F = 4 Hz). 0.05x RFP and 0.05x GFP indicate that a culture was treated with half the established 0.1x dose of pDsRed or pmaxGFP plasmid, respectively. 0.05x GFP + 0.05x RFP indicates a culture simultaneously treated with a half-dose of each plasmid, amounting to the established 0.1x dose. Both plasmid- ($F_{2,18}$ = 9.21; p < 0.01) and field-dependent effects were detected ($F_{1,18}$ = 91.6; p < 0.001; two-way ANOVA;* n = *4). For both field conditions, co-transfection resulted in greater transfection than with either plasmid alone, although this was only shown to be significant compared to pDsRed at 4 Hz; the application of a 4 Hz oscillating magnetic field resulted in a significantly enhanced transfection efficiency for each plasmid alone and in combination (**p < 0.01, ***p < 0.001; Bonferroni's post-tests). (b) Bar graph indicating the proportions of all transfected cells (F = 4 Hz, 0.05x pmaxGFP plus 0.05x pDsRed) which express only RFP, only GFP, or both RFP and GFP. The majority of transfected cells express both transgenes, and significantly more cells were GFP^+/RFP^- than were RFP^+/GFP^- ($F_{2,9}$ = 173; p < 0.001; one-way ANOVA; *p < 0.05, ***p < 0.001; Bonferroni's post-tests;* n = *4).*

3.3.5 MPs can mediate delivery of a therapeutic gene to OPCs

Transfected OPCs, identified by staining for the OPC markers A2B5 and NG2, were observed under all magnetic field conditions and for both the pFGF2-GFP and pAN-GFP plasmids. Cultures transfected with pFGF2-GFP were comparable to both pAN-GFP and plasmid-only controls in terms of the numbers of adherent phase-bright cells, and did not exhibit other signs of toxicity, consistent with pmaxGFP experiments (data not shown). Cells transfected with pAN-GFP exhibited GFP expression throughout the cell body and processes **(Figure 10)**, as was observed for pmaxGFP and pDsRed. However, cells transfected with pFGF2-GFP exhibited GFP expression localised to the nucleus (**Figure 12b-d**; <1% of cells exhibited GFP expression throughout the cell). This is consistent with reports that some FGF2 isoforms are localised to the nucleus, including in astrocytes,[301,302] and demonstrates normal subcellular localisation of the fusion protein by OPCs. For both pFGF2-GFP and pAN-GFP transfected cultures [as was observed for pmaxGFP **(Figure 8b)** and pDsRed transfection (data not shown)], transfected cells were frequently observed in pairs, indicative of a recent cell division **(Figure 13a-b)**. Furthermore, GFP expression in these pairs of cells was typically of comparable intensity, as would be expected following symmetric division of a transfected cell. Such regular appearance of cells with similar intensity of protein expression with a small spatial separation would not be anticipated to result from separate transfection events in neighbouring cells.

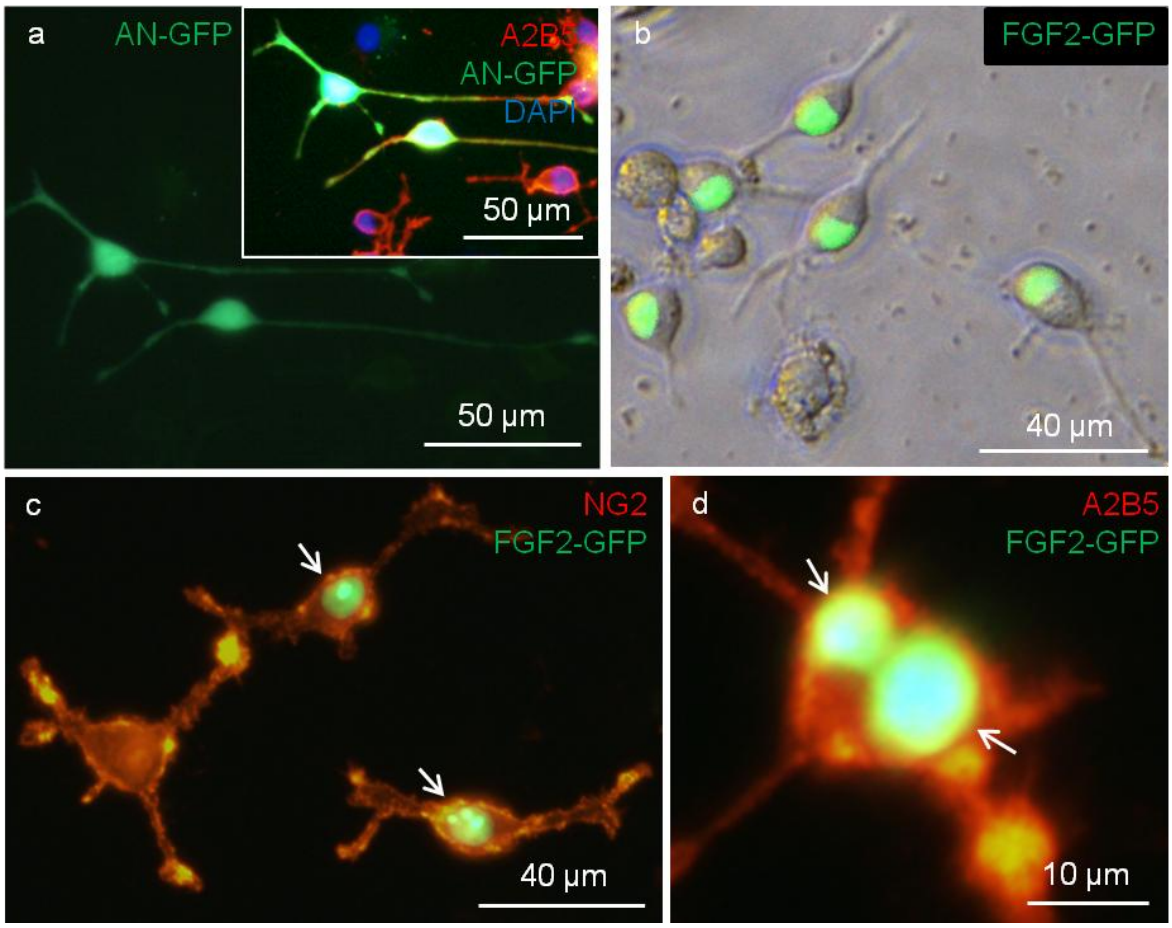

Figure 12: MP-mediated delivery of a therapeutic gene to OPCs. *(a) Fluorescence micrograph of cells transfected with a control plasmid (pAN-GFP; F = 4 Hz). The cells display bipolar morphologies typical of OPCs and exhibit GFP expression throughout the cell body and processes. Inset shows the same cells stained for A2B5 and DAPI. (b) Merged phase and fluorescence micrographs of live cells transfected with a plasmid encoding a therapeutic gene [pFGF2-GFP; encodes fibroblast growth factor 2 (FGF2) tagged with GFP, producing a FGF2-GFP fusion protein], at 24 h post-transfection (F = 4 Hz). The cells display bipolar morphologies typical of OPCs, with GFP expression prominently localised to the nucleus. (c) Fluorescence micrograph of $NG2^+$ cells 48 h post-transfection with pFGF2-GFP (F = 4 Hz). Arrows indicate OPCs with GFP^+ nuclei. (d) Fluorescence micrograph of a proliferating OPC transfected with pFGF2-GFP and stained for A2B5. Both daughter cells have GFP^+ nuclei (arrows indicate daughter nuclei).*

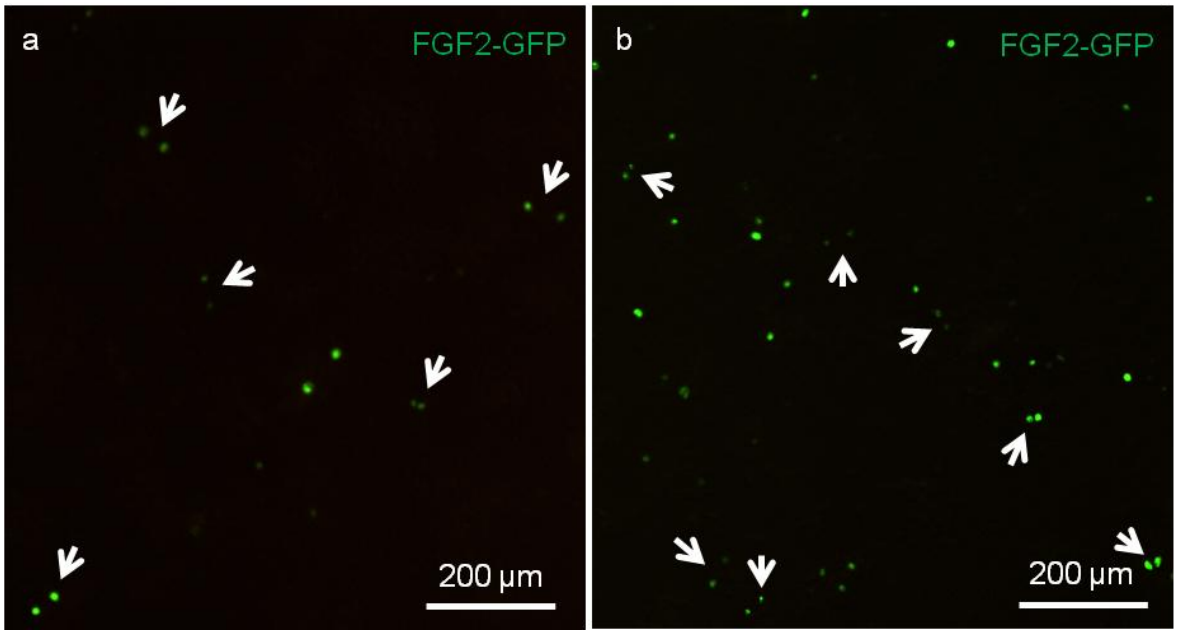

Figure 13: Transgene expressing cells are often observed in pairs, indicative of recent mitosis. *Representative fluorescence micrographs of a live OPC culture magnetofected (F = 4 Hz) with pFGF2-GFP plasmid. Images taken at 12 h (a) and 48 h (b) post-transfection (not the same field). GFP^+ cells are apparent from ~6 h post-transfection and the number of GFP^+ cells increases until peaking at approximately 48 h. Arrows indicate pairs of GFP^+ cells, suggestive of recent proliferation. Note that intensity of GFP expression varies across the field, but is typically similar for each indicated pair.*

Expression of the FGF2-GFP fusion protein was confirmed using an FGF2 antibody. Untreated OPC cultures stained for FGF2 throughout the cell body and processes, but with a marked reduction in signal intensity in the nuclear region **(Figure 14a, c, e)**. This is to be expected, as OPCs show endogenous expression of some isoforms of FGF2,[63] and FGF2 is an essential component of chemically-defined OPC culture medium. In pFGF2-GFP treated cultures, successfully transfected OPCs (with nuclear-localised GFP expression) also exhibited FGF2 staining throughout the cell body and

processes, but with uniform intensity of staining in the nuclear region, indicating a greater presence of nuclear-localised FGF2 than in untransfected cells **(Figure 14b, d, f)**. Untransfected OPCs in these treated cultures stained with identical profiles to OPCs in control cultures, *i.e.* noticeably lower FGF2 staining intensity in the nucleus.

As has been shown for pmaxGFP and pDsRed, the application of both static and oscillating magnetic fields enhanced transfection efficiencies compared to basal levels for pAN-GFP and pFGF2-GFP **(Figure 15)**. An oscillation frequency of 4 Hz produced the greatest transfection efficiencies for both plasmids, significantly enhancing transfection levels compared to a static field, with F = 4 Hz also significantly enhancing efficiency over the F = 1 Hz condition for pFGF2-GFP **(Figure 15)**. Analysis by two-way ANOVA of the transfection efficiency achieved with pmaxGFP, pAN-GFP and pFGF2-GFP (no field versus F = 4 Hz), indicated effects of field ($F_{1,22}$ = 90.1; $p < 0.001$) and plasmid ($F_{2,22}$ = 54.3; $p < 0.001$). With or without a magnetic field, transfection efficiencies for both pAN-GFP and pFGF2-GFP were significantly lower than those achieved using pmaxGFP ($p <$ 0.001 for each of the following comparisons: pAN-GFP versus pmaxGFP, no field; pFGF2-GFP versus pmaxGFP, no field; pAN-GFP versus pmaxGFP, F = 4 Hz; pFGF2-GFP versus pmaxGFP, F = 4 Hz; Bonferroni's post-tests). A regression analysis indicated that increasing plasmid size led to a systematic reduction in transfection efficiency **(Figure 16)**. The equations of the slopes show the x axis intercepts to be approximately 8.9 and 8.7 kb (for the no field and F = 4 Hz conditions respectively), indicating that the percentage of cells transfected tends to zero as plasmid size approaches 9 kb.

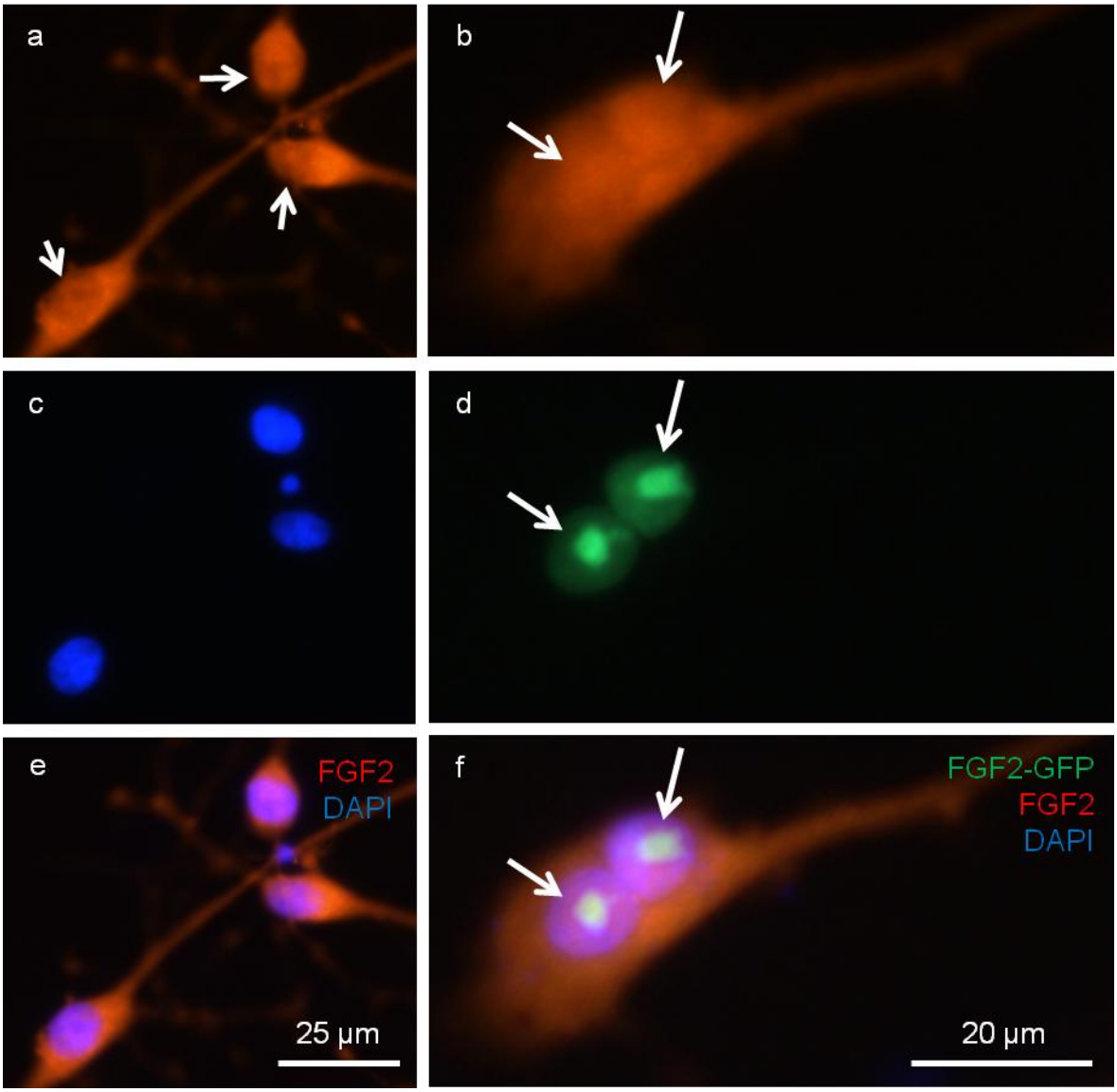

Figure 14: Expression of a therapeutic fusion protein in transfected OPCs. *Fluorescence micrographs of OPC cultures. (a) Untransfected OPCs stained for FGF2 throughout the cell body and processes, but with lower levels of expression in the nucleus. Arrows indicate less intensely-stained regions. DAPI-stained nuclei are shown in counterpart image (c), and (e) shows a merged image. (b) OPCs transfected with pFGF2-GFP (0.1x, F = 4) stained for FGF2 evenly throughout the cell body and processes, including strong staining within the nucleus (arrows). (d) Counterpart image to (b) showing nuclear FGF2-GFP expression. (f) Merged image of (b) and (d), including DAPI-stained nuclei. Arrows indicate the nuclei in (b), (d) and (f).*

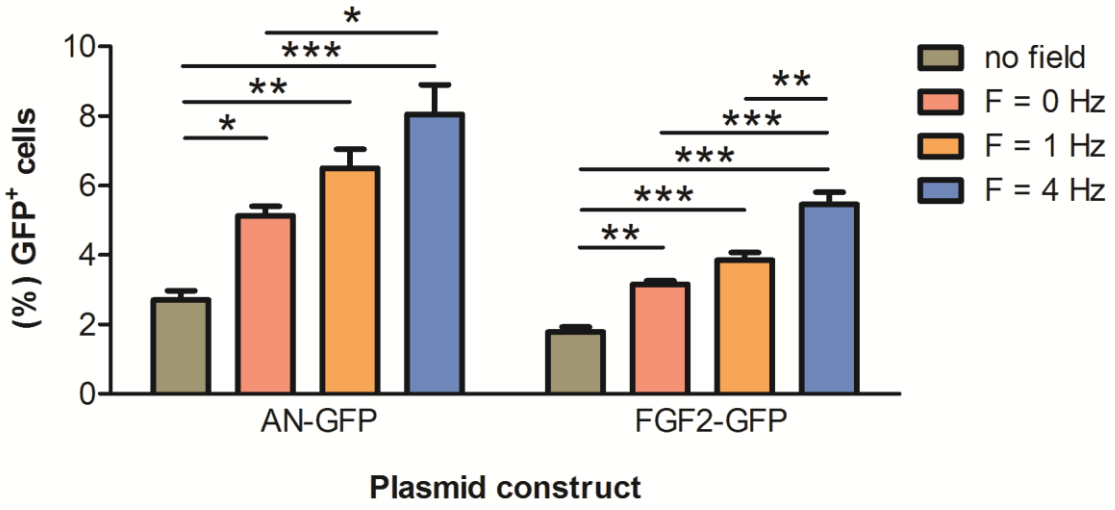

Figure 15: Static and oscillating magnetofection enhances therapeutic gene transfection efficiency in OPCs. *Bar graph illustrating transfection efficiency achieved with and without application of static and oscillating magnetic fields when Neuromag was complexed with either pAN-GFP or pFGF2-GFP. There was a field-dependent effect for pAN-GFP (*$F_{3,12}$ *= 17.7;* $p < 0.001$*; one-way ANOVA;* $n = 4$*) and pFGF2-GFP (*$F_{3,13}$ *= 50.5;* $p < 0.001$*; one-way ANOVA;* $n = 4$*). For both plasmids, all magnetic field conditions significantly enhanced transfection efficiency over basal (no field) levels, with F = 4 Hz also significantly enhancing efficiency compared to the static field condition. For pFGF2-GFP, F = 4 Hz also significantly enhanced transfection efficiency over the F = 1 Hz condition.* *$p < 0.05$, **$p < 0.01$, ***$p < 0.001$*; Bonferroni's post-tests.*

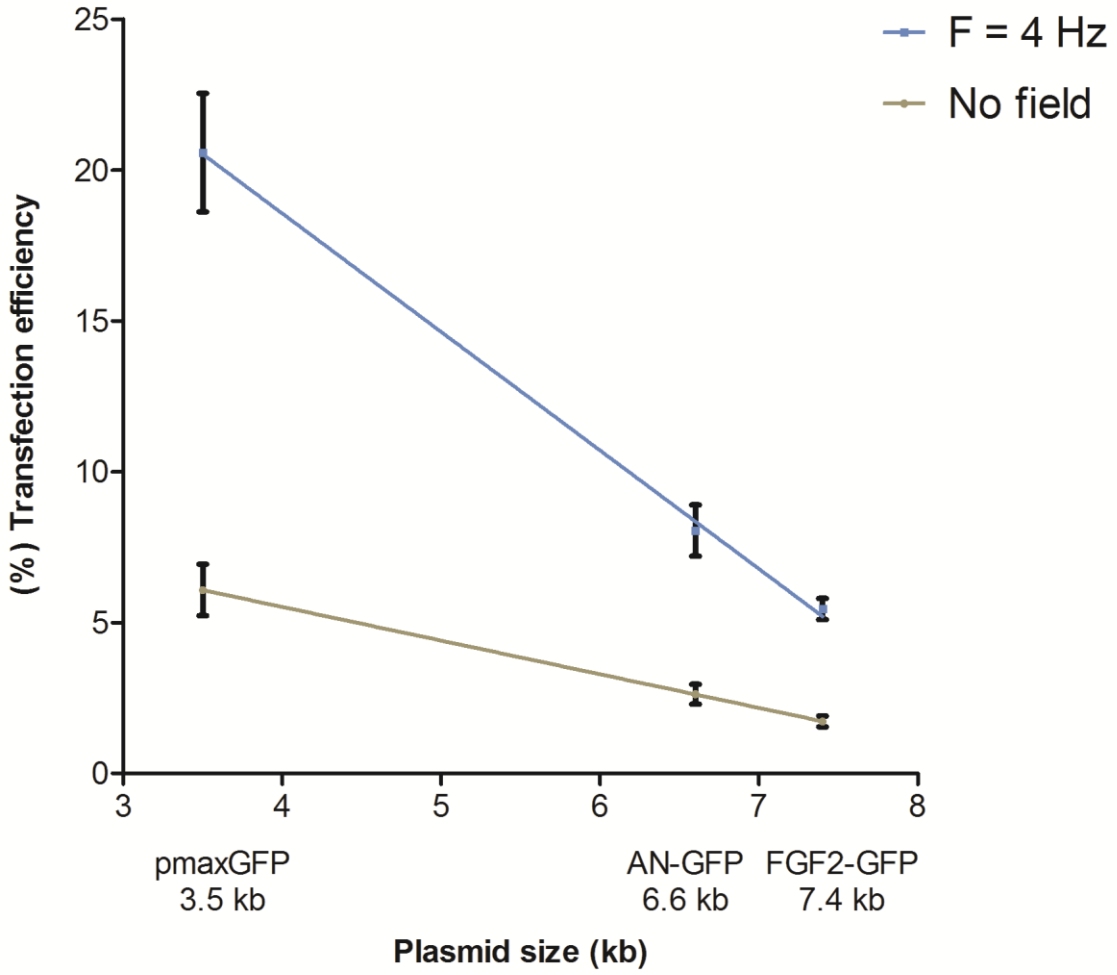

Figure 16: MP-mediated transfection/magnetofection efficiency is inversely related to plasmid size. *Regression analysis using the data provided in Figures 6 and 15, showing that transfection efficiency achieved in OPCs using Neuromag conjugated to different plasmids (0.1x) is inversely related to plasmid size, in the absence of a magnetic field (no field; $r^2 = 0.750$; $p < 0.01$), and also when an oscillating magnetic field is applied (F = 4 Hz; $r^2 = 0.872$; $p < 0.01$). Both basal and magnetofection transfection levels show a systematic reduction along with increasing plasmid size. The equations describing the slopes for the no field and F = 4 Hz conditions are, respectively, (y = 9.987 – 1.116x) and (y = 34.28 – 3.928x). The respective x axis intercepts are 8.949 and 8.726.* $n \geq 3$.

3.3.6 Characterisation of organotypic cerebellar slice cultures

In initial experiments, cerebellar slices were prepared at either 350 or 400 µm thickness then cultured for 10 days. Slices at 350 µm were observed to become thinner over a course of 3 – 5 DIV, whereas 400 µm slices frequently remained at their initial thickness. These thicker slices were of low viability, potentially due to poor penetration of oxygen and nutrients. Therefore, slices were routinely prepared at 350 µm thickness. Slices typically exhibited good cytoarchitectural preservation, with cerebellar folia and axonal tracts being readily identifiable under light microscopy **(Figure 17a)**. After 8 – 10 days in culture, staining for MBP revealed distinct WM tracts **(Figure 17b)**, and live/dead assays revealed that slices were of high viability (>90% live cells; **Figure 18**). After 8 DIV, typically 10 – 12 cerebellar slices per animal were observed to thin sufficiently for use, with clear preservation of WM tracts.

Calbindin staining of slices during these studies demonstrated the presence of Purkinje cells, with soma aligned in the Purkinje cell layer **(Figure 19a-b)**. Slices were also stained for the astrocyte marker GFAP **(Figure 19c-d)** and the OPC marker NG2 **(Figure 20a-c)**, demonstrating the presence of each of these cell types within the slices. These slice cultures remained viable for up to 74 DIV, as demonstrated by live/dead assay **(Figure 20d)**. After this period of time in culture, slices still stained for GFAP, NG2, MBP and calbindin, and WM tracts and cerebellar folia were still identifiable, although less distinct than at earlier time-points.

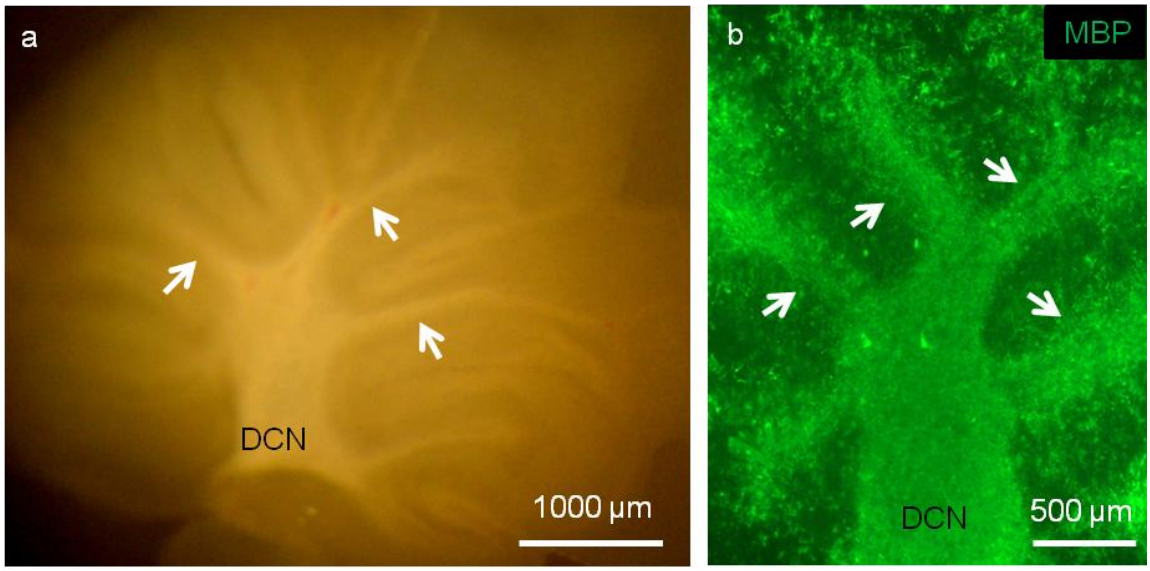

Figure 17: Organotypic cerebellar slices retain cytoarchitectural features of the cerebellum. *(a) Light micrograph of a cerebellar slice culture at 5 days in vitro (DIV), showing preservation of cerebellar features. Arrows indicate white matter (WM) tracts which branch into the cerebellar folia and converge on the deep cerebellar nuclei (DCN). In some of the folia, the molecular and granular layers are apparent. (b) Fluorescence micrograph of a cerebellar slice at 10 DIV stained for the oligodendrocyte marker MBP. WM tracts are apparent (arrows), converging on the DCN from each of the cerebellar folia.*

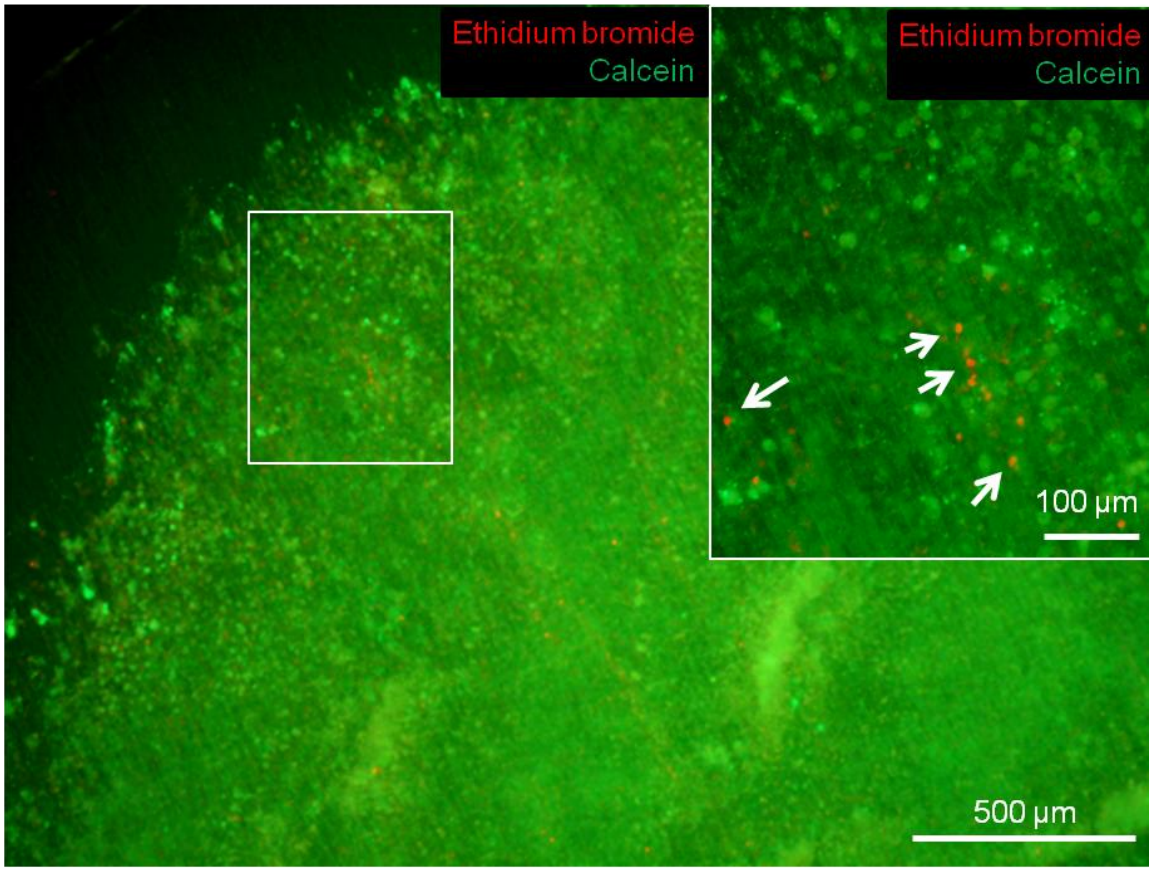

Figure 18: Organotypic cerebellar slices exhibit high viability. *Fluorescence micrograph of a cerebellar slice at 10 DIV, following a viability assay; dead/dying cells are labelled with ethidium bromide, live cells are labelled with calcein. Inset, magnified region (white box) of the same slice. Arrows indicate ethidium-labelled cells.*

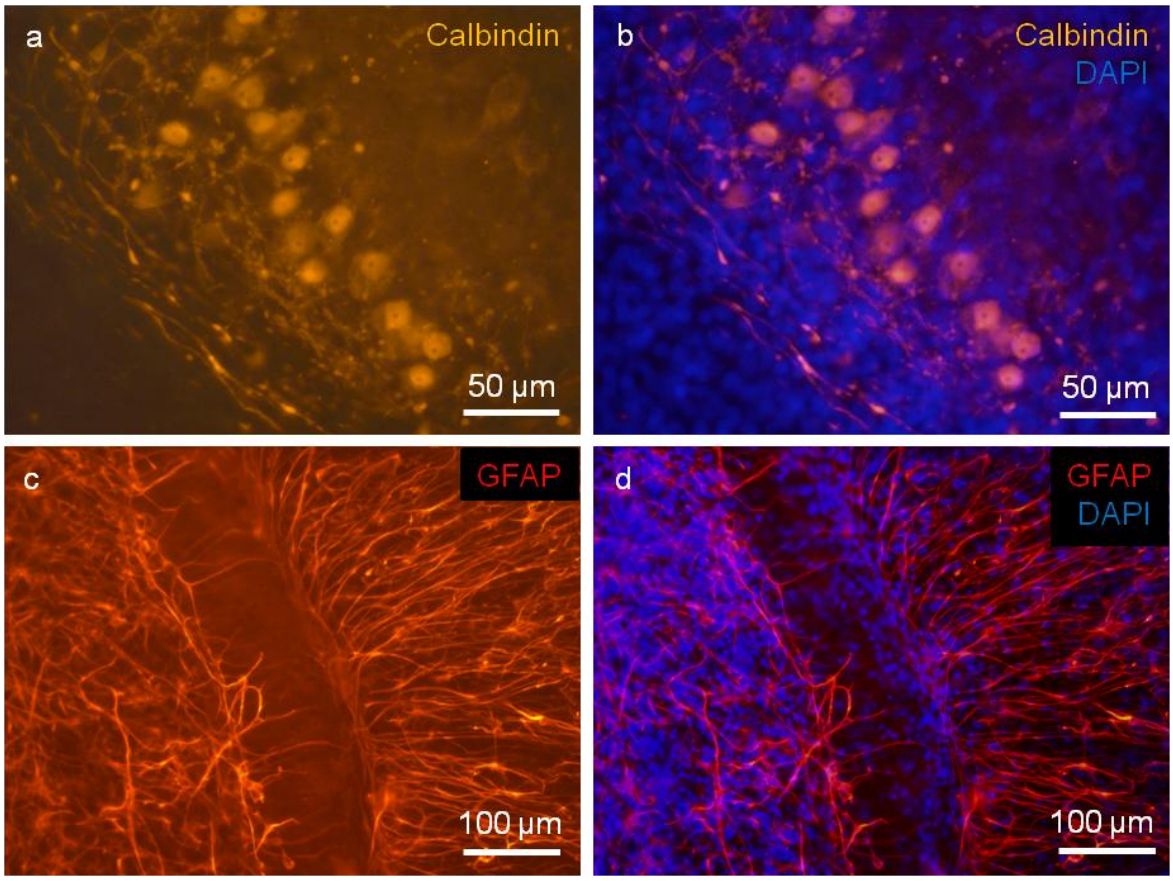

Figure 19: Cerebellar slices retain populations of Purkinje cells and astrocytes. *Fluorescence micrographs of slices stained at 10 DIV for the Purkinje cell marker calbindin (a, b) and the astrocyte marker GFAP (c, d). (b & d) are merged images of (a & c) respectively,including DAPI-labelled nuclei. (a, b) Purkinje cell bodies are present in a thin line, suggesting good preservation of the narrow Purkinje cell layer found in the cerebellum* in vivo.

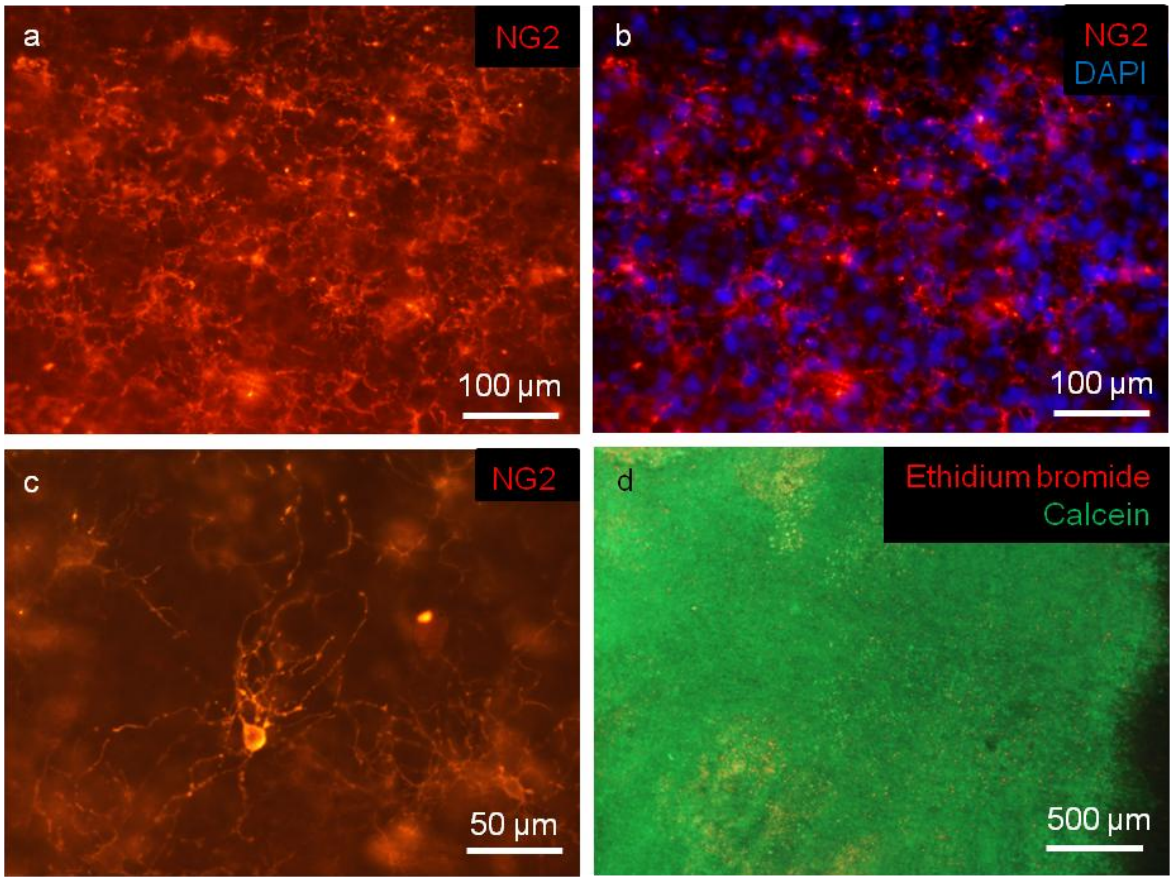

Figure 20: Cerebellar slices retain a population of OPCs, and remain viable for up to 74 days. *(a-c) Fluorescence micrographs of slices stained at 10 DIV for OPC marker NG2. NG2$^+$ cells are present in a syncytium, representative of their arrangement* in vivo. *(b) Counterpart image to (a), merged with DAPI-labelled nuclei. (c) Higher magnification image of a slice stained for NG2, showing a prominent cell with multiple processes. (d) Fluorescence micrograph of a live/dead-stained cerebellar slice at 74 DIV, demonstrating high viability, although with more dead cells apparent than in slices stained at 10 DIV.*

3.3.7 Magnetofected OPC populations transplanted onto cerebellar slice cultures survived, migrated, proliferated and differentiated

Magnetofected (GFP^+) OPCs could be delivered focally to slices by pipette and were readily visualised by fluorescence microscopy **(Figure 21a-b)**. At 24 and 48 h following transplantation, GFP^+ cells could be observed with bipolar morphologies that are characteristic of migratory OPCs **(Figure 21c)** and were frequently observed in pairs, suggestive of proliferation **(Figure 21d)**. Further, transplanted cells were present with multipolar morphologies indicating differentiation **(Figure 21d, inset)**. Confocal microscopy revealed that transplanted cells could be visualised at depth within the slices, rather than being entirely superficial. Transplanted cells also demonstrated co-expression of the OPC marker NG2 with GFP **(Figure 22a)**, and co-expression of the oligodendrocyte marker MBP with GFP **(Figure 22b)**. Transplant populations re-plated into chamber slides with Sato differentiation medium also retained GFP expression, stained for NG2 or MBP, and exhibited normal oligodendroglial morphologies, demonstrating that factors inherent to the slice cultures or slice culture medium (*e.g.* serum) were not necessary to promote survival of the modified cells.

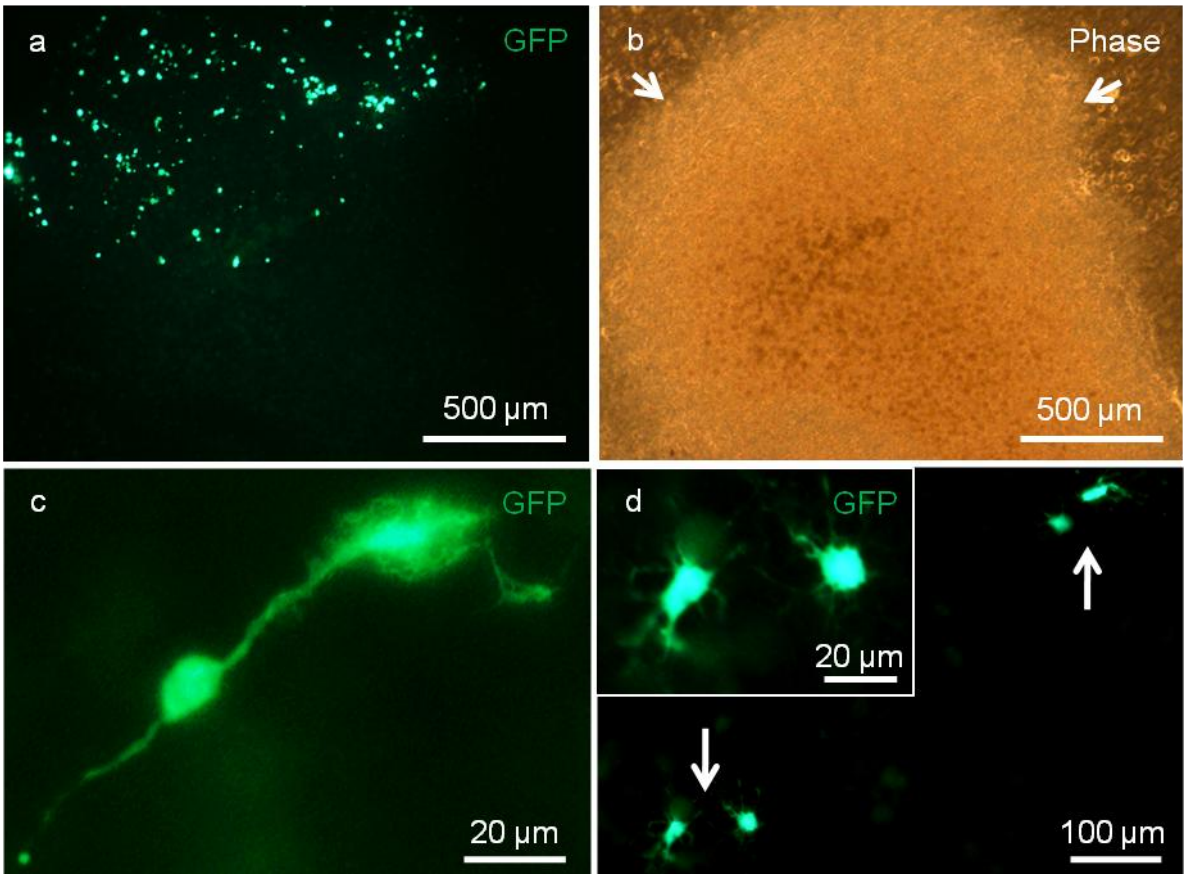

Figure 21. Magnetofected OPCs survive, migrate, proliferate and differentiate following transplantation onto organotypic cerebellar slice cultures. *(a) Magnetofected OPCs were focally delivered to slices, as evidenced by fluorescence microscopy immediately post-transplantation. GFP^+ transplanted cells exhibited the rounded morphology typical of enzymatically detached cells. (b) Counterpart phase image to (a), illustrating slice margin (arrows). Post-transplantation, GFP^+ cells were observed with bipolar morphologies typical of migrating OPCs [24 h; (c)], in pairs, suggestive of proliferation [48 h; (d)], and with multipolar morphologies, indicative of normal differentiation (d, inset).*

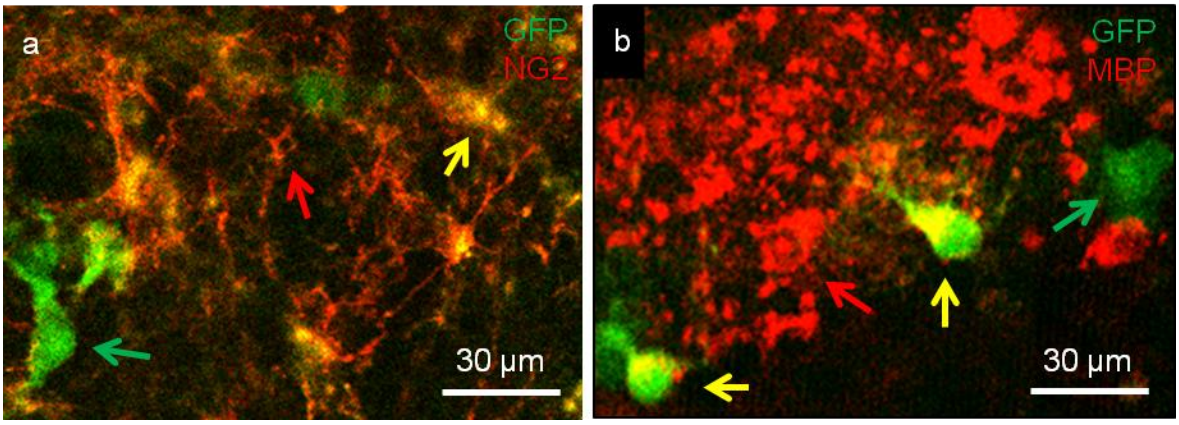

Figure 22. Magnetofected OPCs express OPC and oligodendrocyte markers following transplantation onto organotypic cerebellar slice cultures. *(a) When slices were stained for the OPC marker NG2, 48 h post-transplantation, confocal microscopy revealed $GFP^+/NG2^+$ transplanted OPCs (yellow arrow) against a background of red $NG2^+$ host OPCs (red arrow). Some GFP^+ cells were $NG2^-$ (green arrow). (b) Confocal image of GFP^+ cells stained for the oligodendrocyte marker MBP (yellow arrows) 48 h post-transplantation, indicating OPC differentiation within the slice. Red arrow indicates a MBP^+ host oligodendrocyte; green arrow indicates a GFP^+/MBP^- transplanted cell.*

3.4 Discussion

A number of proof-of-principle studies have been performed: MP-mediated gene delivery to OPCs has been demonstrated for the first time, with transfection efficiency enhanced by employing static and state-of-the-art oscillating magnetofection techniques; these techniques appear to be safe as evidenced by normal proliferation and differentiation profiles of the transfected cells. Both combinatorial gene delivery and therapeutic gene delivery have also been safely demonstrated in OPCs using MP vectors. Further, this is the first use of organotypic neural slices as a safety assay for nanomaterial-modified transplant cells (by studying key regenerative properties of the transfected OPCs following their transplantation onto slices). Use of this assay supports the concept that the transfection protocols developed under this study have a good safety profile and that slice models represent a valuable tool in neural tissue engineering studies.

3.4.1 Magnetofection enhances MP-mediated gene delivery to OPCs

The safety and efficiency of the magnetofection protocol used here show that it could serve as an inexpensive, technically simple alternative to the viral transduction methods which are widely used with OPCs. **Table 1** provides transfection efficiencies achieved in rodent OPCs derived from primary sources using a variety of viral and nonviral methods, showing these to be highly variable. All alternative nonviral vectors tested with OPCs have resulted in significant reductions in cell viability, with most also demonstrating lower levels of transfection than those demonstrated here with MPs. Although some viral methods have produced greater levels of transfection (up to 90%)[50] than reported here, results can vary greatly, with another retroviral study transfecting less

than 0.5% of OPCs.[108] Crucially, toxicity data have rarely been published for viral transduction of OPCs, an omission also common to nonviral techniques, and the lack of detailed data in this regard prevents assessment of the potential for clinical translation of these techniques.

Use of MPs and magnetofection techniques compare favourably with the transfection efficiencies achieved using other nonviral methods, with the critical advantage of high cell viability post-transfection. Techniques such as electroporation and nucleofection produce transient pores in the cell membrane, through which transfection vectors gain cell entry.[303] However, this membrane disruption can result in extensive cell death, and surviving cells are often damaged.[207] An advantage of MPs as vectors is that they exploit the natural endocytotic mechanisms of cells, and avoid membrane disruption. From a translational perspective, it is highly desirable that a cell transplant population demonstrates high viability, as introducing dead/dying cells into a patient may lead to detrimental effects, such as secondary pathology due to necrotic release of the cell contents, and possibly inflammatory responses.[304] Furthermore, in terms of large scale culture of cells for clinical translational applications, a high rate of cell attrition can be predicted to add to the cost of production, especially where limited primary tissue sources are available. MPs additionally offer unique advantages for the development of 'theragnostic' applications, as their multimodality enables therapeutic effects to be combined with diagnostic functionality (*e.g.* non-invasive imaging of MP-labelled cells).[146]

Table 1: Comparative *in vitro* transfection efficiencies in rodent OPCs (derived from primary sources) for viral and nonviral techniques.

Transfection method	Transgene/protein	Transfection efficiency	Viability	Ref
Viral methods				
Lentivirus	GFP	~90%	'Viability not affected'; numerical data not reported	50
Retrovirus	LacZ	~90%	'Viability not affected'; numerical data not reported	50
Retrovirus (LZRS)	CNTF/EGFP	60 – 70%	Data not reported	60
Retrovirus (LZRS)	D15A/EGFP	~60%	Data not reported	64
Retrovirus (MoMuLV)	LacZ	<0.5%	Data not reported	108
Retrovirus	EGFP/p27/p18	Data not reported	Data not reported	305
Adenovirus	EGFP	~70%	Data not reported	290
Adenovirus	LacZ	>50%	Data not reported	306
Adenovirus	p27	Data not reported	~75% (MTT assay)	307
Nonviral methods				
Magnetic particles	GFP	21%	No significant toxicity (established dose)	†
Lipofection (GenePORTER 2)	CASK-EGFP	2 – 5%	Data not reported	290
Lipofection (Lipofectamine, Lipofectin, Cellfectin)	LacZ	1 – 3%	Data not reported; toxic at even low doses (<2 µg)	110
Lipofection (Effectene)	NT3	Data not reported	Data not reported	267
Calcium phosphate precipitation	LacZ	3 – 5%	~10%	108
Calcium phosphate precipitation	LacZ	<2%	Data not reported; induced morphological changes	110
Electroporation	EGFP	~49%	~78%	288*
Electroporation	EGFP	~43%	60%	289*
Electroporation	LacZ	~15%	20 – 25%	110
Electroporation	GFP-KLHL1/MRP2	Data not reported	Data not reported	113

GFP = green fluorescent protein; *β*-Gal = *β*-galactosidase; D15A = multineurotrophin, with brain-derived neurotrophic factor (BDNF) and neurotrophin 3 (NT3) activity; EGFP = enhance green fluorescent protein; CNTF = ciliary neurotrophic factor; MTT = 2-(4,5-dimethyl-2-thiazolyl)-3,5-diphenyl-2H-tetrazolium bromide; CASK = calcium/calmodulin-dependent serine kinase; KLHL1/MRP2 = Kelch-like 1 protein/Mayven-related protein 2, actin binding protein. *Company website. †Reported here.

3.4.2 OPCs are potentially more amenable to transfection during mitosis

Proliferating cells such as OPCs undergo breakdown of the nuclear envelope during mitosis, potentially permitting access of exogenous DNA into the nucleus. It is also reported that proliferating cells have larger nuclear channels and exhibit higher rates of nuclear transport.[176] For all plasmids, transfected cells in OPC cultures were frequently observed in pairs. Presuming that each of these pairs does represent two daughter cells, it is not clear from this evidence whether (i) each is the result of a GFP^+ cell that has divided, with approximately equal inheritance of GFP molecules and/or plasmids by each daughter cell, or (ii) a GFP^- cell (with intracellular Neuromag-plasmid complexes) has divided, and the process of nuclear membrane breakdown during mitosis has permitted approximately equal plasmid entry into the nucleus of both daughter cells. Possibility (ii) implies rapid GFP expression post-mitosis, particularly for cells with intense GFP expression, and therefore seems less likely than (i), which is further supported by the observation that these pairs of cells typically exhibit equal levels of GFP or RFP expression.

3.4.3 Optimising MP-based engineering of OPCs for delivery of therapeutic factors

In addition to delivery of reporter genes, it has been shown here that a therapeutic gene can be delivered to OPCs using MPs as vectors. The therapeutic factor FGF2 was chosen as it is a mitogen for OPCs (and other cell types) and promotes angiogenesis, which are both potentially valuable for promoting CNS regeneration. These experiments demonstrated that transfection efficiency declined as plasmid size increased. As the Neuromag:plasmid ratio was kept constant for all experiments, a possible explanation for this finding is that each Neuromag-pmaxGFP complex (3.5 kb) consists of a higher number

of individual plasmids than each Neuromag-pFGF2-GFP complex (7.4 kb), resulting in OPCs with higher plasmid copy numbers when transfected with smaller plasmids. However, it may be the case that individual plasmids associate with multiple particles, and larger plasmids may result in larger complexes, with potential implications for cellular uptake of these complexes. This is speculative, and it must be considered that plasmids are typically supercoiled, making them highly compacted, as evidenced by the dynamic light scattering (DLS) measurements of Neuromag:pmaxGFP complexes showing only a 35% increase in hydrodynamic diameter over Neuromag alone.[164] Ultrastructural analyses of MP-plasmid complexes [*e.g.* EM, atomic force microscopy (AFM)] and analyses such as DLS (with different sizes of plasmid) would greatly aid the development of these transfection techniques by providing insights into the nature of physico-chemical interactions at the particle-plasmid interface and hence factors that govern effective plasmid delivery. A further factor pertinent to transfection efficiency is likely to be that smaller plasmids may more readily traverse the nuclear membrane and be expressed.[176]

The inverse relationship between transfection efficiency and plasmid size indicates that plasmids should be engineered without unnecessary elements in order to minimise their size. For example, the pFGF2-GFP plasmid used here contains a neomycin resistance sequence, which is unnecessary for transient expression and could be removed. Similarly, for therapeutic effects without fluorescent tagging, the GFP encoding sequence could be removed. If the pmaxGFP plasmid were to be re-engineered, with the *gfp* sequence (~710 bp) replaced by the *FGF2* sequence (867 bp) from the pFGF2-GFP plasmid, the resulting plasmid would be approximately 3.7 kb. From the relationships between plasmid size and transfection efficiency determined here, it can be predicted that this plasmid would result in transfection levels approaching those seen with pmaxGFP (~21%). Most neurotherapeutic growth factor genes have open reading frames of <1.2 kb (*e.g. NT3*: 774

bp, National Centre for Biotechnology Information database, www.ncbi.nlm.nih.gov) and could therefore be incorporated into plasmids of similar size to the pmaxGFP plasmid with the aim of achieving comparable transfection efficiency. Regression analysis predicts that Neuromag particles will not be able to achieve transfection with plasmids larger than approximately 9 kb, but the delivery of large plasmids is desirable in order that multiple therapeutic genes can be delivered simultaneously, with the potential inclusion of complex regulatory elements for region-specific or inducible transgene expression.[63,117] These data highlight the biomedical need for particles capable of delivering plasmids of this size or larger, which may depend upon producing larger particles, or by devising alternative coatings or morphologies in order to increase binding capacity/DNA compaction. Any such particle modifications would require further toxicity testing using procedures similar to those outlined here. Importantly for the development of combinatorial CNS therapies, the delivery of multiple genes to an OPC population has been demonstrated here, with many cells showing expression of both genes. This raises the possibility of producing an OPC transplant population engineered to express two or more therapeutic factors.

3.4.4 Translational considerations for repair of demyelinating lesions

Plasmid-based transfection typically results in transient transgene expression, as observed here. Such transient expression is desirable for promoting CNS remyelination in, for example, MS or SCI lesions. Successful remyelination follows a specific sequence of cellular events, and each phase of the repair process is temporally controlled by precisely regulated expression of repair-promoting signals. This process involves the recruitment of OPCs into lesions sites with subsequent proliferation followed by the differentiation phase and formation of functional myelin sheaths around axons. Notably, maintaining expression

of OPC proliferation- or differentiation-promoting factors for an inappropriate length of time is likely to be detrimental to effective regeneration.[1,6,9,14,29,308] For example, PDGF-AA and FGF2 both have mitogenic and migration promoting effects on OPCs, but also inhibit the late-stages of differentiation into mature oligodendrocytes, and therefore their upregulation should not be prolonged beyond the 'recruitment' phase of regeneration.[63,309] Given this limitation, if multiple therapeutic genes are to be delivered to a transplant population it will be important to select compatible, complementary molecules, such as PDGF-AA and FGF2. However, if sufficient advances are made in particle and plasmid engineering, it may be possible to transfect OPCs with inducible transgenes. For example, the OPC cell line CG4 has been successfully transfected (by calcium phosphate precipitation) with a plasmid encoding FGF2 controlled by the Tet-on system and stably transfected clones isolated by antibiotic selection.[63] By exposing these cells to a tetracycline (*e.g.* Doxycycline), FGF2 expression is activated. In theory, multiple genes could be delivered to OPC transplant populations, using distinct induction signals but the translation of such an approach to the clinical setting would require further research, taking into account critical factors such as the ability of the relevant inducing molecules to cross the BBB.[310]

3.4.5 The underlying mechanisms of oscillating magnetic field enhancement of transfection are not known

If the mechanisms underlying the enhanced transfection efficiency achieved through oscillating magnetofection can be elucidated, it may be possible to further improve these effects, either by modifying the current protocols or potentially modifying the magnetofection device. It is suggested that static magnetofection does not alter the

mechanisms of vector uptake by cells, but merely reduces the time taken for particles to come into contact with adherent cells, and possibly prolongs contact time;[161,185] endocytotic mechanisms remain the proposed method of cellular uptake leading to gene delivery.[186] Based on this, there are a number of theories which could possibly explain the enhanced transfection efficiency observed in the case of oscillating magnetofection: (i) An oscillating field may simply move the MPs laterally (in these experiments, with an amplitude of 200 nm), such that particles in a cell-free area are brought into contact with cells, increasing the likelihood of each particle coming into contact with a cell within a given time. A static magnetic field model predicts that magnetic particles (>10 nm diameter) will accumulate at the centre of a culture well (due to the radial component), potentially with an annulus of slightly greater acuumulation surrounding it (due to the axial component). Therefore, incorporating an oscillating magnetic field may be predicted to overcome these accumulation biases, resulting in a more uniform dispersion of particles.[298] (ii) An oscillating field may cause MPs to distort or stimulate the cell membrane such that endocytosis is more likely to occur.[173,311] It is not clear whether this effect would require that particles be bound (specifically or non-specifically) to the membrane, or whether unbound MPs pulled onto the cell surface by the magnetic field and subsequently manipulated by an oscillating field can have a stimulatory effect.[172] (iii) It may be the case that an oscillating field alters intracellular processing of MPs, for example disrupting endosomal processing and facilitating endosomal escape.[172]

Kamau *et al.* have experimented with a pulsating electromagnetic field approach, showing greatly enhanced MP-mediated transfection of the HeLa cell line.[312] They report that pre-sedimentation using a static magnet followed by the application of a pulsating magnetic field produced optimal results, significantly enhancing efficiency compared to a static field alone, whereas application of a pulsed field followed by a static field

significantly underperformed compared to a static field alone, although still producing greater transfection than seen in the absence of a field. Application of the pulsed field is thought to produce both horizontal (0.75 Hz, 1.5 cm amplitude) and vertical oscillations (50 Hz) of the MPs. The particle movements induced by these oscillations presumably underpin the mechanism by which transfection efficiency is increased by the pulsed field, and these effects are observed after a 10 min exposure to magnetic fields, lending support to the idea that membrane stimulation by MPs in a dynamic magnetic field leads to enhanced cellular uptake, rather than a post-uptake intracellular event. It should be noted that a 5 min exposure to the magnetic field raised the temperature at the surface of the device from 37°C to 42.5°C, which is potentially damaging to cells, but the authors do not report any toxicity data. Similar heating effects have not been observed using the protocols reported here.

The ultimate measure of gene therapy and cell transplantation therapies will be based on functional recovery, or at least inhibition of disease progression, but it remains vital to investigate all possible indications of toxicity or abnormality due to MP and magnetofection applications. With respect to the use of magnetofection, the application of a magnetic field has been reported to affect cells, for example by causing alignment of the cytoskeletal protein F-actin in human fibroblasts exposed to 350 mT for 30 min.[135] However, a review by Smith *et al.* reports that the majority of studies showing these effects have investigated prolonged field exposures (up to 60 h) and often greater field strengths (up to 8 T, compared to 421 mT used here).[313] No obvious effects of magnetic fields on OPCs were observed here, but as microarray analyses of cells exposed to MPs (Fe_3O_4 core of 6 nm diameter, gold coated) demonstrated significant changes in gene expression in the presence of a magnetic field versus absence of a field,[313] it will be of interest to perform

similar microarray analyses of magnetofected OPCs, and also OPCs exposed to MPs with a variety of physico-chemical characteristics.

3.4.6 Safety profiles of nanoengineered OPC transplant populations can be assayed using cerebellar slices: potential refinements of the approach using injury models

Having shown that the magnetofection protocol developed here is safe for OPCs on culture plastic, a more rigorous analysis of cellular behaviour was performed by transplanting modified OPCs onto organotypic neural slices, as a bridge between *in vitro* isolated cell culture and *in vivo* transplantation studies. It should be noted that confocal microscopy demonstrated that transplanted cells were not merely using the slices as a substrate, but could migrate into the slices and integrate into the tissue, shown by the presence of GFP^+ cells beneath the surface layer of cells. The normal behaviour of the modified cells demonstrates the safety of the magnetofection protocols developed in this study and highlights both the potential of the MP platform for clinical translational applications, and the utility of organotypic neural slice cultures to function as 'host' tissue to evaluate cell therapies when used in conjunction with nanotechnology platforms.

The data presented here demonstrate the potential for cerebellar slice cultures in particular, and organotypic CNS slice cultures in general, to serve as a high-throughput screening technique for assessing cell transplant populations. The clinical relevance of this approach can be greatly improved by developing injury/disease models in these slices. Remyelination strategies can be tested by inducing demyelinating lesions in slices, for example by focal injection of ethidium bromide or by adding demyelinating agents to the

culture media (*e.g.* lysolecithin).[314] Furthermore, a number of severely debilitating *in vivo* neurological injury/disease models use animals with severely restricted life expectancy. The slice model technique provides the possibility of establishing organotypic cultures from such animals at an early age, minimising suffering and prolonging the time course over which the relevant pathology can be studied.

Having established that OPCs derived from a primary source can be labelled and transfected using MPs, in the following chapter the capacity for *oligodendrocytes* to be labelled and transfected using Sphero MPs and Neuromag MPs, respectively, will be assessed. These data will be compared with the OPC data in this chapter and Chapter 2, to provide the first systematic intra-lineage comparison of MP-handling.

3.4.7 Conclusions and future directions

The MP platform has significant potential for the genetic engineering of OPCs derived for cell therapies. Further, the slice model approach can offer a simple, high throughput assay to evaluate the survival and regenerative properties of nano-engineered transplant populations. A number of questions have been raised during the course of this study, and further work to enhance MP-based gene delivery methods will need to address a number of issues: (i) To optimise delivery of therapeutic gene sequences, the plasmids will need to be engineered to produce constructs that contain only therapeutic gene sequences and the elements necessary for transcription, thereby minimising their overall size, with the aim of enhancing transfection efficiency. Additionally, the development of alternative transfection-grade MPs (including those with a range of surface coatings and geometries) warrant further investigation, in order to identify physico-chemical parameters that may allow for the attachment and the delivery of larger plasmids and/or greater copy numbers.

Such work will be critically dependent on multidisciplinary collaborations between materials scientists and biologists, and need to be informed by a detailed understanding of the chemical interactions at the organic-inorganic hybrid interface of magnetic particles and biomolecules (for example the associations of large versus small plasmids with the particle surface and their implications for DNA attachment and intracellular release), an area where little information currently exists. (ii) In terms of the magnetofection conditions used, further work will need to test various permutations of oscillation frequencies and amplitudes. The feasibility of combining a repeat transfection ('multifection') approach in conjunction with magnetofection (*i.e.* a 'magneto-multifection' approach)[163] has also not been tested with OPCs to date. As this would involve multiple manipulations, rigorous toxicity testing must be employed to evaluate their potential in the translational context. (iii) To evaluate the remyelinating potential of OPCs genetically modified using MPs, the modelling of demyelinating disease models warrant investigation in cerebellar slice cultures warrants investigation, as this approach can offer a powerful alternative to *in vivo* models. As an example, brief exposure of rat cerebellar slices to the gliotoxin lysolecithin in slice medium at 7 DIV results in extensive myelin damage/loss in slices, but spares Purkinje cell nerve fibres.[314] Limited subsequent remyelination occurs, mimicking many aspects of MS lesions,[4,38,78,315] providing a valuable system in which to study various therapeutic interventions, including transplantation of engineered cell populations, with assessment of the extent of remyelination. Slice cultures can be processed for ultrastructural analyses of WM tracts utilising techniques such as serial sectioning,[316] stereology and 3-D reconstruction.[259,317] Further, by assembling an upright time-lapse microscope, with a temperature- and CO_2-controlled incubation chamber, it will be possible to monitor cells transplanted onto slices in real time and obtain far more accurate data regarding the migratory capacity of the engineered cells, for example, than can be

obtained from fixed tissue. Electrophysiological recordings can be performed in neural slices, including with cerebellar slices, although they are more readily achieved in slices of spinal cord, which can be prepared with long, laminar sections, preserving extensive axonal tracts[73] within which transecting or crush lesions can be induced to simulate SCI.[318] Recordings can be made pre- and post-lesioning, and used to evaluate functional improvement following experimental treatments, including transplantation of modified OPCs, highlighting the versatility of the slice approach for use in neural tissue engineering studies.[b]

[b] Most of the data in sections 3.3.1 – 3.3.3 and 3.3.5 – 3.3.7 have been published. The article is reproduced here as appendix 4.

Chapter 4: Labelling and gene delivery applications of MPs in oligodendrocytes: An intralineage comparison with OPCs

4.1 Introduction

Oligodendrocytes are key targets of disease processes in a range of pathologies such as demyelination conditions and traumatic/hypoxic injury,[7,319] both during adulthood and in a range of neurodevelopmental disorders. Understanding the biology of these cells (for example, elucidating the factors/genes that participate in oligodendrocyte development, their associations with axons and the genesis of myelin) along with the development of effective neuroprotective strategies to promote oligodendrocyte survival, are key goals for regenerative medicine.[290]

Such research into the biology of oligodendrocytes is heavily reliant on the ability to effectively deliver genes to oligodendrocyte populations. In this context, and as with OPCs, viral transduction techniques are commonly employed for gene delivery to oligodendrocytes (both *in vivo* and *in vitro*). As discussed in section 1.7.3, these methods are associated with significant drawbacks, and the direct cytopathic effects associated with viral transduction of oligodendrocytes represent a significant obstacle to progress in understanding oligodendrocyte biology.[108,111,114] Further, the few reported attempts to mediate gene delivery to oligodendrocytes *in vitro* typically report low efficiency, including for example, retroviral transduction.[108,111] Indeed, one *in vivo* study comparing adeno-, retro- and lenti-viral systems found no evidence of oligodendrocyte transduction even at high viral titres.[320] By contrast, another report found evidence that oligodendrocytes can be transduced *in vivo* using adenoviruses, but that gene delivery is complicated by cytopathic effects.[114]

Such findings have added to the demand for the development of nonviral gene delivery techniques, and several such methods have been tested in recent years to genetically modify oligodendrocytes. However, commonly used nonviral transfection

methods such as calcium phosphate precipitation and electroporation yield no/low transfection in oligodendrocytes and are associated with high levels of cell loss.[108,111] Delivery methods such as the gene gun approach and lipofection have yielded the greatest transfection levels in the literature (approximately 20% and 10%, respectively) and appear to be relatively safe, although detailed toxicity data were not provided.[111] However, these transfection levels can still be considered to be relatively low from the point of view of basic research and translational applications. Therefore, the development of an alternative nonviral technique for safe and effective gene delivery to oligodendrocytes is a desirable goal.

While the previous chapters have shown that OPCs (*i.e.* the parent cells of oligodendrocytes) can be labelled and transfected using MPs, it is not clear whether the MP-handling characteristics displayed by the precursor populations will be representative of MP-handling by their daughter cells, owing to the substantial biological differences between these cell types. Cellular morphology alters extensively as OPCs progress through the individual stages of the oligodendroglial lineage, changing from a bipolar cell with very limited membrane, to a highly branched oligodendrocyte, with a complex highly branched morphology, producing extensive quantities of myelin membrane.[9,321,322] Progression through the oligodendroglial lineage, from the highly migratory, mitotic precursor form to the fully differentiated post-mitotic, non-migratory mature oligodendrocyte, is also associated with a series of antigenic shifts, with characteristic patterns of marker expression being associated with each phase of maturation (section 1.2).[7,9,29]

4.1.1 Knowledge gap: Do intralineage differences exist in MP handling between OPCs and oligodendrocytes?

Many of the differences described above between OPCs and oligodendrocytes in relation to their developmental status, have the potential to affect their handling of MPs and indeed synthetic materials in general. For example, the extent of myelin production by oligodendrocytes has been estimated to peak at three times the cell's own weight per day, and to reach a total of one hundred times the weight of the cell body.[7] As a consequence, the production and exocytosis of myelin constituents dominates the metabolic activity and intracellular trafficking mechanisms of these cells.[7] It not clear what effect, if any, this will have on MP-based uptake and transfection in these cells, processes that are critically dependent on endocytotic uptake. There are few studies available in the literature in relation to such issues. One study reports that limited MP-labelling of $GalC^+$ oligodendrocytes was achieved in an undefined mixed neural culture,[222] but MP handling has not been studied in a purified/enriched oligodendrocyte population. Further, it might be expected that oligodendrocytes would exhibit lower MP-mediated transfection efficiency than OPCs, as post-mitotic cells are typically considered intransigent to gene delivery,[177] but few systematic comparisons of this nature exist in the context of nonviral gene delivery in oligodendroglial lineage cells. A critical point to note here is that it is currently unknown if differentiated oligodendrocytes are amenable to MP-mediated transfection, and therefore the effectiveness of the magnetofection methodologies that enhanced transfection efficiency in OPCs (section 3.3.2) is also unknown.

4.1.2 Objectives

The first part of this chapter will address the following questions using the 'test' (Sphero) MP characterised in sections 2.2 and 2.3.2:

(i) Do oligodendrocytes exhibit uptake of MPs?

(ii) Is the rate and extent of MP uptake by oligodendrocytes time- and concentration-dependent?

(iii) Does exposure to these MPs result in acute cytotoxicity in oligodendrocytes?

(iv) Do MP uptake dynamics in oligodendrocytes differ from those in OPCs?

The second part of this chapter will assess the feasibility of MP-mediated gene delivery to oligodendrocytes, using the transfection grade MPs described in section 3.2 (Neuromag) to address the following questions:

(i) Do MP-plasmid complexes, with and without applied magnetic fields, have acute toxic effects on oligodendrocytes?

(ii) Can MPs mediate gene delivery to oligodendrocytes?

(iii) Does static/oscillating magnetofection result in enhanced MP-mediated transfection efficiency in oligodendrocytes?

(iv) Does the amenability of oligodendrocytes to MP-mediated transfection differ from that of OPCs?

4.2 Methods and materials

Oligodendrocyte cultures: Please see section 2.2 for details of the derivation of OPCs from mixed glial cultures. Cultures intended for Sphero uptake studies and transfection studies were plated in parallel to OPC cultures described in sections 2.2 and 3.2, respectively. By plating these OPC and oligodendrocyte cultures in parallel: (i) the purity of the OPC cultures corresponds to the initial purity of the oligodendrocyte cultures, and (ii) confounding biological variability is minimised for the purposes of drawing intralineage comparisons. OPCs were plated on coverslips (0.3 ml/well, at 3 x 10^4 cells/cm^2) in Sato differentiation medium (see section 2.2) and maintained for 7 days (before uptake experiments) or 12 days (before transfection experiments) to generate oligodendrocyte cultures (50% medium changes every 2 – 3 days). After the uptake experiments were performed, the culture time for transfection experiments was extended in an attempt to produce cultures with a greater percentage of MBP^+ cells. Oligodendrocyte differentiation has been reported to be largely complete within 7 – 9 days (*in vitro*), as assessed by the limited changes in gene expression from this point onwards.[323]

Sphero uptake experiments: Oligodendrocytes were treated identically to OPCs, as described in section 2.2, but incubations were conducted in Sato medium.

Transfection experiments: These were performed as described for OPCs in section 3.2, but using Sato medium. Preliminary experiments tested transfection with a 1.0x dose which resulted in obvious toxicity. Therefore the 0.1x dose developed for use with OPCs was used for all data presented here.

Culture purity analysis: The purity of each culture was determined by scoring at least 200 DAPI-stained nuclei for coincidence with MBP staining in fluorescence micrographs.

Assessment of MP-labelling and extent of uptake: These data were obtained in identical fashion to that described for OPCs (section 2.2), except that MBP replaces A2B5. Cells were scored as exhibiting 'low', 'medium' or 'high' levels of MP accumulation by comparing the extent of MP fluorescence with the average area of an oligodendrocyte nucleus, in an identical manner to that described in section 2.2 (OPC and oligodendrocyte nuclei are of comparable size). A minimum of 100 nuclei and three microscopic fields were assessed per treatment group.

Assessment of transfection efficiency: These data were obtained in identical fashion to that described for OPCs (section 3.2), except that MBP replaces A2B5. A minimum of 100 nuclei and three microscopic fields were assessed per treatment group.

Toxicity assessment (uptake and transfection): Fluorescence microscopy was used to count the pyknotic and total (healthy plus pyknotic) nuclei per microscopic field, as measures of MP-related toxicity in both uptake and transfection experiments. For transfection experiments, the percentage of cells expressing MBP was also determined, in order to assess whether there was any MP-related alteration in the expression of this protein, which is a major constituent of myelin. A minimum of 200 nuclei and five fields were assessed for every condition.

Statistical analysis: Data were analysed using GraphPad Prism statistical analysis software. Data are expressed as mean ± SEM. The number of experiments (*n*) refers to the number of mixed glial cultures from which the initial OPC cultures were derived, with

each primary culture being established from a different rat litter. To determine time- and concentration-dependence of the percentage of oligodendrocytes with (i) MP-labelling, (ii) perinuclear MPs, (iii) 'low' levels of MP accumulation or (iv) 'medium' levels of MP accumulation, a two-way ANOVA was performed with Bonferroni's post-tests comparing each concentration with 2 μg/ml at the same time-point and comparing each 4 and 24 h data-point with the same concentration at 1 h. For toxicity analyses, two-way ANOVA was performed at each timepoint to compare (i) the nuclei per field and (ii) percentage of pyknotic nuclei across all MP concentrations. For comparison of (i) the transfection efficiency, (ii) the percentage of MBP^+ cells, (iii) the number of nuclei, and (iv) the percentage of pyknotic nuclei, a one-way ANOVA was performed including each field condition, with Bonferroni's post tests performed for (i). For intralineage comparisons, uptake data for oligodendrocytes were collated with data for OPCs (section 2.3.4; identical Sphero concentrations and incubation times). Transfection data for oligodendrocytes were collated with data for OPCs (section 3.3.2; identical Neuromag-plasmid dose, incubation time and oscillating field protocols). A two-way ANOVA was performed at each time-point to compare the percentage of MP-labelled OPCs with the percentage of MP-labelled oligodendrocytes across all concentrations, with Bonferroni's post tests to compare OPC versus oligodendrocyte data at each concentration. Two-way ANOVA was also used at each time-point to compare the percentage of OPCs exhibiting 'medium'-to-'high' levels of MP accumulation with the percentage of oligodendrocytes exhibiting the same accumulations, for all concentrations. A two-way ANOVA was performed to compare the effects of different field conditions and cell type on transfection efficiency, with Bonferroni's post-tests to compare OPC v oligodendrocyte data for each field condition.

4.3 Results

4.3.1 Oligodendrocyte culture characterisation

Oligodendrocytes were derived from high purity parent OPC cultures, and the majority of cells stained positive for MBP (**Figure 1**). For Sphero uptake studies, 70.3 ± 1.3% of cells were MBP^+ (n = 4); for transfection studies, 75.9 ± 5.4% of cells were MBP^+ (n = 3). Reports typically show that multiple antigenically-distinct stages of the oligodendroglial lineage are typically present in such cultures,[324] and phase contrast microscopy showed that ~80% of MBP^- cells exhibited multi-processed morphologies typical of early oligodendrocytes (see **Figure 1** for examples). Approximately 5% of cells were identified by phase contrast microscopy as microglial contamination, consistent with observations in OPC cultures. Oligodendroglia were phase-bright, with multipolar morphologies, including the complex highly-branched, membrane elaborating morphologies typical of mature oligodendrocytes **(Figure 1)**.

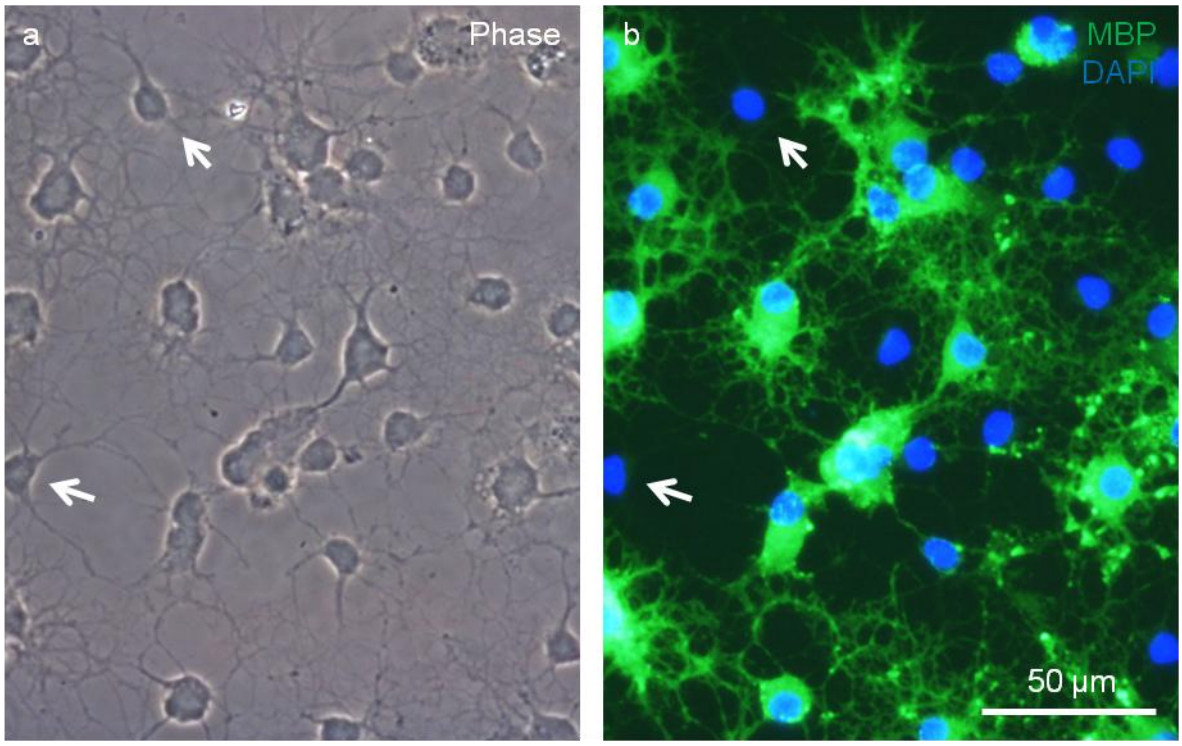

Figure 1: Characterisation of oligodendrocyte cultures. (a) *Representative phase-contrast micrograph of an oligodendrocyte culture, showing multipolar cells with branching processes. (b) Counterpart fluorescence micrograph to (a), showing oligodendrocytes stained for the late-stage oligodendrocyte marker MBP. Arrows indicate the same MBP$^-$ cells in each image, with morphologies typical of early oligodendrocytes. Note the presence of multiple processes under phase microscopy.*

4.3.2 MP uptake in oligodendrocytes is time- and concentration-dependent

Fluorescence microscopy, including z-stack and confocal analyses, confirmed the presence of intracellular Sphero MPs within oligodendrocytes, including perinuclear accumulations (**Figure 2**; confocal images not shown). The percentage of labelled oligodendrocytes was time- and concentration-dependent, with the greatest dose and exposure tested resulting in MP-labelling of *ca.* 45% of MBP$^+$ cells **(Figure 3a)**. MP

concentrations of 20 and 50 µg/ml resulted in the labelling of a significantly greater percentage of MBP^+ cells than 2 µg/ml, at all time-points. Heterogeneity in the extent of MP-uptake by individual cells was apparent, and this was assessed semi-quantitatively using the same criteria employed for OPCs (**Table 1**; criteria detailed in section 2.2). Under all conditions, the majority of MP-labelled cells were judged to exhibit a 'low' level of particle accumulation. At 4 and 24 h, oligodendrocytes with 'medium' levels of MP accumulation were observed, but 'high' levels were observed only at the greatest MP concentration and incubation time **(Table 1)**. Analysis by two-way ANOVA demonstrated a time-dependent effect on the percentage of labelled cells exhibiting perinuclear MPs **(Figure 3b)**.

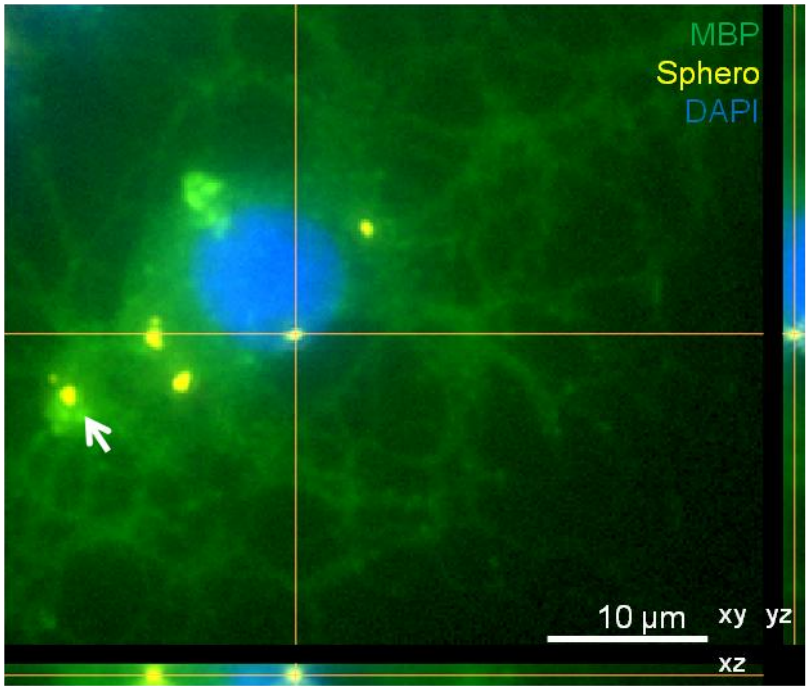

Figure 2: Uptake of Sphero MPs by oligodendrocytes. *Z-stack fluorescence analysis of a Sphero-labelled MBP^+ oligodendrocyte (5 µg/ml, 4 h). Nile red fluorescence indicates the presence of MPs in cytoplasmic and perinuclear (crosshairs) accumulations. White arrow indicates extracellular MPs amongst processes.*

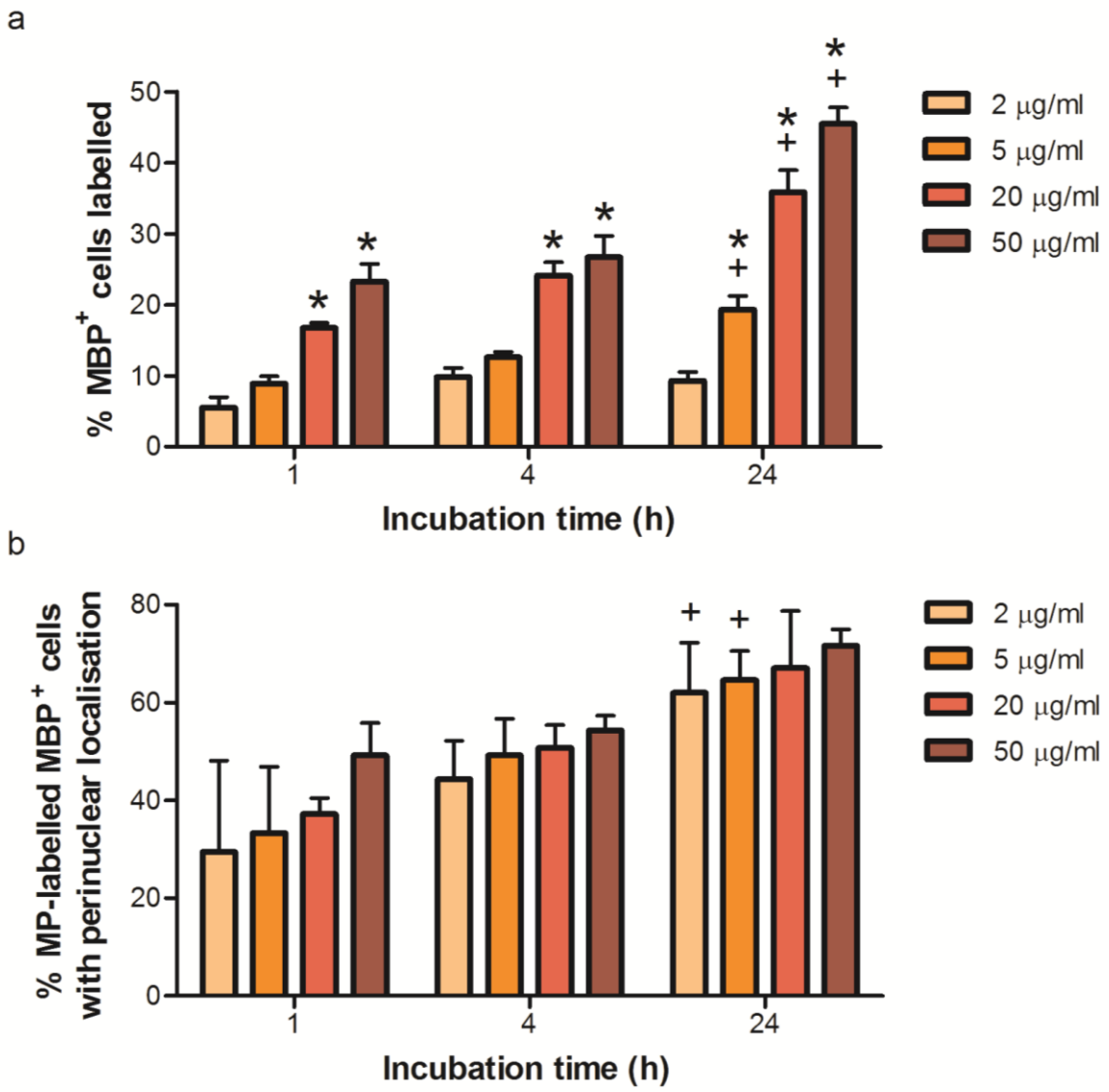

Figure 3: Uptake of Sphero MPs by oligodendrocytes is time- and concentration-dependent, and perinuclear localisation is time-dependent. *(a) Bar chart showing the time- and concentration-dependent labelling of oligodendrocytes with MPs. The percentage of labelled cells is related to both particle concentration ($F_{3,36} = 92.8$; $p < 0.001$) and incubation time ($F_{2,36} = 52.7$; $p < 0.001$; two-way ANOVA; $n = 4$). (b) Bar chart showing that the percentage of oligodendrocytes with perinuclear particles is related to incubation time ($F_{2,36} = 9.95$; $p < 0.001$) but not MP concentration ($F_{3,36} = 1.08$; $p = 0.161$; two-way ANOVA; $n = 4$). For (a) and (b): *$p < 0.05$ versus 2 µg/ml at the same time-point; $^{+}p < 0.05$ versus the same concentration at 1 h (Bonferroni's post-tests).*

Table 1. Semi-quantitative analysis of the extent of Sphero MP uptake by oligodendrocytes.

Incubation time (h)	MP concentration (µg Sphero/ml)	Level of particle accumulation in MP-labelled oligodendrocytes (%)		
		'Low'	'Medium'	'High'
1	**2**	100.0	0.0	0.0
	5	100.0	0.0	0.0
	20	100.0	0.0	0.0
	50	100.0	0.0	0.0
4	**2**	100.0	0.0	0.0
	5	96.2 ± 4.4	3.8 ± 4.4	0.0
	20	93.5 ± 0.4	6.5 ± 0.4	0.0
	50	85.1 ± 3.6†	14.9 ± 3.6**	0.0
24	**2**	98.2 ± 2.1	1.8 ± 2.1	0.0
	5	95.0 ± 5.8	5.0 ± 5.8	0.0
	20	91.6 ± 5.6	8.4 ± 5.6	0.0
	50	86.0 ± 5.4	12.8 ± 5.5*	1.2 ± 1.0

$^{*}p < 0.05$, $^{**}p < 0.01$, versus same concentration at 1 h; $^{\dagger}p < 0.05$, versus 2 µg/ml at the same time-point (Bonferroni's post-tests); $n = 4$.

4.3.3 Sphero MPs are not acutely toxic to oligodendrocytes

At all concentrations and incubation times tested, no significant effects of Sphero MPs were observed in oligodendrocyte cultures with respect to (a) cell adherence, as judged by the number of DAPI-labelled nuclei (either healthy or pyknotic) per microscopic field (concentration: $F_{4,45}$ = 0.913, ns; time: $F_{4,45}$ = 0.569, ns; two-way ANOVA; n = 4; **Figure 4a**), and (b) cell death, as judged by the percentage of cells exhibiting pyknotic nuclei (*i.e.* shrunken or fragmenting morphologies; concentration: $F_{4,45}$ = 0.598, ns; time: $F_{4,45}$ = 0.751, ns; two-way ANOVA; n = 4; **Figure 4b**). For all concentrations and incubation times, oligodendrocyte cultures appeared morphologically similar to controls at 24 h.

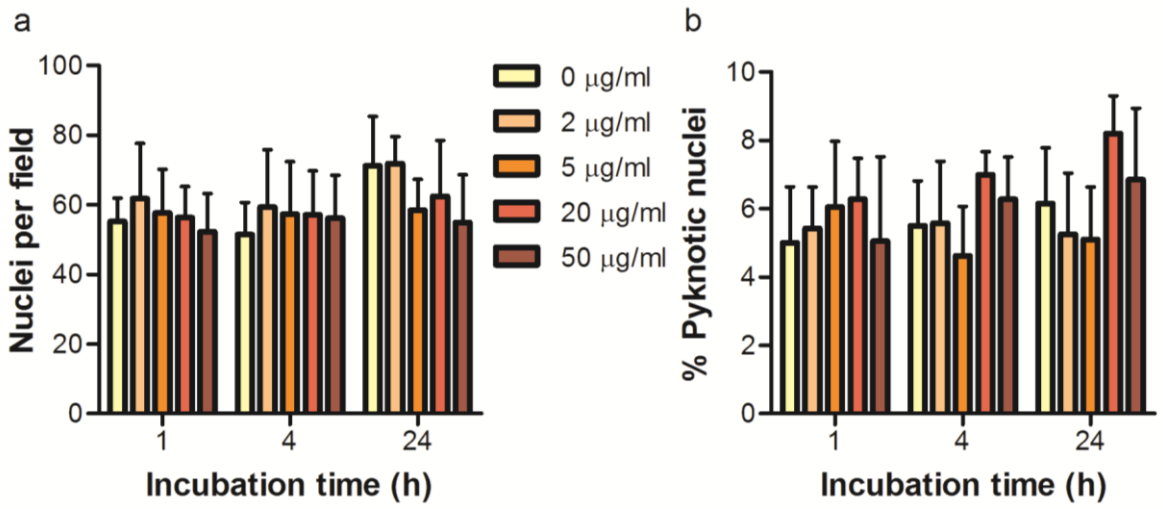

Figure 4: Incubation of oligodendrocytes with Sphero MPs at a range of concentrations does not result in acute cytotoxicity. *Bar graphs of oligodendrocyte time course experiments showing (a) total (healthy plus pyknotic) nuclei per microscopic field, and (b) percentage of nuclei with pyknotic features. No significant differences were found in these parameters either in relation to particle incubation time or particle concentration (*n = *4).*

4.3.4 OPCs are more readily labelled with MPs and show larger MP accumulations than oligodendrocytes

A comparison (two-way ANOVA) of the percentage of MP-labelled OPCs with MP-labelled oligodendrocytes showed a cell type-dependent effect at 4 h ($F_{1,24}$ = 23.5; p < 0.001) and 24 h ($F_{1,24}$ = 7.6; p < 0.05), and a concentration-dependent effect at 1 h ($F_{3,24}$ = 64.7; p < 0.001), 4 h ($F_{3,24}$ = 31.8; p < 0.001) and 24 h ($F_{3,24}$ = 26.9; p < 0.001; n = 4 cultures; **Figure 5a** shows 4 h data). Similar statistical comparisons of the percentage of OPCs and oligodendrocytes exhibiting 'medium'-to-'high' levels of MP accumulation showed both cell type-dependent (1 h: $F_{1,24}$ = 28.8, p < 0.001; 4 h: $F_{1,24}$ = 4.30, p < 0.05) and concentration-dependent (1 h: $F_{3,24}$ = 28.8, p < 0.001; 4 h: $F_{3,24}$ = 12.4, p < 0.001; 24 h: $F_{3,24}$ = 8.72, p < 0.001) effects (n = 4; **Figure 5b** shows 4 h data). Also, for cells scored as demonstrating 'low' levels of uptake, MP accumulations were typically larger in OPCs than in oligodendrocytes (compare **Figure 2** in this chapter with Figure 6b in section 2.3.4, which both show typical levels of MP accumulation, and also see the direct fluorescence and electron microscopy comparisons in sections 5.1 and 5.3.6). Furthermore, in both OPC and oligodendrocyte cultures, cells at more advanced stages of oligodendrocyte differentiation (as judged by number and complexity of processes), contained smaller accumulations of particles than cells with relatively immature and less branched morphologies. This suggests an inverse relationship between the extent of differentiation and capacity for MP uptake in oligodendroglial lineage cells.

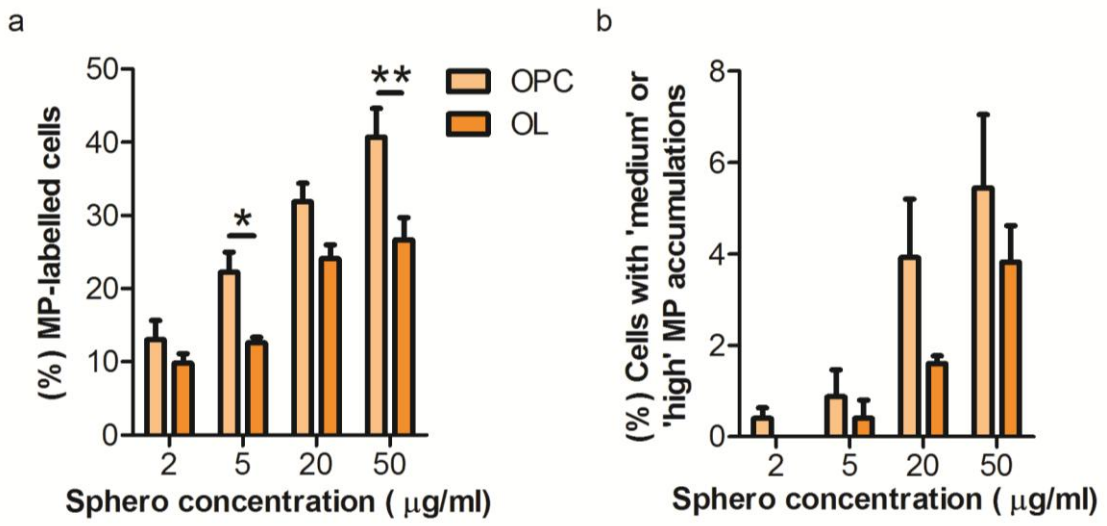

Figure 5: OPCs exhibit a greater percentage of labelled cells than oligodendrocytes. *Bar graphs illustrating (a) the percentage of MP-labelled OPCs and oligodendrocytes and (b) the percentage of OPCs and oligodendrocytes exhibiting 'medium'-to-'high' MP accumulations following 4 h incubation with various concentrations of Sphero particles. Note that a greater percentage of OPCs are labelled than oligodendrocytes at all data-points (*p < 0.05, **p < 0.01; Bonferroni's post tests;* n = *4).*

4.3.5 MP-mediated transfection of oligodendrocytes: A safe magnetofection protocol has been developed

No toxicity was apparent with a 0.1x Neuromag-plasmid dose, under any magnetic field condition, as the percentage of cells which were MBP^+ (MPs: $F_{1,14}$ = 1.76, ns; field: $F_{3,14}$ = 0.297, ns; two-way ANOVA; n = 4; **Figure 6a**), the total healthy nuclei per microscopic field (MPs: $F_{1,16}$ = 0.116, ns; field: $F_{3,16}$ = 0.149, ns; two-way ANOVA; n = 4; **Figure 6b**) and the percentage of nuclei exhibiting pyknosis did not significantly differ from control cultures (MPs: $F_{1,16}$ = 0.0331, ns; field: $F_{3,16}$ = 0.431, ns; two-way ANOVA; n = 4; **Figure 6c**).

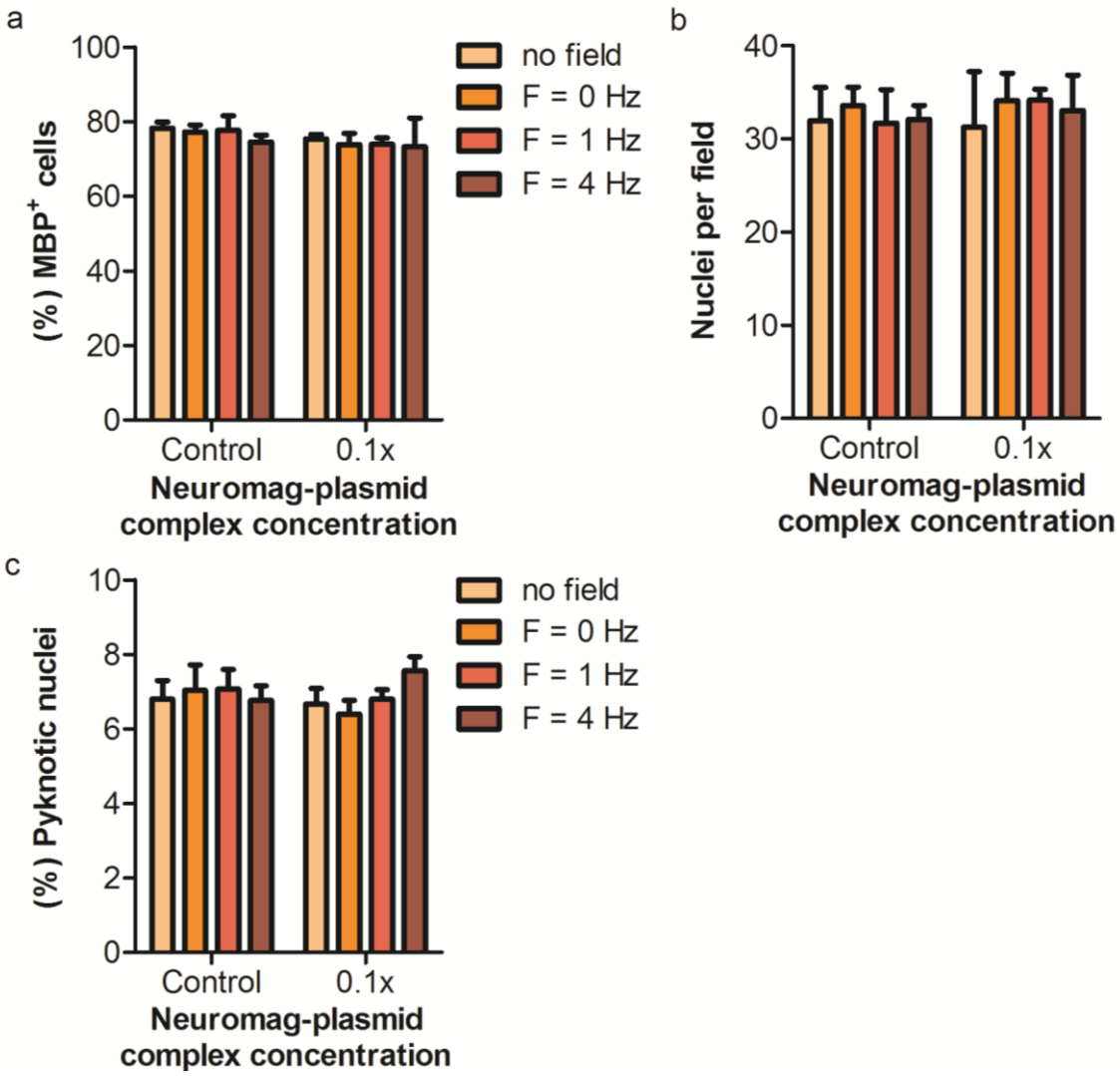

Figure 6: The magnetofection protocols developed for OPCs are also safe for oligodendrocytes. *OPC cultures were maintained in Sato medium for 12 days to produce oligodendrocyte cultures, then transfected (0.1x) and fixed at 48 h post-transfection. (a) Bar graph indicating the percentage of cells staining for the late-stage oligodendrocyte marker MBP for all field conditions tested. (b) Bar graph showing average healthy plus pyknotic nuclei per microscopic field in oligodendrocyte cultures for all fields tested. (c) Bar graph illustrating the percentage of all nuclei that were pyknotic, as judged by DAPI staining. Note that all treatment conditions are similar to controls for all parameters.* n *=3 for all graphs.*

4.3.6 Oligodendrocytes are amenable to MP-mediated gene delivery, which is enhanced by magnetofection

Transfected oligodendrocytes (GFP^+/MBP^+) were observed in oligodendrocyte cultures (**Figure 7a**). The extent of MBP expression in GFP^+ cells ranged from strong expression that matched the extent of GFP expression throughout the cell, to faint expression limited to patches of the cell **(Figure 7b-d)**. Some GFP^+/MBP^- cells were observed and these cells showed morphologies typical of earlier stages of the oligodendroglial lineage. All stages of the oligodendrocyte lineage were observed to have been transfected, including those with a small number of branches and those with highly branched complex morphologies **(Figure 7a-d)**. Compared with basal conditions (no magnetic field; transfection efficiency = 1.9 ± 0.1%), application of a static or 4 Hz oscillating magnetic field increased transfection efficiency between two- and three-fold to 4.9 ± 1.1% (F = 0 Hz) and 6.3 ± 0.6% (F = 4 Hz; **Figure 8**). Although there was a trend towards higher transfection levels at F = 4 Hz, this was not statistically significantly compared with the F = 0 or 1 Hz conditions.

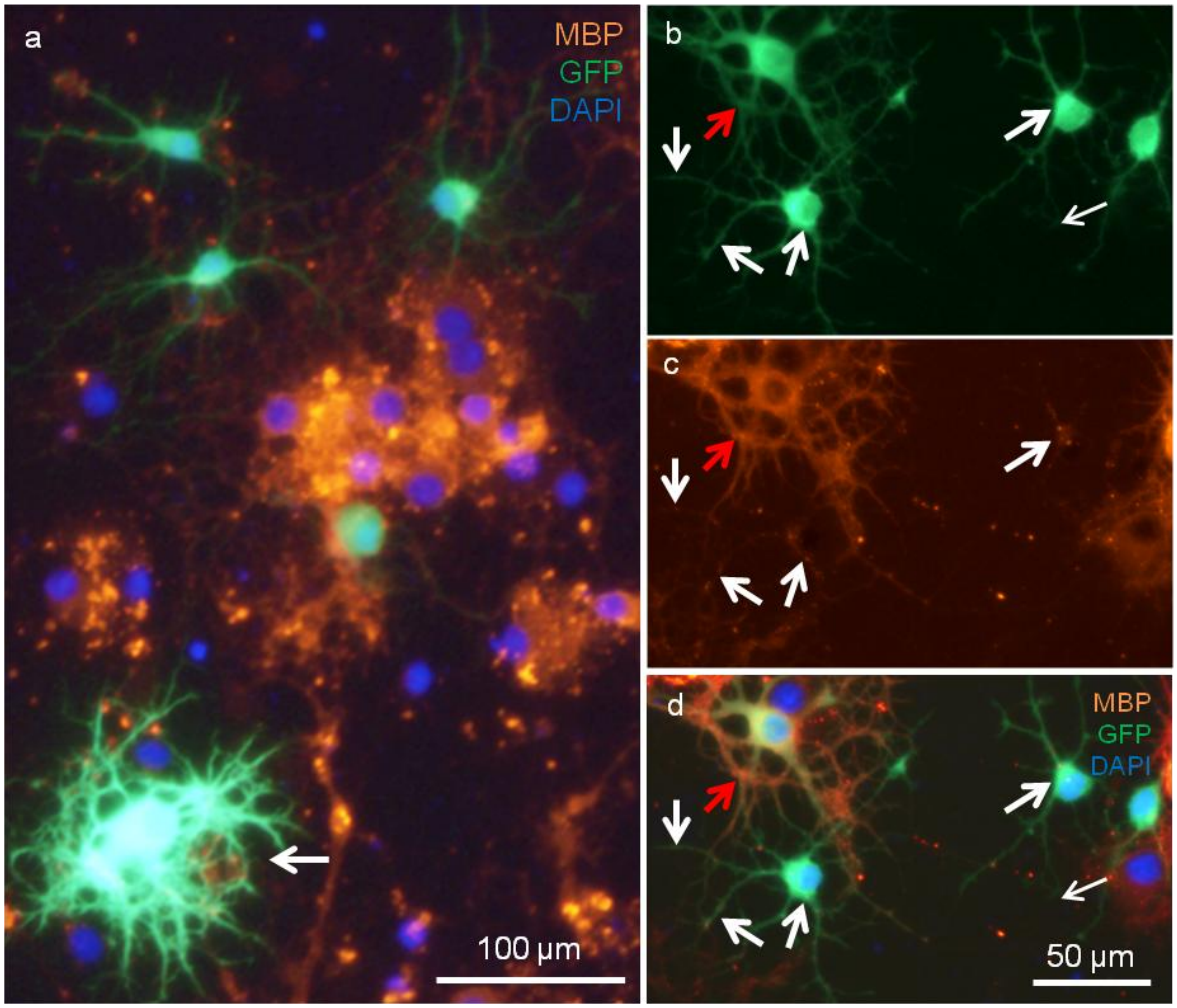

Figure 7: MP-mediated gene delivery to oligodendrocytes. *Fluorescence micrographs of oligodendrocyte cultures 48 h post-magnetofection (0.1x; F = 4 Hz). (a) Oligodendrocyte culture containing cells with various oligodendroglial morphologies, including the highly branched morphology typical of oligodendrocytes (arrow), with most cells staining for MBP. Note that GFP expression is present throughout the cell body and processes of magnetofected cells. (b) Several GFP^+ cells are shown in an oligodendrocyte culture, at various stages of differentiation as judged by bipolar/multipolar status and number of processes. (c) Counterpart fluorescence micrograph to (b) showing MBP expression. (d) Merged image of (b) and (c) showing one GFP^+ cell with clear MBP expression throughout the cell (red arrow), two GFP^+ cells with faint MBP expression (white arrows indicate regions of MBP expression), and a GFP^+/MBP^- cell. Note also two MBP^+/GFP^- cells.*

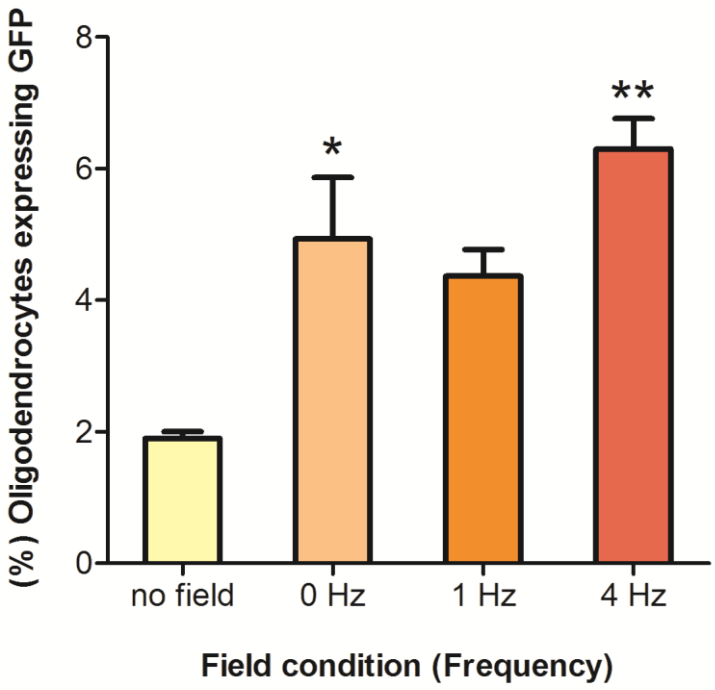

Figure 8: Static and oscillating magnetofection enhances MP-mediated gene delivery to oligodendrocytes. *Bar graph illustrating transfection efficiencies achieved in oligodendrocyte cultures, for all field conditions tested, as judged by the percentage of* MBP^+ *cells expressing GFP. Analysis by one-way ANOVA indicated a field-dependent effect (*$F_{3,8} = 10.7$; $p < 0.01$; $n = 3$*). The F = 0 and 4 Hz magnetic field conditions significantly enhanced transfection levels compared to the no field condition (*$*p < 0.05$, $**p < 0.01$*; Bonferroni's post-tests).*

4.3.7 Oligodendrocytes are less amenable than OPCs to MP-mediated transfection

For all field conditions tested, oligodendrocytes exhibited lower transfection efficiency than OPCs, although this was not shown to be significant for the no field condition **(Figure 9)**. For each field condition, OPC transfection efficiency was typically three-fold greater than oligodendrocyte transfection efficiency **(Figure 9)**.

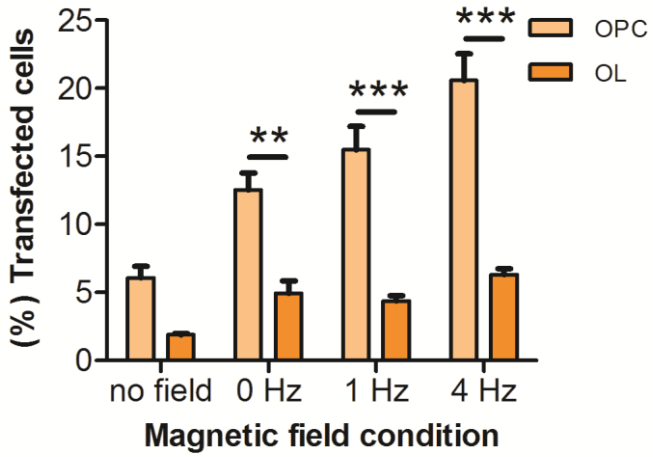

Figure 9: Oligodendrocytes are less amenable than OPCs to magnetofection. *Bar graph illustrating comparative MP-mediated transfection efficiencies achieved in OPCs and oligodendrocytes, under all magnetic field conditions tested. Analysis by two-way ANOVA indicated a cell type- (*$F_{1,24} = 82.0$; $p < 0.001$*) and a field-dependent effect (*$F_{3,24} = 14.5$; $p < 0.001$*).* **$p < 0.01$, ***$p < 0.001$; *Bonferroni's post tests;* $n \geq 3$.

4.4 Discussion

This is the first comparative analysis of MP-mediated cell labelling and transfection between OPCs and mature oligodendrocytes, and, indeed, the first to address intralineage differences in MP-cell interactions in any cell type. Sphero MPs were taken up by oligodendrocytes in a time- and concentration-dependent manner, without acute toxicity (in agreement with OPC data), but the rate and extent of uptake was more limited than that found in OPCs. It has also been shown for the first time that Neuromag:plasmid complexes successfully transfected oligodendrocytes, with efficiency enhanced by both static and oscillating magnetofection techniques, in broad agreement with findings in OPCs. However, transfection levels achieved were significantly lower than those in OPCs.

The fundamental biological question of how alterations in biological properties of cells during differentiation may influence their interactions with synthetic materials, has never previously been addressed. By exploiting the simple technique of plating sister cultures in different media to promote either proliferation or differentiation of OPCs, two different cell types from the same lineage can be derived. Although from the same lineage, OPCs and oligodendrocytes are recognised as distinct cell types due to the dramatic alterations that take place during the maturation process.[9] The elegant culture model employed here therefore allows the robust dissection of the influence of biological parameters such as proliferation/differentiation status that may govern neural cell-nanomaterial interactions (and consequently, successful nanomaterial uptake/transfection in neural cells), whilst excluding differences in cell behaviour which may be inherent to the *different lineages* of the cell types in question (*e.g.* comparing astrocyte behaviour with microglial behaviour).

4.4.1 MP-based transfection and effects of magnetofection strategies in oligodendrocytes

Use of a range of magnetofection conditions showed that the application of magnetic fields (F = 0 and 4 Hz) could enhance transfection efficiency over the no field condition. However transfection levels achieved using these protocols were considerably lower than that obtained using some other nonviral methods (**Table 2)**. This comparison shows that, so far, the gene gun has demonstrated the greatest transfection efficiency in oligodendrocytes *in vitro.* This method may therefore remain the technique of choice for oligodendrocyte transfection. However, the safety and simplicity of the magnetofection protocol developed here highlights the need for detailed investigation into strategies to further enhance MP-based transfection and magnetofection approaches in oligodendrocytes (for example, by testing a range of transfection grade MPs, varying magnetofection conditions such as different oscillating frequencies applied at a range of amplitudes, or by utilising different magnetofection protocols such as the 'magneto-multifection' protocol as described by Pickard *et al.*,[163] which employs repeated magnetofection procedures).

Table 2: Comparative *in vitro* transfection efficiencies in rat oligodendrocytes (derived from primary sources) for viral and nonviral vectors.

Method	Transgene	Source of cells	Efficiency	Toxicity	Ref
Viral methods					
Retrovirus	*lacZ*	P15 – 20	<0.1%	Data not reported	[111]
Retrovirus (MoMuLV)	*lacZ*	P28 – 42	0%	Data not reported	[108]
Nonviral methods					
Gene gun (gold particles)	*lacZ*	P15 – 20	20%	Data not reported	[111]
Lipofection	*lacZ*	P15 – 20	10%	Data not reported	[111]
Lipofection	*lacZ*	P28 – 42	0%	Data not reported	[108]
Magnetofection (magnetic particles)	*gfp*	P1 – 3	6%	Not significant at established dose	*
Calcium phosphate precipitation	*lacZ*	P28 – 42	<3%	90% cell death	[108]
Calcium phosphate precipitation	*lacZ*	P15 – 20	<2%	"*Most cells died"*	[111]
Electroporation	*lacZ*	P28 – 42	Data not reported	"*Drastic*" cell death	[108]

MoMuLV = Moloney murine leukaemia virus; *lacZ* = *β*-Galactosidase; P# = postnatal day #; gfp = green fluorescent protein; *Reported here.

4.4.2 Intercellular differences in MP uptake and MP-mediated transfection

The observation that it was possible to label a greater percentage of OPCs than oligodendrocytes, with marked differences between the cell types with respect to MP accumulation, suggests that as OPCs differentiate into oligodendrocytes the rate of MP uptake may diminish. It is not clear whether the larger accumulations of MPs seen in OPCs were taken up in a single endocytotic event, or formed inside the cell following uptake of MPs in several events. Oligodendrocytes typically display small MP accumulations, often potentially a single particle (as judged by measurements in fluorescence and electron micrographs; data to be shown in section 5.3.6), suggesting that these cells may not be able to endocytose several MPs in a single endocytotic event. Detailed comparisons of the surface interactions of OPCs and oligodendrocytes with synthetic particles (for example using the OTOTO methodology described in section 2.3.9) would be useful in elucidating such issues.

Mature MBP^+ oligodendrocytes proved to be far less amenable to MP-mediated transfection than $A2B5^+$ OPCs, even under a variety of magnetofection conditions. This reduction in transfection efficiency is consistent with studies using various protocols that suggest that post-mitotic cells are typically less readily transfected than mitotic populations.[178,179] Indeed, for other gene delivery techniques, both viral and nonviral, OPCs are typically more amenable than oligodendrocytes, demonstrating that there are cell-intrinsic differences with respect to the capacity for transfection/transduction. In this context, it should be noted that the task of determining the underlying causes for differences in transfection capability is complicated by the diversity of approaches employed with oligodendroglial cells **(Table 2)**, which exploit different mechanisms of gene delivery. Data derived from cell lines are of little value for discerning differences

between OPCs and oligodendrocytes, as the 'true' differentiation status of such cells is at best difficult to ascertain, and it may not be possible to categorise such cells as either OPCs or oligodendrocytes due to their contradictory morphological, behavioural or antigenic profiles. For example, the OLN-93 cell line is proliferative and described as morphologically resembling bipolar OPCs, yet these cells stain $A2B5^{-}/MBP^{+}$.[244] It is not clear how such cell lines should be categorised within the oligodendroglial lineage, and therefore transfection data obtained using cell lines will be excluded from the following discussion.

4.4.3 Underlying reasons for differences in MP uptake and MP-mediated transfection efficiency

A number of speculations can be made as to the underlying reasons for the differences in MP-handling observed between OPCs and oligodendrocytes, and these have been summarised in **Figure 10**. First, it is not clear which regions of membrane (*i.e.* what proportion/which regions of the cell body and/or cellular processes) are capable of endocytosis. For both OPCs and oligodendrocytes, Sphero particle uptake appears to be restricted to the cell body, as although particles were sometimes observed in association with cellular processes, particularly the extensive oligodendrocyte processes, these MPs were never deemed to be intracellular under either confocal or TEM analysis. This suggests that the total membrane elaborated by the cell is not necessarily reflective of the capacity for particle uptake, as more limited particle uptake was observed in oligodendrocytes than in OPCs, suggesting that a only a small proportion of the oligodendrocyte membrane is capable of endocytosis.

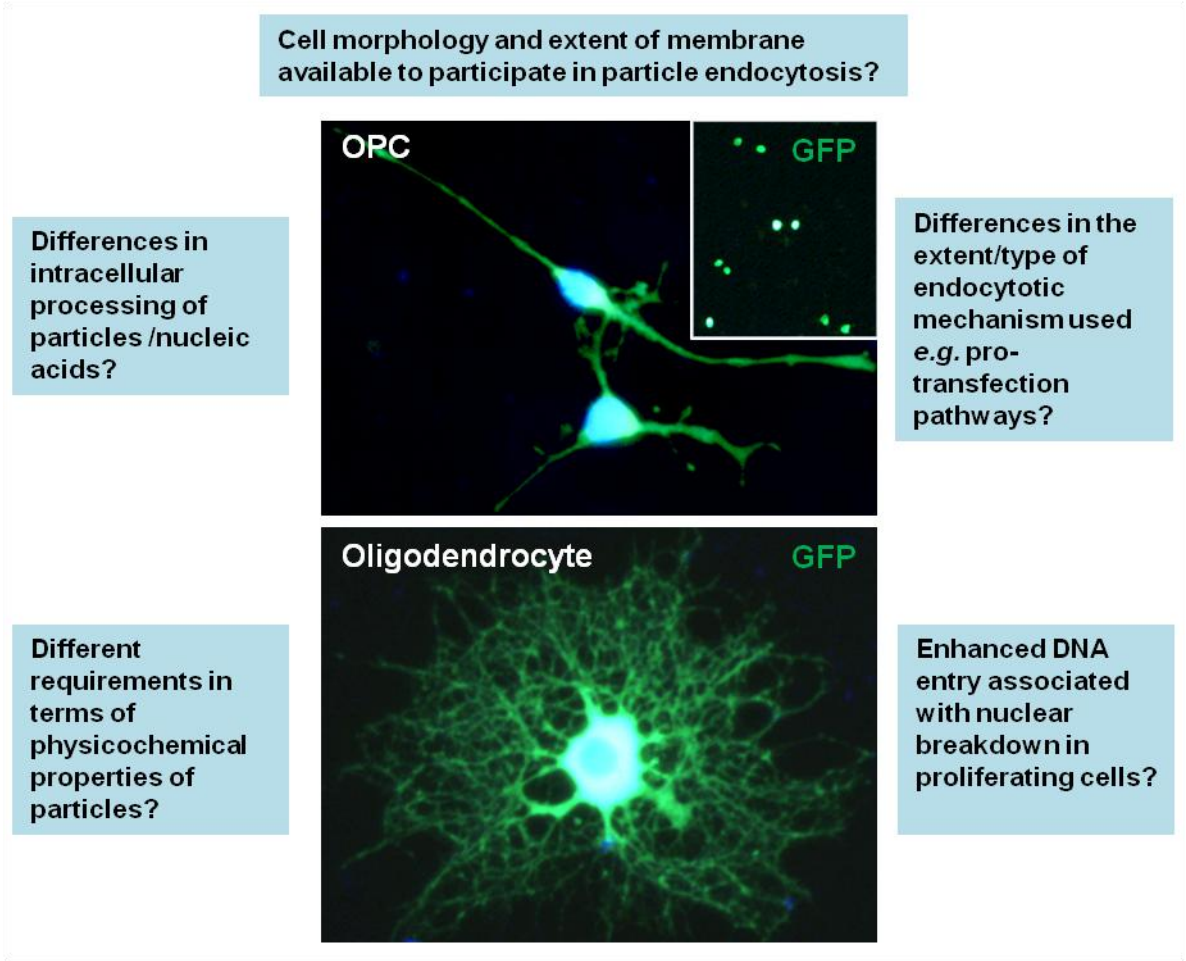

Figure 10: Schematic summary of the potential factors underlying the differences in MP uptake and amenability to transfection in OPCs versus oligodendrocytes. *Representative fluorescence micrographs are included of GFP^+ OPCs and a GFP^+ oligodendrocyte, in order to highlight the morphological differences between the two cell types. The OPCs display typical morphologies with few processes and a nucleus occupying a large proportion of the small oval cell body. GFP^+ OPCs were frequently observed in pairs, indicative of recent mitosis (inset). Note that the oligodendrocyte has a similar sized nucleus to OPCs, but a larger cell body and substantially more membrane elaborations. Although less amenable to transfection than OPCs, even mature oligodendrocytes could be transfected, as indicated by the complex highly-branched morphology of the transfected cell shown here.*

A second parameter is the particular combination of endocytotic mechanisms employed by each cell type. During differentiation, the capacity to use an individual endocytotic mechanism may be lost or gained, and such a change in endocytotic profile could significantly affect MP uptake dynamics. Even if both cell types exhibit the same endocytotic processes, the basal *rates* of each endocytotic process may differ between OPCs and oligodendrocytes. For example, based on the observation that neuronal signals can up-regulate oligodendrocyte endocytosis of PLP,[325] Kippert *et al.* cultured the oligodendroglial cell line Oli-neu with and without neuronal conditioned medium and assessed endocytotic activity.[322] The authors demonstrated a reduction in the rate of macropinocytosis in Oli-neu cells in neuronal conditioned medium, but reductions in other endocytotic mechanisms were not detected. This suggests that *in vivo*, as cells commit to oligodendrocyte differentiation and interact with neurons, they will experience a reduction in macropinocytotic activity, in line with reports from other physiological systems of the downregulation of endocytotic activity during differentiation.[22] Such a reduction in macropinocytosis could potentially explain the smaller MP accumulations observed in oligodendrocytes compared to OPCs reported here.

However, the reduction in transfection efficiency observed in oligodendrocytes (typically a three-fold difference) is more dramatic than might be predicted by a simple comparison of the percentage of MP-labelled cells (typically less than a two-fold difference) and may be further related to the smaller accumulations of Sphero MPs (particularly that of perinuclear MPs) in oligodendrocytes compared to OPCs. This suggests that a greater plasmid copy number may be present in OPCs, although other contributory factors may include differing tendencies between the cell types for vacuolar localisation of MP:plasmid complexes, potential degradation of the complexes, or damage to the nucleic acid cargo (*e.g.* by nucleases). One indication that developmental changes

occurring during the maturation of oligodendroglial cells may impact on their intrinsic amenability to plasmid based transfection is provided by a microarray comparison of gene expression between immature and mature oligodendrocytes. Findings from this study showed that of the genes exhibiting two-fold or greater differences between the cell types in levels of expression, 5% of 341 genes in immature oligodendrocytes and <0.5% of 368 genes in mature oligodendrocytes, were related to nuclear trafficking.[326] If such difference in gene expression manifest as a reduction in nuclear transport activity, then this in turn could limit nuclear delivery of plasmids in oligodendrocytes, limiting transfection efficiency.

The lower transfection efficiency observed in oligodendrocytes compared to OPCs may also be speculated to be related, at least in part, to their mitotic status. Proliferating cells such as OPCs have larger nuclear channels and undergo breakdown of the nuclear envelope during mitosis, readily permitting access of exogenous (but intracellular) DNA into the nucleus.[176] By comparison, the oligodendrocytes (a major post-mitotic population) may therefore be relatively refractory to transfection. In support of the nuclear breakdown hypothesis, GFP expression is consistently found in cells that appear to have recently undergone mitosis. However, an earlier study in primary human fibroblasts has suggested that for virus-independent transfection methods, a round of cell division (with dissolution of the nuclear membrane) is *not* a pre-requisite for DNA to enter the nucleus.[327] Indeed, it has been shown here that complex, highly processed, post-mitotic cells can be transfected using MPs. Therefore the relationship between cell proliferation, nuclear breakdown and the extent of transfection in oligodendroglial cells is currently unresolved.

Finally, the size of MPs used here may affect both uptake and intracellular processing. For example, the smaller MP accumulations observed in oligodendrocytes

compared to OPCs may suggest that the endocytotic size limit is lower in oligodendrocytes, possibly restricting uptake to single Sphero particles, whereas small clusters of MPs were frequently observed associated with OPC membrane and intracellularly, suggesting that these cells may be able to endocytose larger numbers of particles per endocytotic event than oligodendrocytes. In turn, this may be related to the specific uptake mechanism used. For example, OPCs may use both macro- and micro-pinocytosis, but oligodendrocytes may only employ micropinocytosis. It should be noted that macropinocytosis is more likely to result in transfection than is clathrin-mediated endocytosis.[240] Systematic analyses of oligodendrocyte handling of different MPs and the related uptake mechanisms will be required to determine whether the differences between OPCs and oligodednrocytes are indeed due to differences in macropinocytotic activity. This, in turn, will inform the development of MPs suitable for engineering oligodendroglial lineage cells.

4.4.4 Conclusions and future directions

Within the oligodendroglial lineage, the differentiation status of the cells influences both the capacity for MP uptake and the amenability to MP-mediated transfection. These findings have broader implications for the translation of OPC transplantation therapies as they suggest the major need to maintain transplant populations at an early, precursor form of the oligodendroglial lineage in order to effectively label or transfect cells using MPs. The presence of 'contaminants' in the form of more differentiated phenotypes can be predicted to reduce the overall efficiency of MP-based applications. Whilst a number of potential causative factors have been suggested here in order to explain the differences between precursor and differentiated cell forms, our knowledge of the reasons governing

such findings is currently limited and warrants detailed investigation. Such information will allow for the identification of key parameters that support or limit MP applications in neural cells, providing possibilities for the enhancement of such applications for neural tissue engineering. Ideally such research will employ particles possessing a wide range of physico-chemical properties in combination with cell biology and ultrastructural methods and genomic/proteomic analysis, to evaluate interactions at the particle-cell interface, and to elucidate intracellular trafficking mechanisms, including the fate of internalised particles and plasmids.

This is the first report to study *intralineage* differences in particle uptake and gene delivery potential, and the next chapter will build on this comparative analysis by performing a global, cross-cellular comparison of MP-handling across the four major CNS glial cell types.[c]

[c] The data relating to oligodendrocyte transfection, and the comparative analysis of OPC and oligodendrocyte transfection have been published. The article is reproduced here as appendix 5.

Chapter 5: Differences in MP-handling by CNS glial subclasses: Competitive MP uptake in glial co-cultures

5.1 Introduction[d]

The preceding chapters have studied MP interactions with cells derived from a single neural (oligodendroglial) cell lineage, viz. the OPCs and their progeny the oligodendrocytes. These studies revealed differences between these cell types in terms of MP handling, including differences in the accumulation of intracellular MPs (section 4.3.4) and marked differences in amenability to transfection (section 4.3.7). Having shown that intralineage differences exist, it is important to address the wider issue regarding the differences in MP-handling between oligodendroglia and the other major glial lineages of the CNS, namely the microglia and astrocytes. Each of these cell types has unique structural, functional and molecular properties related to their specific roles, and can therefore be predicted to show important differences in their uptake and handling of synthetic materials. For example, microglia have a haematopoietic origin, arising from uncommitted myeloid progenitors that infiltrate the CNS during development.[328] Microglia are located throughout the CNS parenchyma, and they are the primary CNS phagocytes.[328] Even in a 'resting' ramified state, microglia constantly monitor their environment with

[d] **Note:** *In this chapter, data on MP uptake and toxicity in OPCs and oligodendrocytes (from Chapters 2 and 4) have been collated with previously published data derived from astrocyte*[240] *(article reproduced as appendix 6) and microglial*[241] *cultures that were obtained using the same MP formulation (Sphero) and identical treatment conditions (methodology detailed in Appendix 2, section 2.2 and section 5.2). Pooling of the data in this manner has allowed, here, for a systematic cross-cellular comparison of MP uptake by the four major neuroglial subpopulations of the CNS. Based on this cross-cellular analysis, a hypothesis has been developed regarding particle handling in mixed glial populations; testing of this hypothesis is the main focus of this chapter.*

highly motile processes, phagocytosing or endocytosing nutrients, debris and damaged/dying cells; microglia exhibit all endocytotic mechanisms.[241,329] Following CNS insults, these cells become activated, proliferate, migrate to lesion sites, and secrete several cytokines/immunomodulatory factors.[330]

Astrocytes perform a variety of functions in the CNS, chiefly the maintenance of homeostasis.[331,332] They are a major constituent of the BBB, regulate ionic fluxes in the extracellular milieu, recycle neurotransmitters, and are involved in the function of virtually all synapses.[328] Astrocytes also supply metabolites to neurons and are highly active in the secretion of various signalling molecules, including trophic factors.[328] Given these functions, astrocytes are highly endocytotically active, and exhibit all of the main mechanisms, including phagocytosis.[191,333] The roles of OPCs and oligodendrocytes in myelin genesis have been discussed in detail in sections 1.2 and 1.3. No information is available regarding endocytotic mechanisms in primary OPCs, and most oligodendrocyte studies focus on the role of endocytosis in the cycling of membrane/myelin proteins, rather than uptake of extracellular molecules.[322,325]

Together, these neuroglial populations form an extensive cellular network in the CNS and outnumber neurons by a factor of approximately ten,[334,335] consequently it can be predicted that elucidating the mechanisms of particle handling by this major class of cells will be a critical component in understanding interactions between biomaterials and the CNS as a whole. Such knowledge will be vital for the development of MP-based neural engineering tools for use *in vivo* and *in vitro*. Despite this, there are few reports in the literature of MP handling by glial cells, and many of these relate to either cell lines, which may not be representative of *in vivo* behaviour (see section 1.10), or poorly characterised co-cultures,[222] in which case it can be difficult to delineate the intrinsic behaviours of individual cell types.

This laboratory has reported Sphero MP uptake dynamics in astrocytes[240] and microglia.[241] By collating these published data with similar analyses for OPCs and oligodendrocytes, reported for the first time in this thesis, information relating to Sphero MP uptake are now available for all four major CNS glial cell types, allowing for comparative MP uptake dynamics and MP-related toxicity in these cells to be described (statistical methods detailed in **Appendix 2**). Major findings from these analyses are: (i) In time-course experiments, cultures fixed and stained after 1 h incubation (20 µg/ml) showed rapid labelling of microglia (96.9 ± 1.0%), and markedly fewer labelled cells in astrocyte (30.4 ± 10.1%), OPC (16.6 ± 1.2%) and oligodendrocyte (16.8 ± 0.8%) cultures. (ii) The extent of accumulation also differed greatly between the glial cell types at 1 h, with 79.5 ± 4.4% of all microglia exhibiting 'medium'-to-'high' levels of MP accumulation, compared to 10.3 ± 4.4% of all astrocytes, while no OPCs or oligodendrocytes exhibited 'medium' or 'high' levels of uptake at this time-point. Marked differences in particle accumulation were also evident at 24 h, with heterogeneity evident in the extent of MP accumulation within individual, non-microglial cells (**Figure 1a-d** shows typical examples of MP accumulation by the different glial subtypes). (iii) Comparing the extent of MP uptake at 4 h highlights the rapid labelling of >88% of microglia, even with the lowest MP concentrations tested, compared to the gradual time- and concentration-dependent uptake observed in the other cell types **(Figure 2a)**. Within this time frame and with the maximum MP concentration used, 85 – 100% of microglia and astrocytes could be labelled with MPs, but in contrast, an average of 40% of OPCs and 27% of oligodendrocytes could be labelled (**Figure 2a**). (iv) Following 24 h MP exposure, toxicity was not observed in OPCs, oligodendrocytes, or astrocytes but was marked in microglial cultures at an identical applied MP concentration **(Figure 2b)**. (v) Perinuclear localization of particles was observed in all the cell types, but

with marked differences in the proportions of cells containing MPs in the perinuclear region **(Figure 2c)**.

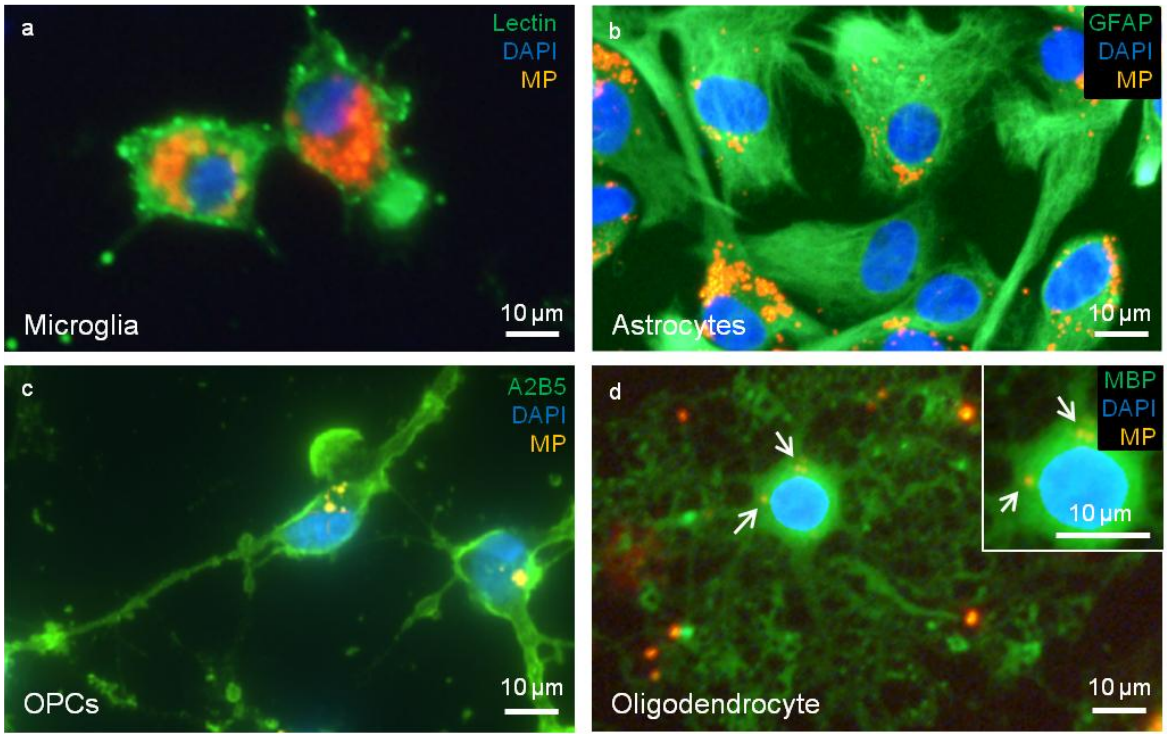

Figure 1: Characteristic MP uptake profiles of glial cell types. *Fluorescence micrographs of glia (high purity microglial, astrocyte and OPC cultures, and an enriched oligodendrocyte culture) following incubation with Sphero MPs (20 µg/ml, 24 h). (a) Microglia stain for the marker lectin and exhibit high levels of MP uptake, with large perinuclear accumulations. (b) Astrocytes stain for the marker GFAP and exhibit heterogeneity in the extent of MP uptake. Note flattened cells, large quantities of membrane relative to nucleus in cross-section, and greater extent of uptake compared to (c) and (d). (c) OPCs stain positive for the marker A2B5, and exhibit typically small clusters of MPs compared to (a) and (b). Note bipolar forms and potentially limited quantity of membrane available to undertake endocytosis. (d) Oligodendrocyte stained with MBP, and exhibiting a highly branched, mature morphology. Very small accumulations of MPs are present (white arrows, and enlarged in inset). Despite extensive membrane elaboration, MPs are mainly extracellular.*

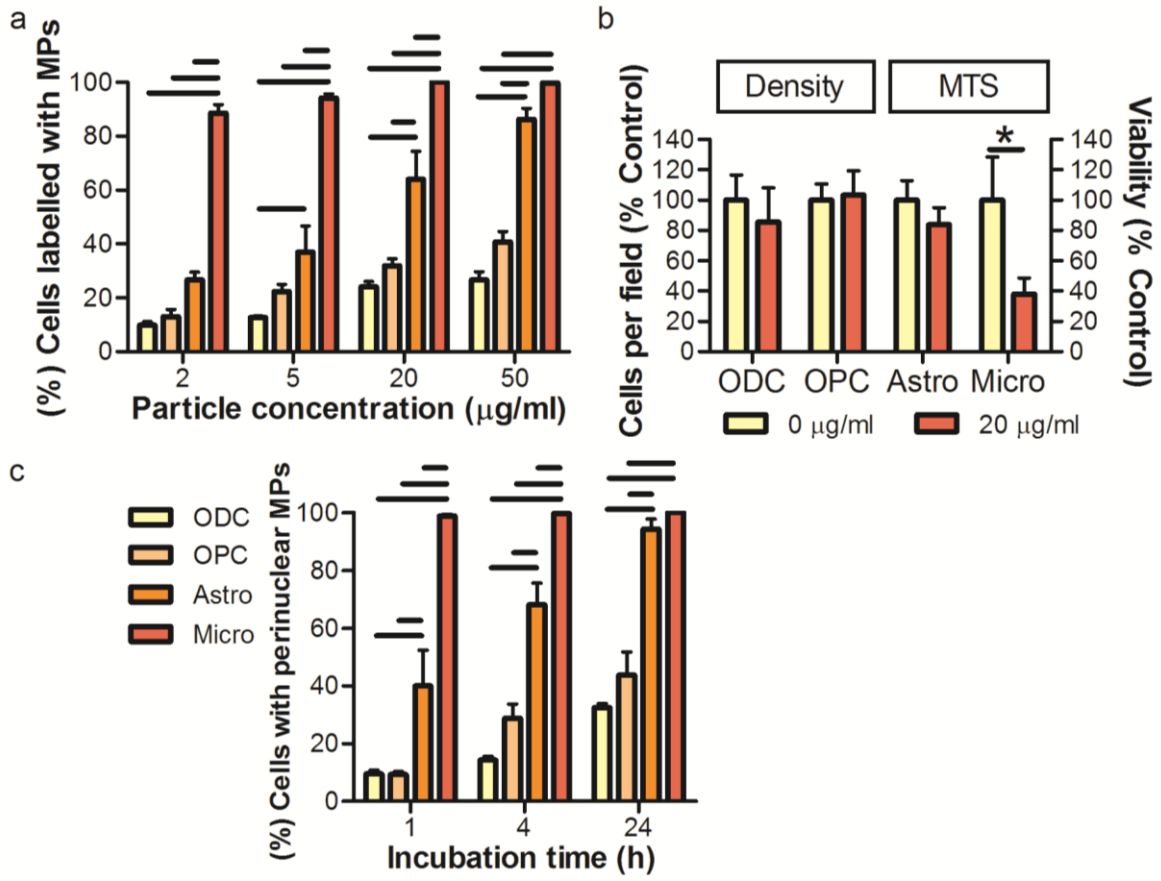

Figure 2: The extent and rate of glial MP uptake are cell type-specific. *(a) Bar graph comparing Sphero-labelling of each glial cell type (4 h). Note the rapid microglial uptake compared to the other cell types. The percentage of cells labelled was cell type- ($F_{3,40}$ = 310;* $p < 0.001$*) and concentration-dependent ($F_{3,40}$ = 44.8;* $p < 0.001$*; two-way ANOVA with Bonferroni's post-tests; lines on graph indicate* $p < 0.05$*). (b) Bar graph comparing MP-related toxicity in neuroglial cells (24 h, 20 µg/ml;* *$p < 0.05$*). (c) Bar graph showing the percentage of all cells exhibiting perinuclear MPs (50 µg/ml). Note the rapid perinuclear accumulation in virtually all microglia, compared to the gradual accumulation in the other glial cell types. The percentage of cells with perinuclear MPs was cell type- ($F_{3,30}$ = 171;* $p < 0.001$*) and time-dependent ($F_{2,30}$ = 32.8;* $p < 0.001$*; two-way ANOVA with Bonferroni's post-tests; lines on graph indicate* $p < 0.05$*). ODC = MBP$^+$ cells in enriched oligodendrocyte cultures; OPC = A2B5$^+$ cells in high purity OPC cultures; Astro = GFAP$^+$ cells in high purity astrocyte cultures; Micro = OX42$^+$ cells in high purity microglial cultures. For all graphs,* $n = 4$ *for OPCs and oligodendrocytes; for astrocytes and microglia,* $n = 3$ *for (a) and (c),* $n = 5$ *for (b).*

5.1.1 Knowledge gap: Do microglial cells exhibit competitive uptake dynamics in relation to other neuroglial subtypes?

The cross-cellular comparison of MP uptake above reveals clear differences between individual glial classes in the rate and extent of MP accumulation, with the relationship with respect to these parameters being: microglia > astrocytes > OPCs > oligodendrocytes. The rapidity and avidity of particle accumulation by microglia suggests that these cells could exhibit competitive uptake in the presence of other glial cells thereby constituting an 'extracellular barrier' to MP uptake in the other cell types, a phenomenon that will have major implications for the use of the MP platform within mixed neural cell populations for neuroengineering applications. Therefore, a mixed glial system will be developed here to test the prediction that microglia will outcompete other glial cell types in terms of particle uptake when these cells are co-cultured. The basic premise of this system is that the presence of substantial numbers of microglia will limit MP uptake by a second cell type, in a two-glial-cell-type co-culture.

Current mixed cell type culture models have significant drawbacks, notably high variability in the cell source (for example combined use of cell lines with primary cells, or CNS with peripheral nervous system cells) limiting the utility of these studies, and therefore an appropriate co-culture technique is required, in order to test these competitive uptake predictions. A defined glial co-culture system, with all cells being derived in parallel from a single primary cell source, will reduce such variability, yielding more reliable data in relation to intrinsic differences in MP uptake by neuroglial subpopulations. While such an approach could also be attempted in organotypic slice cultures, less control can be brought to bear on the precise stoichiometry of cells present and this will therefore limit a robust quantification of relative MP uptake by individual cell types.

A further observation made from the cross cellular comparison is that incubation with MPs at 20 µg/ml for 24 h resulted in significant toxicity in microglial cultures but not in the other cell types **(Figure 2b)**. The underlying basis for this difference is unknown, and, in general, the mechanisms of intracellular processing of MPs across neuroglial subtypes are unclear. These considerations have therefore prompted a cross cellular TEM analysis of MP uptake and stability in individual neuroglial subpopulations, with the aim of taking the first step towards elucidating particle fate within these cells, to provide a mechanistic basis for the observed toxicity.

5.1.2 Objectives

i. To develop a glial co-culture system to test the hypothesis that microglia act as an 'extracellular barrier' to MP uptake in other neuroglial subtypes. The model will be used to specifically test whether co-culture with microglia limits the extent of MP uptake by OPCs and astrocytes.

ii. To conduct a cross-cellular transmission electron microscopical analysis of MP stability and fate within neuroglial subpopulations, to attempt to discern the underlying reasons for inter-cellular differences in particle-related toxicity.

5.2 Materials and Methods

Reagents and equipment: Trypsin, biotin-conjugated lectin (from *Lycopersicon esculentum*, tomato), monoclonal anti-biotin FITC-conjugated secondary antibody (clone BN-34) were from Sigma (Poole, Dorset, UK).

Sphero and Neuromag particles: These are described in sections 2.2 and 3.2, respectively.

Dynamic light scattering (DLS) and zeta-potential of Sphero MPs: In order to prove that differences in MP uptake are due to cell intrinsic biological differences in neuroglia, it is important to rule out the effects on cellular MP uptake of different culture media,and the potential for particle aggregation with time. To evaluate the effects of the culture medium on particle size and charge, measurements of hydrodynamic diameter and zeta potential were made using a Malvern Zetasizer Nano ZS. Particles were added to various biological media: deionised water, D10, OPC-MM and Sato. Media were incubated (37°C, 5% CO_2/95% humidified air) before analysis, to ensure measurements were made at the same pH as that at which cells were cultured.

OPC cultures: OPC cultures were derived from primary mixed glial cultures as described in section 2.2.

Development of the co-culture models: The development of the co-culture system requires that different cell types are cultured in the same medium. OPCs are usually cultured in a chemically-defined medium (OPC-MM), but in pilot experiments microglia and astrocytes did not tolerate this medium. When OPCs were cultured in the D10 medium used for microglia and astrocytes, most cells began to differentiate within 24 h, including differentiation into type 2 astrocytes, which stain for GFAP and are considered an artefact of *in vitro* culture.[336] All three cell types can be cultured together in D10 in the primary

mixed glial cultures from which they are derived, with astrocyte-derived factors preventing OPC differentiation. Therefore, a co-culture medium was developed consisting of D10 medium supplemented with 20% conditioned medium from primary mixed glial cultures, which was sterile filtered (D10-CM). Under these conditions, OPCs largely retained their bipolar morphologies and few type 2 astrocytes were observed (~1%).

Furthermore, it was important to ensure that each of the cell types required for a co-culture was ready for plating within a short period of time, to ensure that the highly proliferative astrocytes did not significantly alter their plating density and/or reach confluence, at which point their behavior might be altered. Therefore, mixed glial cultures were prepared as described in section 2.2, but flasks were plated at differing densities, such that they would reach confluence at different rates **(Figure 3)**. OPCs were plated on PDL-coated coverslips in 24-well culture plates (0.3 ml D10-CM; 4 x 10^5 cells/ml for OPC cultures, 2 x 10^5 cells/ml for co-cultures) and cultured for 24 h to allow the cells to attach and recover their processes. At this point, astrocyte cultures were trypsinized and plated on PDL-coated coverslips in 24-well culture plates (0.3 ml D10-CM; 4 x 10^5 cells/ml for astrocyte cultures, 2 x 10^5 cells/ml for co-cultures). Microglia were plated on PDL-coated coverslips in the same 24-well culture plates in high purity cultures (0.3 ml D10-CM; 4 x 10^5 cells/ml) and onto previously prepared OPC and astrocyte cultures to form co-cultures (0.3 ml D10-CM, replacing the medium already present; 2 x 10^5 cells/ml). Microglia attach to coverslips rapidly (typically <1 h), at which point uptake or transfection experiments could be performed. High purity cultures of OPCs, astrocytes and microglia were studied in parallel with the co-cultures.

Culture:	Mixed glial (a)	Astrocytes	Mixed glial (b)	Mixed glial (c)
Plating density (cells/flask)	20 x 10^6		5 x 10^6	10 x 10^6
Day 6	Confluent; shake overnight for 2 nights			
Day 8	Trypsinise; re-plate as astrocytes	Plated from (a)		Confluent; shake for 1 h for microglia; shake overnight for OPCs
Day 9				Plate OPCs
Day 10		Sub-confluent; Plate astrocytes	Shake for 1 h; Plate microglia	

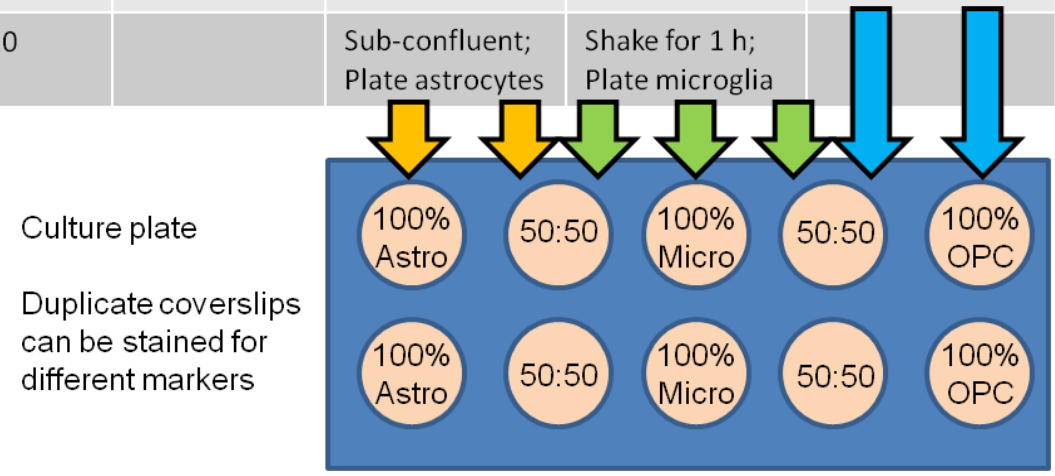

Figure 3: Schematic indicating procedure to produce different glial cell types for co-cultures. *Mixed glial cultures were established at differing initial plating densities such that they became confluent at different rates. Astrocytes (Astro), OPCs and microglia (Micro) were then derived from these cultures and plated as high purity cultures (100%) and at half density for co-cultures (50:50).*

Competitive Sphero uptake experiments: Once microglia had adhered to coverslips, all cultures were incubated with Sphero particles (20 µg/ml). At 24 h after MP treatment,

cultures were washed with PBS, fixed with 4% PFA and immunostained as described in section 2.2, using FITC secondary antibodies. Identically treated coverslips were stained with A2B5 or lectin for pure OPC and microglial cultures, as well as OPC:microglia cocultures. Lectin was found to stain astrocytes, and so for pure astrocyte cultures and for astrocyte:microglia cocultures one coverslip was stained for GFAP, and the other was unstained. For pure microglial cultures, one coverslip was stained for GFAP, and the identically treated counterpart was stained for lectin.

Fluorescence microscopy and uptake analysis: Stained co-cultures were imaged and analysed in identical fashion to that described in section 2.2.

TEM sample preparation: Cells were plated on polyornithine-coated aclar (0.3 ml/well, at 6 x 10^4 cells/cm^2; OPCs in OPC-MM for 24 h; for oligodendrocytes, OPCs were plated in Sato and maintained for 8 d; microglia in D10 for 24 h) then incubated with 20 µg/ml Sphero MPs for 24 h and processed and imaged in an identical manner to that described in section 2.2. Sphero MPs were also processed on polyornithine-coated aclar in D10 without cells to study the shape and size of particles alone.

Statistical analysis: Data were analysed using GraphPad Prism statistical analysis software, with statistical tests as detailed in the text. Data are expressed as mean ± SEM. The number of experiments (*n*) refers to the number of mixed glial cultures from which OPC cultures were derived, with each primary culture being established from a different rat litter. For analysis of MP uptake in co-cultures, unpaired two-tailed *t*-tests were performed for each cell type to compare the following in pure versus co-cultures: (i) the percentage of MP-labelled cells, (ii) the percentage of cells showing 'medium' levels of uptake, and (iii) the percentage of cells showing 'high' levels of MP uptake.

5.3 Results

5.3.1 Sphero MPs exhibit similar characteristics in different culture media

The Sphero particles used in all the uptake studies compared here have been characterised in sections 2.2 and 2.3. However, the astrocyte and microglial experiments involved culturing cells in different media than was used in the isolated OPC/oligodendrocyte cultures, therefore further characterisation was performed to address the possibility that the particles may adopt different properties once added to these different media. Limited differences in hydrodynamic diameter were observed in the three culture media used to propagate each of the cell types, suggesting limited aggregation of particles immediately after addition to media **(Table 1)**. Comparison of 5 min and 24 h measurements in Sato medium showed that a small amount of particle aggregation occurred, as the particle size increased by a factor of *ca.* 2. The mean diameter of these particles was shown to be ~360 nm (range 200 – 390 nm) by SEM analysis (section 2.2), but the mean hydrodynamic diameter was in the range 843 – 961 nm. These values were determined by DLS, a technique that measures the hydrodynamic diameter of the particle surrounded by the solvation layers. Measurements by DLS are more accurate for soft materials, such as proteins, with the size of more dense materials commonly being overestimated.[280,337] These observations are consistent with the literature relating to magnetic particles, where different methods of size-determination can produce conflicting data.[139,280] The zeta potential measurements showed that these particles carry a negative charge in all media, attributable to the carboxylic surface groups, with small differences observed across the media. As the charge on a particle is pH-dependent, the zeta potential would not be expected to vary across these culture media, as all are of similar pH values.

Together, these results suggest that MP characteristics do not substantially vary across culture conditions, and are not the reason for the observed differences in MP uptake between neuroglial subtypes.

Table 1. Physical characteristics of Sphero MPs in various biological media.

Medium	Relevant cell type(s)	ζ-potential (mV)[a]	d_{DLS} (nm)[a]	
		Incubation time: 5 min	5 min	24 h
H_2O	-	-	843	-
OPC-MM	OPCs	-14.6	867	-
Sato	Oligodendrocytes	-14.3	850	1650
D10	Astrocytes; Microglia	-13.7	961	-

d_{DLS} = Hydrodynamic diameter, determined by dynamic light scattering (DLS). [a]Average values of three measurements.

5.3.2 Characteristics of glial co-cultures: Competitive uptake assays

High purity OPC cultures were produced, as judged by A2B5 staining (98.3 ± 0.7% $A2B5^+$; n = 4). Astrocyte cultures largely consisted of cells with the flattened, polygonal morphologies typical of type 1 astrocytes, with <1% exhibiting the complex, branching morphologies of type 2 astrocytes. These cultures were of high purity, as judged by staining for GFAP (98.7 ± 0.8%; n = 3). Microglial cultures were of high purity, as judged by staining for the microglial marker lectin **(**97.9 ± 0.9%; n = 4). Characterisation of co-cultures of OPCs with microglia by staining duplicate coverslips revealed that both cell types were present and in proportions approximating the target 50:50 ratio ($A2B5^+$ cells:

55.6 ± 4.5%; lectin^{+} cells: 44.8 ± 5.6%; *n* = 4 cultures). Characterisation of co-cultures of astrocytes with microglia by staining duplicate coverslips revealed that 56.1 ± 2.9% of cells were GFAP^{+}; n = 3 cultures. However, lectin staining was found to be a non-specific microglial marker as it also stained astrocytes. Therefore quantification of microglial proportions in the co-cultures was not feasible using immunohistochemical staining, and this marker was excluded from further astrocyte-microglia co-culture experiments. However, the microglial phenotype could be inferred from (i) a GFAP^{-} staining profile associated with the DAPI-stained nuclei, and (ii) the distinct rounded morphologies of microglia under phase microscopy, compared with the flattened morphologies of astrocytes, enabling a clear distinction to be made between the two cell types for quantification of cell-specific MP uptake.

5.3.3 Microglial uptake of MPs is rapid and extensive compared to astrocytes and OPCs

After 90 min incubation, astrocyte and OPC cultures demonstrated an even distribution of particles across the culture wells, with few cell-associated aggregations **(**MPs identified by nile red fluorescence, **Figure 4a-b & d-e**; extracellular MPs were identified by agitating the culture plate, causing the particles to move**)**. In stark contrast, microglial cultures rapidly showed large accumulations of nile red fluorescence, within ~100% of cells, readily judged to be within cells by the characteristic perinuclear aggregations, which remained static during agitation of the culture plate **(Figure 4c-f)**.

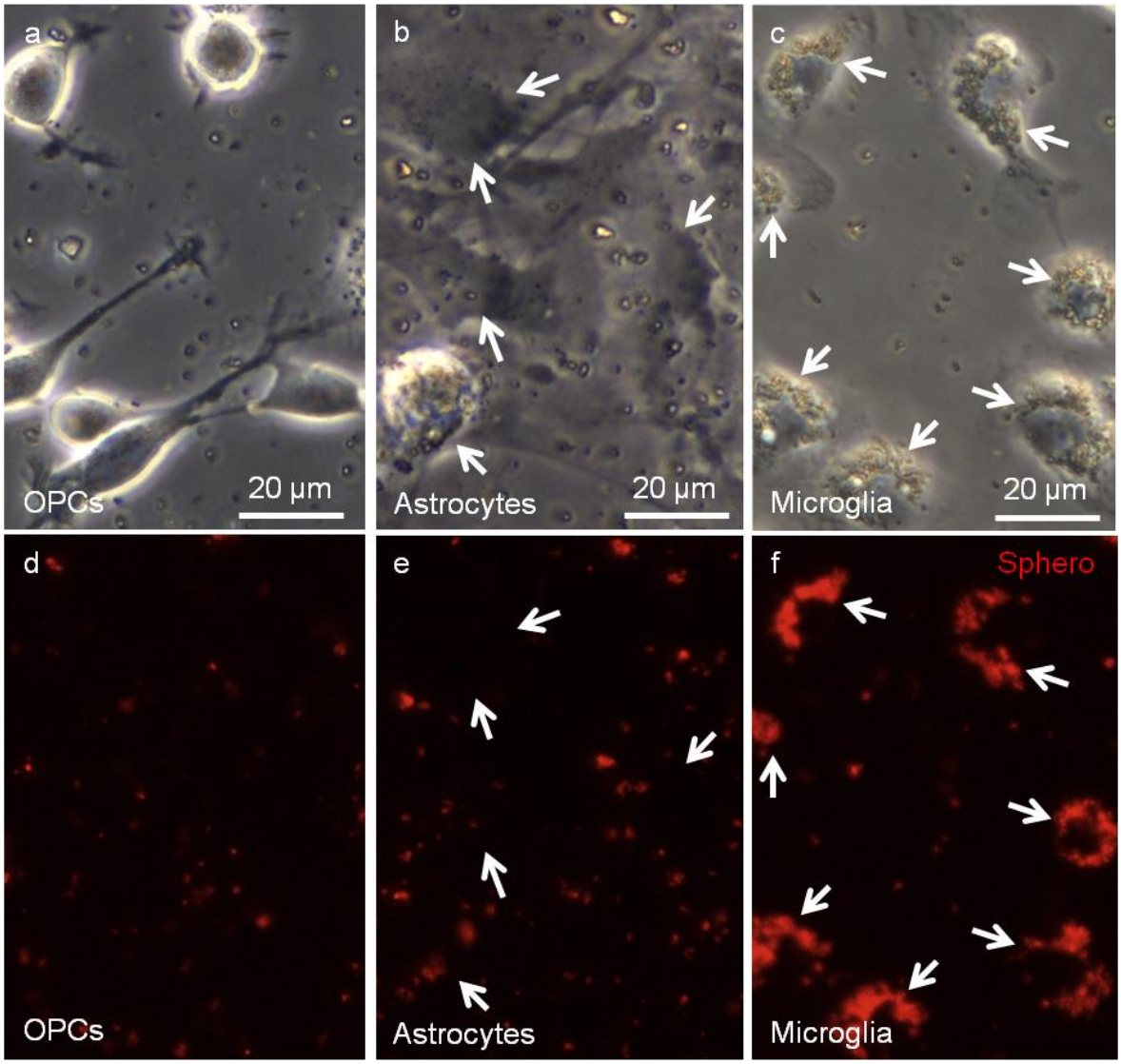

Figure 4: Microglial uptake of MPs is far more rapid than OPC or astrocyte uptake. *Representative phase-contrast images of high purity live OPC (a), astrocyte (b) and microglial (c) cultures after 90 min incubation with MPs (Sphero, 20 µg/ml), with counterpart fluorescence micrographs, respectively (d), (e) and (f). Astrocytes (flattened morphologies) and microglia are indicated with arrows. Sphero MPs, identified by fluorescence, are distributed evenly across the OPC and astrocyte culture wells, with few labelled cells, but microglia exhibit extensive MP uptake with clear perinuclear localisation. As these are live cultures, many particles are suspended in the medium, rather than being attached to the substrate/cells, and could be determined as such by gently agitating the plate.*

5.3.4 MP uptake by OPCs is dramatically reduced when co-cultured with microglia

Co-culture of OPCs with microglia resulted in a dramatic reduction in the proportion of MP-labelled OPCs, and in the extent of MP accumulation in OPCs, compared to high purity OPC cultures **(Figure 5)**. Approximately 75% of OPCs in pure cultures were MP-labelled, and over 50% of OPCs demonstrated 'medium'-to-'high' levels of MP accumulation **(Figure 6)**. In stark contrast, when co-cultured with microglia there was a significant reduction in the percentage of MP-labelled OPCs (to an average of approximately 35%), with many regions of the cultures showing no uptake in OPCs **(Figure 5b-d)**. Less than 4% of OPCs exhibited 'medium' levels of particle accumulation, and no OPCs were observed with 'high' levels of uptake **(Figure 6)**. In pure microglial cultures, ~100% of microglia were MP-labelled, with ~54% showing 'high' levels of particle accumulation. Approximately 100% of microglia in co-cultures with OPCs were also MP-labelled, but with a significant increase in the percentage showing 'medium'–to-'high' levels of MP accumulation.

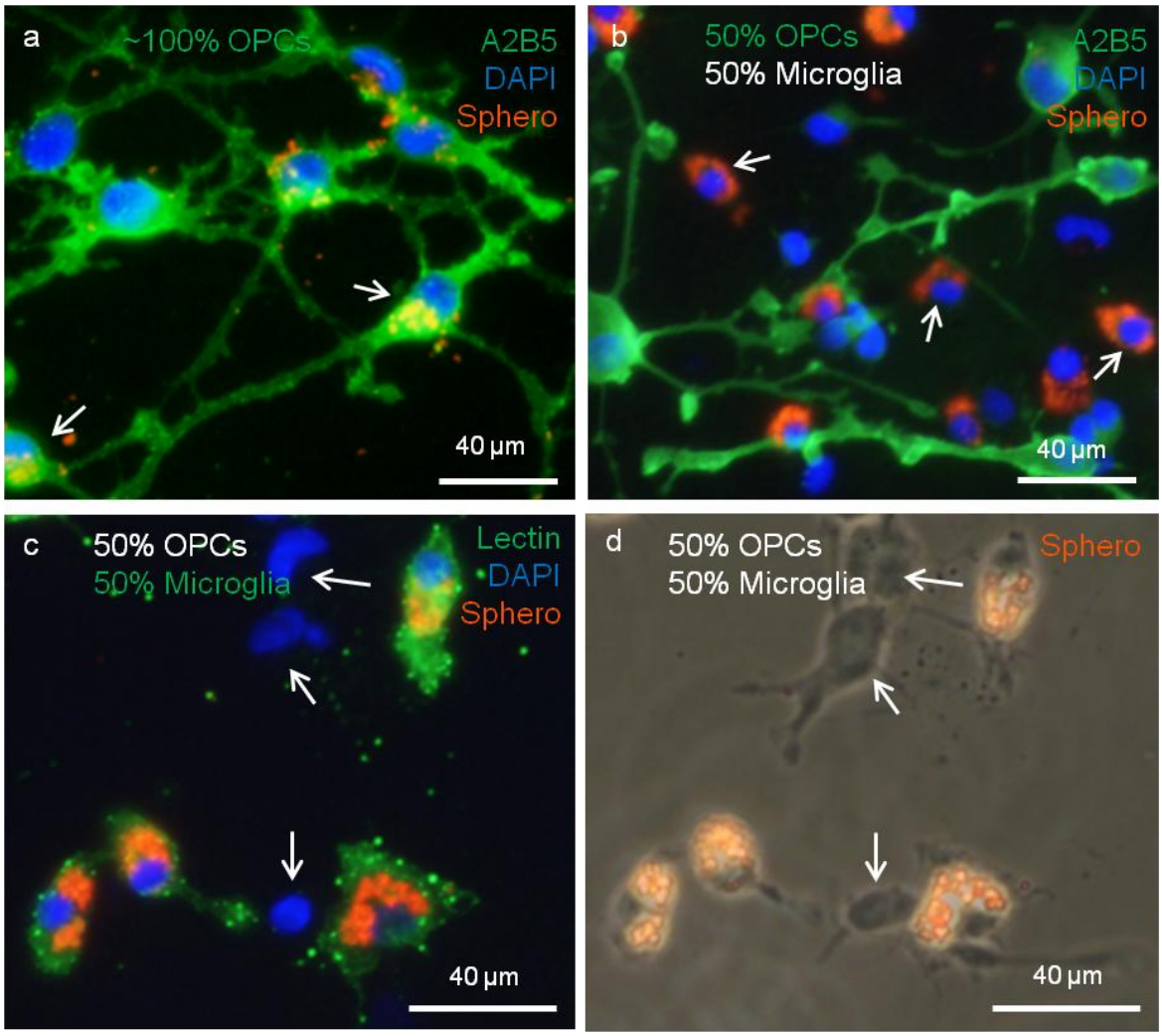

Figure 5: Reduction in MP uptake by OPCs in the presence of microglia. *(a) Fluorescence micrograph of a high purity OPC culture (stained for A2B5; <2% microglia) demonstrating a high proportion of MP-labelled cells. Arrows indicate OPCs scored as having a 'high' level of MP accumulation. (b) Fluorescence micrograph of an OPC:microglia co-culture (~50% microglia) showing extensive accumulation of MPs in DAPI-labelled A2B5$^-$ cells (some indicated by arrows), identified as microglia by phase contrast microscopy (not shown). Note the almost complete lack of MP-labelling of A2B5$^+$ OPCs. (c) Fluorescence micrograph of an OPC:microglia co-culture (~50% microglia) showing extensive accumulation of MPs in cells identified as microglia by lectin staining. Note the lack of MP-labelling in DAPI-labelled lectin$^-$ cells, identified by phase contrast microscopy as OPCs. (d) Phase contrast counterpart to (c). Arrows indicate the same OPCs in (c) and (d). All cultures incubated for 24 h at 20 µg Sphero/ml.*

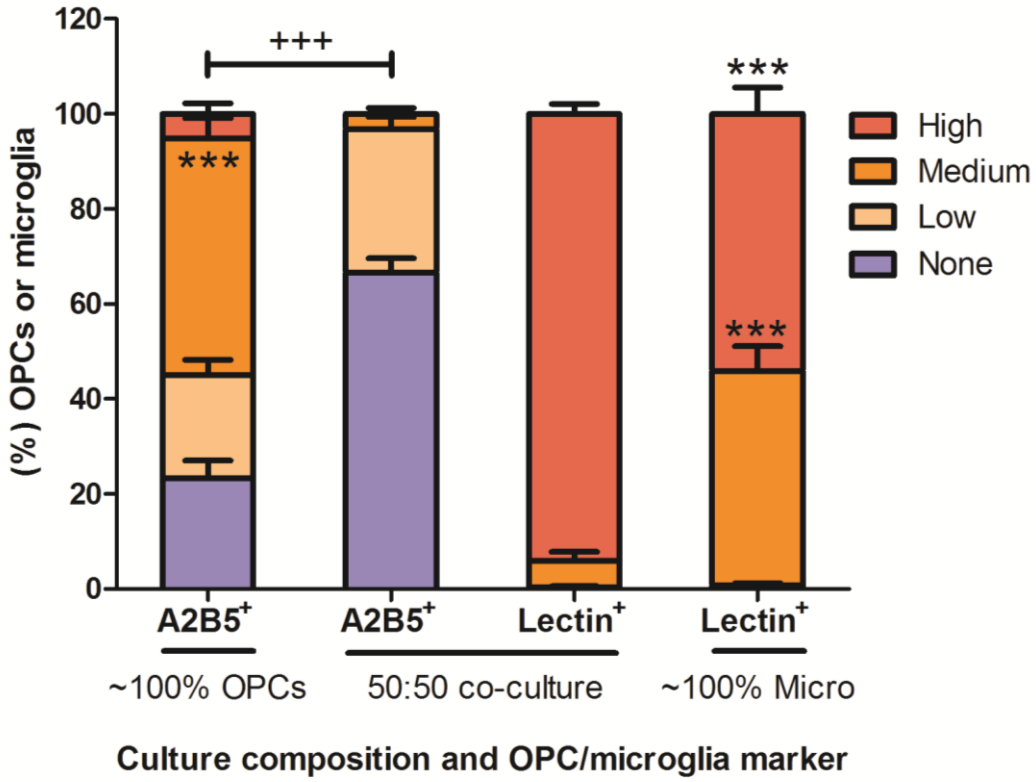

Figure 6: The proportion of MP-labelled OPCs and the extent of MP accumulation by OPCs is markedly reduced in the presence of microglia. *Bar graph illustrating the percentage of MP-labelled cells and the extent of MP accumulation by OPCs and microglia in high purity isolated cultures (left and right hand bars, respectively) and in 50:50 co-cultures (central bars, OPCs to the left and microglia to the right). When co-cultured with microglia, the percentage of MP-labelled OPCs was significantly reduced (*$^{+++}$*p < 0.001;* n = 4*). A greater percentage of OPCs exhibited 'medium' (***p < 0.001;* n = 4*) accumulations of MPs in high purity OPC cultures than in co-cultures. A greater percentage of microglia exhibited 'medium' levels of uptake in high purity microglial cultures than in co-cultures (***p < 0.001; n = 4), and a greater percentage of microglia exhibited 'high' levels of uptake in co-culture than in high purity culture (***p < 0.001; n = 4). ~100% OPCs = high purity OPC culture (>98% A2B5*$^{+}$*); 50:50 co-culture = OPCs and microglia in a 50:50 co-culture; ~100% Micro = microglia in a high purity culture (~98% lectin*$^{+}$*).*

5.3.5 MP uptake by astrocytes is dramatically reduced when co-cultured with microglia

Co-culture of microglia with astrocytes resulted in a marked reduction in the proportion of MP-labelled astrocytes, and in the extent of MP accumulation in astrocytes, compared to high purity astrocyte cultures **(Figure 7)**. Approximately 100% of cells were labelled in pure astrocyte cultures, with ~94% of astrocytes showing 'medium' or 'high' levels of MP accumulation **(Figure 8)**. This is in stark contrast to the restricted astrocyte uptake observed in the presence of microglia, where MP-labelling was reduced to ~70% of astrocytes, with some regions of the cultures showing near complete abolition of MP uptake in astrocytes (illustrative examples are shown in **Figure 7b**). Less than 30% of astrocytes accumulated 'medium'-to-'high' levels of particles; **Figure 8**). The presence of astrocytes did not significantly affect microglial uptake of MPs, with 100% of microglia in these co-cultures showing MP-labelling, and ~65% of microglia exhibiting 'high' levels of MP accumulation. This was comparable to microglial uptake in high purity microglial cultures, where ~100% of microglia were MP-labelled, with ~54% of microglia showing 'high' levels of MP uptake **(Figure 8)**.

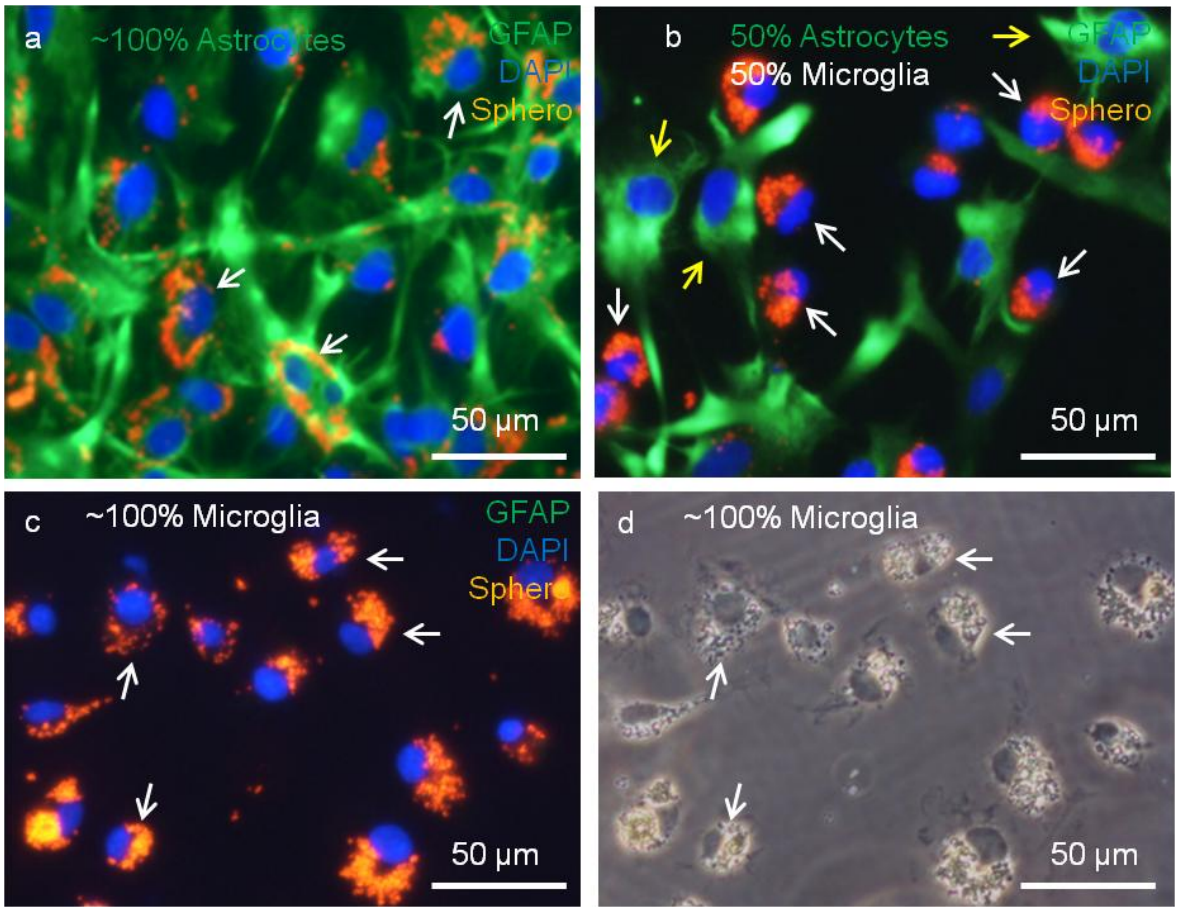

Figure 7: Reduction in MP uptake by astrocytes in the presence of microglia. *(a) Fluorescence micrograph of a high purity astrocyte culture (stained for GFAP; <2% microglia) demonstrating a high proportion of MP-labelled cells. Arrows indicate astrocytes scored as having a 'high' level of MP accumulation. (b) Fluorescence micrograph of an astrocyte:microglia co-culture (~50% microglia) showing extensive accumulation of MPs in DAPI-labelled GFAP$^-$ cells (some indicated by white arrows), identified as microglia by phase contrast microscopy (not shown). Note the reduction in MP-labelling of GFAP$^+$ astrocytes (unlabelled astrocytes indicated by yellow arrows). (c) Fluorescence micrograph of a high purity microglial culture (~98% lectin$^+$; data not shown) exhibiting extensive accumulation of MPs in cells identified as microglia by phase contrast microscopy and by a lack of GFAP staining. (d) Phase contrast counterpart to (c). Arrows indicate the same microglia in (c) and (d). All cultures incubated for 24 h at 20 µg Sphero/ml.*

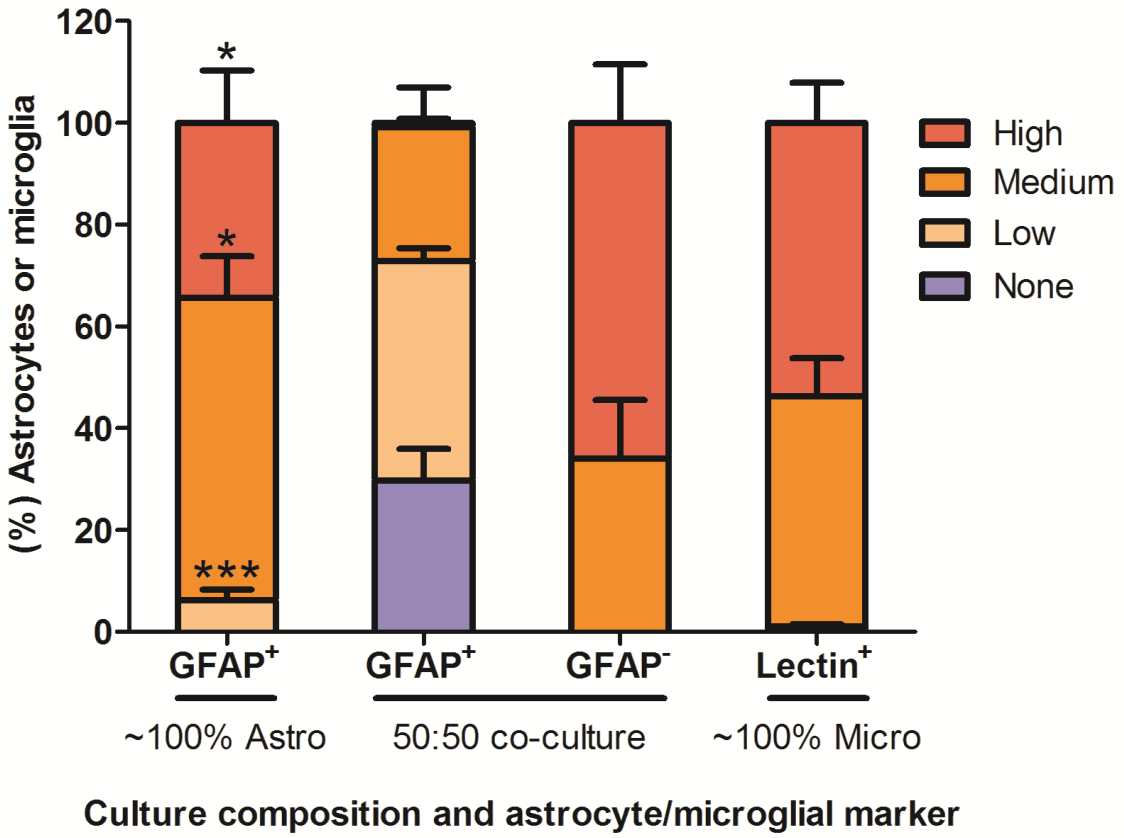

Figure 8: The proportion of MP-labelled astrocytes and the extent of MP accumulation by astrocytes is markedly reduced in the presence of microglia. *Bar graph illustrating the percentage of MP-labelled cells and the extent of MP accumulation by astrocytes and microglia in high purity isolated cultures (left and right hand bars, respectively) and in 50:50 co-cultures (central bars, astrocytes to the left and microglia to the right). A greater percentage of astrocytes exhibited 'medium'* (*$p < 0.05$; $n = 3$) *or 'high'* (*$p < 0.05$; $n = 3$) *accumulations of MPs, and significantly fewer exhibited 'low' uptake* (***$p < 0.001$; $n = 3$), *in high purity astrocyte cultures than in co-cultures. No differences were shown between pure microglial and co-cultures in terms of the percentage of MP-labelled microglia, or the extent of MP uptake. ~100% Astro = high purity astrocyte culture (>98% GFAP$^+$); 50:50 co-culture = astrocytes and microglia in a 50:50 co-culture; ~100% Micro = microglia in a high purity culture (~98% lectin$^+$).*

5.3.6 The intracellular processing of Sphero MPs, and associated toxicity, is glial cell type-specific

TEM analyses of glia incubated with Sphero MPs were compared. Electron dense MPs were readily identifiable in electron micrographs of astrocytes (unpublished image shown from a previous study by this lab),[240] OPCs and oligodendrocytes, and were observed to be free in the cytosol, including the perinuclear accumulations **(Figure 9a-c)**. The intracellular particles exhibited the same characteristic ring of iron oxide around the polystyrene core as was seen when particles were processed for TEM in D10 medium without cells **(Figure 9a, inset)**, suggesting that they were morphologically intact within these cell types. Particle clusters were typically smaller in oligodendrocytes than in OPCs, and strikingly smaller in OPCs and oligodendrocytes compared with astrocytes, supporting the observations made using fluorescence microscopy (compare **Figure 1b-d** and **Figure 9a-c**). TEM analyses of microglia revealed extensive particle accumulations which were often associated with multilamellar bodies **(Figure 9d & 10a)**. In contrast to astrocytes, OPCs and oligodendrocytes, MPs within microglia appeared to be undergoing extensive sequestration and degradation, likely within lysosomes **(Figure 10b)**.

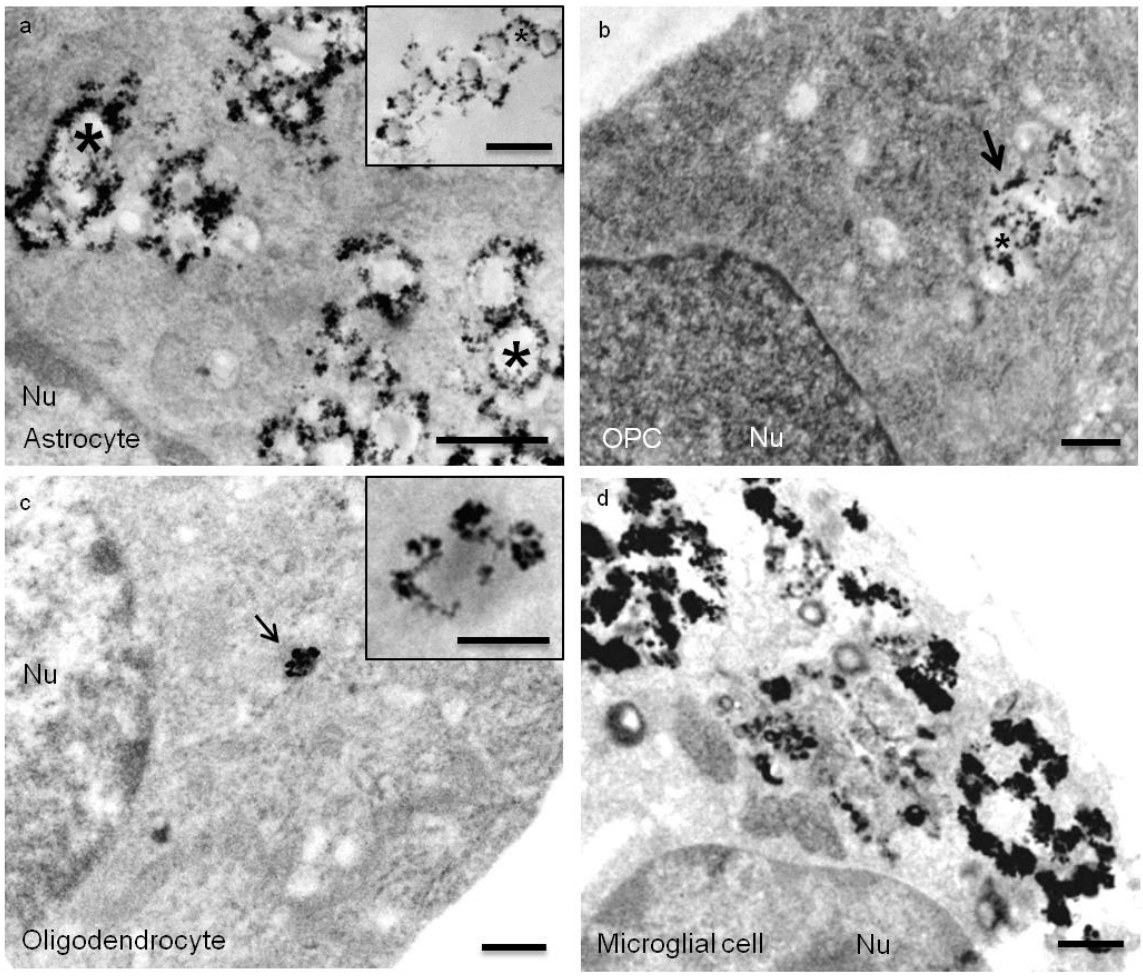

Figure 9: Intracellular fate of MPs is cell type-dependent. *TEM analyses of glial cells following 24 h incubation with 20 µg Sphero/ml. (a) An astrocyte with intact intracellular MPs, as evidenced by the presence of electron dense rings of iron surrounding the polystyrene cores (*). Inset, intact MPs in D10 medium without cells (24 h), for comparison of particle shape and structure. (b) An OPC showing intact MPs in a small cluster in the cell cytosol (arrow). (c) An oligodendrocyte showing a single MP in the cytosol (arrow). Inset shows magnified image of the MP. Note the relative size of the MP accumulations in (a), (b) and (c), which are typical of astrocytes, OPCs and oligodendrocytes. (d) A microglial cell showing large intracellular accumulations of MPs. Note that particles appear to be undergoing degradation, as evidenced by comparison with intact MPs [see (a), inset]. * indicates polystyrene core of MPs; Nu indicates nucleus; Scale bars indicate 0.5 µm, except (c, inset) where scale bar indicates 200 nm.*

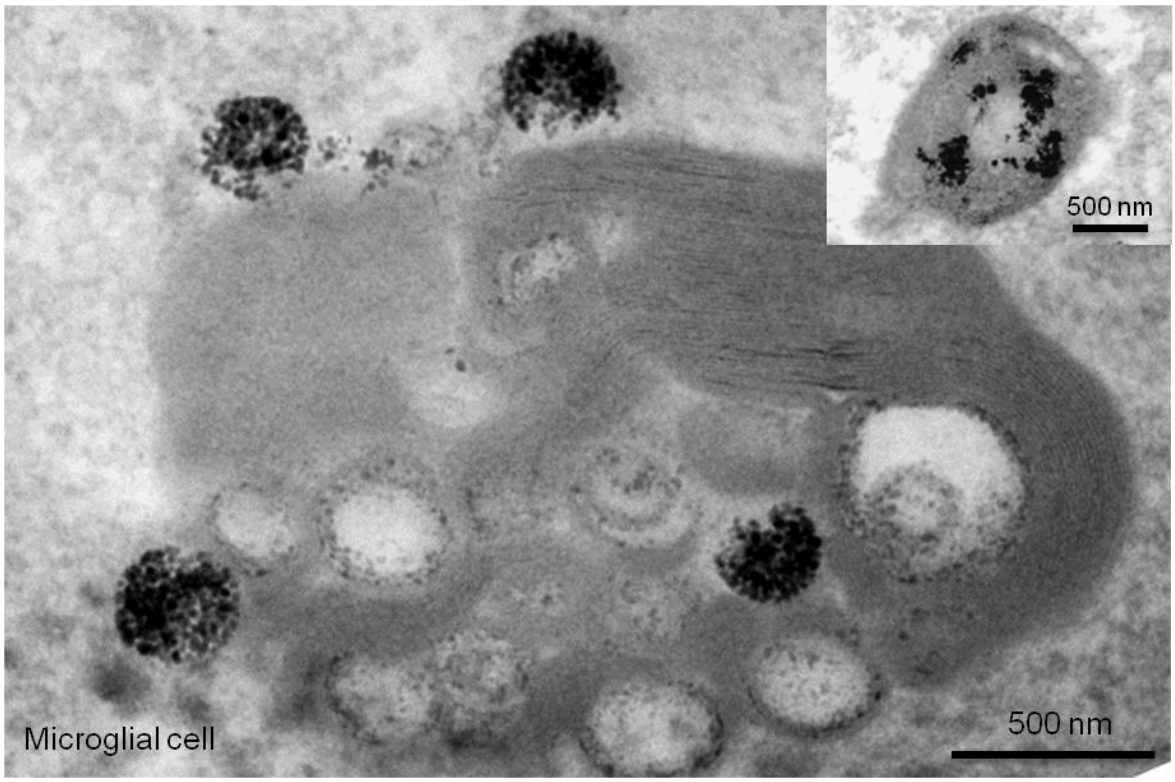

Figure 10: Microglia sequester and degrade MPs. *A microglial cell, showing particles associated with an electron dense multilamellar body. Note that the electron dense iron particles are not accumulated in rings, but appear to be condensing into clusters, suggesting that particles are undergoing degradation. Inset shows extensive MP degradation within a lysosome, as evidenced by dispersion of iron deposits.*

5.4 Discussion

This is the first reported systematic comparison of MP handling by the major classes of CNS glia (using purified or enriched cultures, derived from the same primary source, viz. neonatal rat cortex). For Sphero particles, the glial cell types exhibit key differences in the rate and extent of MP uptake, and subsequent intracellular processing of particles, as well as their susceptibility to MP-related toxicity. There are also differences between the glial subtypes in their amenability to MP-mediated gene delivery as shown in chapters 3 and 4 for OPCs and oligodendrocytes, and by comparison with previously published astrocyte[164] and microglial[241] data.

Based on these observations, it can be predicted that these variations will exert important influences on the biological utility of MP platforms for neural engineering applications. These findings have broad implications for the design of novel neurocompatible materials, and the development of protocols for their use, especially in the presence of mixed neural populations. A schematic summary of these cell type-specific MP-handling characteristics is shown below **(Figure 11)**, and this discussion will now address the significance of each of these findings in turn.

	Microglia	Astrocytes
Cells labelled	100%†	>95%‡
Extent of uptake	High	Medium-High
Particle stability	Lysosomal degradation, iron leaching evident	Appear stable
Cytotoxicity	Yes†	Not evident
Perinuclear localisation	Yes	Yes
Transfection levels achievable	Negligible (<1%)†	Up to 54%¥ Optimal at F = 1 Hz

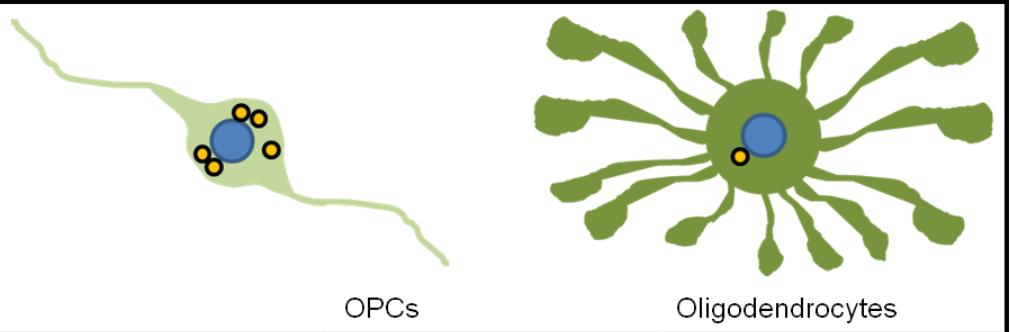

	OPCs	Oligodendrocytes
Cells labelled	~57%	~45%
Extent of uptake	Low (>ODC)	Low (<OPC)
Particle stability	Appear stable	Appear stable
Cytotoxicity	Not evident	Not evident
Perinuclear localisation	Yes	Yes
Transfection levels achievable	Up to 21% Optimal at F = 4 Hz	Up to 6%

Figure 11: Schematic overview of intercellular differences in MP-processing by glia and relevance to neural tissue engineering applications. *Diagrams illustrate typical cell morphologies, relative levels of MP-accumulation, extent of perinuclear localisation and degradation of MPs. MPs are indicated by yellow circles. Tables summarise MP-handling characteristics for each cell type, relating to cell labelling efficiency, cytotoxicity and transfection levels achievable. ODC = oligodendrocyte. References: †*[241]*, ‡*[240]*, ¥*[164]*.*

5.4.1 Microglial MP uptake is rapid and extensive compared to other glial cell types

Microglial uptake of Sphero MPs is far more rapid and extensive than is seen in astrocytes, OPCs or oligodendrocytes. Various MP-based applications may depend upon loading cells with a sufficient quantity of particles, for example non-invasive detection of transplanted cells will require cells with sufficient label for effective detection by MRI. Astrocytes and microglia are likely to be readily labelled with sufficient particles for such an application, with potentially 100% of cells detectable by MRI and histological techniques. However, for the concentrations and incubation times tested, it was not possible to label 100% of an OPC or oligodendrocyte culture, and as discussed in section 2.4.1, it remains possible that one or more subpopulations exist in primary oligodendroglial cultures which are not amenable to MP-labelling, at least with the Sphero particle. These suppositions would need to be assessed empirically, and MRI contrast capability of the labelled cells would also depend upon particle properties. For example, employing a high-contrast particle (*e.g.* the Fe_3O_4-PEI-RITC particles studied in Chapter 2) may facilitate adequate accumulation of MRI-compatible contrast agent in cells which exhibit typically 'low' levels of MP accumulation per cell.

5.4.2 Unlike other glial cell types, microglia sequester and degrade MPs, and exhibit MP-related toxicity

Intracellular Sphero MPs were observed in all glial cell types, but important differences were noted in their subsequent intracellular processing. For astrocytes, OPCs and oligodendrocytes, TEM analyses indicate that the particles are intact and commonly free in the cell cytosol, rather than being within endosomes/vesicles or associated with structures such as the nuclear membrane, Golgi apparatus or endoplasmic reticulum (in

agreement with the previously published astrocyte data).[240] However, TEM analyses of microglia suggest that these cells sequester MPs in vesicles, including multilamellar bodies, and also undergo degradation within lysosomes, with iron leaching from the particles. These findings could provide a mechanistic basis for the differences in MP toxicity observed in the different glial subtypes, information that is vital to assessing the potential for translation of MP-based engineering techniques.

Differences in intracellular processing of MPs can determine whether toxic effects are produced, as illustrated by Chen *et al.*[338] The authors exposed a human glioma cell line (U251) to two different DMSA-coated iron oxide MPs and assessed whether ROS were produced.[338] In a neutral environment (pH 7.4, typical of cytosol) no toxic effects were observed. However, in an acidic environment (pH 4.8; pH 4.5 – 5.0 is typical of a lysosome)[198] MPs catalysed the production of ROS (hydroxyl radicals) from H_2O_2, with concomitant MP-dose-dependent cytotoxicity. TEM analyses of these cells revealed the presence of MPs within lysosomes, and the authors offer this intracellular localisation as an explanation for the toxicity observed with these MPs, potentially explaining why MP-related toxicity was observed in microglia in the current study (*i.e.* in the only cell type where intralysosomal MPs were observed).

In contrast to these findings, Hohnholt *et al.* (this report is also discussed in section 2.4.3) assessed the toxicity of DMSA-coated iron oxide MPs in the OLN-93 oligodendroglial cell line and did not find evidence of increased ROS levels or acute cytotoxicity.[273] Their findings indicate that OLN-93 cells metabolise iron from these particles, although it is not clear by what mechanism the iron is released from the MPs. No evidence was seen of Sphero MPs undergoing breakdown in OPCs or oligodendrocytes, in contrast to Hohnholt *et al.*,[273] but future work should attempt to study this issue further by measuring particle breakdown products and associated toxic by-products, such as ROS,

using particles with a range of physico-chemical properties. Such studies may indicate which formulations are the most stable within cells.

Direct *in vivo* delivery of MPs as contrast agents exploits microglia/macrophage activity allowing for the mapping of CNS lesions. The data presented here in relation to toxic effects of MPs in microglia raise the possibility of secondary toxic effects, as microglia may take up large quantities of MPs and succumb to cell death within lesion sites, potentially exacerbating immune responses. The potential for such an outcome highlights the need for detailed toxicity assessments of synthetic materials intended for biomedical applications.

5.4.3 Amenability to MP-mediated transfection, and optimal magnetofection conditions, differ between glial cell types

A further point to note here is that all glial cell types demonstrated perinuclear accumulation of Sphero MPs, suggesting the feasibility of MP-mediated gene delivery. This has previously been shown to be possible with astrocytes,[164] and gene delivery to OPCs and oligodendrocytes has now been demonstrated here (section 3.3.1 and 4.3.6, respectively). The most effective magnetofection condition for astrocytes was the application of a 1 Hz oscillating field. However, for OPCs, a 4 Hz oscillating field proved most effective. The reasons for these intercellular differences are unknown, but as recent data from this laboratory (submitted for publication) shows that NSCs are also optimally transfected at 4 Hz, it may be speculated that these differences may be related to cellular morphology. Both OPCs and NSCs have small spherical or oval cell bodies, with few processes, whereas astrocytes adopt broad flat morphologies. For broad, flat cells (*e.g.* astrocytes), membrane associated MPs are likely to be on top of the cell, oriented such that

an oscillating field would move/agitate them approximately parallel to the membrane, whereas for small, spherical cells (*e.g.* OPCs, NSCs), there may be an approximately equal chance that cell membrane associated particles are attached to the side of the cell, in which case an oscillating field would move/agitate them perpendicular to the membrane. If the direction of particle agitation relative to the membrane affects uptake then this could explain the frequency-dependent differences in transfection efficiency observed. Oscillating magnetofection of other cell types with broad flat morphologies (similar to astrocytes, *e.g.* fibrocytes) should be investigated, to determine whether they are also more effectively transfected at low frequencies. The efficiency of magnetofection of oligodendrocytes differed little between F = 0, 1 and 4 Hz, and therefore no conclusions can be drawn with respect to cell morphology influencing the effectiveness of the field conditions. Overall, these data indicate that effective MP-mediated gene delivery requires that a protocol be tailored for each specific cell type.

Initial attempts to transfect microglia (with the same Neuromag MPs as used in chapters 3 and 4, and with static but not oscillating magnetofection) resulted in very low transfection efficiency (<1%).[241] Based on the TEM analyses of Sphero MPs in microglia, it seems likely that Neuromag-plasmid complexes may also be sequestered or degraded by microglia, without gene delivery to the nucleus, providing a reason for the limited transfection observed in these cells. In recent preliminary competitive transfection experiments, oscillating magnetofection techniques (0.1x dose, F = 4 Hz) have been tested with OPC and microglial co-cultures, and although some GFP expression was observed in cells identified as microglia, the pattern of expression differed greatly from that seen in all other cell types. Whereas transfected OPCs in the same cultures exhibited uniform green fluorescence throughout the cell body and processes, GFP expression in microglia was punctate, in numerous round structures with variable intensity **(Figure 12)**, suggesting that

GFP had been expressed by the cell, but that it was subsequently sequestered within vesicles. It is not clear from the analyses performed so far whether this 'abnormal' GFP expression is cytotoxic to microglia, but some microglia which had undergone these 'aborted transfection' events showed evidence of pyknotic nuclei.

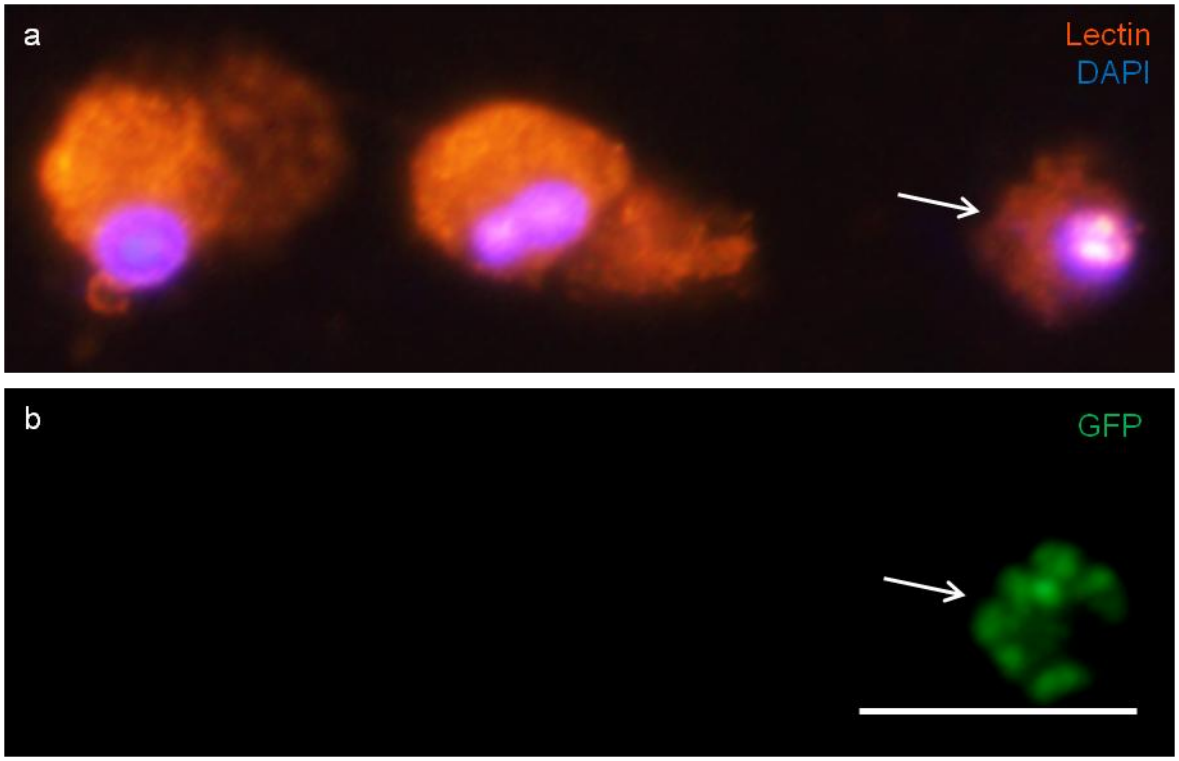

Figure 12: Microglia demonstrate 'abnormal' GFP expression following oscillating magnetofection. *Fluorescence micrographs of an OPC:microglial co-culture 48 h following magnetofection (Neuromag MPs, pmaxGFP plasmid, 0.1x dose, F = 4 Hz). (a) Lectin^{+} microglia. Arrow indicates a microglial cell with a rounded morphology and shrunken, potentially pyknotic nucleus. (b) Counterpart image to (a) showing abnormal GFP expression in a microglial cell (arrow). Note that GFP appears to be sequestered in multiple intracellular regions, rather than evenly expressed throughout the cell. Scale bar = 20 µm.*

5.4.4 Microglia represent an 'extracellular barrier' to MP-based engineering of other glial subtypes

To the best of my knowledge, this is the first report of a stoichiometrically-defined neural co-culture system being developed with cells derived from a common primary origin. The method of co-culture of individual glial subtypes that I have developed here has allowed for the co-propagation of cells that usually require different media. The success of the method is evidenced by microscopic observations which revealed that cells within the co-cultures demonstrated their characteristic morphological and antigenic staining profiles. The observation that near 50:50 glial mixtures could be achieved, suggests that the cell plating densities and relative timings of cellular additions can potentially be refined further to result in varying cell to cell ratios, as required (for example 90:10 or 70:30).

In this context, it is noteworthy that whilst other studies have compared cellular responses to a single particle across a variety of cell types (in purified/enriched cultures), these studies have frequently employed cell lines[220] (see section 1.10 for details of the drawbacks of cell line-derived data), and rarely attempted to include multiple cell types from a single tissue source. Some studies have attempted to evaluate particle uptake in undefined mixed cell cultures established from dissociated neural tissue. For example, Pinkernelle *et al.* established mixed cultures from P5 – 8 rat cerebellum.[222] Commercially available MPs (magnetite core, 185 – 190 nm diameter) were added to these cultures and the authors conclude that *"...most MNPs [magnetic nanoparticles] were phagocytosed by the microglial cells in the mixed cultures which presumably reduce the amount of MNPs for uptake by other cells*".[222] Without demonstrating greater MP uptake in isolated high purity cultures of these non-microglial cell types (as has been reported in this thesis) than

was shown in the mixed cultures, it is clear that this conclusion cannot be reached from this single study. Furthermore, there are significant limitations to this culture system as a model to compare uptake between neural cells. These mixed neural cultures were not well characterised, were highly variable in composition, and underwent significant stoichiometric changes during culture, presumably due to cell proliferation, differentiation or death. While the authors provided a percentage composition of several cell types, actual cell counts were not reported. Also, the oligodendroglial lineage is assessed in limited detail, with the use of a single oligodendrocyte marker, which suggested the presence of a low proportion of oligodendroglial cells in these cultures, questioning the validity of the interpretations with respect to competitive uptake dynamics between microglia and oligodendrocytes.

Using the co-culture approach developed here to perform competitive uptake assays has confirmed the hypothesis that microglia act as a significant 'extracellular barrier' to MP-based engineering of other glial cell types. Both astrocytes and OPCs exhibited a dramatic reduction in the percentage of cells labelled, and a reduction in the extent of MP accumulation when co-cultured with microglia. On average, individual microglia exhibited a greater extent of particle accumulation when co-cultured with OPCs. This was presumably due to the fact that, in these co-cultures, each microglial cell is 'competing' for particles with a reduced number of neighbouring microglia, which have been replaced with another, less avid, cell type (the OPC). This effect was not noted for microglial co-culture with astrocytes, which is consistent with the greater levels of uptake seen in astrocytes than in OPCs, suggesting that astrocytes will compete with microglia more effectively than will OPCs. Despite the greater 'competitive' uptake shown by astrocytes, it should be noted that the microglial 'barrier' significantly limited the extent of MP accumulation by astrocytes in co-cultures.

5.4.5 Glial co-cultures as complex models to mimic the interactions of mixed CNS cell populations with synthetic materials

In agreement with findings from the co-culture model developed here, competitive uptake dynamics in glial cell populations have been previously reported following MP delivery to the CNS *in vivo*, with uptake dominated by microglia, highlighting the predictive value of the approach utilised here. For example, Fleige *et al.* tested uptake of MPs in three glioma cell lines, showing that incubation with MPs for 30 minutes (at three different concentrations) resulted in all cell lines demonstrating similar concentration-dependent accumulation of particles.[339] In a separate experiment, *in vivo* injections of a GFP-expressing tumour cell line (F98) were made in the rat putamen in order to produce GFP^+ gliomas at this site.[339] Acute forebrain slices from these animals were incubated with MPs for 30 minutes and the authors report "*massive*" particle uptake by activated ameboid microglia and invading macrophages, but "*almost no*" uptake by glioma cells, suggesting that the presence of microglia and blood macrophages can act as an 'extracellular barrier' to MP uptake by glioma cells. The authors further tested the capacity of glia in co-cultures to take up MPs by culturing microglia over a monolayer of primary astrocytes (undefined ratio). Following incubation of these co-cultures with particles for 30 min, they report that microglial uptake is "*evident*" but that there is "*almost no detectable*" labelling of astrocytes,[339] further supporting the concept that competitive uptake mechanisms exist between microglia and other glial cell types.

5.4.6 Conclusions and future directions

Microglia are one of the most abundant cell types in the CNS and demonstrate rapid and efficient uptake of MPs. Therefore, any MP-based applications intended for use in the CNS *in vivo* must give consideration to their presence, especially in the context of CNS lesions where microglia will be more numerous and more active than in healthy tissue. As such the microglia can be considered a substantial barrier to MP-mediated gene or drug delivery, as they are likely to sequester and probably digest such functionalised particles, reducing the likelihood of a successful functional outcome. Further, the MP-associated toxicity in microglia, as reported here, could potentially become a cause of significant secondary pathology in CNS lesions. Despite the lack of success with gene delivery, transfection of microglial cells remains a significant goal in regenerative medicine. As a neural population that readily migrates to CNS lesions and releases a wide variety of cytokines, microglia are a major target for gene therapy, whether by the introduction of exogenous genes or by the regulation of endogenous genes.

If it is intended that MPs are to be delivered to a specific CNS cell type other than the microglia, it will be necessary to design a particle that evades microglial uptake. Such 'stealth' particles are currently being investigated by numerous laboratories.[340–342] If microglial uptake is successfully limited, astrocytes seem the next most likely cell type to exhibit uptake of MPs in the CNS, due to their abundance and the greater accumulation of MPs seen here compared to oligodendroglial cells, and the low level of particle uptake reported in primary neurons.[222] If a MP is intended to reach an oligodendroglial population, it may be necessary to employ a specific targeting strategy, such as the incorporation of a ligand or antibody directed towards an oligodendroglial-specific receptor,[133,261,343] owing to the inherently low levels of uptake in these cells compared to other glia.

Lastly, the co-culture system developed here could be expanded to include additional neural cell types (*e.g.* oligodendrocytes, neurons or NSCs), in defined ratios, and with the desired extent of differentiation/activation [*e.g.* mature oligodendrocytes, activation of microglia by granulocyte-macrophage colony-stimulating factor (GM-CSF)] to match particular CNS regions or disease states. Introducing these additional levels of refinement can potentially provide superior models with enhanced cellular complexity for the testing of interactions of synthetic materials with the CNS.

Chapter 6: Conclusions and general discussion

6.1 Summary of thesis findings

It has been shown in this thesis that OPCs and oligodendrocytes are amenable to MP-based cell labelling and transfection (including magnetofection strategies), albeit with notable cell type-dependent differences. Through intercellular comparisons of particle uptake and handling by the major neuroglial subtypes, it has become apparent that substantial differences exist between individual cell subclasses.

The findings presented in this thesis can be summarised as follows:

- OPCs derived from a primary source were safely labelled with MPs (up to 60% of cells) of two physico-chemically different (and well-characterised) formulations, without the need for specific cell targeting strategies. MP-labelled OPCs displayed normal differentiation profiles and could retain their label for up to 30 days.
- The OTOTO SEM protocol enabled the ultrastructural visualisation of OPC-MP interactions, including the identification of endocytotic events.
- OPCs were safely transfected using MPs, with transfection efficiency enhanced by magnetofection techniques. An oscillating magnetic field (4 Hz) has proved optimal with the protocols tested so far. Genetically modified OPCs transplanted onto organotypic cerebellar slice cultures survived and displayed normal migration, proliferation and differentiation profiles.
- Combinatorial and therapeutic gene delivery to OPCs was safely achieved using MPs, but MP-mediated transfection efficiency is inversely proportional to plasmid size.
- Oligodendrocytes were safely labelled with MPs (up to 45% of cells), without the need for cell-targeting strategies, albeit with smaller MP accumulations than observed in OPCs.

- Oligodendrocytes were safely transfected using MPs, with transfection efficiency enhanced by static and oscillating magnetofection techniques. Transfection levels under all magnetofection conditions were significantly lower than those obtained in OPCs.
- A cross-cellular comparison of data from this thesis with data previously published by this laboratory, shows that astrocytes are more amenable to MP-mediated gene delivery than OPCs, which are more amenable than oligodendrocytes. The most effective oscillating field condition for transfection varies between cell types.
- The same cross-cellular comparison of MP uptake and handling shows that microglial MP uptake is far more rapid and extensive than the other glial cell types, and a glial MP uptake hierarchy is apparent: microglia > astrocytes > OPCs > oligodendrocytes.
- MP-based toxicity (associated with lysosomal MP degradation) was observed in microglia, but not in astrocytes, OPCs or oligodendrocytes, all of which contained intact cytosolic MPs, at identical MP concentrations and incubation times.
- A protocol has been developed for the co-culture of different glial subtypes with defined stoichiometry. Using this model, the hypothesis that microglia constitute an 'extracellular barrier' to MP-based engineering of other cell types has been confirmed in defined co-cultures with astrocytes, and with OPCs.

The immediate implications of these findings have been discussed in detail within each chapter, and the discussion here will consider broader implications for the use of the MP platform in conjunction with neural tissue engineering. Here, I propose further directions for developments in the fields of MP design/analysis, genetic engineering of transplant populations, and *in vitro* transplant modelling.

6.2 Implications of findings and future directions

The design of neurocompatible MPs will require systematic analyses of MP interactions with neural cells on a cell-by-cell basis, including OPCs, which is a vast undertaking. The development of automated analytical systems would be of benefit in this regard for high-throughput MP screening. The most detailed information about cell-particle interactions, including uptake, comes from ultrastructural studies, but these are typically low throughput. The OTOTO SEM technique developed here begins to address the need to gather quantifiable data across large numbers of cells, but the process could be further developed by introducing automation of both the sample processing and imaging/analysis stages. The processing of coverslips for OTOTO SEM consists of a simple procedure of adding and removing solutions, which could easily be automated, followed by the packaging of coverslips in filter paper for critical point drying. Although this packaging step may prove difficult to automate, the critical point drying would not. Having prepared the samples, the imaging and analysis could be amenable to software-based automation for detection and quantification of particles[344] and endocytotic events. The development of such technologies represents commercial opportunities for industry, with the equipment and software likely being translatable to various other purposes (*e.g.* studying membrane interactions and uptake mechanisms for viral vectors, or quantifying the effects of stimulatory/inhibitory molecules on the extent of endocytotic membrane ruffling or pit formation).

The successful labelling and transfection of OPCs shown in this thesis illustrates the considerable potential for the development of *multimodal* MPs for use with neural transplant populations. The prototype Fe_3O_4-PEI-RITC particles tested here were designed to deliver such multifunctionality, providing MRI contrast, histological detection by

fluorescence or iron staining, and incorporating PEI as a transfection agent. However, low transfection levels (<1%) were achieved in astrocytes using these particles, even with static field magnetofection techniques.[102] The reasons for this low efficiency are unclear, but are apparently not due to limited MP uptake, as ~100% of astrocytes were successfully labelled with MP:plasmid complexes, even without magnetofection.[102] The high iron content of these particles, and hence high density, may lead to rapid sedimentation of these MPs, such that magnetofection does not significantly enhance vector-cell contact.[102] Therefore the limited gene delivery observed may be related to MP-plasmid interactions, or intracellular processing of the complexes, and further particle development will seek to address these issues.[102] For example, the quantity and conformation of DNA bound by the particles should be investigated, and the rate of release of the plasmid from the complex, necessary for nuclear import, should be assessed. Such information will inform the modification of the current prototype, and the design of novel particles. The prototype particle tested here may prove to be amenable to magnetic cell targeting approaches (aided by the high iron content), but yet further functionality could also be incorporated into multimodal MPs, producing so-called 'smart nanostructures'. This concept refers to particles that react to intracellular physiological changes, or external stimuli (*e.g.* heat, light), with this reaction often being proposed to result in a conformational change in the particle, releasing a drug payload from an internal compartment.[345] However, the interesting possibility has also been raised that a structural change in the particle could be detectable non-invasively in real-time, signalling an event such as a change in pH (*e.g.* reporting lysosomal localisation of the particle).[99]

This research interface between materials chemistry and cell transplant biology is an area of high scientific interest, and the development of MPs as cellular engineering tools would be aided by standardised reporting of at least some particle characteristics, such as

the size, shape and charge of particles. The lack of routine characterisation of synthetic materials (which are frequently novel, and even when not, may exhibit significant batch-to-batch variability), in conjunction with the fact that the choice of model cell type(s) is not standardised, hampers progress in the field of tissue engineering as findings cannot readily be compared and contrasted between studies. Therefore, sound conclusions cannot be drawn in respect of which particle properties influence their utility for cellular engineering (*e.g.* it is not clear how particle charge affects the extent of cellular uptake; see section 1.9). Agreement also needs to be reached regarding which particle characteristics should be reported, and which analyses are most appropriate to determine each of these properties (*e.g.* the limitations of hydrodynamic diameter as a measure of MP size have been discussed in section 5.3.1; and although determining zeta potential in a physiological medium rather than water may be more biologically relevant, there may not be a medium upon which standardisation could be agreed).

The proofs-of-principle of MP-mediated delivery of multiple reporter genes and a therapeutic gene to OPCs indicate that multiple therapeutic genes could be delivered to an OPC transplant population, allowing a combination of goals to be targeted. However, further to this, the combinatorial therapies likely required for CNS regeneration would be more effectively delivered with *temporal* control of transgene expression. Through further vector and plasmid engineering it may be possible to deliver multiple therapeutic genes to a transplant population, each under the control of a different promoter. A number of inducible promoter systems have been developed, whereby transgene expression can be triggered by drugs (*e.g.* tetracycline, rapamycin, or tamoxifen).[117] To provide more clinical control of the process, the promoters could be designed to be manipulable through external signalling, potentially in real-time. For example, the technology developed to perform hyperthermia therapy in tumours can be adapted for use with thermoinducible

promoters.[346] An oscillating magnetic field can be used to raise the temperature in the vicinity of MPs (this technology is based on the fact that tumour cells are more sensitive to this heating than normal cells) activating this thermoinducible promoter and hence triggering expression of the associated transgene.[347]

With reference to the translational relevance of these findings, clinical transplant populations are likely to be derived either from primary foetal tissue or from *in vitro* differentiation of human ESCs or NSCs.[34] In the first instance, the cell source will likely be heterogeneous (consisting of OPCs at various stages of differentiation, and potentially including different subtypes), and of indeterminate age (human conception can only be estimated to within 1 – 2 weeks),[348,349] and furthermore it will be difficult to predict what approximate age and quantity of cells will become available for a treatment. This scenario will be more accurately modelled by studies using cells from primary sources, than by studies employing cell lines (see section 1.10), and the heterogeneous uptake dynamics noted in the cross-cellular comparison of astrocyte, OPC and oligodendrocyte populations from primary sources is likely to be representative of human foetal tissue, although this will need to be established empirically. The fact that oligodendrocytes display lower amenability to manipulation than OPCs should be investigated further, with MP handling by defined oligodendroglial stages being studied. These stages can be derived by immunopanning,[305,323] and evaluated in isolation, and by determining the amenability to engineering of each stage/subtype, it may be possible to predict the amenability to labelling/transfection of a donor cell population based on that population's antigenic profile. Such data may allow the determination of developmental windows within which donor populations are most/least amenable to MP-based engineering. It will be of interest to determine whether MP uptake and transfection efficiency decreases continuously as the cells differentiate and mature. Furthermore, it will be of interest to test MP handling and

transfection efficiency in cell types that precede OPCs in development (*e.g.* NSCs, ESCs) to determine whether there is a step-wise decrease in amenability to MP uptake/transfection throughout development. If this is found to be the case, it raises interesting questions about whether it may be more effective in general to manipulate cells at a precursor/antecedent stage and then induce differentiation, rather than attempting to manipulate the desired cell type directly. For cell transplant populations derived from ESCs or NSCs, an industrial opportunity is available, as these cells are likely to be expanded and differentiated *in vitro* using automated cell culture machines. As the oscillating magnetofection protocol developed here is technically simple, it could be incorporated into such machinery, automating the process of transfection, and limiting the risks of pathogenic contamination by confining these manipulations within a single device.

Two models consisting of multiple cell types have been utilised in this thesis: slice cultures and defined co-cultures. The organotypic cerebellar slice culture system employed here has already been adapted to serve as an injury model of both focal and diffuse demyelination, including traumatic injury (see section 1.6), but it has only begun to be exploited as 'host' tissue for genetically modified neural cell transplantation strategies, with one report of the transplantation of GFP-expressing OPCs,[4] in addition to the report in this thesis, and has not yet been used to test *therapeutically*-modified OPC transplant populations. The clinical relevance of this organotypic model can be improved by seeking to establish slice cultures from human tissue,[37,350] and potentially from patients with myelin-related disease (*e.g.* MS). This will involve collaboration with hospitals/tissue banks, application(s) for ethical clearance, and regulation by the Human Tissue Authority (HTA), but given the lack of translation of treatments developed in many animal models,[67,68] such an approach could yield data of far greater predictive value for the clinic. This model could be combined with the transplantation of neural cells derived from human

ESCs and NSCs, and also primary human neural cells (although these are less readily available), to further enhance the translational relevance of the studies. Furthermore, these models provide an opportunity to test MP-based engineering of human cells/tissue, including transplantation modelling. In this context, there are no reports of MP-mediated gene delivery to non-tumourigenic primary human neural cells (there is one report of static magnetofection of primary glioblastoma cells),[351] representing a significant knowledge gap. It is unknown whether inter-species differences exist in the amenability of neural cells to MP-based engineering in general, or to magnetofection techniques in particular, either static or oscillating. Furthermore, it is not known whether species-specific differences in MP-based toxicity exist, and it is unknown whether the human oligodendroglial lineage will exhibit a similar reduction in amenability to MP-labelling/transfection as is shown by rat OPCs/oligodendrocytes; the prolonged developmental period for humans[348,349] may provide a longer developmental window in which OPCs can be effectively engineered, compared to rats. The defined co-culture system developed during this thesis can be expanded to include additional cell types (subject to the development of suitable media), at defined ratios, and the stages of differentiation/activation of each cell type can be influenced. Stoichiometrically-representative models can potentially be produced of various CNS regions and/or disease states, including the production of models with pre-immunosuppressed microglia, of relevance to the modelling of corticosteroid-treated patients, for example some MS patients.[352,353]

The demonstration that microglia constitute an 'extracellular barrier' limiting MP delivery to other glial cell types has implications for *in vivo* usage of MPs, which can be predicted to typically result in extensive accumulation by microglia, limiting their delivery to other neural cell types, with oligodendrocytes anticipated to demonstrate the lowest levels of uptake of the neuroglia. It will be of interest to perform comparable MP studies

with neurons, including competitive uptake studies in co-cultures, to determine how neurons fit into the 'uptake hierarchy' determined in this thesis for the neuroglia. By obtaining a sufficient number of data-points at various times and concentrations, it should be possible to develop a mathematical model of the rate and extent of uptake by each cell type, and these models could be used to make predictions of competitive uptake outcomes, which could then be tested in co-cultures, including co-cultures of three or more cell types. If these models demonstrate that the hierarchy of MP uptake suggested by comparing pure glial cultures also describes MP uptake in cultures with all glial cell types, then it can be anticipated that *in vivo* delivery of MPs to the CNS will typically be an ineffective method for engineering OPCs, and especially for engineering oligodendrocytes. Such applications would likely require specific cell targeting strategies, possibly combined with methods to evade microglial uptake, sequestration and breakdown.

In terms of approval for clinical translation, synthetic materials, including magnetic particles, are regulated by the FDA in identical manner to other diagnostic and therapeutic agents, requiring studies of systemic clearance, biodistribution and toxicology;[218,354,355] regulations in the EU are similar. Although extensive work is required to gain FDA or EU approval, several iron oxide-based particles have been approved for use as contrast agents,[143,183] for the treatment for iron-deficiency anaemia,[356,357] or for hyperthermic tumour therapy.[347] Therefore, by rigorously testing MPs in primary cells and relevant models that mimic the complexity of the CNS, to ensure neurocompatibility, followed by pre-clinical animal testing, it is feasible that an iron oxide-based MP designed for neural engineering could enter clinical trials.

This thesis has demonstrated the utility of MPs for labelling and transfecting OPC transplant populations, and highlighted a number of ways in which the effectiveness of

these applications could be enhanced, through further research. Additionally, intercellular differences in glial MP handling have been described, and their implications discussed, particularly with reference to the role of microglia as an ‘extracellular barrier’ to particle uptake by other cell types. By developing effective tools for the engineering of neural cell transplant populations, and employing well-designed combinatorial strategies, it is hoped that such work will enable a step-change in the treatment of debilitating CNS injury/disease, from palliative approaches, to regenerative therapies.

Appendix 1: Particle calculations (Sphero and Fe_3O_4-PEI-RITC)

This calculation for Fe_3O_4-PEI-RITC particles was kindly provided by Dr H H P Yiu (Heriot-Watt University, Edinburgh, UK).

The unfunctionalised iron oxide core is ~25 nm in diameter, and has a density of 5 g/cm^3.

The volume ($4/3\ \pi r^3$) of one particle is 8181 nm^3.

The mass (density x volume) of one particle is 4.1×10^{-17} g.

Therefore, 1 µg contains approximately 24 billion particles.

Once functionalised with PEI and RITC, the organic content has been determined to be ~20%.

Correcting for this organic component, there are estimated to be 19.2 billion particles/µg.

To compare the concentration of Fe_3O_4-PEI-RITC particles with Sphero particles: Sphero particles are supplied at 1% w/v (10 mg/ml) and reported by the manufacturer to contain 2.59×10^{11} microspheres (particles) per ml.

Therefore, 1 mg contains 2.59×10^{10} particles, and 1 µg contains 2.59×10^7 particles.

At 50 µg/ml, this equates to 1.295 billion Sphero particles/ml ($2.59 \times 10^7 \times 50$).

For Fe_3O_4-PEI-RITC particles at 5 µg/ml, there are 96 billion particles/ml (19.2 x 5).

This gives a ratio of 1:74, Sphero:Fe_3O_4-PEI-RITC.

For equal w/v concentrations (*e.g.* 20 µg/ml), the particle number ratio is 1:741.

Appendix 2: Statistical analyses for the cross-cellular comparison of MP uptake

To compare the rate and extent of MP uptake by different glial cell types (section 5.1), published data relating to astrocytes and microglia were collated with novel data reported in this thesis for OPCs and oligodendrocytes. All astrocyte, microglial and OPC cultures (section 2.4) were of high purity, and oligodendrocyte cultures were enriched (section 4.3). The phrase 'each cell type' refers to: all $GFAP^+$ cells in pure astrocyte cultures (n = 3 cultures for uptake; n = 5 for toxicity), all $OX42^+$ cells in pure microglial cultures (n = 3 cultures for uptake; n = 5 for toxicity), all $A2B5^+$ cells in pure OPC cultures, and all MBP^+ cells in enriched oligodendrocyte cultures. All of the data was obtained using Sphero MPs, which are characterised in section 2.2, and all experiments were performed with identical ranges of concentrations and incubation times.

Rate of MP labelling: data-points were compared at (a) 1 h, 20 µg/ml, (b) 4 h, 2 µg/ml, and (c) 4 h, 50 µg/ml for the percentage of each cell type exhibiting MP labelling.

Extent of MP accumulation: data-points were compared at 1 h, 20 µg/ml for the percentage of each cell type that exhibited either 'medium' or 'high' levels of MP accumulation ('medium' and 'high' data were summated).

Figure 1e, Rate of MP labelling: data-points were compared at 4 h for all concentrations (2, 5, 20 and 50 µg/ml) for the percentage of each cell type exhibiting MP labelling.

Figure 1f, Toxicity: Data-points were compared following 24 h incubation with particles at 20 µg/ml. For oligodendrocytes, the number of MBP^+ cells in MP-treated cultures was expressed as a percentage of the number of MBP^+ cells in control cultures, giving a percentage viability assessment. For OPCs, the same procedure was performed for

A2B5^{+} cells. For astrocytes and microglia, MTS assays were performed, and absorbance readings from MP-treated cultures were expressed as a percentage of absorbance readings from controls, giving a percentage viability assessment. Unpaired two-tailed *t* tests were then performed comparing each viability assessment with controls (100%).

Figure 1g, Perinuclear localisation: data-points were compared at (a) 1 h, 50 µg/ml, (b) 4 h, 50 µg/ml, and (c) 24 h, 50 µg/ml for the percentage of each cell type exhibiting any perinuclear MPs.

Appendix 3: Article published by Nanomedicine (London).

Much of the data included in chapters 2, 4 and 5 has now been accepted for publication by Nanomedicine.

This appendix consists of the unformatted article, accepted for publication on 30/08/2012.

Adapted from Nanomedicine 2012 (Ahead of Print) with permission of Future Medicine Ltd (08/10/2012)..

Differences in Magnetic Particle (MP) Uptake by Central Nervous System (CNS) Neuroglial Subclasses: Implications for Neural Tissue Engineering

Stuart I Jenkins, Mark R Pickard, David N Furness, Humphrey HP Yiu, Divya M Chari

Keywords: Magnetic particles, endocytosis, neuroglia, uptake, oligodendrocyte precursor cell

Abstract

Aims: To analyze magnetic particle (MP) uptake and intracellular processing by the four main non-neuronal subclasses of the central nervous system (CNS) [viz. oligodendrocyte precursor cells (OPCs), oligodendrocytes, astrocytes and microglia].

Materials and Methods: MP uptake and processing were studied in rat OPCs and oligodendrocytes, using fluorescence and transmission electron microscopy, and results collated with previous data from microglia and astrocytes.

Results: Significant intercellular differences were observed between glial subtypes, with microglia demonstrating the most rapid/extensive particle uptake, followed by astrocytes, with OPCs and oligodendrocytes showing significantly lower uptake. Ultrastructural analyses suggest that MPs are extensively degraded in microglia but are relatively stable in other cells.

Conclusions: Intercellular differences in particle uptake and handling exist which will have important implications for the utility of the MP platform for biological applications involving neuroglial cells, including their genetic modification, transplant cell labeling and direct biomolecule delivery to mixed CNS cell populations *in vivo*.

Introduction

Magnetic particles (MPs) have emerged in recent years as an important platform for advanced biomedical technology, due to innovations in their large-scale synthesis and complex surface functionalization [1,2]. These advanced materials are used in key applications such as drug/gene delivery, magnetic drug targeting, thermotherapies, stem cell targeting, and in diagnostic imaging (as contrast agents) [2–6]. The size and surface chemistry of MPs can be tailored for molecules with which they are to be 'functionalized', enabling the construction of multimodal particles that can mediate combinations of cellular applications, whilst retaining nanoscale dimensions [7]. The unique versatility achievable with their structural design therefore confers on MPs the ability to serve as a 'theragnostic platform' to integrate therapeutic strategies with diagnostic methods such as MRI [8].

Despite their proven therapeutic potential, the use of MPs for central nervous system or CNS (*ie.* brain and spinal cord) applications has been a relatively underexploited area to date [2]. Their utility is being increasingly demonstrated for a range of regenerative applications including neural progenitor/stem cell transplant imaging [9,10], gene delivery deploying novel 'magnetofection' methods [11–15] and diagnostic imaging in neurological injury [16]. However, there are critical gaps in our knowledge of fundamental biological parameters governing the utility of this emergent technology for CNS applications, especially the factors that determine MP uptake and intracellular processing in neural cells. The influence of parameters such as MP size, coating and charge on particle uptake have been studied in non-neural cell types [17-20] but the influence of neural cell *subtype* on particle uptake has never been assessed. This is especially pertinent when considering MP applications in CNS tissue; the latter is uniquely complex and contains several, specialist, interacting cell types meaning that data obtained from other physiological systems cannot be extrapolated to the CNS. The neurons mediate electrical conduction but a diverse population of *non-neuronal* cells, collectively termed the 'neuroglia' undertake distinct and critical functions such as immune surveillance, blood-brain barrier maintenance, genesis of myelin (the insulating sheath around neurons) and regulation of electrochemical signalling [21-23]. Neuroglial subclasses consist of the oligodendrocytes [that co-exist with their parent population- the oligodendrocyte precursor cells (OPCs)], microglia, and astrocytes. These subclasses have unique structural, functional and molecular properties and can therefore be predicted to show important differences in their uptake and handling of synthetic materials. Indeed, our recent studies point to significant intercellular differences in toxicity and transfection levels between neuroglia, the reasons for which are unknown [12,14,24]. The neuroglia form an extensive cellular network and outnumber neurons by a factor of approximately ten, consequently, understanding particle handling by this major class of cells will be a critical component in understanding interactions between biomaterials and the CNS as a whole.

A small number of studies have reported MP uptake by neuroglial cells [25,26] but whether differences in particle uptake and handling exist between different neuroglial subtypes in CNS tissue, is unknown. To address this issue, we have assessed the uptake and intracellular processing of a single type of MP (of specific size and formulation) by oligodendrocyte lineage cells *ie.* oligodendrocytes and OPCs derived from primary cell cultures. These findings were collated with data from our previous studies in astrocytes [27] and microglia [24] (also derived from primary cultures) to provide, for the first time, comparative data on the uptake characteristics and particle handling by these major subclasses of CNS cells.

Materials and Methods

Reagents and equipment: Tissue culture-grade plastics, media, and media supplements were from Fisher Scientific (Loughborough, UK) and Sigma-Aldrich (Poole, UK). Recombinant human platelet-derived growth factor (PDGF-AA) and basic fibroblast growth factor (FGF2) were from Peprotech (London, UK). Monoclonal rat anti-MBP was from Serotech (Kidlington, UK), monoclonal mouse anti-A2B5 was from Sigma-Aldrich (Poole, UK), and secondary antibodies (FITC-conjugated) were from Jackson ImmunoResearch Laboratories Inc. (West Grove, PA, USA). Mounting medium with DAPI (4',6-diamidino-2-phenylindole) was from Vector Laboratories (Peterborough, UK). Paramagnetic, carboxyl-modified Sphero^{TM} nile red fluorescent MPs (diameter 0.20 – 0.39 μm, iron content 15 – 20% w/v) were obtained from Spherotech Inc. (Lake Forest, Illinois, USA). We have observed that their fluorophore does not leach, and their emission spectra remain stable following long periods of storage, making these an optimal choice for this study.

Particle characterization: FTIR (Fourier transform infrared) spectroscopic analysis was carried out using a Perkin Elmer Spectrum 100 spectrometer fitted with an ATR (attenuated total reflection) sampling unit. For the sample measurement, 32 scans in the region from 650 to 4000 cm^{-1} were accumulated with a resolution of 4 cm^{-1}. Powder XRD (X-ray diffraction) analysis on the iron oxide component of the particles was carried out using a Bruker D8 Advance diffractometer with Cu $K\alpha_1$ radiation (λ = 1.542 Å). The diffraction pattern was collected from 2θ = 5° to 80°, at a step size of 0.009° and a step time of 120 s. The particle size of iron oxide was estimated using Scherrer analysis on the most intense peak (311). Assessments of hydrodynamic size and zeta-potential of particles in various medium were made using a Malvern Zetasizer Nano ZS. To evaluate the effects of time on particle aggregation, size measurements were made at 5 min and 24 h after particle addition to Sato medium (37ºC). To evaluate the effects of different culture media on particle size and zeta potential, measurements were made after particle addition to all three media used for the maintenance of the individual cell types used in these studies and compared with particle size in deionized water. All media were incubated (37ºC, 5% CO_2/95% humidified air) before analysis, to ensure measurements were made at the same *p*H as that at which cells were cultured.

OPC and oligodendrocyte cultures for uptake experiments: The care and use of animals was in accordance with the Animals (Scientific Procedures) Act of 1986 (United Kingdom) with approval by the local ethics committee. Primary mixed neuroglial cultures were prepared from cerebral cortices of Sprague-Dawley rats at postnatal day 1 – 3, based on an established protocol [28]. Cultures were maintained in D10 medium (DMEM supplemented with 10% fetal bovine serum, 2 mM glutaMAX-I, 1 mM sodium pyruvate, 50 U mL^{-1} penicillin, and 50 μg mL^{-1} streptomycin) at 37°C in 5% CO_2/95% humidified air for 8 – 10 days, then shaken for 2 h on a rotary shaker at 200 rpm. This medium, containing largely microglia was discarded, fresh D10 medium added, and flasks shaken overnight at 200 rpm. The resulting medium, containing largely OPCs, was transferred to non-tissue-culture grade petri dishes, to reduce residual microglial contamination. After 30 min, unattached cells were resuspended in either OPC maintenance medium (OPC-MM: DMEM supplemented with 2 mM glutaMAX-I, 1 mM sodium pyruvate, 10 nM biotin, 10 nM hydrocortisone, 30 nM

sodium selenite, 50 µg mL^{-1} transferrin, 5 µg mL^{-1} insulin, 0.1% bovine serum albumin, 50 U mL^{-1} penicillin, 50 µg mL^{-1} streptomycin, 10 ng mL^{-1} PDGF-AA, and 10 ng mL^{-1} FGF2) for OPC cultures, or in Sato medium (DMEM supplemented with 2 mM glutaMAX-I, 1 mM sodium pyruvate, 1X N2 supplement, 30 nM thyroxine, 30 nM triiodothyronine, 50 U mL^{-1} penicillin, and 50 µg mL^{-1} streptomycin) to generate oligodendrocyte cultures. Cells were plated onto poly-D-lysine (PDL) coated glass coverslips in 24-well plates (0.3 mL/well, at 3 x 10^4 cells/cm^2). OPC cultures were maintained for 24 h before incubation with MPs, to allow cell adherence and re-growth of processes. Oligodendrocyte cultures were maintained for 7 days (50% medium changes every 2 – 3 days) to allow cell differentiation, before incubation with MPs. Cells were then incubated with 2 – 50 µg mL^{-1} MPs for 1 – 24 h. For long-term studies, OPCs were pulse-labeled with MPs for 24 h, then switched to Sato medium and maintained for 1 month. Control cultures were treated with equal volumes of fresh medium, without MPs. Samples were washed with phosphate buffered saline (PBS), then fixed and either immunostained, or processed for Perl's Prussian blue histochemical staining. OPC and oligodendrocyte cultures are not as strongly adherent to PDL-coated coverslips as microglial and astrocyte cultures. This presented a methodological problem for particle uptake experiments with regard to the removal of extracellular particles when terminating incubations. In previous work, extensive washing with PBS was necessary to reduce non-specific binding of MPs to minimal levels, and this was well tolerated by microglial and astrocyte cultures, resulting in minimal cell detachment. In the present study a similar washing protocol resulted in the loss of many OPCs and oligodendrocytes, even without the prior addition of MPs. Consequently, to minimize the loss of cells, several washes were performed by gently applying PBS to the walls of culture wells.

Toxicity assessment: Initial experiments used a 3-[4,5-dimethylthiazol-2-yl]-2, 5-diphenyltetrazolium bromide (MTS) assay to assess MP toxicity in OPCs and oligodendrocytes, as described earlier, for comparison with astrocyte and microglia data [24,27]. However, in these cell types, typically low levels of MTS reduction to formazan were consistently found in both control and MP-treated cultures, which was not deemed sufficiently sensitive to accurately assess toxicity. Therefore, epifluorescence microscopy was used to count the pyknotic and total (healthy plus pyknotic) nuclei per microscopic field, as measures of MP-related toxicity. A minimum of five fields were counted for every condition.

Immunocytochemistry: Washed cells were fixed with 4% paraformaldehyde [PFA; room temperature (RT); 25 min] then washed again. For staining, cells were incubated with blocking solution [5% serum in PBS, with 0.3% Triton X-100 for MBP (myelin basic protein); RT; 30 min], then with primary antibody in blocking solution (A2B5 1:200; MBP 1:200; 4°C; overnight). A2B5 and MBP are widely-used markers of the oligodendroglial lineage: the A2B5 antibody recognizes cell surface ganglioside epitopes; MBP is one of the major protein constituents of myelin, and is used to label late-stage oligodendrocytes. Cells were then washed with PBS, incubated with blocking solution (RT; 30 min), and incubated with the appropriate FITC-conjugated secondary antibody in blocking solution (1:200; RT; 2 h). Finally, coverslips were washed with PBS and mounted with the nuclear stain DAPI.

Fluorescence microscopy & image analysis: Samples were imaged using fixed exposure settings on an Axio Scope A1 fluorescence microscope (Carl Zeiss MicroImaging GmbH, Goettingen, Germany), and the images merged using Adobe Photoshop CS3 (version 10.0.1). The purity of each culture was determined by scoring at least 100 DAPI-stained nuclei for coincidence with A2B5 or MBP staining. Z-stack fluorescence images of samples were created using fixed exposure settings on a Nikon Eclipse 80i microscope fitted with a CA742-95 camera (Hamamatsu Photonics, Hamamatsu, Japan), with manual focus stepping at 0.5 or 1.0 µm, and the image manipulations performed using Nikon NIS Elements (version 3.00). The proportion of $A2B5^+$ OPCs or MBP^+ oligodendrocytes with coincident nile red fluorescence was assessed (minimum 100 DAPI-stained nuclei for each concentration and time point), with the proportion of MP-labeled cells exhibiting any perinuclear MPs also being recorded. Some samples were also imaged using a BioRad MRC1024 confocal laser scanning microscope.

Semi-quantitative assessment of MP uptake: It was deemed unsuitable to assess levels of uptake by means of a fluorescence plate reader, or in terms of incorporated iron per cell, as these techniques quantify the total fluorescence or iron present in a culture, and therefore assume an even distribution between cells. Such techniques would not enable the determination of uptake heterogeneity within the cell population, as observed in our cultures. A flow cytometry approach was also considered and rejected, as it is likely that extracellular MPs adherent to the plasma membrane would lead to a number of 'false positives' and this technique cannot distinguish cytoplasmic versus nuclear accumulations of particles within cells. Microscopic cell counting analysis was therefore considered the most appropriate method to assess whether MPs were intracellular, or merely extracellularly attached to plasma membrane. To ensure that cellular uptake was judged correctly, z-stack analyses were performed for both OPC and oligodendrocyte cultures to confirm that MPs were intracellular, rather than adherent to the plasma membrane (minimum of 100 cells analyzed for all concentrations and timepoints). Analysis of oligodendrocyte cultures proved particularly problematic, as MPs were often observed amongst their extensive, lipid-rich processes. However, from the z-stack analyses it was apparent that MPs were external to the oligodendrocyte processes. Therefore, for these analyses, only MPs that were clearly within the oligodendrocyte soma, the main cell body, were considered to be intracellular, and all other particles were deemed to be extracellular. The level of MP uptake in individual cells was assessed in a semi-quantitative manner by comparison with the average cross-sectional area of an OPC/oligodendrocyte nucleus, and scored as either 'low' (<10% of the area of an average nucleus), 'medium' (10 – 50%), or 'high' (>50%). We consider that such detailed microscopic assessment of MP uptake more accurately reflects the heterogeneity that is typically found in primary cell cultures.

Cross cellular comparison of MP uptake across neuroglial subpopulations: Selected datapoints from OPC and oligodendrocyte uptake experiments were combined with equivalent datapoints obtained from rat astrocytes [27] and microglia [24] using identical particle concentrations and timings of exposure. In both cases, the cells were derived from mixed glial cultures (as used for derivation of OPCs and oligodendrocytes) however these two cells were maintained in D10 medium (which is detailed above) for uptake analyses. The relative plating densities used in these experiments were 3×10^4 cells/cm^2 (OPCs and oligodendrocytes), 4 x

10^4 cells/cm^2 (astrocytes) and 6 x 10^4 cells/cm^2 (microglia). Toxicity data (MTS assays) for astrocytes and microglia were obtained from references [27] and [24], respectively.

Perls' Prussian blue staining: Washed samples were fixed with 4% PFA (RT; 25 min), then washed again. Samples were incubated with 2% potassium ferricyanide in 2% HCl for 30 min, then washed three times with distilled water and mounted without DAPI. Images were then taken using light microscopy, to visualize intracellular iron, and fluorescence microscopy, to visualize nile red particle fluorescence. Images were merged to assess colocalization of iron deposits with fluorescence.

Scanning electron microscopy (SEM): MPs in OPC-MM were air-dried onto aluminium stubs and visualized uncoated using a high resolution field emission scanning electron microscope (Hitachi S4500) operated at an accelerating voltage of 5 kV.

Transmission electron microscopy (TEM): Microglial, oligodendrocyte, astrocyte and OPC cultures were established on PDL- or polyornithine-coated aclar sheet (microglial [24] and astrocyte [27] cultures were prepared as described previously), cut to fit a 24-well plate (0.3 mL/well, at 6 x 10^4 cells/cm^2), then incubated with 20 µg mL^{-1} MPs for 4 or 24 h. Samples were fixed with 2.5% glutaraldehyde [in sodium cacodylate buffer (SCB); RT; 2 h], then washed with SCB. Samples were postfixed with 1% osmium tetroxide in SCB for 1 h, washed with SCB, dehydrated in a graded series of ethanol, then infiltrated with Spurr resin, before polymerization at 60°C for 16 h. To obtain sections, the block was trimmed to expose the aclar sheet which was peeled off, leaving the cells in the resin. Ultrathin sections were then cut parallel to the original plane of the sheet on a Reichert Ultracut E ultramicrotome, mounted on 200 mesh thin bar copper grids, and stained with 2% uranyl acetate in 70% ethanol (RT; 20 min) and 2% Reynolds lead citrate (RT; <5 min). A minimum of three sections were examined for each cell type using a JEOL 100-CX transmission electron microscope operated at 100 kV. Images were acquired using a SIS systems Megaview III digital camera (Olympus).

Statistical analysis: Data were analyzed using GraphPad Prism statistical analysis software. Data are expressed as mean ± SEM. The number of experiments (n) refers to the number of mixed glial cultures from which OPC or oligodendrocyte cultures were derived, with each primary culture being established from a different rat litter. Data were analyzed by two-way analysis of variance (ANOVA), with Bonferroni's multiple comparison post-tests for *post hoc* analysis

Results

Characterization of MPs

The MPs used here have a multilayered design **(Figure 1a)**, comprising a polystyrene core (stained with the fluorophore nile red), coated with a polystyrene/iron oxide composite layer; thus the fluorophore is encapsulated within the particle structure and we have found that these are stable in physiological media and consistently perform robustly under our experimental conditions, justifying their use in this study. These 'test' MPs are relatively large (200 – 390 nm diameter; mean = 360 nm); we have previously justified the use of particles of this diameter for *in vivo* biological applications [24]. Indeed, particles of up to 1 µm diameter have been used to image cells transplanted into the CNS without demonstrable effects on even complex biological functions such as myelination [29] and other particles, including functionalized transfection grade ones are of comparable diameter [29–32].

Batch-to-batch variability can occur during MP synthesis, and particle size is an important factor in cellular uptake and processing [19]. Therefore, MPs were analyzed by SEM for size and shape assessments; our data were consistent with our previous findings, showing that the particles used here were regular in shape, and within the size range reported by the manufacturer **(Figure 1b)**. Perls' Prussian blue staining of cells which had been pulse-labeled with these MPs for 24 h revealed the presence of iron coincident with nile red fluorescence at 24 h **(Figures 1c & d)**, and at 30 days post-treatment (data not shown). This demonstrates the reliability of fluorescence as an indicator of MP presence, and suggests the stability of MPs in the culture media and the cells. No blue staining was observed after Perls' staining of control cultures. The particles carry ca. 1.63 × 106 carboxyl groups per particle (data provided by supplier, Spherotech Inc.). The hydrodynamic size of the particles was similar in Sato or OPC-MM, with a slight increase in D10 medium, therefore no differences in aggregation were observed in the three types of media used **(Table 1)**. Comparison of 5 min and 24 h measurements in Sato medium showed that a small amount of particle aggregation occurred, as the particle size increased by a factor of ca. 2. The mean diameter of these particles was shown to be 360 nm by SEM analysis, but the hydrodynamic diameter was in the range 843 – 961 nm. These values were determined by dynamic light scattering (DLS), a technique that measures the hydrodynamic diameter of the particle surrounded by the solvation layers. Measurements by DLS are more accurate for soft materials, such as proteins, with the size of more dense materials commonly being overestimated [33]. These observations are consistent with the literature relating to magnetic nanoparticles [34].

The zeta potential measurements showed that the particles carried negative charge in all media, which can be attributed to the carboxylic acid groups (**Table 1**). The difference in zeta potential among particles in different media was found to be small (indeed, as the charge on a particle is *p*H dependent, the zeta potential of the particles would not be expected to vary significantly as the media used for the cell culture experiments are all of similar *p*H values).

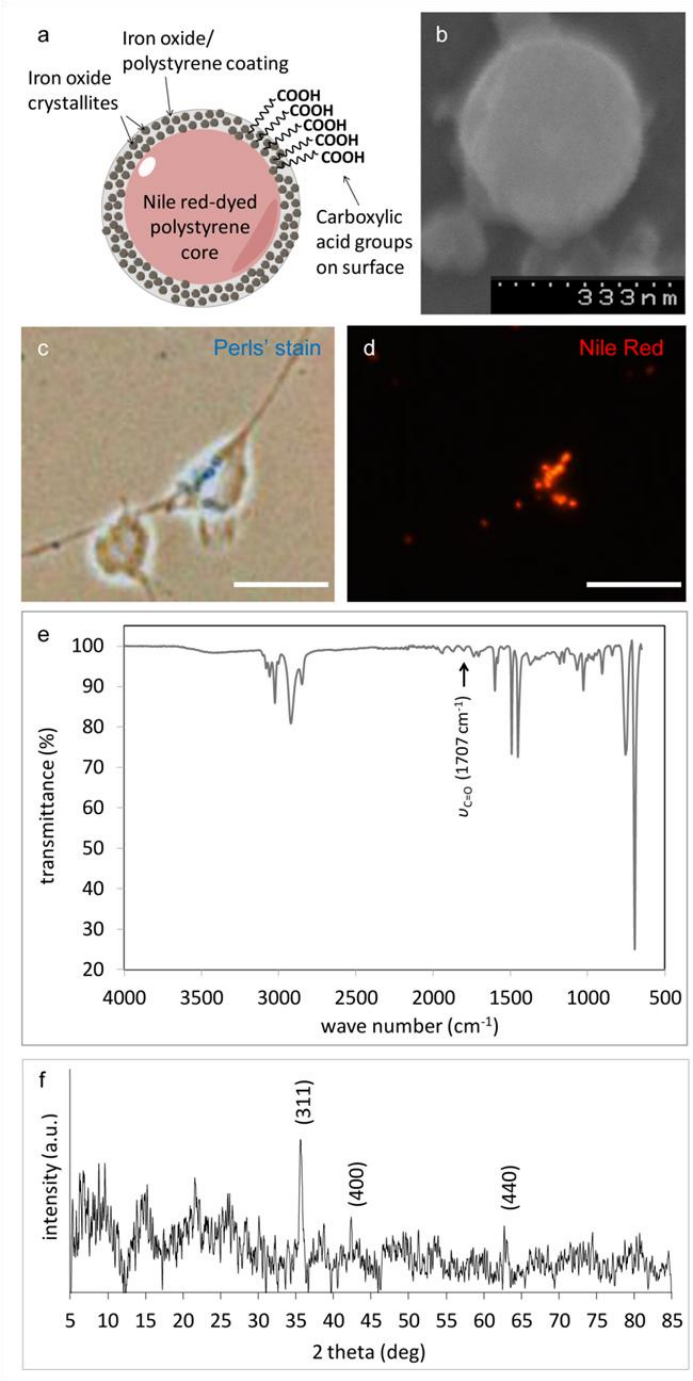

Figure 1: Multi-layered MP structure with particle visualization by fluorescence and histochemical staining. *(a) Schematic diagram of an idealized particle, illustrating the polystyrene core stained with nile red fluorophore, surrounded by a magnetite layer (Fe_3O_4), with a carboxyl-modified coating (layers not drawn to scale). (b) Scanning electron micrograph of an individual particle, showing typical size and shape. (c) Phase-contrast micrograph, showing Perls' Prussian blue staining of iron within an OPC (24 h incubation with 20 µg mL^{-1} MPs). (d) Counterpart fluorescence micrograph image to (c), showing nile red fluorescence is coincident with iron accumulations. Scale bar = 20 µm in (c) and (d). (e) FTIR spectroscopic analysis of MP shows a major polystyrene component characterized by peaks between the region 3083 – 3025 cm^{-1} (C-H stretch, aliphatic) and 2923 – 2851 cm^{-1} (C-H stretch, aromatic ring). The peaks within the fingerprint region 1601, 1492 and 1452 cm^{-1} correspond to the C=C stretch in an aromatic system. The strong peaks at 755 and 696 cm^{-1} correspond to the C-H bending mode of the benzene ring. A small number of carboxylic acid groups were detected at 1707 cm^{-1} (C=O stretching), indicated by an arrow. (f) Powder XRD pattern of particles showing an inverse spinel structure of iron oxide crystallites in particles (a.u. = arbitrary units).*

The FTIR spectrum of these Spherotech particles was dominated by the polystyrene component (**Figure 1e**) with a small number of carboxylic groups, shown as $\nu_{C=O}$ (C=O stretching) at 1707 cm^{-1}. The powder XRD pattern (**Figure 1f**) revealed that the iron oxide crystallites in the particles are of an inverse spinel structure, *eg.* Fe_3O_4 (magnetite) or gamma-Fe_2O_3 (maghemite). However, due to the small crystal size or low crystallinity of the iron oxide, the diffraction peaks are broad and of low intensity. This is also partly due to the predominant amount of polystyrene (*ca.* 80%) present in the particles. The average crystal size was estimated to be around 18.5 nm in diameter using Scherrer analysis on the diffraction peak (311).

Table 1. *Physical characteristics of Sphero MPs in various biological media*

		ζ-potential [mV][a]	d_{DLS} [nm][a]	
Medium	Relevant cell type(s)	Incubation time: 5 min	5 min	24 h
H_2O	-	-	843	-
Sato	Oligodendrocytes	-14.3	850	1650
D10	Astrocytes; Microglia	-13.7	961	-
OPC-MM	OPCs	-14.6	867	-

d_{DLS} = Hydrodynamic diameter, determined by dynamic light scattering (DLS). [a]Average values of three measurements

OPC Culture Characteristics

Phase contrast microscopy of untreated and MP-treated cultures revealed phase-bright cells with bipolar morphologies characteristic of OPCs **(Figure 2a)**. High purity OPC cultures were routinely derived, as assessed by immunostaining for the OPC marker A2B5 (95.4 ± 0.9%; n = 4), and DAPI-staining showed typical round or oval nuclei (Figure 2a, inset).

Concentration- and Time-Dependence of MP Uptake and Perinuclear Localization in OPCs

Fluorescence microscopy, including z-stack and confocal analyses, confirmed the intracellular localization of MPs in OPCs (**Figure 2b**; confocal data not shown) with particles typically observed in small clusters. MP uptake was time- and concentration-dependent, with the highest dose and longest exposure tested resulting in labeling of *ca.* 60% of $A2B5^+$ cells **(Figure 2c)**. Concentrations of 20 and 50 µg mL^{-1} labeled a significantly greater percentage of cells than 2 µg mL^{-1}, at all time points. The extent of MP-uptake by individual cells was heterogeneous, therefore a semi-quantitative approach was employed to classify categories of uptake as described previously [24,27]. Under all conditions, the majority of MP-labeled OPCs exhibited a 'low' level of particle accumulation. At 4 and 24 h, a small percentage of MP-labeled cells exhibited 'medium' levels of uptake at all concentrations with 'high' levels of uptake rarely observed (**Table 2**). The percentage of labeled OPCs with MPs in a perinuclear localization was time- and concentration-dependent **(Figure 2d)**. Intranuclear particles were not observed using confocal or z-stack analyses.

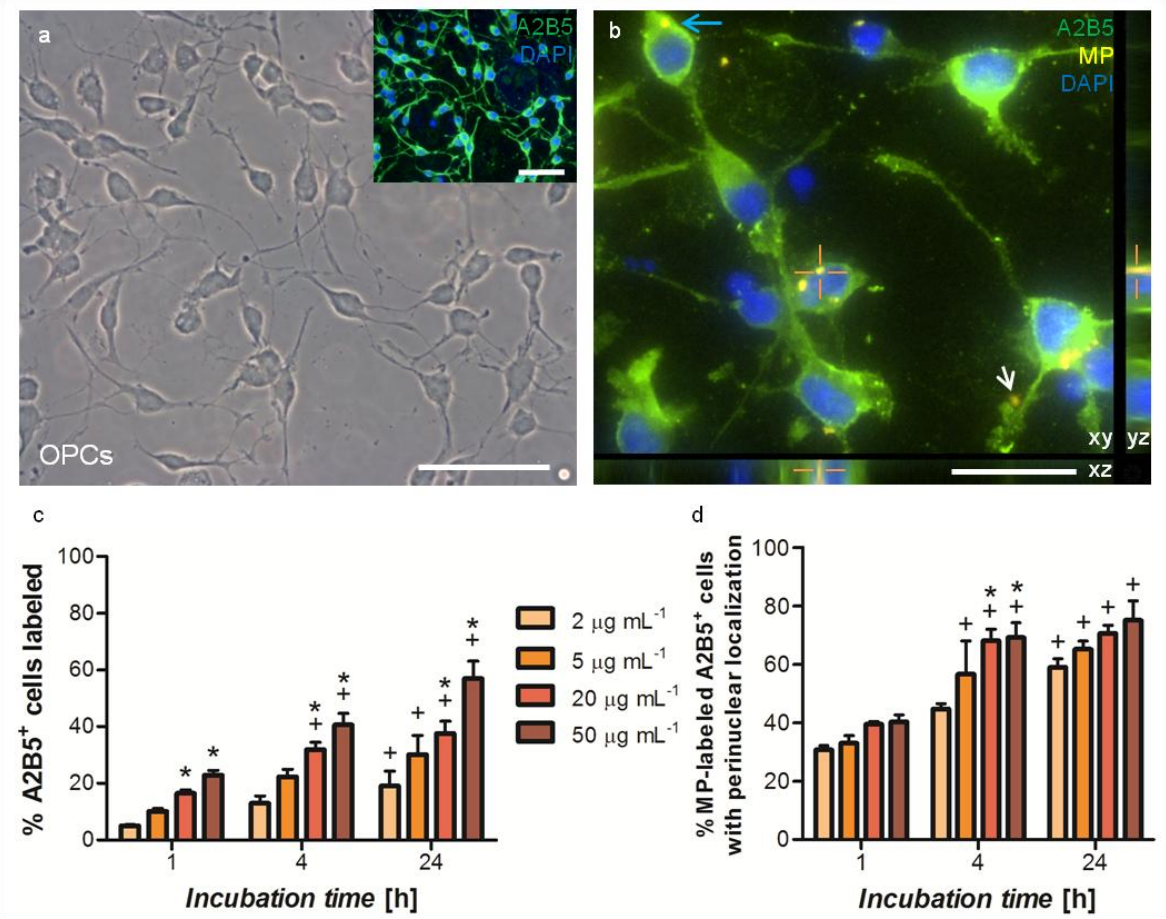

Figure 2: Uptake and perinuclear localization of MPs by OPCs is time- and concentration-dependent. *(a) Typical phase-contrast micrograph of OPCs, with counterpart fluorescence micrograph, inset, showing A2B5 staining. (b) Z-stack fluorescence analysis of cells incubated with 5 µg mL^{-1} MPs for 4 h. Nile red fluorescence reveals MPs in cytoplasmic accumulations (blue arrow), perinuclear accumulations (crosshairs), and attached to the substratum (white arrow). (c) Bar chart showing the time- and concentration-dependent labeling of OPCs with MPs. The proportion of labeled cells is related to particle concentration and incubation time ($p<0.001$ for each factor; two-way ANOVA; n = 4). (d) Bar chart showing the time- and concentration-dependence of perinuclear particle localization in MP-labeled OPCs. Perinuclear localisation was related to both particle concentration and incubation time ($p<0.001$ for each factor; two-way ANOVA; n = 4). For (c) and (d): [*$p<0.05$ versus 2 µg mL^{-1} at the same timepoint; $^{+}p<0.05$ versus the same concentration at 1 h (Bonferroni's post-tests)]. Scale bar = 50 µm in (a), 20 µm in (b).*

Oligodendrocyte Culture Characteristics

Oligodendrocytes were derived from high purity parent OPC cultures **(Figure 3a),** with 70.3 ± 1.3% of cells staining positive for the late-stage oligodendrocyte marker myelin basic protein (MBP; Figure 3a, inset). All stages of the oligodendroglial lineage are typically present in such cultures [35], and our own analyses show that a further ~25% stain for earlier markers such as NG2 and O4, with the remainder (<5%) being microglial contamination (data not shown). Cells were phase-bright, with multipolar morphologies, including the complex highly-branched, membrane elaborating morphologies typical of mature oligodendrocytes.

Table 2. *Semi-quantitative analysis of extent of MP uptake by OPCs*

Incubation time [h]	MP concentration [µg mL^{-1}]	Proportion of labeled OPCs (%)		
		'Low'	'Medium'	'High'
1	**2**	100.0%	0.0%	0.0%
	5	100.0%	0.0%	0.0%
	20	100.0%	0.0%	0.0%
	50	95.0 ± 1.0%	5.0 ± 1.0%	0.0%
4	**2**	99.6 ± 0.5%	0.4 ± 0.5%	0.0%
	5	96.7 ± 2.6%	3.3 ± 2.6%	0.0%
	20	88.2 ± 4.1%	11.8 ± 4.1%	0.0%
	50	87.0 ± 3.1%	12.1 ± 2.2%	0.9 ± 1.0%
24	**2**	97.3 ± 1.9%	2.7 ± 1.9%	0.0%
	5	95.9 ± 2.2%	4.1 ± 2.2%	0.0%
	20	86.8 ± 4.3%	12.2 ± 3.6%	1.1 ± 0.7%
	50	85.1 ± 4.3%	13.3 ± 3.0%	1.6 ± 1.5%

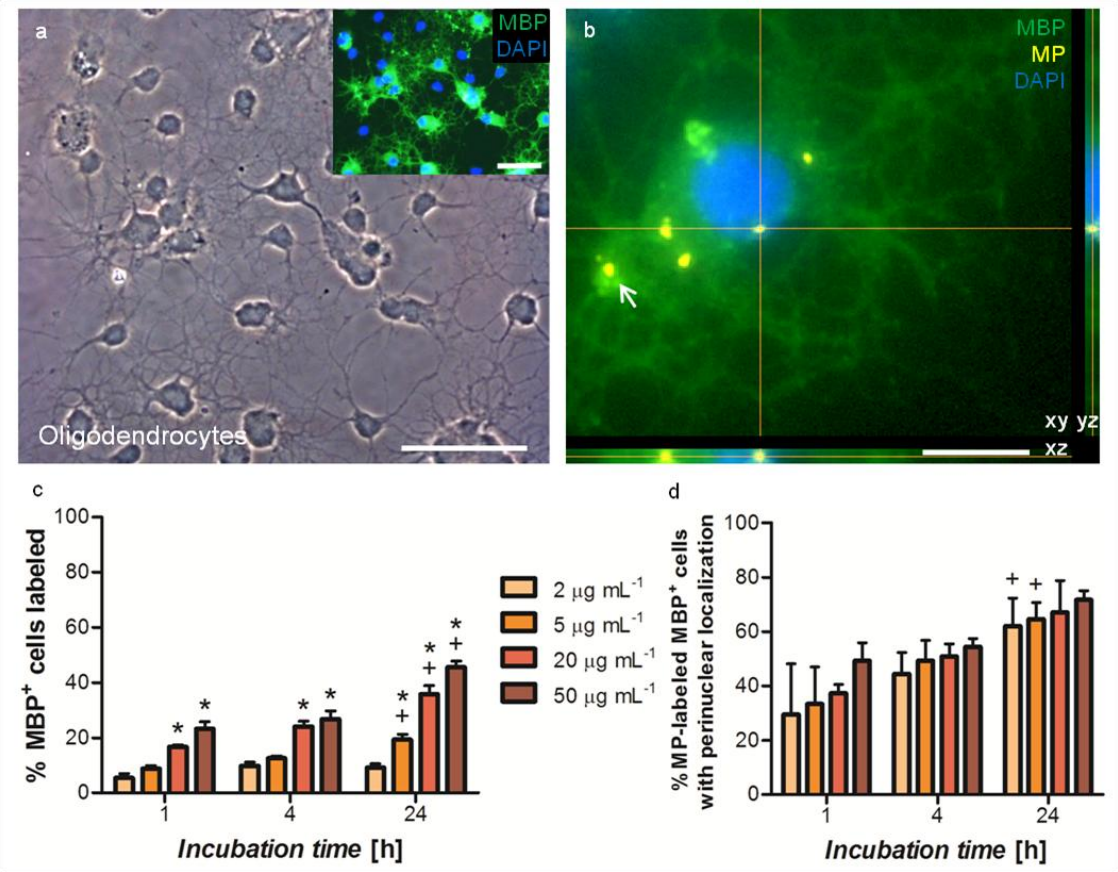

Figure 3: Uptake of MPs by oligodendrocytes is time- and concentration-dependent, and perinuclear localization is time-dependent. *(a) Representative phase-contrast and fluorescence (inset) micrographs of oligodendrocytes. (b) Z-stack fluorescence analysis of an MBP$^+$ oligodendrocyte, incubated with 5 µg mL^{-1} MPs for 4 h. Nile red fluorescence indicates the presence of MPs in cytoplasmic and perinuclear (crosshairs) accumulations. White arrow indicates extracellular MPs amongst processes. (c) Bar chart showing the time- and concentration-dependent labeling of oligodendrocytes with MPs. The percentage of labeled cells is significantly related to both particle concentration and incubation time ($p<0.001$ for each factor; two-way ANOVA; n = 4). (d) Bar chart showing that the percentage of oligodendrocytes with perinuclear particles is significantly related to incubation time but not MP concentration ($p<0.001$ and $p = 0.161$ respectively; two-way ANOVA; n = 4). For (c) and (d): [*$p<0.05$ versus 2 µg mL^{-1} at the same timepoint; $^+p<0.05$ versus the same concentration at 1 h (Bonferroni's post-tests)]. Scale bar = 50 µm in (a), 10 µm in (b).*

Concentration- and Time-Dependence of MP Uptake and Perinuclear Localization in Oligodendrocytes

Z-stack and confocal fluorescence analyses, confirmed the presence of intracellular MPs in oligodendrocytes, including perinuclear accumulations (**Figure 3b**; confocal data not shown). The percentage of labeled oligodendrocytes was time- and concentration-dependent, with the greatest dose and exposure tested resulting in MP-labeling of *ca*. 45% of MBP^+ cells **(Figure 3c)**. MP concentrations of 20 and 50 µg mL^{-1} labeled a significantly greater percentage of MBP^+ cells than 2 µg mL^{-1}, at all timepoints. Heterogeneity in uptake was apparent and this was assessed semi-quantitatively using the same criteria used for scoring OPCs **(Table 3)**. Under all conditions, the majority of MP-labeled cells exhibited a 'low' level of particle accumulation. At 4 and 24 h, oligodendrocytes with 'medium' levels of MP accumulation were observed with 'high' levels of accumulation rarely observed (only at the greatest MP concentration and incubation time; Table 3). By 24 h, cultures exposed to 2 and 5 µg mL^{-1} MPs exhibited a time-dependent increase in the percentage of MP-labeled MBP^+ oligodendrocytes with perinuclear particles **(Figure 3d)**.

Table 3. *Semi-quantitative analysis of extent of MP uptake by oligodendrocytes*

		Proportion of labeled oligodendrocytes (%)		
Incubation time [h]	MP concentration [µg mL^{-1}]	'Low'	'Medium'	'High'
1	2	100%	0.0%	0.0%
	5	100%	0.0%	0.0%
	20	100%	0.0%	0.0%
	50	100%	0.0%	0.0%
4	2	100%	0.0%	0.0%
	5	96.2 ± 4.4%	3.8 ± 4.4 %	0.0%
	20	93.5 ± 0.4%	6.5 ± 0.4%	0.0%
	50	85.1 ± 3.6%	14.9 ± 3.6%	0.0%
24	2	98.2 ± 2.1%	1.8 ± 2.1%	0.0%
	5	95.0 ± 5.8%	5.0 ± 5.8%	0.0%
	20	91.6 ± 5.6%	8.4 ± 5.6%	0.0%
	50	86.0 ± 5.4%	12.8 ± 5.5%	1.2 ± 1.0%

Comparison of MP Uptake in OPCs and Oligodendrocytes

When data for OPCs and oligodendrocytes were compared, the proportions of labeled cells were similar at 1 h post-MP addition (Figures 2c & 3c). At subsequent time points, a greater percentage of OPCs than oligodendrocytes were MP-labeled with the exception of the 24 h incubation with 20 µg mL^{-1} MP (Tables 2 and 3). With respect to cells scored as having 'low' levels of uptake, the accumulations of MPs present within OPCs were typically larger than those within oligodendrocytes (compare Figures 2b and 3b, which show representative levels of MP accumulation). Further, cells at more advanced stages of oligodendrocyte differentiation (judged by number/complexity of processes), contained smaller particle accumulations than cells with relatively immature and less branching morphologies (data not shown). This suggests an inverse relationship between cellular maturity and capacity for MP uptake. For both cell types, the percentage of cells with 'medium-high' levels of MP uptake was time- ($p<0.001$; two-way ANOVA; n =

4) and concentration-dependent (p<0.001; two-way ANOVA; n = 4), suggesting that the uptake mechanism is non-saturable in the time-frame examined.

Assessment of MP Toxicity in OPCs and Oligodendrocytes

No significant effects of MPs were observed in OPC or oligodendrocyte cultures with respect to (a) cell adherence, judged by number of DAPI-labeled nuclei (either healthy or pyknotic) per microscopic field **(Figures 4a & b)**, and (b) cell death, judged by the percentage of nuclei exhibiting pyknotic features **(***ie.* shrunken or fragmenting morphologies; **Figures 4c & d**). OPC and oligodendrocyte cultures appeared morphologically similar to controls at 24 h, and this was also true for oligodendrocytes at one month post-pulse labeling with MPs (data not shown). No effects of MPs were noted on the time taken to reach confluence or extent of membrane elaboration in OPC or oligodendrocyte cultures.

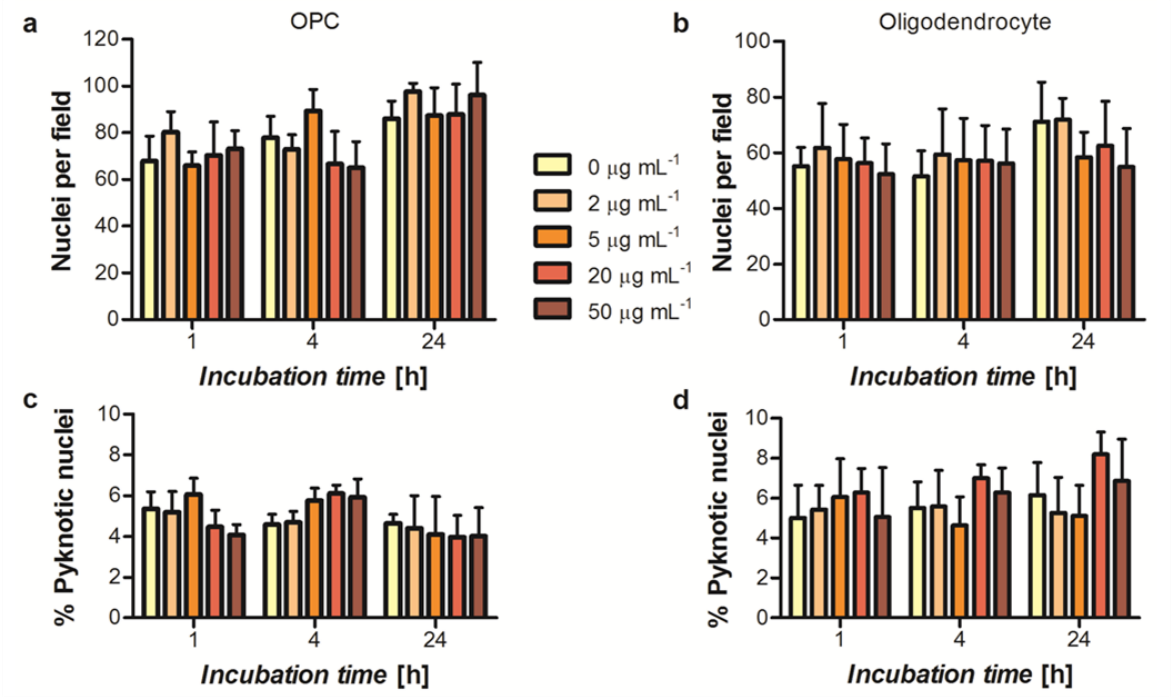

Figure 4: Incubation with MPs at a range of concentrations does not result in acute cytotoxicity in OPCs or oligodendrocytes. *Bar graphs of time course experiments showing total (healthy plus pyknotic) nuclei per microscopic field for (a) OPC and (b) oligodendrocyte cultures, and percentage of nuclei with pyknotic features for (c) OPC and (d) oligodendrocyte cultures. No significant differences were found in these parameters either in relation to particle incubation time or particle concentration (p>0.05; two-way ANOVA; n = 4 for all graphs).*

Intercellular Differences in Extent of MP Uptake

Data from OPCs and oligodendrocytes were combined with data obtained from rat astrocytes [27] and microglia [24] using identical particle concentrations and timings of exposure. From these analyses, there are clear differences between individual neuroglial classes in the rate and extent of MP accumulation, with the relationship with respect of these parameters being: microglia > astrocytes > OPCs > oligodendrocytes **(Figures 5a-d)**. Comparing the extent of MP-uptake at 4 h, highlights the rapid labeling of >90% of microglia, even with low MP concentrations, compared to the gradual time- and concentration-dependent

uptake observed in the other cell types **(Figure 5e)**, using an identical MP dose. Intercellular differences in perinuclear particle localization were also apparent with a representative dose of 50 µg mL^{-1}, with microglia showing the most rapid and extensive accumulation **(Figure 5f)**.

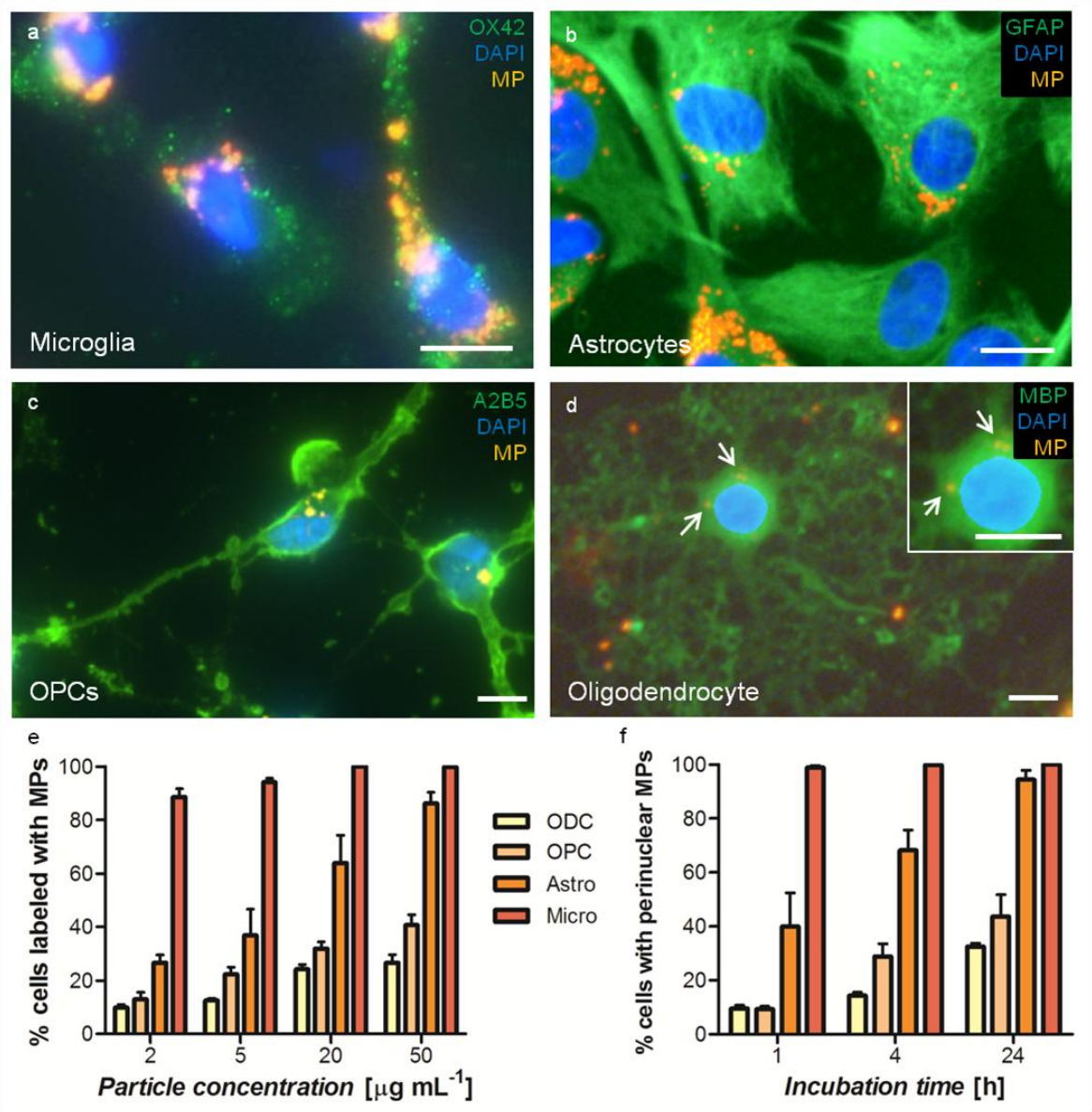

Figure 5: The extent and rate of MP uptake by neuroglia are cell-type specific. Fluorescence micrographs of neuroglia, following incubation with MPs (20 µg mL^{-1}, 24 h). (a) Microglia are stained with the marker OX42, in characteristic punctate fashion, and exhibit high levels of MP uptake, including large particle clusters and perinuclear accumulations. (b) Astrocytes stain for the marker GFAP, and exhibit heterogeneity in the extent of MP uptake. Note flattened cells, large quantities of cytoplasm relative to nucleus in cross-section, and greater extent of uptake compared to (c) and (d). (c) OPCs stain positive for the marker A2B5, and exhibit typically small clusters of MPs compared to (b). Note bipolar forms and potentially limited quantity of membrane available to undertake endocytosis. (d) Oligodendrocyte stained with the late-stage oligodendrocyte marker MBP, and exhibiting a highly branched, mature morphology. Very small accumulations of MPs are present (white arrows, and enlarged in inset). Despite extensive membrane elaboration, MPs are mainly extracellular. (e) Bar graph illustrating comparative MP-labeling in enriched/purified cultures of each neuroglial cell type after 4 h exposure to MPs. (f) Bar graph showing the percentage of all cells having perinuclear MPs in enriched/purified cultures of each neuroglial cell type (50 µg mL^{-1}). For (e) and (f), data for astrocytes and microglia were obtained from references [27] and [24], respectively; ODC = MBP^+ cells in oligodendrocyte cultures; OPC = $A2B5^+$ cells in OPC cultures; Astro = $GFAP^+$ cells in astrocyte cultures; Micro = $OX42^+$ cells in microglial cultures. All scale bars are 10 µm.

Intercellular Differences in MP Processing in Cells

TEM analyses were used to study the intracellular disposition of MPs. This is a time consuming and technically demanding method compared with other histological approaches, but we consider that this is the most robust ultrastructural approach to obtain morphological data on modes of particle uptake, evidence of vacuolar internalization, perinuclear trafficking, and lysosomal degradation/end products of MP breakdown, with high resolution. Electron dense MPs were easily identified within cells using TEM. Astrocytes, OPCs and oligodendrocytes contained intact MPs **(Figures 6a-c)**, morphologically similar to particles incubated in medium alone (Figure 6a, inset), that were generally observed to be free in the cytosol including the perinuclear accumulations [27]. MP clusters were smaller in oligodendrocytes compared with OPCs, and strikingly smaller in OPCs and oligodendrocytes compared with astrocytes (Figures 6a-c), supporting our observations using fluorescence microscopy. By contrast, microglia revealed extensive MP accumulations which were often associated with multilamellar bodies **(Figure 6d & e)**. In contrast to astrocytes and OPCs, MPs appeared to be undergoing extensive degradation in microglia, likely within lysosomes (Figure 6e, inset). Following 24 h MP exposure, toxicity was not observed in OPCs, oligodendrocytes, or astrocytes [27], but was marked in microglial cultures at an identical applied MP concentration **(Figure 6f)** [24].

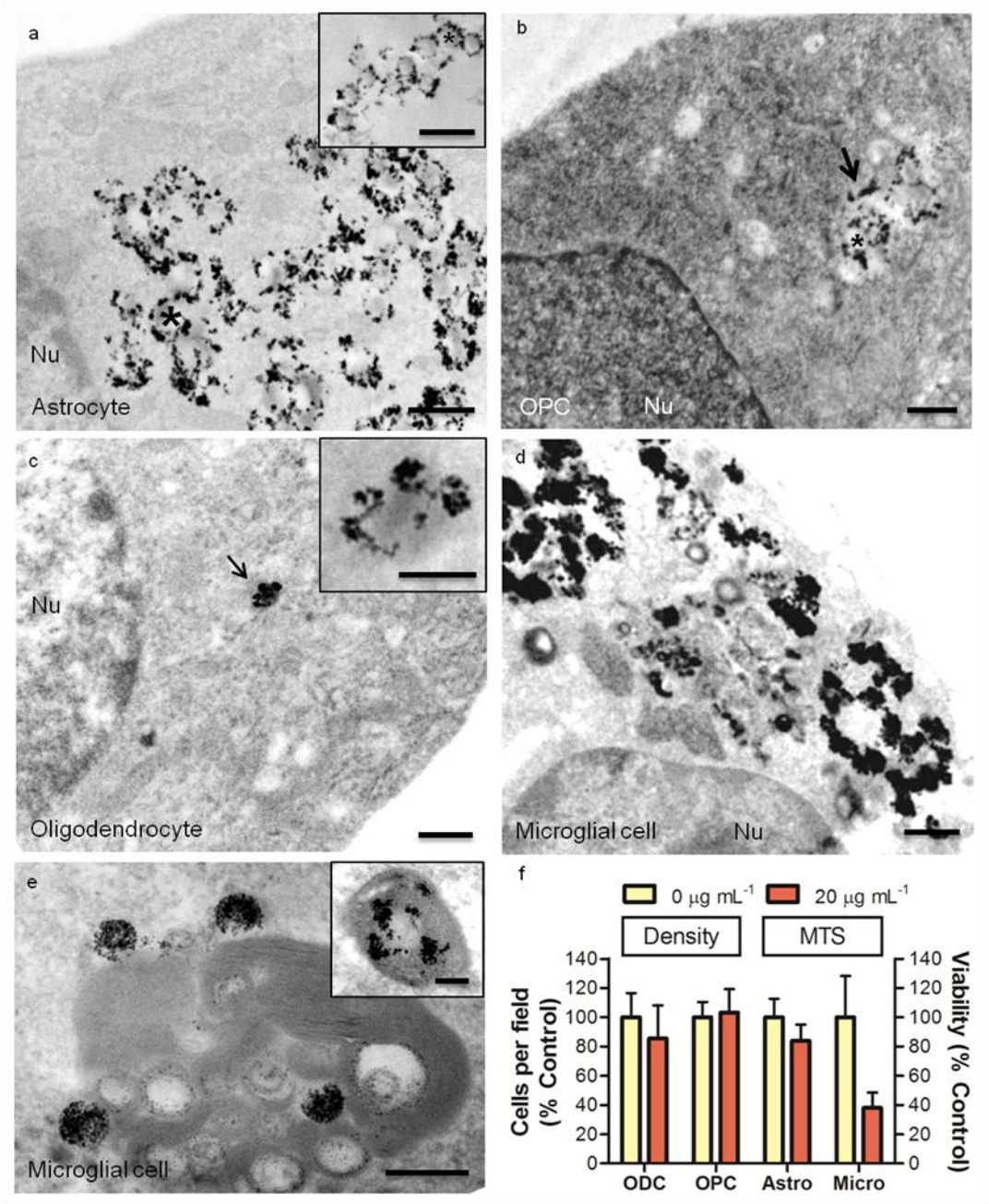

Figure 6: Intracellular fate of MPs is cell-type dependent. *(a-e) TEM analyses of glial cells following 24 h incubation with 20 µg mL^{-1} MPs. (a) An astrocyte where MPs appear to be intact, as evidenced by the presence of electron dense rings of iron surrounding the polystyrene cores (*). Inset, intact MPs in D10 medium without cells (24 h incubation), for comparison of particle shape and structure. (b) An OPC showing intact MPs in a small cluster in the cell cytosol (arrow). (c) An oligodendrocyte showing a single MP in the cytosol (arrow). Inset shows increased magnification image of the MP. Note the relative size of the MP accumulations in (a), (b) and (c), which are typical of astrocytes, OPCs and oligodendrocytes. (d) A microglial cell showing large intracellular accumulations of MPs. Note that these particles appear to be undergoing degradation, as evidenced by comparison with intact MPs [see (a), inset]. (e) A microglial cell, showing particles associated with an electron dense multilamellar body. Note that the electron dense iron particles are not accumulated in rings, but appear to be condensing into clusters, suggesting that particles are undergoing degradation. Inset, extensive MP degradation within a lysosome, as evidenced by dispersion of iron deposits. (f) Bar graph comparing MP-related toxicity in neuroglial cells following 24 h incubation with 20 µg mL^{-1} MPs. Toxicity in OPC and oligodendrocyte (ODC) cultures is assessed by cell number per field (left y-axis) while toxicity to astrocytes (Astro) and microglia (Micro) is assessed by MTS assay (right y-axis); data for astrocytes and microglia were obtained from references [27] and [24], respectively. Nu indicates nucleus. Scale bars indicate 0.5 µm, except (c, inset) where scale bar indicates 200 nm.*

Discussion

To the best of our knowledge, this is the first investigation into intercellular differences in MP uptake and handling by the major neuroglial subtypes. Our data reveal that these subpopulations exhibit key differences in the uptake and intracellular processing of MPs, which reflect cell intrinsic differences and cannot be attributed to differences in experimental conditions used to propagate the individual cell types. For example, astrocytes and microglia are cultured in the same medium (D10) in isolated culture experiments, but show significant differences with respect of particle uptake and accumulation. Indeed, in recent experiments, where microglia and astrocytes were *co-cultured* in a 1:1 ratio in D10 medium (*ie.* identical cell densities and medium), we found dramatic differences in the extent of MP uptake between these cells, with particles localized almost exclusively to microglial cells. Few differences were noted in particle size and charge in the different media, and all cell types were derived from primary mixed glial cultures, eliminating variability in the cell source seen in previous work evaluating intercellular differences in particle handling by neural cells [36]. This lends further support to the notion that the variations observed represent true cell specific properties. We consider that such variations could have important implications for the biological utility of MP platforms for neural tissue engineering applications. As such, we consider that the findings have broader implications for the design and development of novel neurocompatible materials for regenerative medicine, and associated protocols for their use.

Most work to date evaluating cellular MP uptake and handling has utilized cell lines [37-41]. This has yielded valuable data but warnings about cell line identity have been made since the 1950s, with many instances of published work carried out in misidentified cell lines [42-44]. Cell lines possess an altered physiology compared with the corresponding primary cells and behave in a relatively homogenous clonal manner. Consequently, their properties may not represent biological variations that exist *in vivo* that reflect cell proliferation, differentiation and varying states of biological activation (particularly relevant in neurological injury), all of which will influence the outcomes of MP use. Cell lines show relatively high survival/proliferation rates and resistance to adverse stimuli such as cell death signals. Continuous passage of cells without robust quality control also risks chronic contamination by mycoplasma - such 'cryptic' contamination can alter cell structure, metabolism and growth, all of which can impact the interpretation of data [45]. These considerations, combined with the risk of cellular aneuploidy, can make cell lines a relatively poor model for toxicity testing [45,46]. This is an issue of high relevance to nanotechnology, where the neurotoxicity of nano- and micro-sized particles is currently an issue of major public and scientific concern. As such, we contend that cells derived from primary cultures, as used here, are of higher biological relevance than cell lines, particularly when developing protocols for translational applications.

MP uptake is dependent on endocytosis (macropinocytosis, clathrin-, and caveolin-mediated uptake) in mammalian cells [2,19,47] but limited data exist on MP uptake mechanisms in primary neuroglia. The cells studied here display a range of endocytotic mechanisms overall, and differences in MP accumulation likely relate to variations in basal levels of endocytosis. We can predict that the specific endocytotic pathways utilized by each cell type, and their levels of activity, closely correlate with the *functional* role for each cell type. For example, microglia are phagocytic cells and continuously survey their microenvironment

using highly motile processes, removing debris and foreign materials; they utilize all endocytotic mechanisms, including receptor-mediated endocytosis, macropinocytosis and phagocytosis [24,48]. The astrocytes, in turn, have a major role in uptake of extracellular biomolecules and possess well-developed endocytotic machinery; we recently showed that astrocytes take up the MPs studied here by macropinocytosis and coated pit mechanisms [27]. In line with their broad regulatory and defence roles, microglia and astrocytes showed extensive and rapid particle uptake. By contrast, cells of the oligodendrocyte lineage have specialist roles in generating oligodendrocytes and the myelin sheath [23]. As such, we can predict that endocytotic cycling in these cells is lower, an expectation strikingly reflected in the finding that percentages of labeled oligodendroglial cells are about half that observed in astrocytes and microglia, along with substantially lower levels of MP accumulation. We are not aware of studies quantifying endocytotic mechanisms across neuroglial cells, and such a comparison will be a pre-requisite to providing formal proof of this idea.

A further factor influencing uptake could be the relative extent of cell membrane available to undertake endocytosis. Astrocytes display characteristically flattened morphologies and large amounts of membrane. By contrast, OPCs and oligodendrocytes have small oval or round cell bodies, and, as far as we are aware, their processes are not involved in particle uptake - observations supported by our histological analyses. Differences in cell surface area may account for the differences in particle uptake, and it is not clear whether using particles of altered dimensions or geometry may result in greater MP accumulation [19,49].

In line with their phagocytic role, microglial cells appear to inactivate particles by sequestration within vesicles and active lysosomal degradation. Extensive particle accumulation in conjunction with iron toxicity post-degradation is the likely pathological correlate of MP toxicity in these cells [50]. By contrast, in the other cell types, particles appeared to be relatively stable morphologically with negligible associated toxicity.

We consider that the overall profiles of MP uptake and handling exhibited by neuroglia, as reported here, have broader predictive value with biological implications regarding MP use in neural tissue engineering (see **Figure 7** for a schematic overview). First, if using MPs for cell labeling and imaging of neural transplant populations, then protocols will need to be individually tailored by cell type, with OPCs requiring higher particle concentrations and incubation times, to achieve high efficiency labeling. A previous study in an OPC cell line suggests that sub-10 nm magnetic nanoparticles show extensive accumulation in these cells [9] indicating that MP physicochemical properties (such as size, shape, coating, geometry and charge) may need to be tailored to achieve optimal labeling [8].

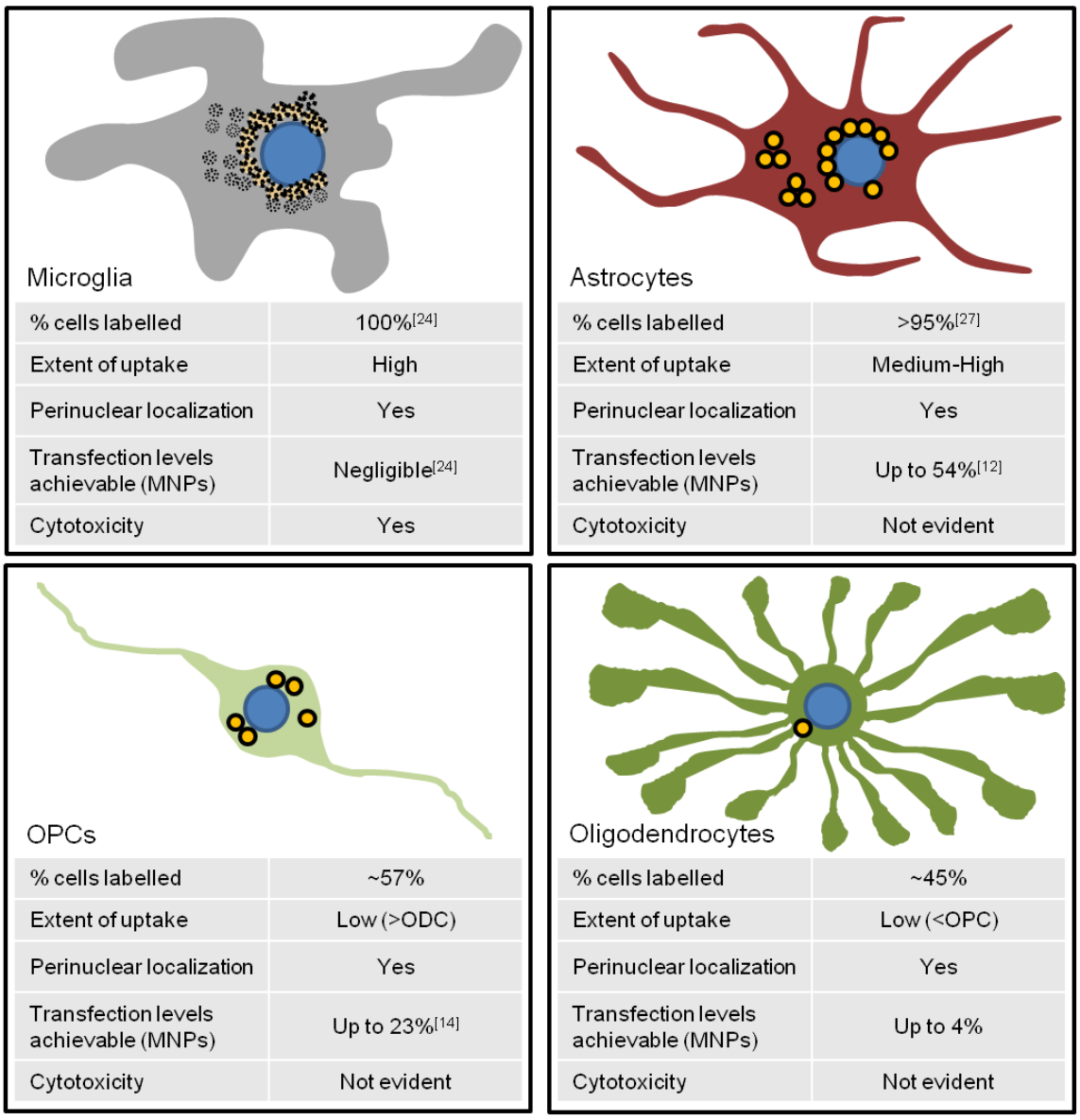

Figure 7: Schematic overview of intercellular differences in MP-processing by neuroglia and relevance to neural tissue engineering applications. *Diagrams illustrate typical cell morphologies, relative levels of MP-accumulation, extent of perinuclear localization and degradation of MPs. Tables summarize related effects on labeling and transfection levels achievable in individual cell types, and associated cytotoxicity. ODC = oligodendrocyte.*

Second, while MPs are effective transfection agents, the specific mode of intracellular trafficking of particles will exert an important influence on transfection levels achieved. Efficient perinuclear accumulation of MPs (a pre-requisite for DNA delivery [51]) in microglia, suggests that MPs could act as effective transfection agents in these cells, but we recently reported that microglial transfection was rarely achieved using transfection grade MPs [24]; particle sequestration and breakdown provides a reasonable explanation for our observations and indeed, there are few reports of non-viral, plasmid based transfection of microglia. Microglial transfection is a desirable goal, allowing immunomodulation in neurological injury, but our results indicate that there are significant 'intracellular barriers' to MP-mediated transfection in microglia that will need to be overcome, using strategies such as MP targeting to particular intracellular compartments to evade

degradation mechanisms. By contrast, the relative stability and non-sequestration of MPs in astrocytes and OPCs is in line with our findings that both cell types can be transfected (with the same transfection grade MPs tested in microglia), albeit with major differences in maximal transfection levels achieved (*ca.* 55% for astrocytes [12] versus *ca.* 23% for OPCs [14]). This trend correlates with the relative extent of basal MP uptake in astrocytes versus OPCs. There is a sharp drop in MP mediated transfection of oligodendrocytes (up to 4%; unpublished observations) despite perinuclear MP accumulation. This could be related to lower particle uptake but successful transfection may also depend on other factors. For example, nuclear breakdown during mitosis may facilitate entry of nucleic acids, so proliferative populations such as astrocytes/OPCs may be relatively amenable to MP-mediated transfection compared to non-dividing cells such as oligodendrocytes [17,51].

Third, robust microglial uptake of MPs is beneficial for imaging sites of CNS injury/disease [52]. However, rapid and extensive particle uptake by endogenous microglia may limit particle uptake by other cell types where mixed populations of neural cells exist, for example, neurological injury sites [24]. Such considerations suggest that microglial MP uptake is a significant ‘extracellular barrier' when considering applications such as direct MP mediated drug/gene delivery to the CNS, that may potentially require strategies such as immunosuppression, cell targeting approaches or variations in particle physiochemical properties, to reduce microglial uptake. Further, MP related toxicity in microglia could become a cause of secondary CNS pathology, therefore particle doses and formulations must be selected with caution.

Conclusions

CNS neuroglial subclasses show considerable variability in MP uptake and intracellular handling. Such variations are likely related to differences in (a) their functional roles; (b) basal endocytotic activity; and (c) extent of membrane elaboration. We predict that the differences have implications for use of the MP platform in neural tissue engineering and translational applications such as imaging, cell labeling and gene/drug delivery. It is therefore essential for future work to take account of the complexity of neuroglial responses to synthetic materials, in order to optimize and refine the use of MPs for neural regeneration. Such work will need to be informed by a detailed understanding of the relationship between the physicochemical properties of MPs and neuroglial uptake, processing and toxicity - parameters that are poorly documented at present.

Future Perspective

There is a critical knowledge gap in nanotechnology and neurotoxicology, regarding the influence of the chemistry of materials platforms on the biology of CNS cells [53]. Such information is vital to robustly evaluate the utility of novel materials for the development and optimization of new therapeutics. Further studies will need to characterize neuroglial cell interactions with MPs of a range of physicochemical properties to identify those with optimal features for specific biomedical applications. For each cell type, such investigations should include ultrastructural analyses of particle fate; endocytotic blocker studies to establish specific uptake mechanisms; microarray analyses for detailed toxicity analysis; evaluation of

vesicular trafficking of MPs, to develop particles with the potential for endosomal escape or to suggest the specific endocytotic mechanisms to which MPs should be preferentially targeted.

Summary points

- Non-neuronal cells of the CNS, termed the neuroglia, derived from primary cultures, show significant intrinsic differences in MP uptake.
- Microglia show the most rapid and extensive MP uptake followed by astrocytes; oligodendrocyte precursor cells and oligodendrocytes show comparatively less uptake.
- MPs undergo extensive degradation in microglia whereas particles appear relatively intact in the other cell types. Significant microglial toxicity was observed at concentrations that were non-toxic in the other cell types.
- The differences in the extent of MP uptake and processing in the neuroglia could have significant implications for MP use in neural tissue engineering applications.
- Rapid uptake and degradation of MPs in microglia could represent a significant 'extracellular barrier' for direct MP use (in gene/drug delivery) in the CNS. Such degradation is also a major 'intracellular barrier' in applications such as transfection.
- MP stability in astrocytes and oligodendroglial cells indicates that MPs are compatible with these cells, but the relative levels of cellular uptake will determine the efficacy of MP use.
- Utilising cells derived from primary cultures, as in the current study, offers several advantages over cell lines that are widely employed in bio-nanotechnology research.
- Future studies will need to characterize relationships between MP physicochemical properties and cellular uptake, processing and toxicity in CNS cells, to identify optimal neurocompatible materials.

Acknowledgements

We thank Dr Rosemary Fricker and Dr Rowan Orme for access to and assistance with z-stack fluorescence microscopy. We thank Professor Chris Exley and Dr James Beardmore for access to and assistance with DLS and zeta-potential measurements. This work was supported by research grants from the US National Multiple Sclerosis Society, Royal Society UK and a New Investigator Award from the British Biotechnology and Biological Sciences Research Council, UK.

References

[1] Tartaj P, del Puerto Morales M, Veintemillas-Verdaguer S, Gonzalez-Carreno T, Serna CJ. The preparation of magnetic nanoparticles for applications in biomedicine. *J. Phys. D: Appl. Phys.* 36, R182-R197 (2003).

[2] Shubayev VI, Pisanic TR 2nd, Jin S. Magnetic nanoparticles for theragnostics. *Adv. Drug Delivery Rev.* 61, 467-477 (2009).** Describes the potential of magnetic nanoparticle (MNP) platforms for combined therapeutic and diagnostic modalities.

[3] Yellen B, Forbes Z, Halverson D *et al.* Targeted drug delivery to magnetic implants for therapeutic applications. *J. Magn. Magn. Mater.* 293, 647-654 (2005).
[4] Pankhurst QA, Thanh NKT, Jones SK, Dobson J. Progress in applications of magnetic nanoparticles in biomedicine. *J. Phys. D: Appl. Phys.* 42, 224001 (2009).** Comprehensive review of use of MNPs for biomedical applications.
[5] Dobson J. Magnetic micro- and nano-particle-based targeting for drug and gene delivery. *Nanomedicine (Lond.)* 1, 31-37 (2006).
[6] Frank JA, Miller BR, Arbab AS *et al.* Clinically applicable labeling of mammalian and stem cells by combining superparamagnetic iron oxides and transfection agents. *Radiology* 228, 480-487 (2003).
[7] Berry CC. Progress in functionalization of magnetic nanoparticles for applications in biomedicine. *J. Phys. D: Appl. Phys.* 42, 224003 (2009).** Excellent review of biomedical applications of MNPs.
[8] Yiu HHP, Pickard MR, Olariu CI, Williams SR, Chari DM, Rosseinsky MJ. Fe(3)O(4)-PEI-RITC magnetic nanoparticles with imaging and gene transfer capability: Development of a tool for neural cell transplantation therapies. *Pharm. Res.* 29, 1328-1343 (2012).
[9] Bulte JWM, Zhang S, van Gelderen P *et al.* Neurotransplantation of magnetically labeled oligodendrocyte progenitors: Magnetic resonance tracking of cell migration and myelination. *Proc. Natl Acad. Sci.USA* 96, 15256-15261 (1999).* Study describing the use of MNPs for imaging of neural cell transplant populations, a major application for MNPs.
[10] Bulte JWM, Duncan ID, Frank JA. *In vivo* magnetic resonance tracking of magnetically labeled cells after transplantation. *J. Cereb. Blood Flow Metab.* 22, 899-907 (2002).
[11] Plank C, Schillinger U, Scherer F *et al.* The magnetofection method: Using magnetic force to enhance gene delivery. *Biol. Chem.* 384, 737-747 (2003).
[12] Pickard MR, Chari DM. Enhancement of magnetic nanoparticle-mediated gene transfer to astrocytes by "magnetofection": Effects of static and oscillating fields. *Nanomedicine (Lond.)* 5, 217-232 (2010).
[13] Scherer F, Anton M, Schillinger U *et al.* Magnetofection: Enhancing and targeting gene delivery by magnetic force *in vitro* and *in vivo*. *Gene Ther.* 9, 102-109 (2002).** Seminal paper describing the use of the magnetofection technology to enhance MNP mediated gene transfer.
[14] Jenkins SI, Pickard MR, Granger N, Chari DM. Magnetic nanoparticle-mediated gene transfer to oligodendrocyte precursor cell transplant populations is enhanced by magnetofection strategies. *ACS Nano* 5, 6527-6538 (2011).
[15] Sapet C, Laurent N, de Chevigny A *et al.* High transfection efficiency of neural stem cells with magnetofection. *BioTechniques* 50, 187-189 (2011).
[16] Muja N, Bulte JWM. Magnetic resonance imaging of cells in experimental disease models. *Prog. Nucl. Magn. Reson. Spectrosc.* 55, 61-77 (2009).
[17] Patel LN, Zaro JL, Shen WC. Cell penetrating peptides: Intracellular pathways and pharmaceutical perspectives. *Pharm. Res.* 24, 1977-1992 (2007).
[18] Schlorf T, Meincke M, Kossel E, Glüer CC, Jansen O, Mentlein R. Biological properties of iron oxide nanoparticles for cellular and molecular magnetic resonance imaging. *Int. J. Mol. Sci.* 12, 12-23 (2010).
[19] Verma A, Stellacci F. Effect of surface properties on nanoparticle-cell interactions. *Small* 6, 12-21 (2010).* Discussion on the effects of physicochemical properties of nanoparticles on cellular uptake.
[20] Jing Y, Mal N, Williams PS *et al.* Quantitative intracellular magnetic nanoparticle uptake measured by live cell magnetophoresis. *FASEB J.* 22, 4239-4247 (2008).
[21] Du Y, Dreyfus CF. Oligodendrocytes as providers of growth factors. *J. Neurosci. Res.* 68, 647–654 (2002).
[22] Kim SU, de Vellis J. Microglia in health and disease. *J. Neurosci. Res.* 81, 302-313 (2005).
[23] Baumann N, Pham-Dinh D. Biology of oligodendrocyte and myelin in the mammalian central nervous system. *Physiol. Rev.* 81, 871-927 (2001).
[24] Pickard MR, Chari DM. Robust uptake of magnetic nanoparticles (MNPs) by central nervous system (CNS) microglia: Implications for particle uptake in mixed neural cell populations. *Int. J. Mol. Sci.* 11, 967-81 (2010).
[25] Geppert M, Hohnholt MC, Thiel K *et al.* Uptake of dimercaptosuccinate-coated magnetic iron oxide nanoparticles by cultured brain astrocytes. *Nanotechnology* 22, 145101 (2011).
[26] Fleige G, Nolte C, Synowitz M, Seeberger F, Kettenmann H, Zimmer C. Magnetic labeling of activated microglia in experimental gliomas. *Neoplasia* 3, 489-499 (2001).
[27] Pickard MR, Jenkins SI, Koller C, Furness DN, Chari DM. Magnetic nanoparticle labelling of astrocytes derived for neural transplantation. *Tissue Eng., Part C* 17, 89-99 (2011).
[28] McCarthy KD, de Vellis J. Preparation of separate astroglial and oligodendroglial cell cultures from rat cerebral tissue. *J. Cell Biol.* 85, 890-902 (1980).

[29] Dunning MD, Lakatos A, Loizou L *et al.* Superparamagnetic iron oxide-labeled Schwann cells and olfactory ensheathing cells can be traced *in vivo* by magnetic resonance imaging and retain functional properties after transplantation into the CNS. *J. Neurosci.* 24, 9799-9810 (2004).
[30] Franklin RJM, Blaschuk KL, Bearchell MC *et al.* Magnetic resonance imaging of transplanted oligodendrocyte precursors in the rat brain. *Neuroreport* 10, 3961-3965 (1999).
[31] McBain SC, Griesenbach U, Xenariou S *et al.* Magnetic nanoparticles as gene delivery agents: Enhanced transfection in the presence of oscillating magnet arrays. *Nanotechnology* 19, 405102 (2008).
[32] Yang J, Liu J, Niu G *et al. In vivo* MRI of endogenous stem/progenitor cell migration from subventricular zone in normal and injured developing brains. *NeuroImage* 48, 319-328 (2009).
[33] De Palma R, Peeters S, Van Bael MJ *et al.* Silane ligand exchange to make hydrophobic superparamagnetic nanoparticles water-dispersible. *Chem. Mater.* 19, 1821-1831 (2007).
[34] Olariu CI, Yiu HHP, Bouffier L *et al.* Multifunctional Fe3O4-PEI-RITC nanoparticles for targeted bi-modal imaging of pancreatic cancer. *J. Mater. Chem.* 21, 12650-12659 (2011).
[35] Tang DG, Tokumoto YM, Raff MC. Long-term culture of purified postnatal oligodendrocyte precursor cells: Evidence for an intrinsic maturation program that plays out over months. *J. Cell Biol.* 148, 971-984 (2000).
[36] Pinkernelle J, Calatayud P, Goya GF, Fansa H, Keilhoff G. Magnetic nanoparticles in primary neural cell cultures are mainly taken up by microglia. *BMC Neurosci.* 13, 32 (2012)
[37] Prijic S, Scancar J, Romih R. Increased cellular uptake of biocompatible superparamagnetic iron oxide nanoparticles into malignant cells by an external magnetic field. *J. Membr. Biol.* 236, 167-179 (2010).
[38] Chaudhari KR, Ukawala M, Manjappa AS *et al.* Opsonization, biodistribution, cellular uptake and apoptosis study of PEGylated PBCA nanoparticle as potential drug delivery carrier. *Pharm. Res.* 29, 53-68 (2011).
[39] Soenen SJH, Himmelreich U, Nuytten N, Pisanic TR 2nd, Ferrari A, De Cuyper M. Intracellular nanoparticle coating stability determines nanoparticle diagnostics efficacy and cell functionality. *Small* 6, 2136-2145 (2010).
[40] dos Santos T, Varela J, Lynch I, Salvati A, Dawson KA. Quantitative assessment of the comparative nanoparticle-uptake efficiency of a range of cell lines. *Small* 7, 3341-3349 (2011).
[41] Kim JS, Yoon TJ, Yu KN *et al.* Cellular uptake of magnetic nanoparticle is mediated through energy-dependent endocytosis in A549 cells. *J. Vet. Sci.* 7, 321-326 (2006).
[42] American Type Culture Collection Standards Development Organization Workgroup ASN-0002, Cell line misidentification: the beginning of the end. *Nat. Rev. Cancer* 10, 441–448 (2010).
[43] Nardone RM. Curbing rampant cross-contamination and misidentification of cell lines. *BioTechniques* 45, 221-227 (2008).
[44] Buehring GC, Eby EA, Eby MJ. Cell line cross-contamination: How aware are mammalian cell culturists of the problem and how to monitor it? *In Vitro Cell. Dev. Biol. Anim.* 40, 211-215 (2004).
[45] Freshney RI. Cell line provenance. *Cytotechnology* 39, 55-67 (2002).
[46] Hughes P, Marshall D, Reid Y, Parkes H, Gelber C. The costs of using unauthenticated, over-passaged cell lines: How much more data do we need? *BioTechniques* 43, 575-586 (2007).
[47] Musyanovych A, Dausend J, Dass M, Walther P, Mailänder V, Landfester K. Criteria impacting the cellular uptake of nanoparticles: A study emphasizing polymer type and surfactant effects. *Acta Biomater.* 7, 4160-4168 (2011).
[48] Park JY, Kim KS, Lee SB *et al.* On the mechanism of internalization of alpha-synuclein into microglia: Roles of ganglioside GM1 and lipid raft. *J. Neurochem.* 110, 400-411 (2009).
[49] Sohaebuddin SK, Thevenot PT, Baker D, Eaton JW, Tang L. Nanomaterial cytotoxicity is composition, size, and cell type dependent. *Part. Fibre Toxicol.* 7, 22-38 (2010).
[50] Long TC, Tajuba J, Sama P *et al.* Nanosize titanium dioxide stimulates reactive oxygen species in brain microglia and damages neurons *in vitro*. *Environ. Health Perspect.* 115, 1631-1637 (2007).
[51] van der Aa MAEM, Mastrobattista E, Oosting RS, Hennink WE, Koning GA, Crommelin DJA. The nuclear pore complex: The gateway to successful nonviral gene delivery. *Pharm. Res.* 23, 447-459 (2006).
[52] Bulte JWM. *In vivo* MRI cell tracking: Clinical studies. *Am. J. Roentgenol.* 193, 314-325 (2009).
[53] Yang Z, Liu ZW, Allaker RP *et al.* A review of nanoparticle functionality and toxicity on the central nervous system. *J. R. Soc. Interface* 7, S411-422 (2010).

Appendix 4: Article published by ACS Nano.

This appendix contains an article published in ACS Nano, containing a subset of the data from chapter 3.

Jenkins SI, Pickard MR, Granger N, Chari DM

Magnetic nanoparticle-mediated gene transfer to oligodendrocyte precursor cell transplant populations is enhanced by magnetofection strategies

ACS Nano vol. 5, no. 8, 6527-6538, 2011

Magnetic Nanoparticle-Mediated Gene Transfer to Oligodendrocyte Precursor Cell Transplant Populations Is Enhanced by Magnetofection Strategies

Stuart I. Jenkins,[†] Mark R. Pickard,[†] Nicolas Granger,[‡] and Divya M. Chari[†,*]

[†]Cellular and Neural Engineering Group, Institute for Science and Technology in Medicine, Keele University, Keele, Staffordshire, ST5 5BG, United Kingdom and [‡]MRC Centre for Stem Cell Biology and Regenerative Medicine, and Department of Veterinary Medicine, University of Cambridge, Madingley Road, Cambridge, CB3 0ES, United Kingdom

ABSTRACT This study has tested the feasibility of using physical delivery methods, employing static and oscillating field "magnetofection" techniques, to enhance magnetic nanoparticle-mediated gene transfer to rat oligodendrocyte precursor cells derived for transplantation therapies. These cells are a major transplant population to mediate repair of damage as occurs in spinal cord injury and neurological diseases such as multiple sclerosis. We show for the first time that magnetic nanoparticles mediate effective transfer of reporter and therapeutic genes to oligodendrocyte precursors; transfection efficacy was significantly enhanced by applied static or oscillating magnetic fields, the latter using an oscillating array employing high-gradient NdFeB magnets. The effects of oscillating fields were frequency-dependent, with 4 Hz yielding optimal results. Transfection efficacies obtained using magnetofection methods were highly competitive with or better than current widely used nonviral transfection methods (*e.g.*, electroporation and lipofection) with the additional critical advantage of high cell viability. No adverse effects were found on the cells' ability to divide or give rise to their daughter cells, the oligodendrocytes—key properties that underpin their regeneration-promoting effects. The transplantation potential of transfected cells was tested in three-dimensional tissue engineering models utilizing brain slices as the host tissue; modified transplanted cells were found to migrate, divide, give rise to daughter cells, and integrate within host tissue, further evidencing the safety of the protocols used. Our findings strongly support the concept that magnetic nanoparticle vectors in conjunction with state-of-the-art magnetofection strategies provide a technically simple and effective alternative to current methods for gene transfer to oligodendrocyte precursor cells.

KEYWORDS: oligodendrocyte precursor cells · magnetic nanoparticles · magnetofection · transplantation · organotypic slice culture · gene therapy · transfection

Oligodendrocyte precursor cells (OPCs) are a major transplant population to promote repair following myelin damage (as occurs in neurological diseases such as multiple sclerosis) and in spinal cord injury (SCI).[1−5] The beneficial effects of OPCs are primarily due to the production of new myelin by oligodendrocytes, the daughter cells of OPCs.[6] Myelin is the lipid-based insulating sheath covering nerve fibers that aids in the efficient conduction of electrical signals and exerts neuroprotective effects on axons.[7,8] Cell replacement studies have noted a down-regulation of genes associated with tissue damage and inflammation following OPC transplantation, indicating additional mechanisms by which OPCs may exert tissue-sparing effects.[9] These cells are abundant in fetal and adult brain, and relatively pure OPC populations can be obtained from CNS tissue using FACS/antibody selection; protocols have also been established to derive OPCs from rodent/human embryonic stem cells (hESCs), highlighting their translational potential for clinical cell transplantation therapies.[9−11] The major therapeutic and translational potential of OPCs is evidenced by the commencement of human clinical trials in regenerative medicine, for example that by Geron Corporation (CA, USA) of their product GRNOPC1, consisting of hESC-derived OPCs for repair of SCI.[12]

While cell transplantation therapies have major potential to mediate neural repair, successful therapeutic interventions are likely to require so-called "combinatorial" approaches (*e.g.*, delivery of cells *plus* therapeutic factors to injury foci), as neural repair is a complex process requiring multiple goals to be achieved for successful regeneration.[13−17] Consequently, engineering the repair properties of transplanted OPCs, for example by introducing genes encoding therapeutic factors, constitutes a key strategy to improve neural repair. OPCs can be modified to deliver therapeutic proteins such as fibroblast growth factor 2 (FGF2), ciliary neurotrophic factor

* Address correspondence to d.chari@hfac.keele.ac.uk.

Received for review May 22, 2011 and accepted July 1, 2011.

Published online July 01, 2011
10.1021/nn2018717

(CNTF), and neurotrophin 3 (NT3) following transplantation.[14,15,18,19] Such interventions make lesion environments more conducive to repair, enhance both graft-mediated and endogenous cellular repair, encourage axonal outgrowth in lesions, and promote angiogenesis.[20−24]

From a technical perspective, it is important to note that previous studies have relied heavily on viral methods to achieve gene transfer to OPCs.[14,15,25,26] Viral methods are efficient and have yielded valuable information in experimental studies on neural repair. However, despite recent technological advances, there are still significant risks and disadvantages associated with viral-mediated gene transfer, primarily safety issues such as toxicity, nonspecific cellular uptake, inflammatory responses, and oncogenic effects leading to abnormal cellular growth.[25,27−32] Concerns have been raised that viral vectors may themselves cause alterations in OPC proliferation and differentiation, oligodendrocyte death, and myelin damage.[27] There are also major limitations with viral delivery in terms of limited plasmid insert size and achieving large-scale production for clinical applications, leading to a major international drive for the development and evaluation of nonviral transfection methods.[31,32] Despite this, many of the nonviral methods used for neural gene transfer also have major associated disadvantages. For example, nonviral vectors have lower transfection efficacies than their viral counterparts, leading to the adoption of physical gene delivery methods, such as biolistic transfection and electroporation, which can be associated with adverse effects such as membrane damage, abnormal cell physiology, and substantial cell death (up to 80% cell loss).[30,33]

In this context, magnetic nanoparticle (MNP)-based vector platforms have emerged as an essential tool for advanced biomedical technology, due to progress in recent years in both the large-scale synthesis and complex surface functionalization of such particles.[29,34] These next-generation nanomaterials are used in major areas of biological research and medicine, including drug/gene therapy, magnetic targeting (*e.g.*, cancer therapies), and diagnostic imaging (as contrast enhancers).[35−40] The particles consist of a superparamagnetic core, within a biocompatible surface coating, allowing attachment of specific functional groups to the surface coating (Figure 1). MNP size and surface chemistry can be adapted to suit the "functionalizing" molecule, and a tailored combination of surface functionalizations can potentially be achieved to construct complex particles that can mediate multiple applications (*e.g.*, real-time imaging of neural transplant populations plus drug/gene therapy) while retaining nanoscale dimensions.[34,40,41] For example, MNP platforms have been shown to have key applications for noninvasive MR imaging of a range of transplant cells, notably, for tracking of myelin-generating cell populations: MNP-labeled primary Schwann and olfactory ensheathing cells (OECs),[42] as well as CG4 cells

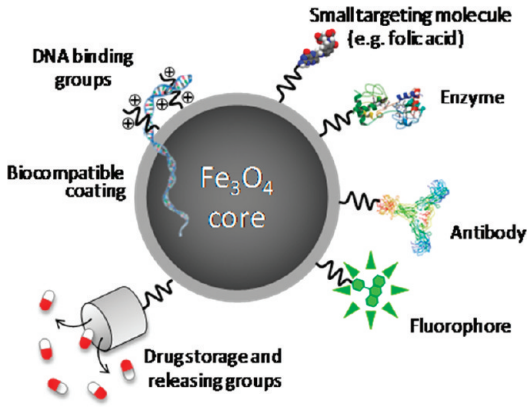

Figure 1. Schematic diagram depicting the multilayered design of magnetic nanoparticles, illustrating the magnetic iron oxide (magnetite) core and biocompatible coating, with examples of potential functionalization for biomedical applications.

(an OPC cell line),[43] could all be detected by MRI following transplantation into areas of brain and spinal cord pathology, without adverse effects on transplant cell migration, cell fate, or repair potential.

In terms of MNP-based transfection, a key feature of MNP vectors is their compatibility with novel magnetofection techniques, *viz.*, the application of magnetic fields to assist gene transfer.[44−47] These methods have the major safety advantage that they exploit the natural uptake pathways (endocytotic mechanisms) of cells during the transfection process, without disrupting the cell membrane, resulting in high cell viabilities post-transfection.[48−52] We have recently demonstrated the significant potential of MNPs to mediate gene transfer to key neural transplant cell populations [such as astrocytes[53] and neural stem cells (NSCs)].[54] We proved that transfection efficacies could be dramatically improved using magnetofection approaches, the latter including use of an oscillating array system utilizing high-gradient NdFeB magnets applied at a range of frequencies.[53] To date, however, the use of MNPs to mediate safe gene transfer to the major transplant population of OPCs has not been assessed. The current study aims to address this issue by employing OPCs derived from primary rat mixed glial cell cultures to assess (i) whether OPCs can be transfected using MNP vectors, (ii) if novel static and oscillating field magnetofection techniques can enhance transfection efficiencies, (iii) whether these transfection protocols affect the survival or differentiation potential of OPCs, and (iv) the transplantation potential of MNP-transfected OPCs using organotypic cerebellar slice cultures as host tissue.

RESULTS AND DISCUSSION

Cell Cultures. These experiments were performed using untransformed OPCs, derived from primary rat mixed glial cultures, to eliminate the potential problems commonly encountered with the use of cell lines, which include transformation-induced abnormalities

in cell physiology, microbial contamination, karyotyping necessitated by the risk of cellular aneuploidy, and genetic instability. Highly pure cultures of OPCs were consistently obtained, as judged by cellular morphology and A2B5 (OPC marker) staining (94.3 ± 2.3%; $n = 5$). Light microscopic observations showed that cells displayed an elongated bipolar morphology with oval cell bodies characteristic of OPCs.

Choice of Particles and Particle Concentrations. Neuromag particles are transfection-grade MNPs that were originally designed for use with primary neurons and in which they have a history of "safe" usage. We have utilized these particles to demonstrate MNP-mediated transfection and the efficacy of magnetofection approaches, in a range of neural cell types [astrocytes,[53] NSCs,[54] OECs, and oligodendrocytes (unpublished data)], making them the nanoparticle of choice in our laboratory. In terms of incubation times required to achieve optimal transfection, removal of particle–plasmid complexes after 1 h incubation (as per the protocol developed by ourselves for transfection of astrocytes)[53] resulted in negligible transfection (typically <1%) over a 48 h monitoring period, for all field conditions. By contrast, increasing the length of OPC exposure to complexes to 48 h resulted in a dramatic increase in reporter protein expression over a similar monitoring period. This exposure time was not associated with toxicity, and qualitative microscopic observations on the extent of green fluorescent protein (GFP) expression in OPCs over a three-week observation period revealed that protein expression peaks at 48 h, consistent with the timing of peak expression reported earlier for plasmid-based transfection.[19,53] Therefore, in all experiments, toxicity and transfection efficiency were routinely assessed by fluorescence microscopy at 48 h.

Establishment of Safe Particle–Plasmid Concentrations and Field Conditions. As cell survival and phenotypic stability are key considerations in cell replacement strategies, a battery of assays was used to assess the toxicity of Neuromag–*gfp* (pmaxGFP plasmid) complexes and magnetofection techniques on OPCs. At every concentration and applied magnetic field condition, plasmid alone controls were found to be without any effect on OPC morphology or survival and never resulted in GFP expression (Figure 2A). The particle concentration routinely used to safely transfect neurons (1.0×) as recommended by the manufacturer resulted in the obvious presence of rounded, detaching cell profiles and dramatic loss of OPCs. Therefore, lower concentrations (0.5× and 0.1×) of Neuromag–*gfp* were evaluated; irrespective of the applied magnetic field, treatment with 0.5× Neuromag–*gfp* was also found to result in a decrease in cell number per field, the presence of nonadherent cells, and an increase in pyknotic nuclei (Figure 2A and B). In contrast, 0.1× Neuromag–*gfp* had no statistically significant effects on any of these parameters under all magnetic field conditions used (Figures 2A). It was deemed unnecessary to test for

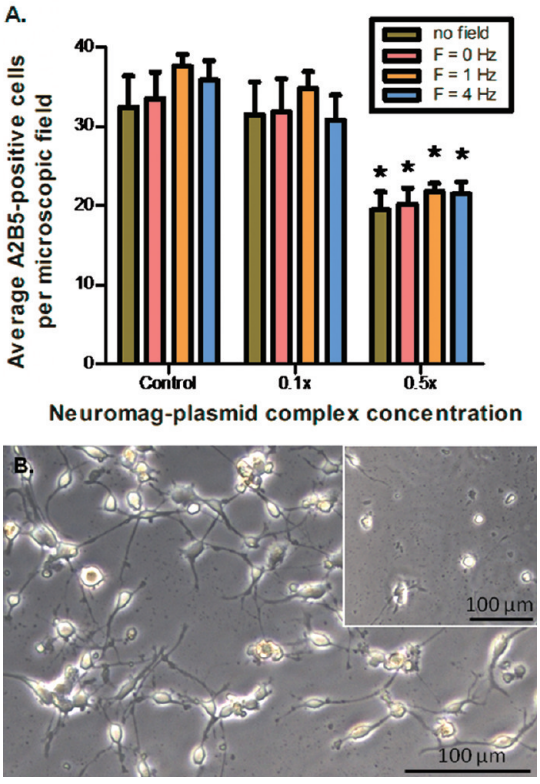

Figure 2. Establishment of safe particle dose and magnetic field conditions for OPC magnetofection. (A) Bar chart showing average number of cells stained for the OPC marker A2B5 per microscopic field, 48 h post-transfection with Neuromag–plasmid complexes. For all magnetic field conditions tested and the no field condition, the number of A2B5$^+$ cells per field was markedly reduced at 0.5× complex concentration, but not at 0.1×, compared to control cultures exposed to plasmid alone. *$p < 0.05$ *versus* control, no field; $n = 5$ cultures. (B) Representative phase-contrast micrograph of OPCs, 48 h post-transfection with 0.1× Neuromag–plasmid complexes. Note phase-bright cells with mostly bipolar morphologies. Inset shows OPCs 48 h post-transfection with 0.5× Neuromag–plasmid complexes. Note reduced density of cells and lack of processes.

toxicity of the particles alone, as Neuromag MNPs have been specifically developed as transfection grade particles and, as such, have no intended usage without conjugation of nucleic acids. However, in pilot experiments, 0.1× Neuromag particles alone were not found to be associated with any adverse effects on OPC viability or proliferative/differentiation potential. Additionally, OPCs could be incubated with 0.1× Neuromag–*gfp* complexes for up to 48 h without induction of significant toxic effects, and no alterations were observed in the morphology or A2B5 staining profiles of OPCs at this concentration. This was therefore deemed the "safe" dose for transfection applications.

These data highlight the need for rigorous dose-optimization prior to MNP use. When considering the development of optimal magnetofection methodologies for cells of neural origin, it is of note that experimental protocols required to prevent toxicity vary between individual neural cell types. This underscores

the critical importance of tailoring particle dosing regimens on a cell-by-cell basis with respect to (i) particle concentration and (ii) incubation time, in order to develop safe protocols for biomedical applications. First, the particle concentration routinely used to safely transfect neurons is toxic not only to OPCs, as shown here, but also to astrocytes[53] and NSCs,[54,55] necessitating the use of lower MNP concentrations for these non-neuronal cell types. Second, at a given particle concentration, the duration of particle exposure that can be considered "safe" also varies between cell types. For example, in a previous study, it was necessary to limit astrocyte incubation time with 0.1× Neuromag−*gfp* complexes to 1 h to prevent toxicity,[53] whereas in the present study, OPCs could be safely incubated with the same particle−plasmid complex concentration for a prolonged period of time (48 h).

It is not clear what specific cellular mechanisms account for these intercellular differences. As uptake of MNPs is known to occur *via* endocytotic mechanisms such as macropinocytosis and receptor-mediated uptake (for example clathrin- and caveolin-mediated), we can speculate that differences in the mechanisms and/or activity of endocytosis between astrocytes and OPCs account for differences in the extent of particle uptake and toxicity.[48,50,52] This may in turn be related to the specific neurophysiological functions performed by the cell type in question (*e.g.*, homeostasis, immune surveillance).

Assessment of Magnetofection Techniques for Transfection of OPCs. *OPC Transfection Studies and Effects of Applied Magnetic Fields (Magnetofection).* Transfection efficacy was assessed at 0.1× Neuromag−*gfp* concentrations, with and without application of static and oscillating magnetic fields. Basal GFP expression was observed, *i.e.*, in the absence of a magnetic field (mean transfection efficiency: 6.1 ± 1.0%; range: 3.1−8.1%; Figure 3A). All magnetofection conditions produced transfection efficiencies significantly higher than basal levels (Figure 3A). Specifically, the application of a static magnetic field resulted in a transfection efficiency that was approximately 2-fold that in the absence of a field (F = 0 Hz: 12.5 ± 1.2%; range 10.8−17.0%). The oscillating magnetic field conditions resulted in transfection efficiencies that were approximately 2.5-fold (F = 1 Hz: 15.5 ± 1.9%; range 9.3−19.9%) and 3.5-fold (F = 4 Hz: 20.6 ± 2.2%; range 15.9−26.3%) that in the absence of a field. Importantly, the 4 Hz oscillating magnetic field condition produced significantly greater transfection efficiency than the static magnetic field condition (Figure 3A). However, no significant difference was found between the 1 Hz oscillating field condition and either the static or 4 Hz oscillating field conditions. In all experiments, transfected OPCs were observed to be phase bright and exhibited normal cell adherence. Cells expressed GFP throughout the cell body and processes (Figure 3B). Transfected cells retained their characteristic bipolar phenotypes and exhibited normal staining profiles for the OPC marker A2B5, and DAPI-stained nuclei appeared healthy with no evidence of increased chromatin condensation or pyknosis (Figure 3C).

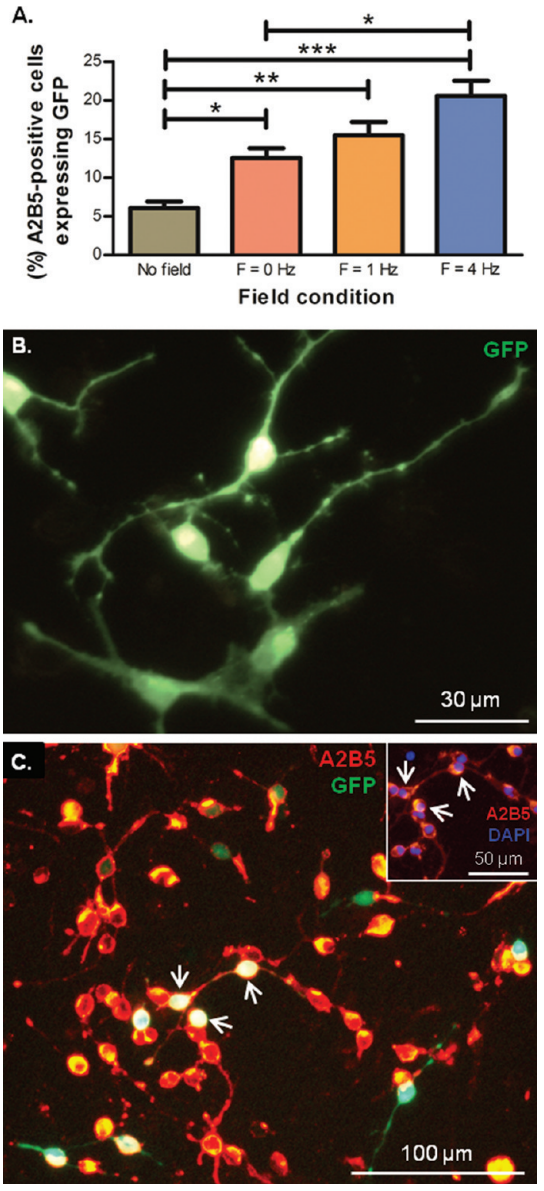

Figure 3. Application of static or oscillating magnetic arrays (magnetofection) enhances MNP-based OPC transfection without affecting cellular morphology or staining profiles. (A) Bar chart showing transfection efficiencies achieved in OPCs 48 h post-transfection using Neuromag−*gfp* complexes (0.1× complex concentration), as judged by the percentage of A2B5$^+$ cells expressing GFP (A2B5 is an OPC marker). Static and oscillating magnetic field conditions significantly enhanced transfection efficiency compared to the basal level (no field). Importantly, application of the 4 Hz oscillating magnetic field significantly enhanced transfection efficiency compared to the static magnetic field condition. *$p < 0.05$, **$p < 0.01$, ***$p < 0.001$; $n = 5$ cultures. (B) Representative image of transfected OPCs with bipolar morphologies, expressing GFP throughout the cell body and processes. (C) Representative image of transfected OPCs. Note co-localization of GFP expression with A2B5 staining, and (inset) morphologically normal DAPI-stained nuclei. Arrows indicate same transfected cells in main image and inset.

TABLE 1. Comparative Transfection Efficiencies in Rat OPCs for Viral and Nonviral Vectors[a]

transfection method	gene	transfection efficiency	viability	ref
Viral Methods				
retrovirus (MoMuLV)	β-Gal	0.005−0.5%	not reported	56
retrovirus (LZRS)	D15A/EGFP	60%	not reported	14
retrovirus (LZRS)	CNTF/EGFP	60−70%; adult OPCs	not reported	15
adenovirus (AdLacZ)	β-Gal	>50%; did not distinguish OPCs and astrocytes	not reported	38
Nonviral Methods				
magnetic nanoparticles	GFP	21%	no significant toxicity	current study
lipofection	β-Gal	1−3%	not reported; toxic at even low doses (<2 μg)	30
calcium phosphate precipitation	β-Gal	3−5%	~10%	56
calcium phosphate precipitation	β-Gal	<2%	not reported; induced morphological changes	30
electroporation	EGFP	~43%	60%	57[b]
electroporation	β-Gal	10−15%	20−25%	30

[a] β-Gal = β-galactosidase; D15A = multineurotrophin, with brain-derived neurotrophic factor (BDNF) and neurotrophin 3 (NT3) activity; EGFP = enhanced green fluorescent protein; CNTF = ciliary neurotrophic factor; GFP = green fluorescent protein. [b] Company Web site.

A range of nonviral methods have been tested previously for OPC transfection (Table 1). Our data show that magnetofection strategies compare favorably with such methods, in terms of both transfection efficiency and cell viability. There is considerable variability in transfection efficiencies reported previously for OPCs, and all nonviral alternatives have resulted in reduced cell viability. For example, calcium phosphate-based transfection of OPCs produced <5% transfection efficiency and resulted in abnormal morphological changes in cells.[56] The lipofection agents Lipofectamine, Lipofectin, and Cellfectin were found to be toxic to OPCs, even at low concentrations, and resulted in <3% of cells being transfected,[30] while electroporation has been reported to result in efficiencies ranging from 10% to 15% (20−25% cell viability)[30] to approximately 43% (60% viability).[57] In terms of virus-mediated gene delivery, although retroviral transduction has been reported to yield a gene transfer efficiency of up to 70% in OPCs,[15] results can vary greatly, with another study reporting only 0.005−0.5% transfection using retroviral methods[56] (OPC viability not reported in either study). Irrespective of the efficiencies of other techniques, it must be stressed that MNPs offer a combination of advantages for neural cell transplantation therapies (compared with existing vector platforms), owing to their unique multifunctionality for "theragnostic" applications, *i.e.*, the fusion of therapeutic approaches, such as gene/drug delivery, with imaging methods such as MRI.[29,34−36,38,41]

In keeping with our previous findings,[53,54] the efficacy of oscillating fields was found to be frequency-dependent (optimal frequency = 4 Hz for OPCs). We have described previously the efficacy of magnetofection strategies in NSCs[54] and astrocytes[53] and discussed the basis for their effects; this finding is in contrast to the optimal oscillation frequency for astrocyte transfection (F = 1 Hz) but identical to that for NSC monolayers. It is not clear what mechanisms are responsible for the cell-to-cell variation in optimal transfection-promoting frequencies. The oscillating movements may serve to reduce biases in magnetic field strength across the cellular monolayer, thereby improving cellular access to particles and hence transfection levels. The lateral motion imparted by oscillating magnetic fields may also increase the likelihood of particle−cell contact and stimulate endocytosis; we cannot rule out the induction of pro-transfection uptake mechanisms such as macropinocytosis by the oscillating fields.[38,53,59] If this is the case, differences in cell size/plating density and extent of membrane elaboration by cells may account for such frequency-dependent effects. Combined with the significant variations in the timing of particle exposure and extent of transfection between cells, these results highlight further the need to tailor MNP transfection protocols for individual cell types, as protocols for one neural cell type cannot be extrapolated to another. Further analyses using blockers of specific endocytotic pathways and detailed TEM analyses to systematically compare MNP uptake are necessary to establish the basis of intercellular variability in the efficacy of magnetofection methods.

Effects of Magnetofection on OPC Fate (Proliferation and Differentiation). MNP-mediated transfection did not alter the proliferative capacities of OPCs, as comparative counts of OPC densities per field between cultures treated with particle−plasmid complexes and plasmid only controls revealed no significant differences at 48 h (Figure 2A). Additionally, transfected progeny (immature oligodendrocytes) with daughter nuclei in close apposition and therefore appearing to result from recent OPC divisions could be observed (Figure 4A), supporting the finding that MNP-based transfection does not alter the proliferative potential of OPCs. Furthermore, transfected OPCs differentiated into GFP^+/MBP^+ oligodendrocytes (myelin basic protein, MBP, is a late-stage oligodendrocyte marker) with mature, highly branched morphologies, comparable to that observed in control cultures (Figure 4B). Counts of MBP^+ cells from untreated cultures *versus* MNP transfected

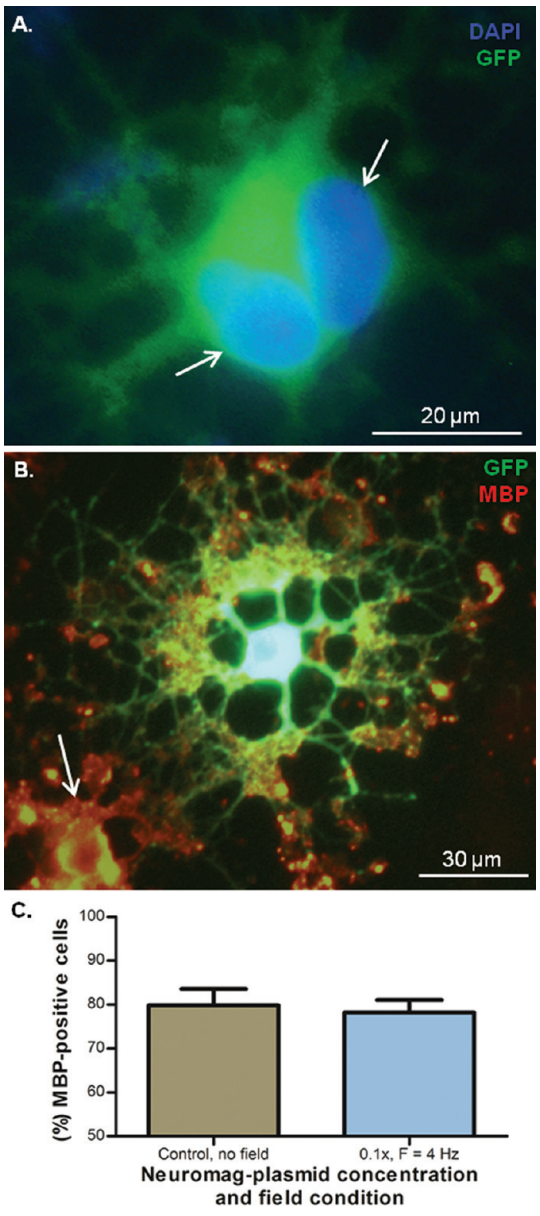

Figure 4. Transfection of OPCs using magnetofection does not affect proliferation or differentiation potential. (A) Following culture in Sato differentiation medium, transfected OPCs developed multipolar morphologies typical of early-stage oligodendrocytes. Arrows indicate two nuclei, suggestive of a recent cell division, and therefore normal proliferative activity. (B) Following culture in Sato differentiation medium, transfected OPCs developed morphologies typical of mature oligodendrocytes, expressed GFP throughout their processes, and stained for myelin basic protein (a late-stage oligodendrocyte marker). Arrow indicates MBP^+/GFP^- cell. (C) Bar chart showing percentage of MBP^+ cells, 12 days post-transfection. The percentage of MBP^+ cells in transfected cultures (0.1× complex concentration; $F = 4$ Hz) was not significantly different from controls (without complexes or magnetic field). $n = 4$ cultures.

cultures ($F = 4$ Hz) (cultured in differentiation-promoting medium) revealed no significant difference in the percentage of MBP^+ cells at 12 days post-transfection (Figure 4C). Transfected OPCs and their progeny were observed to display the full range of morphological

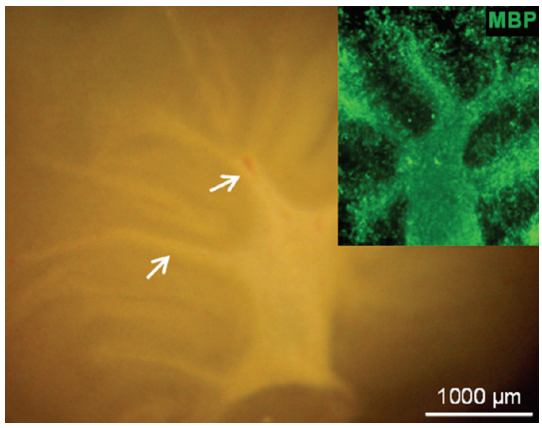

Figure 5. Cerebellar slice cultures (10 days in culture) retain structural and anatomical organization. (A) Representative image of slice culture, with clearly visible white matter tracts (arrows) branching from the base. Inset illustrates that these white matter tracts are distinctly revealed by MBP staining, a marker for mature oligodendrocytes.

phenotypes observed as standard within differentiating cultures of the oligodendroglial lineage, from bipolar unbranched cells to multipolar, highly branched, complex forms with extensive membrane elaboration, lending further support to the finding that the differentiation potential of OPCs is unaffected by the transfection protocols used in this study. Longer term monitoring of cultures revealed that expression of GFP persisted within oligodendrocytes for up to 22 days (the latest time point observed). However levels of expression declined with time, and at 22 days approximately 5% of peak levels of transfection were observed. Such transient expression is especially desirable in the context of myelin repair, where regeneration-promoting molecules are expressed in a temporally specific pattern, such that each stage of the repair process occurs in the appropriate sequence; maintaining pro-proliferation or pro-differentiation environments for inappropriate periods has been suggested to be detrimental to repair.[6,7,17,60–62] For example, platelet-derived growth factor (PDGF-AA) and FGF2 induce proliferation and migration of OPCs, but also inhibit late-stage oligodendrocyte differentiation, and so their upregulation should not be prolonged beyond the "recruitment" phase of repair.[18,63]

Evaluation of Transplantation Potential of Transfected OPCs. *Organotypic Cerebellar Slice Cultures As Host Tissue.* The study has employed organotypic models for the introduction and subsequent monitoring of OPC transplant cells. Such three-dimensional, *in vitro* models are widely used in experimental neurology research, providing an excellent bridge between isolated cell cultures (which lack tissue organization and environmental cues that can influence transplant cell behavior) and *in vivo* investigations that are typically expensive, time-consuming, and difficult to monitor in real time.[64–67] Slice cultures demonstrated high viability, as judged by

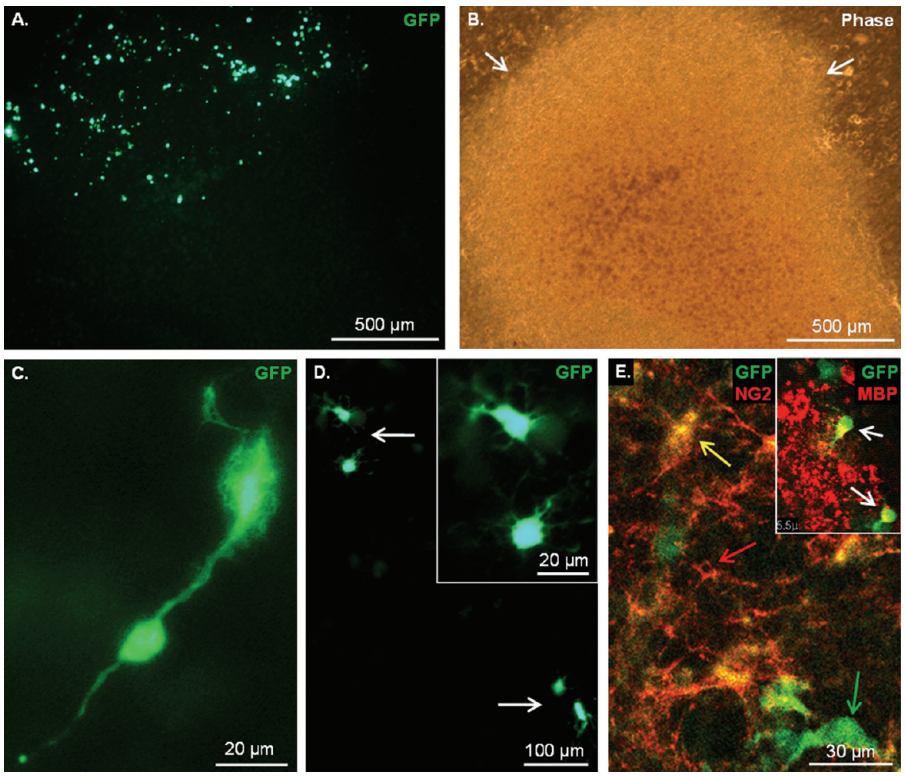

Figure 6. Transfected OPCs survive, migrate, proliferate, and differentiate following transplantation into organotypic slice cultures. (A) Transfected OPCs could be focally delivered to slices, as evidenced by fluorescence microscopy immediately post-transplantation. GFP$^+$ transplanted cells exhibited the rounded morphology typical of enzymatically detached cells. (B) Counterpart phase image to (A), illustrating slice margin (arrows). Post-transplantation, GFP$^+$ cells were observed with bipolar morphologies typical of migrating OPCs (24 h; C), in pairs, suggestive of proliferation (48 h; D), and with multipolar morphologies, indicative of normal differentiation (D, inset). (E) When slices were stained for the OPC marker NG2, 48 h post-transplantation, confocal microscopy revealed GFP$^+$/NG2$^+$ transplanted OPCs (yellow arrow) against a background of red NG2$^+$ host OPCs (red arrow). Some GFP$^+$ cells were NG2$^-$ (green arrow). Inset shows confocal image of GFP$^+$ cells stained for the oligodendrocyte marker MBP 48 h post-transplantation (arrows), indicating OPC differentiation within the slice.

live/dead staining (Viability kit, Invitrogen, UK; data not shown). Well-preserved white matter (WM) tracts could be clearly observed using phase contrast microscopy (Figure 5). This was confirmed by fluorescence microscopy following MBP immunostaining (Figure 5, inset), and WM tracts showed similar anatomical organization to that found *in vivo*.[66]

OPC Transplantation onto Cerebellar Slices. Transplants were performed with 15 slices in total, from four animals. Slices imaged immediately post-transplantation showed that focal delivery of OPCs could be achieved. Delivery of the cells was by simply pipetting onto the slices, rather than by invasive injection. From an experimental perspective, this approach has the major advantage of greatly reduced trauma to both cells and slice host tissue. The transplantation procedure produced passive spread with a radius of 700 μm (Figure 6A and B), due to the force of the transplantation procedure alone. Immediately after transplantation, OPCs were clearly observed to express GFP and displayed rounded morphologies characteristic of enzymatically detached cells (Figure 6A). Post-transplantation, cells were observed to recover their characteristic cellular morphologies. At 24–48 h post-transplantation, GFP$^+$ cells showed evidence of (1) migration, as indicated by the presence of cells with elongated bipolar morphologies that are characteristic of migratory OPCs (Figure 6C), and (2) proliferation, indicated by the striking occurrence of GFP$^+$ cells in pairs (Figure 6D). Slices were stained for either NG2, an OPC marker, or MBP, a late-stage oligodendrocyte marker, to establish the cellular identity of transplant cells. Confocal microscopy revealed the presence of GFP$^+$/NG2$^+$ cells against a background of host NG2$^+$ cells, confirming the OPC identity of the transplanted cells (Figure 6E). There was also clear evidence of OPC differentiation in slices, as demonstrated by the presence of multipolar cells (Figure 6D, inset), and GFP$^+$/MBP$^+$ cells, detected in slices using confocal microscopy (Figure 6E, inset). Transplant populations replated into chamber slides with Sato differentiation medium also retained GFP expression and exhibited normal oligodendroglial morphologies, supporting the observations that MNP transfection protocols do not alter the differentiation capabilities of the transfected, transplanted cells.

These results demonstrate the transplantation potential of MNP-transfected OPCs. They further prove

that cellular properties of OPCs that are key to their regenerative potential, such as the ability to divide, migrate, and give rise to myelin-generating cells, are unimpaired following the transfection protocols. These findings emphasize the safety of the protocols developed and suggest that the MNP platform has considerable potential for clinical translational OPC applications involving *ex vivo* CNS gene transfer. In terms of the transplantation methods used here, tissue engineering approaches using brain and spinal cord slice cultures to evaluate cell replacement therapies represent a key recent advance in the reduction, replacement, and refinement (3Rs) of experimental animal usage in neurological research. We have extensively documented the suitability of organotypic model systems for assessing the transplantation potential of key neural cells, including NSCs and astrocytes, using high-throughput analyses.[50,53,55] Our current data lend support to our previous work and further demonstrate that the slice model can be successfully used to monitor the survival and fate of transplanted OPC populations. It is important to note that cerebellar slice models offer unique advantages as host tissue within which to evaluate OPC transplantation approaches, as these retain large, well-defined, axonal (WM) tracts that undergo myelination *in vitro*.[66,67] Additionally, slices can be prepared from dysmyelinating mutants (including those with limited postnatal survival), and focal/disseminated demyelinating lesions can be induced in normal slice WM tracts, highlighting the translational potential of cerebellar slices for evaluating the regeneration-promoting effects of OPC transplantation therapies.[66−68]

MNP-Mediated Delivery of Plasmid Encoding Therapeutic Growth Factor. The preceding experiments were conducted with the pmaxGFP plasmid, which encodes a reporter gene only. To assess the potential of the optimized magnetofection protocol for functional gene delivery, OPC cultures ($n = 4$) were transfected using MNPs conjugated with a plasmid encoding the therapeutic protein FGF2 tagged with GFP (FGF2-GFP; 7.4 kb); FGF2 is a major growth factor that promotes neural regeneration due to its mitogenic properties (including for OPCs) and angiogenesis-promoting effects. A recommended plasmid (AN-GFP; 6.6 kb) lacking the FGF2 insert was used as a control. It should be noted that both these plasmids are considerably larger than the pmaxGFP plasmid (3.5 kb) used in earlier experiments. Magnetofection of OPCs with these plasmids, using the optimized protocol (oscillating magnetic field of $F = 4$ Hz), revealed cellular GFP expression using both the therapeutic and control plasmids (Figure 7A−C). For the FGF2-encoding plasmid, GFP expression was largely restricted to the nucleus (Figure 7A and B). These findings are consistent with several reports, demonstrating endogenous expression of nuclear isoforms of FGF2 in glia, notably astrocytes.[69,70] Occasional rounded profiles consistent with dividing OPCs could be observed

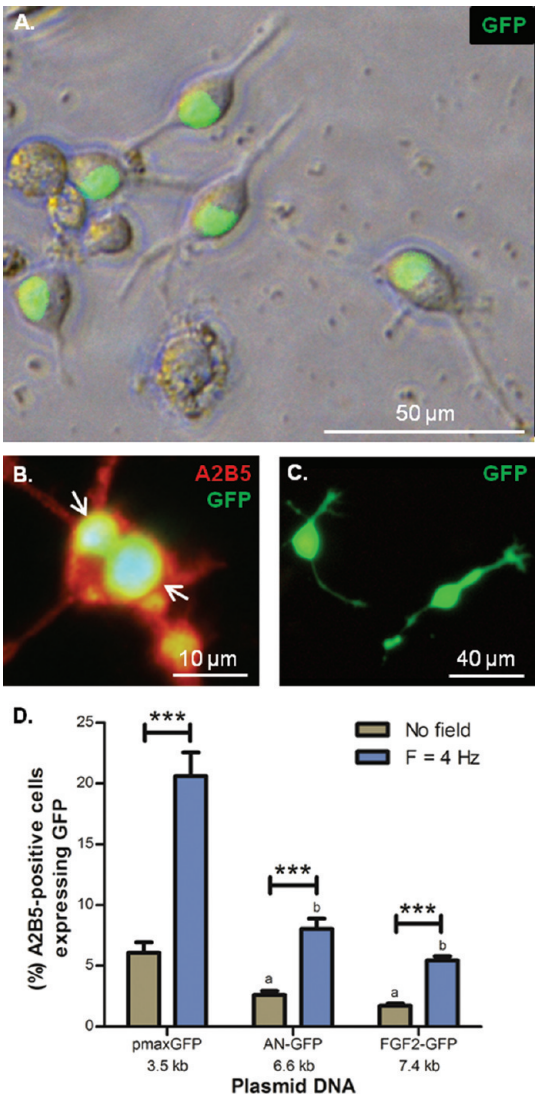

Figure 7. MNP-mediated delivery of therapeutic genes to OPCs. (A) Representative phase image of live cells transfected using the FGF2-GFP plasmid, which encodes fibroblast growth factor 2 (FGF2) tagged with green fluorescent protein (GFP) at 24 h post-transfection. Transfected cells exhibit bipolar morphologies typical of OPCs with GFP expression prominently localized to the nucleus. (B) Fluorescence image of a proliferating OPC transfected with the FGF2-GFP plasmid and stained for the OPC marker A2B5; both daughter cells appear to express GFP (arrows indicate daughter nuclei). (C) Representative fluorescence image of cells transfected using the AN-GFP control plasmid. Note that GFP expression is present throughout the cell body and processes. (D) Bar chart illustrating transfection efficiencies achieved in OPCs using Neuromag (0.1×) conjugated to various plasmids, as judged by percentage of $A2B5^+$ cells expressing GFP. Data are shown for transfection without a magnetic field and with applied oscillating field ($F = 4$ Hz). For each plasmid, the 4 Hz oscillating field significantly enhances transfection efficiency over the no field condition (*$p < 0.001$). Transfection efficiency for both the AN-GFP and FGF2-GFP plasmids is significantly lower compared to pmaxGFP, for the corresponding field conditions ($^a p < 0.001$ compared to pmaxGFP no field condition; $^b p < 0.001$ compared to pmaxGFP $F = 4$ Hz). $n = 5$ cultures for pmaxGFP studies; $n = 4$ cultures for AN-GFP and FGF2-GFP studies. Data in B−D were at 48 h post-transfection.**

with both daughter cells appearing to inherit the introduced gene (Figure 7B). For the control plasmid, the pattern of GFP expression (Figure 7C) was similar to that seen in earlier experiments with the pmaxGFP plasmid (Figure 3B and C), *i.e.*, with GFP expression evident throughout the cell body and extending into the processes of cells. In immunostaining studies, all transfected cells were found to clearly express the OPC-specific marker A2B5 (for example see Figure 7B). Determination of transfection efficiencies yielded values of $5.5 \pm 0.4\%$ for the FGF2-GFP plasmid and $8.1 \pm 1.0\%$ for the AN-GFP control plasmid with applied oscillating magnetic fields, both of which were significantly higher than the corresponding values determined in the absence of a magnetic field (Figure 7D).

It is clear from these data that use of larger plasmids results in a systematic decrease in MNP-mediated transfection efficacy. This strongly indicates that experimental protocols will need to be modified to account for variations in plasmid size. This issue could be addressed using a range of strategies, including (i) reduction of overall plasmid size by removal of the reporter protein component and other elements of the constructs; (ii) use of particles with different polymer coatings/sizes to further enhance the DNA binding capacity of the particles; and (iii) testing of different oscillation frequencies to determine if the optimal frequency differs with plasmid size, with additional optimization of the duration of field application.

In terms of the translational applications of our findings to clinical cell transplantation therapies, a number of studies have demonstrated that repair mechanisms can be enhanced by genetic manipulation of OPC transplant populations.[14,15,18,19] The optimal transfection efficiency for neural repair following *ex vivo* gene delivery will ultimately need to be determined by evaluation of functional recovery post-transplantation of transfected OPCs in a range of experimental pathologies; such effects can be predicted to be dependent on the nature of the pathology, the functional gene under study, and extent of the neural injury. Cao *et al.* (2010) retrovirally transfected adult rat primary OPCs (transfection efficacy approximately 70%) with CNTF, then transplanted them into adult spinal cord, 9 days post-contusion.[15] At 7 weeks post-transplantation, rats that received transplants of CNTF-OPCs demonstrated 4-fold greater survival of transplanted OPCs, a greater number of myelinated axons, and a greater level of functional recovery, compared to rats that received transplants of unmodified OPCs. Previous studies suggest that transfection of 20–50% of a neural progenitor transplant population can help to promote effective functional recovery (*via* angiogenesis and neuroprotection, for example).[22,23] In addition, the unmodified OPC transplant populations *per se* have an intrinsic repair capability;[9,13] therefore our results indicate that the OPC transfection levels obtained here (with protocol optimization to account for plasmid size variations as described above) may be sufficient to promote neural repair; this will need to be tested using functional genes in neural injury models. Further work is being carried out to measure the migratory capacity and long-term integration of transfected OPCs following transplantation into slice cultures.

In summary, MNPs can be used to transfect OPCs, with transfection efficiency enhanced by application of a static/oscillating magnetic field. Transfected OPCs can be successfully transplanted into cerebellar tissue slices, where they survive, migrate, proliferate, and differentiate into oligodendrocytes, highlighting the translational potential of the MNP platform for OPC transplantation therapies.

EXPERIMENTAL SECTION

Reagents and Equipment. Tissue culture-grade plastics, media, and media supplements were from Fisher Scientific (Loughborough, UK) and Sigma-Aldrich (Poole, UK). Recombinant human platelet-derived growth factor (PDGF-AA) and basic fibroblast growth factor (FGF2) were from Peprotech (London, UK). Polyclonal rabbit anti-NG2, Omnipore membrane (JHWP01300), and Millicell culture inserts were obtained from Millipore (Watford, UK). Monoclonal rat antimyelin basic protein was from Serotech (Kidlington, UK), monoclonal mouse anti-A2B5 was from Sigma-Aldrich (Poole, UK), and secondary antibodies (Cy3-conjugated) were from Jackson ImmunoResearch Laboratories Inc. (West Grove, PA, USA). Mounting medium with DAPI (4′,6-diamidino-2-phenylindole) was from Vector Laboratories (Peterborough, UK). The pmaxGFP plasmid (3.5 kb) was from Amaxa Biosciences (Cologne, Germany), and both the pCMV6-FGF2-GFP plasmid (encodes the open reading frame of human FGF2 with a carboxy-terminal turboGFP tag; 7.4 kb, FGF2-GFP) and the recommended control plasmid, pCMV6-AN-GFP (6.6 kb, AN-GFP), were from OriGene Technologies (Rockville, MD, USA).

Neuromag transfection-grade MNPs were purchased from Oz Biosciences (Marseille, France). These positively charged particles have an average diameter of 160 nm (range 140–200 nm). DNA binding curves showed that these particles bind DNA effectively with DNA binding increasing particle size by 35%, assessed using a Malvern Zetasizer 3000. The MAGNEFECT-NANO oscillating magnetic array system was from NanoTherics Ltd. (Stoke-on-Trent, UK). This system allows 24-well plates to be placed over a horizontal array of 24 neodymium (NdFeB) magnets, grade N42, which match the plate configuration. The magnetic array can be programmed to oscillate laterally beneath the culture plate *via* a computerized motor; both the frequency and the amplitude of oscillation can be varied. The field strength at the face of each magnet is 421 ± 20 mT (NanoTherics Ltd., personal commun.).

Cell and Tissue Culture Procedures. The care and use of animals was in accordance with the Animals (Scientific Procedures) Act of 1986 (United Kingdom) with approval by the local ethics committee.

OPC Cell Cultures. Primary mixed glial cell cultures were first prepared from cerebral cortex of Sprague–Dawley rats at postnatal day 1–3 (P1–3), using an established protocol.[71] Medium (D10) was DMEM supplemented with 10% fetal bovine serum, 2 mM glutaMAX-I, 1 mM sodium pyruvate, 50 U/mL penicillin, and 50 μg/mL streptomycin. After 8–10 days culture at 37 °C in 5% CO_2/95% humidified air, flasks were shaken for 2 h on a

rotary shaker at 200 rpm, and the medium, containing mainly microglia, was discarded. Fresh D10 medium was then added, and the flasks were shaken overnight at 200 rpm. This medium, containing mainly OPCs, was transferred to nontissue culture grade Petri dishes, to which microglia (but not OPCs) will readily attach in order to reduce microglial contamination. After 30 min, unattached cells were resuspended at 2×10^5 cells/mL in OPC maintenance medium (OPC-MM, comprising DMEM, 2 mM glutaMAX-I, 1 mM sodium pyruvate, 10 nM biotin, 10 nM hydrocortisone, 30 nM sodium selenite, 50 μg/mL transferrin, 5 μg/mL insulin, 0.1% BSA, 50 U/mL penicillin, 50 μg/mL streptomycin, 10 ng/mL PDGF-AA, 10 ng/mL FGF2). OPCs were plated (0.3 mL/well of a 24-well plate) either on PDL-coated coverslips for assessment of transfection efficiency or on PDL-coated wells for transplantation experiments. This plating density (3×10^4 cells/cm^2) yields optimal cell survival, as lower OPC densities can result in significant cell death, likely due to loss of paracrine effects.

Organotypic Cerebellar Slice Cultures. Brains were extracted from P9−14 rats into ice-cold slicing medium (EBSS buffered with 25 mM HEPES). Cerebella were dissected and meninges removed; then 350 μm parasagittal slices were prepared using a McIlwain tissue chopper. Slices were incubated on ice for 30 min, then transferred to pieces of Omnipore membrane on Millicell culture inserts in six-well plates containing slice culture medium (50% MEM, 25% heat-inactivated horse serum, 25% EBSS, supplemented with 36 mM D-glucose, 50 U/mL penicillin, and 50 μg/mL streptomycin). Slices were incubated at 37 °C in 5% CO_2/95% humidified air for at least 8 days before transplantation, with medium changes every 2−3 days.

Toxicity Experiments. It was necessary to determine the maximum safe dose of Neuromag−plasmid complexes for transfection and to determine whether magnetofection conditions affected toxicity. Neuromag MNPs are recommended for use with neurons at a final concentration of 7 μL/mL in medium (referred to here as 1.0×), but lower concentrations have been required for safe use with other neural cells (astrocytes, NSCs).[53−55] Control cultures were treated with pmaxGFP plasmid alone, without Neuromag. The DNA-binding capacity of Neuromag MNPs is maximal at a ratio of 3.5 μL Neuromag to 1 μg DNA;[53] this ratio was therefore routinely used in the present study. Plasmid-based transfection is often reported to result in peak expression at 48 h,[19,53] and the results of preliminary experiments were consistent with this timing; therefore in all cases transfection efficiency was assessed at 48 h. Accordingly, Neuromag−*gfp* toxicity was assessed by incubating OPCs with various concentrations of complexes (1.0×, 0.5×, and 0.1×), with and without exposure to magnetic fields (no field, static field, 1 Hz oscillating field, and 4 Hz oscillating field). Exposure to a magnetic field was for 30 min, and total incubation time for all conditions was 48 h, at which point cells were fixed. Several parameters of cytotoxicity were assessed by microscopy, specifically (i) whether cells were processed, phase bright, and adherent; (ii) the presence of pyknotic nuclei, as judged by DAPI staining; (iii) expression of the OPC marker A2B5; and (iv) cell counts per microscopic field, which are indicative of proliferative capacity.

Transfection (Magnetofection) Experiments. Transfection protocols were based on those supplied with the Neuromag MNPs; however the specific protocols used in this study were tailored for the OPC densities used (3×10^4 cells/cm^2). In preliminary experiments, Neuromag−*gfp* concentrations at 0.1×, 0.5×, 1.0×, 2.0×, and 4.0× were tested rather than simply adopting the 0.1× dose devised for use with astrocytes as reported by ourselves previously.[53] In terms of DNA quantity, we have previously generated DNA binding curves for Neuromag MNPs to determine the particle:DNA ratio that results in maximal binding;[53] this ratio was maintained constant while varying particle concentrations. The combination of parameters resulting in optimal OPC survival and maximal DNA binding that yielded transfection without cytotoxicity were used in this study. For the transfection step, at 2 h after OPC plating, medium was replaced with 0.225 mL of fresh antibiotic-free OPC-MM. After a further 24−48 h, transfection complexes (per well, at 0.1×) were prepared by mixing 60 ng of pmaxGFP in 75 μL of DMEM base medium, then gently mixing this with 0.21 μL of Neuromag. For control wells, pmaxGFP was mixed in DMEM, but no Neuromag was included. After 20 min incubation, the entire complex mix was added dropwise to cells, while gently swirling the plate. For magnetofection, immediately following application of complexes to cells, the 24-well plate was placed above a 24-magnet array on the MAGNEFECT-NANO device, which had been prewarmed in the incubator. The array either remained static or was programmed to oscillate with an amplitude of 0.2 mm and a frequency (F) of 1 or 4 Hz. After 30 min, the plate was removed from the magnetic array. For the no field condition, plates were returned to the incubator without application of a magnetic field. Cells were incubated with complexes for 48 h in total, then fixed. Experiments to assess the delivery of the plasmid FGF2-GFP (which encodes the functional gene FGF2 tagged with turboGFP) and the appropriate control plasmid AN-GFP (which encodes turboGFP alone) were conducted in an identical manner. Transfections were performed either without application of a magnetic field or with the initial application of an oscillating magnetic field of $F = 4$ Hz.

Differentiation Potential of Transfected OPCs and Long-Term GFP-Expression in Oligodendrocyte Progeny. At 48 h post-transfection, cells were washed with PBS, then switched to Sato medium (DMEM supplemented with 2 mM glutaMAX-I, 1 mM sodium pyruvate, 30 nM triiodothyronine, 30 nM thyroxine, 1% N2 supplement, 50 U/mL penicillin, and 50 μg/mL streptomycin) to induce oligodendrocyte differentiation. Cells were monitored to assess the extent of cellular expression of GFP and to evaluate potential adverse effects on OPC differentiation for up to 3 weeks. Medium was changed every 2−3 days.

Transplantation of Transfected OPCs onto Slice Cultures. At 24 h post-magnetofection ($F = 4$ Hz), OPCs were washed with PBS, then detached using accutase-DNase I. Cells were resuspended at 2×10^7 cells/mL Sato medium, and 0.5 μL was pipetted onto cerebellar slice cultures. Passive spread of cells due to the pipetting procedure was assessed by transferring cerebellar slices to a small quantity of PBS on a microscope slide, then transplanting cells onto these slices and viewing immediately using fluorescence microscopy. At the end of the transplant procedure, remaining cells were also plated at 2×10^5 cells/mL Sato medium directly on PDL-coated chamber slides. Samples were fixed and stained 24−48 h post-transplantation to assess the survival and morphology of the transplanted and replated cells.

Immunocytochemistry and Immunohistochemistry. Cells and slices were washed with PBS, fixed with 4% paraformaldehyde [room temperature (RT); 25 min], then washed again. For staining, samples were incubated with blocking solution (5% serum in PBS, with 0.3% Triton X-100 for NG2 and MBP; RT; 30 min), then with primary antibody in blocking solution (A2B5 1:200, NG2 1:150, MBP 1:200; 4 °C; overnight). The A2B5 antibody recognizes cell surface ganglioside epitopes, while the NG2 antibody recognizes a cell surface chondroitin sulfate proteoglycan; MBP is a major protein constituent of myelin and is used to detect late-stage oligodendrocytes. All the above markers are widely used to label cells of the oligodendrocyte lineage. Samples were then washed with PBS, incubated with blocking solution (RT; 30 min), and then incubated with the appropriate Cy3-conjugated secondary antibody in blocking solution (1:200; RT; 2 h). Samples were then washed with PBS and mounted with DAPI.

Fluorescence Microscopy and Image Analysis. Samples were imaged using fixed exposure settings on an Axio Scope A1 fluorescence microscope (Carl Zeiss MicroImaging GmbH, Goettingen, Germany), and the images merged using Adobe Photoshop CS3 (version 10.0.1). For toxicity and transfection experiments, a minimum of 200 nuclei per treatment per culture were scored for association with A2B5 staining (for culture purity) or for GFP expression (for transfection efficiency). For OPC differentiation experiments, a minimum of 100 nuclei per treatment per culture were scored for MBP expression. Slices were imaged post-transplantation using the AxioScope and, in some experiments, using a BioRad MRC1024 confocal laser scanning microscope.

Statistical Analysis. Data were analyzed using GraphPad Prism statistical analysis software. Data are expressed as mean ± SEM. The number of experiments (n) refers to the number of OPC

cultures used, each from a different rat litter. To determine whether transfection conditions affected toxicity or transfection efficiency, data (the number of $A2B5^+$ cells per field and the percentage of $A2B5^+$ cells expressing GFP, respectively) were analyzed by one-way ANOVA, with Bonferroni's multiple comparison test for *post hoc* analysis. To determine whether transfection conditions affected the differentiation of OPCs into MBP^+ oligodendrocytes, the percentage of MBP^+ cells in cultures without Neuromag and without application of a magnetic field was compared to magnetofected cultures using a two-tailed paired *t*-test. To compare the transfection efficiencies for the pmaxGFP, FGF2-GFP, and AN-GFP plasmids, with and without the application of an oscillating magnetic field, the percentage of $A2B5^+$ cells expressing GFP was analyzed by one-way ANOVA, with Bonferroni's multiple comparison test for *post hoc* analysis.

Acknowledgment. We thank D. Furness for expert assistance with confocal microscopy. This work was supported by a research grant from the Royal Society, UK, and a New Investigator Award from the British Biotechnology and Biological Sciences Research Council, UK.

REFERENCES AND NOTES

1. Ben-Hur, T.; Einstein, O.; Bulte, J. W. M. Stem Cell Therapy for Myelin Diseases. *Curr. Drug Targets* **2005**, *6*, 3–19.
2. Kulbatski, I.; Mothe, A. J.; Parr, A. M.; Kim, H.; Kang, C. E.; Bozkurt, G.; Tator, C. H. Glial Precursor Cell Transplantation Therapy for Neurotrauma and Multiple Sclerosis. *Prog. Histochem. Cytochem.* **2008**, *43*, 123–176.
3. Moreno-Flores, M. T.; Avila, J. The Quest to Repair the Damaged Spinal Cord. *Recent Pat. CNS Drug Discovery* **2006**, *1*, 55–63.
4. Ruff, R. L.; McKerracher, L.; Selzer, M. E. Repair and Neurorehabilitation Strategies for Spinal Cord Injury. *Ann. N.Y. Acad. Sci.* **2008**, *1142*, 1–20.
5. Willerth, S. M.; Sakiyama-Elbert, S. E. Cell Therapy for Spinal Cord Regeneration. *Adv. Drug Delivery Rev.* **2008**, *60*, 263–276.
6. Franklin, R. J. M.; ffrench-Constant, C. Remyelination in the CNS: from Biology to Therapy. *Nat. Rev. Neurosci.* **2008**, *9*, 839–855.
7. Rodriguez, M. A Function of Myelin is to Protect Axons from Subsequent Injury: Implications for Deficits in Multiple Sclerosis. *Brain* **2003**, *126*, 751–752.
8. Stangel, M. Neuroprotection and Neuroregeneration in Multiple Sclerosis. *J. Neurol.* **2008**, *255*), 77–81.
9. Keirstead, H. S.; Nistor, G.; Bernal, G.; Totoiu, M.; Cloutier, F.; Sharp, K.; Steward, O. Human Embryonic Stem Cell-Derived Oligodendrocyte Progenitor Cell Transplants Remyelinate and Restore Locomotion after Spinal Cord Injury. *J. Neurosci.* **2005**, *25*, 4694–4705.
10. Buchet, D.; Baron-Van Evercooren, A. In Search of Human Oligodendroglia for Myelin Repair. *Neurosci. Lett.* **2009**, *456*, 112–119.
11. Windrem, M. S.; Nunes, M. C.; Rashbaum, W. K.; Schwartz, T. H.; Goodman, R. A.; McKhann, G., 2nd; Roy, N. S.; Goldman, S. A. Fetal and Adult Human Oligodendrocyte Progenitor Cell Isolates Myelinate the Congenitally Dysmyelinated Brain. *Nat. Med.* **2004**, *10*, 93–97.
12. http://www.geron.com/GRNOPC1Trial/grnopc1-backgrounder.pdf (accessed May 20, 2011).
13. Bambakidis, N. C.; Miller, R. H. Transplantation of Oligodendrocyte Precursors and Sonic Hedgehog Results in Improved Function and White Matter Sparing in the Spinal Cords of Adult Rats after Contusion. *Spine J.* **2004**, *4*, 16–26.
14. Cao, Q.; Xu, X. M.; DeVries, W. H.; Enzmann, G. U.; Ping, P.; Tsoulfas, P.; Wood, P. M.; Bunge, M. B.; Whittemore, S. R. Functional Recovery in Traumatic Spinal Cord Injury after Transplantation of Multineurotrophin-Expressing Glial-Restricted Precursor Cells. *J. Neurosci.* **2005**, *25*, 6947–6957.
15. Cao, Q.; He, Q.; Wang, Y.; Cheng, X.; Howard, R. M.; Zhang, Y.; DeVries, W. H.; Shields, C. B.; Magnuson, D. S.; Xu, X. M.; *et al.* Transplantation of Ciliary Neurotrophic Factor-Expressing Adult Oligodendrocyte Precursor Cells Promotes Remyelination and Functional Recovery after Spinal Cord Injury. *J. Neurosci.* **2010**, *30*, 2989–3001.
16. Stangel, M.; Trebst, C. Remyelination Strategies: New Advancements Toward a Regenerative Treatment in Multiple Sclerosis. *Curr. Neurol. Neurosci. Rep.* **2006**, *6*, 229–235.
17. Blakemore, W. F. Regeneration and Repair in Multiple Sclerosis: the View from Experimental Pathology. *J. Neurol. Sci.* **2008**, *265*, 1–4.
18. Magy, L.; Mertens, C.; Avellana-Adalid, V.; Keita, M.; Lachapelle, F.; Nait-Oumesmar, B.; Fontaine, B.; Baron-Van Evercooren, A. Inducible Expression of FGF2 by a Rat Oligodendrocyte Precursor Cell Line Promotes CNS Myelination *in Vitro*. *Exp. Neurol.* **2003**, *184*, 912–922.
19. Rubio, N.; Rodriguez, R.; Arevalo, M. A. *In Vitro* Myelination by Oligodendrocyte Precursor Cells Transfected with the Neurotrophin-3 Gene. *Glia* **2004**, *47*, 78–87.
20. Himes, B. T.; Liu, Y.; Solowska, J. M.; Snyder, E. Y.; Fischer, I.; Tessler, A. Transplants of Cells Genetically Modified to Express Neurotrophin-3 Rescue Axotomized Clarke's Nucleus Neurons after Spinal Cord Hemisection in Adult Rats. *J. Neurosci. Res.* **2001**, *65*, 549–564.
21. Holland, E. C.; Varmus, H. E. Basic Fibroblast Growth Factor Induces Cell Migration and Proliferation after Glia-Specific Gene Transfer in Mice. *Proc. Natl. Acad. Sci. U. S. A.* **1998**, *95*, 1218–1223.
22. Martinez-Serrano, A.; Lundberg, C.; Horellou, P.; Fischer, W.; Bentlage, C.; Campbell, K.; McKay, R. D.; Mallet, J.; Bjorklund, A. CNS-Derived Neural Progenitor Cells for Gene Transfer of Nerve Growth Factor to the Adult Rat brain: Complete Rescue of Axotomized Cholinergic Neurons after Transplantation into the Septum. *J. Neurosci.* **1995**, *15*, 5668–5680.
23. Maurer, M. H.; Thomas, C.; Burgers, H. F.; Kuschinsky, W. Transplantation of Adult Neural Progenitor Cells Transfected with Vascular Endothelial Growth Factor Rescues Grafted Cells in the Rat Brain. *Int. J. Biol. Sci.* **2007**, *4*, 1–7.
24. McTigue, D. M.; Horner, P. J.; Stokes, B. T.; Gage, F. H. Neurotrophin-3 and Brain-Derived Neurotrophic Factor Induce Oligodendrocyte Proliferation and Myelination of Regenerating Axons in the Contused Adult Rat Spinal Cord. *J. Neurosci.* **1998**, *18*, 5354–5365.
25. Blits, B.; Bunge, M. B. Direct Gene Therapy for Repair of the Spinal Cord. *J. Neurotrauma* **2006**, *23*, 508–520.
26. Jiang, S.; Seng, S.; Avraham, H. K.; Fu, Y.; Avraham, S. Process Elongation of Oligodendrocytes is Promoted by the Kelch-Related Protein MRP2/KLHL1. *J. Biol. Chem.* **2007**, *282*, 12319–12329.
27. Franklin, R.; Quick, M.; Haase, G. Adenoviral Vectors for *in Vivo* Gene Delivery to Oligodendrocytes: Transgene Expression and Cytopathic Consequences. *Gene Ther.* **1999**, *6*, 1360–1367.
28. Hermens, W. T.; Verhaagen, J. Viral Vectors, Tools for Gene Transfer in the Nervous System. *Prog. Neurobiol.* **1998**, *55*, 399–432.
29. Jeffery, N. D.; McBain, S. C.; Dobson, J.; Chari, D. M. Uptake of Systemically Administered Magnetic Nanoparticles (MNPs) in Areas of Experimental Spinal Cord Injury (SCI). *J. Tissue Eng. Regen. Med.* **2009**, *3*, 153–157.
30. Krueger, W. H.; Madison, D. L.; Pfeiffer, S. E. Transient Transfection of Oligodendrocyte Progenitors by Electroporation. *Neurochem. Res.* **1998**, *23*, 421–426.
31. Pichon, C.; Billiet, L.; Midoux, P. Chemical Vectors for Gene Delivery: Uptake and Intracellular Trafficking. *Curr. Opin. Biotechnol.* **2010**, *21*, 640–645.
32. Ryan, D. A.; Federoff, H, J. Translational Considerations for CNS Gene Therapy. *Expert Opin. Biol. Ther.* **2007**, *7*, 305–318.
33. Guo, Z.; Yang, N. S.; Jiao, S.; Sun, J.; Cheng, L.; Wolff, J. A.; Duncan, I. D. Efficient and Sustained Transgene Expression in Mature Rat Oligodendrocytes in Primary Culture. *J. Neurosci. Res.* **1996**, *43*, 32–41.
34. Berry, C. C. Progress in Functionalization of Magnetic Nanoparticles for Applications in Biomedicine. *J. Phys. D: Appl. Phys.* **2009**, *42*, 1–9.

35. Dobson, J. Magnetic Micro- and Nano-Particle-Based Targeting for Drug and Gene Delivery. *Nanomedicine (London)* **2006**, *1*, 31–37.
36. de la Fuente, J. M.; Berry, C. C.; Riehle, M. O.; Curtis, A. S. G. Nanoparticle Targeting at Cells. *Langmuir* **2006**, *22*, 3286–3293.
37. Kempe, M; Kempe, H; Snowball, I.; Wallen, R.; Arza, C. R.; Gotberg, M.; Olsson, T. The Use of Magnetite Nanoparticles for Implant-Assisted Magnetic Drug Targeting in Thrombolytic Therapy. *Biomaterials* **2010**, *31*, 9499–9510.
38. McBain, S. C.; Yiu, H. H.; Dobson, J. Magnetic Nanoparticles for Gene and Drug Delivery. *Int. J. Nanomed.* **2008**, *3*, 169–180.
39. Tandon, P.; Nordstrom, R. J. Next-Generation Imaging Development for Nanoparticle Biodistribution Measurements. *Wiley Interdiscip. Rev. Nanomed. Nanobiotechnol.* **2011**, *3*, 5–10.
40. Yiu, H. H.; McBain, S. C.; Lethbridge, Z. A.; Lees, M. R.; Dobson, J. Preparation and Characterization of Polyethylenimine-Coated Fe3O4-MCM-48 Nanocomposite Particles as a Novel Agent for Magnet-Assisted Transfection. *J. Biomed. Mater. Res. A* **2010**, *92*, 386–392.
41. Hanessian, S.; Grzyb, J. A.; Cengelli, F.; Juillerat-Jeanneret, L. Synthesis of Chemically Functionalized Superparamagnetic Nanoparticles as Delivery Vectors for Chemotherapeutic Drugs. *Bioorg. Med. Chem.* **2008**, *16*, 2921–2931.
42. Dunning, M. D.; Lakatos, A.; Loizou, L.; Kettunen, M.; ffrench-Constant, C.; Brindle, K. M.; Franklin, R. J. M. Superparamagnetic Iron Oxide-Labeled Schwann Cells and Olfactory Ensheathing Cells can be Traced *in Vivo* by Magnetic Resonance Imaging and Retain Functional Properties after Transplantation into the CNS. *J. Neurosci.* **2004**, *24*, 9799–9810.
43. Bulte, J. W. M.; Zhang, S.-C.; van Gelderen, P.; Herynek, V.; Jordan, E. K.; Duncan, I. D.; Frank, J. A. Neurotransplantation of Magnetically Labeled Oligodendrocyte Progenitors: Magnetic Resonance Tracking of Cell Migration and Myelination. *Proc. Natl. Acad. Sci. U. S. A.* **1999**, *96*, 15256–15261.
44. Laurent, N.; Sapet, C.; Le Gourrierec, L.; Bertosio, E.; Zelphati, O. Nucleic Acid Delivery Using Magnetic Nanoparticles: the Magnetofection Technology. *Ther. Delivery* **2011**, *2*, 471–482.
45. Plank, C.; Schillinger, U.; Scherer, F.; Bergemann, C.; Remy, J. S.; Krotz, F.; Anton, M.; Lausier, J.; Rosenecker, J. The Magnetofection Method: Using Magnetic Force to Enhance Gene Delivery. *Biol. Chem.* **2003**, *384*, 737–747.
46. Sapet, C.; Laurent, N.; de Chevigny, A.; Le Gourrierec, L.; Bertosio, E.; Zelphati, O.; Beclin, C. High Transfection Efficiency of Neural Stem Cells with Magnetofection. *Biotechniques* **2011**, *50*, 187–189.
47. Scherer, F.; Anton, M.; Schillinger, U.; Henke, J.; Bergemann, C.; Kruger, A.; Gansbacher, B.; Plank, C. Magnetofection: Enhancing and Targeting Gene Delivery by Magnetic Force *in Vitro* and *in Vivo*. *Gene Ther.* **2002**, *9*, 102–109.
48. Huth, S.; Lausier, J.; Gersting, S. W.; Rudolph, C.; Plank, C.; Welsch, U.; Rosenecker, J. Insights into the Mechanism of Magnetofection using PEI-based Magnetofectins for Gene Transfer. *J. Gene Med.* **2004**, *6*, 923–936.
49. Khalil, I. A.; Kogure, K.; Akita, H.; Harashima, H. Uptake Pathways and Subsequent Intracellular Trafficking in Nonviral Gene Delivery. *Pharmacol. Rev.* **2006**, *58*, 32–45.
50. Pickard, M. R.; Jenkins, S. I.; Koller, C. J.; Furness, D. N.; Chari, D. M. Magnetic Nanoparticle Labelling of Astrocytes Derived for Neural Transplantation. *Tissue Eng. Part C* **2010**, *17*, 89–99.
51. Plank, C.; Scherer, F.; Schillinger, U.; Bergemann, C.; Anton, M. Magnetofection: Enhancing and Targeting Gene Delivery with Superparamagnetic Nanoparticles and Magnetic Fields. *J. Liposome Res.* **2003**, *13*, 29–32.
52. Smith, C. A.; de la Fuente, J.; Pelaz, B.; Furlani, E. P.; Mullin, M.; Berry, C. C. The Effect of Static Magnetic Fields and tat Peptides on Cellular and Nuclear Uptake of Magnetic Nanoparticles. *Biomaterials* **2010**, *31*, 4392–4400.
53. Pickard, M. R.; Chari, D. M. Enhancement of Magnetic Nanoparticle-Mediated Gene Transfer to Astrocytes by "Magnetofection": Effects of Static and Oscillating Fields. *Nanomedicine (London)* **2010**, *5*, 217–232.
54. Pickard, M. R.; Chari, D. M. *Magnetic Nanoparticle Applications for Neural Stem Cell Transplantation Therapies*. *Programme of the Fourth Annual Scientific Conference of the UK National Stem Cell Network*, University of York, March 30—April 1, **2011**. Abstract: Poster number 83.
55. Pickard, M. R.; Barraud, P.; Chari, D. M. The Transfection of Multipotent Neural Precursor/Stem Cell Transplant Populations with Magnetic Nanoparticles. *Biomaterials* **2011**, *32*, 2274–2284.
56. Lubetzki, C.; Goujet-Zalc, C.; Evrard, C.; Danos, O.; Rouget, P.; Zalc, B. Gene Transfer of Rat Mature Oligodendrocytes and Glial Progenitor Cells with the LacZ Gene. *Ann. N.Y. Acad. Sci.* **1990**, *605*, 66–70.
57. http://www.lonzabio.com/fileadmin/groups/marketing/Downloads/Protocols/Generated/Optimized_Protocol_99.pdf (accessed May 20, 2011).
58. Hermens, W. T. J. M. C.; Giger, R. J.; Holtmaat, A. J.; Dijkhuizen, P. A.; Houweling, D. A.; Verhaagen, J. Transient Gene Transfer to Neurons and Glia: Analysis of Adenoviral Vector Performance in the CNS and PNS. *J. Neurosci. Methods* **1997**, *71*, 85–98.
59. McBain, S. C.; Griesenbach, U.; Xenariou, S.; Keramane, A.; Batich, C. D.; Alton, E. W. F. W.; Dobson, J. Magnetic Nanoparticles as Gene Delivery Agents: Enhanced Transfection in the Presence of Oscillating Magnet Arrays. *Nanotechnology* **2008**, *19*, 405102.
60. Baumann, N.; Pham-Dinh, D. Biology of Oligodendrocyte and Myelin in the Mammalian Central Nervous System. *Physiol. Rev.* **2001**, *81*, 871–927.
61. Chari, D. M. Remyelination in Multiple Sclerosis. *Int. Rev. Neurobiol.* **2007**, *79*, 589–620.
62. de Castro, F.; Bribian, A. The Molecular Orchestra of the Migration of Oligodendrocyte Precursors During Development. *Brain Res. Rev.* **2005**, *49*, 227–241.
63. Baron, W.; Metz, B.; Bansal, R.; Hoekstra, D.; de Vries, H. PDGF and FGF-2 Signaling in Oligodendrocyte Progenitor Cells: Regulation of Proliferation and Differentiation by Multiple Intracellular Signaling Pathways. *Mol. Cell. Neurosci.* **2000**, *15*, 314–329.
64. Gahwiler, B. H.; Capogna, M.; Debanne, D.; McKinney, R. A.; Thompson, S. M. Organotypic Slice Cultures: a Technique has Come of Age. *Trends Neurosci.* **1997**, *20*, 471–477.
65. Sundstrom, L.; Morrison, B., 3rd; Bradley, M.; Pringle, A. Organotypic Cultures as Tools for Functional Screening in the CNS. *Drug Discovery Today* **2005**, *10*, 993–1000.
66. Xiang, Z.; Reeves, S. A. Simvastatin Induces Cell Death in a Mouse Cerebellar Slice Culture (CSC) Model of Developmental Myelination. *Exp. Neurol.* **2009**, *215*, 41–47.
67. Birgbauer, E.; Rao, T. S.; Webb, M. Lysolecithin Induces Demyelination *in Vitro* in a Cerebellar Slice Culture System. *J. Neurosci. Res.* **2004**, *78*, 157–166.
68. McKenzie, I. A.; Biernaskie, J.; Toma, J. G.; Midha, R.; Miller, F. D. Skin-Derived Precursors Generate Myelinating Schwann Cells for the Injured and Dysmyelinated Nervous System. *J. Neurosci.* **2006**, *26*, 6651–6660.
69. Forget, C.; Stewart, J; Trudeau, L.-E. Impact of Basic FGF Expression in Astrocytes on Dopamine Neuron Synaptic Function and Development. *Eur. J. Neurosci.* **2006**, *23*, 608–616.
70. Gomez-Pinilla, F.; Vu, L.; Cotman, C. W. Regulation of Astrocyte Proliferation by FGF-2 and Heparan Sulfate *in Vivo*. *J. Neurosci.* **1995**, *15*, 2021–2029.
71. McCarthy, K. D.; de Vellis, J. Preparation of Separate Astroglial and Oligodendroglial Cell Cultures from Rat Cerebral Tissue. *J. Cell Biol.* **1980**, *85*, 890–902.

Appendix 5: Article published by Nano LIFE.

The oligodendrocyte transfection data from chapter 4, and the comparisons with OPC transfection, have now been accepted for publication by *Nano LIFE*.

Magnetic nanoparticle mediated gene transfer to oligodendrocytes: A comparison of differentiated cells versus precursor forms, Stuart I. Jenkins, Mark R. Pickard, Divya M. Chari, Nano LIFE, Vol. 3, No. 1, Copyright 2013 World Scientific Publishing Company.

This appendix consists of the formatted author's proof.

Nano LIFE
Vol. 3, No. 1 (2013) 1243001 (8 pages)

DOI: 10.1142/S1793984412430015

World Scientific
www.worldscientific.com

MAGNETIC NANOPARTICLE MEDIATED GENE TRANSFER TO OLIGODENDROCYTES: A COMPARISON OF DIFFERENTIATED CELLS VERSUS PRECURSOR FORMS

STUART I. JENKINS, MARK R. PICKARD and DIVYA M CHARI*
Cellular and Neural Engineering Group
Institute for Science and Technology in Medicine
Keele University, Staffordshire ST5 5BG, UK
**d.chari@hfac.keele.ac.uk*

Received 29 June 2012
Accepted 25 July 2012
Published

Magnetic nanoparticles (MNPs) have emerged as a major platform for the formulation of magnetic vectors for nonviral gene delivery. Notably the application of "magnetofection" strategies (use of magnetic fields to increase MNP−cell interactions) can significantly enhance MNP mediated gene transfer. Despite the potential of this approach, the use of MNPs and magnetofection for gene delivery to oligodendrocytes (the cells that make and maintain myelin, the insulating sheath around nerve fibers in the central nervous system) has never been tested. Here, we prove the feasibility of using MNPs in conjunction with applied static or oscillating gradient magnetic fields (the "magnetofection" method) to deliver genes to oligodendrocytes; all applied magnetic field conditions resulted in greater transfection than the no field condition but overall transfection levels obtained were typically low (*ca.* $< 6\%$). Oligodendrocyte transfection levels under all magnetic field conditions were less than a third compared with their parent cell population, the oligodendrocyte precursor cells. We demonstrate for the first time that, within cells of a specific neural lineage, the amenability to transfection is dependent on the differentiation status of the cell.

Keywords: Oligodendrocytes; oligodendrocyte precursors; magnetic nanoparticles; gene delivery; transfection.

1. Introduction

Oligodendrocytes are a major class of neuroglial cells of the central nervous system (CNS), and arise during development from migratory and mitotic precursors called oligodendrocyte precursor cells (OPCs). The oligodendrocytes are responsible for the production and maintenance of myelin — the fatty, insulating sheath around CNS nerve fibers — which plays a major role in aiding rapid conduction of electrical impulses and is increasingly believed to have a neuroprotective function.[1−3] Loss of myelin (a process termed "demyelination") is a major pathological finding in a range of neurological injuries/diseases, therefore genetic modification of oligodendrocytes, in order to understand their biology and devise effective therapeutic approaches, is a major goal in experimental neurology.

Efforts so far to achieve genetic modification of oligodendrocytes have largely relied on the use of viral transduction methods that can be associated

with a range of drawbacks including oligodendrocyte death and demyelination, suggesting the need to find alternative methods for gene transfer to these cells.[4–7] In this context, magnetic nanoparticles (MNPs) have recently emerged as a major nanotechnology platform for the formulation of magnetic vectors for gene transfer, that are additionally amenable to "magnetofection" strategies (*viz.* the application of magnetic fields to assist transfection). MNP mediated gene transfer, enhanceable by magnetofection, is feasible in a range of neural cells including neurons,[8] neural stem cells,[9] astrocytes[10] and OPCs.[11] Despite this potential, the use of MNPs deployed with magnetofection methods to achieve gene delivery to oligodendrocytes has never been attempted. The aim of this study was twofold: (i) To assess the feasibility of MNP based transfection in oligodendrocytes; and (ii) to determine whether transfection efficiency varies with the differentiation status of oligodendroglial lineage cells, by comparing transfection in oligodendrocytes versus OPCs, under various magnetofection conditions.

2. Methods

2.1. *Materials*

Tissue culture-grade plastics, media and media supplements were from Fisher Scientific (Loughborough, UK) and Sigma-Aldrich (Poole, UK). Recombinant human platelet-derived growth factor (PDGF-AA) and basic fibroblast growth factor (FGF2) were from Peprotech (London, UK). Monoclonal rat anti-myelin basic protein (MBP; a late stage oligodendrocyte marker) was from Serotech (Kidlington, UK), and secondary antibodies (Cy3-conjugated) were from Jackson ImmunoResearch Laboratories Inc. (West Grove, PA, USA). Mounting medium with DAPI (4',6-diamidino-2-phenylindole) was from Vector Laboratories (Peterborough, UK). The pmaxGFP plasmid (3.5 kb) was from Amaxa Biosciences (Cologne, Germany). Neuromag transfection-grade MNPs were purchased from Oz Biosciences (Marseille, France); their physicochemical properties have been previously described.[9,10] The magnefectnano^{TM} oscillating magnetic array system was from nanoTherics Ltd. (Stoke-on-Trent, UK) and the details of this system have been previously published.[10]

2.2. *Cell culture procedures*

The care and use of animals was in accordance with the Animals (Scientific Procedures) Act of 1986 (United Kingdom) with approval by the local ethics committee. Primary mixed glial cell cultures were prepared from cerebral cortex of Sprague-Dawley rats at postnatal day 1−3 (P1−3), and purified OPC cultures derived from these using an established protocol.[12] OPCs were plated on PDL-coated glass coverslips in 24-well plates (0.3 ml/well; 3×10^4 cells/cm^2). To induce differentiation into oligodendrocytes, OPCs were cultured in Sato differentiation medium (DMEM supplemented with 2 mM glutaMAX-I, 1 mM sodium pyruvate, 30 nM 3,5,3′-triiodothyronine, 30 nM thyroxine, 1% N2 supplement, 50 U/ml penicillin and 50 μg/ml streptomycin) for 12 days. Before transfection, culture medium was replaced with 225 μl fresh medium. Neuromag-plasmid complexes were formed by mixing plasmid (60 ng per well) with DMEM (75 μl/well), then gently mixing this with Neuromag particles (0.21 μl). Complexes were allowed to form for 20 min, then added dropwise to the culture wells. Plates were then incubated either in the absence of a magnetic field or magnetofected using a static (frequency, $F = 0$) or oscillating ($F = 1$ or 4 Hz) magnetic field (30 min incubation). The concentration of Neuromag used here, termed 0.1X, represents 10% of the dose recommended by the manufacturers for use with neurons, and this protocol has been developed in our laboratory for safe use with OPCs.[11]

Control cultures were incubated with plasmid alone; in preliminary experiments, we found that plasmid alone controls showed similar cell numbers, morphologies and staining profiles to untreated controls (data not shown), validating the control group used here. Cells were fixed (4% paraformaldehyde) and stained for MBP at 48 h post-transfection as described previously.[11]

2.3. *Assessment of particle toxicity in oligodendrocyte cultures*

A battery of assays was used to assess particle toxicity following 48 h exposure to complexes. Cell adherence and survival were evaluated by quantifying the percentage of MBP$^+$ cells, average number of nuclei and percentage of pyknotic nuclei per field. It was deemed unnecessary to test for toxicity

of the particles alone as Neuromag MNPs have been specifically developed as transfection grade particles and, as such, have no intended usage without conjugation of nucleic acid.

2.4. *Fluorescence microscopy and image analysis*

Samples were imaged using fixed exposure settings on an Axio Scope A1 fluorescence microscope (Carl Zeiss MicroImaging GmbH, Goettingen, Germany), and the images merged using Adobe Photoshop CS3 (version 10.0.1). For toxicity and transfection experiments, a minimum of 200 nuclei per treatment per culture, selected from a minimum of five random fields, were scored for various parameters of toxicity, association with MBP staining (to assess oligodendrocyte culture purity) and for GFP expression (to quantify transfection efficiency).

2.5. *Statistical analysis*

Data were analyzed using GraphPad Prism statistical analysis software. Numerical and graphical data for transfection and toxicity experiments are presented as mean ± SEM. All data were analyzed by one-way ANOVA with Bonferroni's multiple comparison test for *post hoc* analysis. The number of experiments (n) refers to the number of cultures used, each established from a different rat litter. Transfection data obtained for each field condition were compared with previous transfection data for OPCs obtained under identical treatment conditions.[11]

3. Results

3.1. *Oligodendrocyte culture purity*

High purity OPC cultures (95.1% ± 1.4% of cells stained for the OPC marker A2B5; $n = 3$ cultures) were used to produce oligodendrocytes; a high proportion of the latter stained for MBP at seven days post-differentiation (75.9% ± 5.4%; $n = 3$ cultures) [Fig. 1(a)]. An additional 20% of cells stain for earlier markers of the lineage such as NG2 and O4, with the remainder (∼5%) being microglial contamination (data not shown). MBP^+ cells were phase-bright, with multipolar morphologies, including the complex highly-branched, membrane elaborating morphologies typical of mature oligodendrocytes [Figs. 1(a) and 1(a), inset).

3.2. *Assessment of MNP toxicity in oligodendrocytes*

Following incubation with MNP−DNA complexes ± magnetic field application, cells appeared phase bright and showed normal adherence on microscopic examination, with all stages of cell maturation observed in terms of cell phenotype and process elaboration. In the presence of particle−plasmid complexes, no toxicity was apparent under any magnetic field condition, as the percentage of MBP^+ cells [Fig. 1(b)], the total nuclei per microscopic field [Fig. 1(c)] and the percentage of nuclei exhibiting pyknosis [Fig. 1(d)] did not significantly differ from control cultures.

3.3. *MNP-mediated transfection in oligodendrocytes and effects of magnetofection*

Under all field conditions, plasmid alone controls never resulted in GFP expression. Following incubation with Neuromag−pmaxGFP complexes, GFP^+/MBP^+ cells were observed in oligodendrocyte cultures. From morphological evaluations, all stages of the oligodendrocyte lineage were observed to have been transfected, ranging from cells with a small number of processes to those with complex morphologies elaborating extensive myelin sheets [Figs. 2(a)−2(c)]. The extent of MBP expression in GFP^+ cells ranged from strong expression that overlapped GFP expression throughout the cell including processes, to faint expression limited to patches of the cell [Figs. 2(a)−2(c)].

The basal level of transfection with plasmid conjugated MNPs (no field condition) was 1.9% ± 0.1% [Fig. 2(d)]. Application of a static or oscillating magnetic field increased transfection efficiency between two- and three-fold to 4.9% ± 1.1% ($F = 0$ Hz), 4.4% ± 0.5% ($F = 1$ Hz) and 6.3% ± 0.6% ($F = 4$ Hz). The static and $F = 4$ Hz (but not $F = 1$ Hz) conditions significantly enhanced efficiency relative to the no field condition. Although there was a trend towards higher transfection levels at $F = 4$ Hz compared with the $F = 0$ Hz or 1 Hz conditions, this was not statistically significantly [Fig. 2(d)].

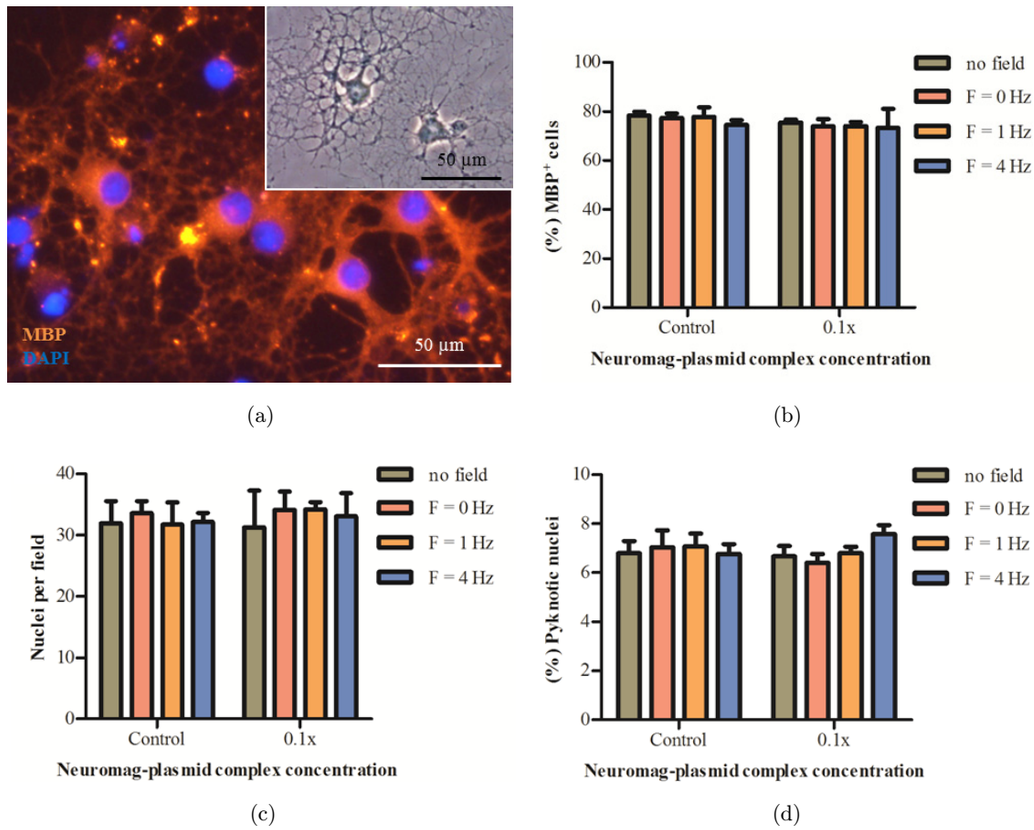

Fig. 1. Magnetofection protocols are not acutely toxic to oligodendrocytes. (a) Fluorescence micrograph of an oligodendrocyte culture stained for the late-stage oligodendrocyte marker MBP, with cells displaying the highly branched morphology typical of oligodendrocytes (also see phase-contrast micrograph, inset). (b) Bar graph indicating the average percentage of MBP^+ cells, at all field conditions tested ($p > 0.05$ versus control, no field; one-way ANOVA with Bonferroni's post-test; $n = 3$ cultures). (c) Bar graph showing average number of healthy nuclei per microscopic field in oligodendrocyte cultures for all field conditions tested. No differences were found between any treatment condition and the no particle, no field control ($p > 0.05$; one-way ANOVA with Bonferroni's post-test; $n = 3$ cultures). (d) Bar graph illustrating the percentage of all nuclei that were pyknotic, as judged by DAPI staining ($p > 0.05$ versus control, no field; one-way ANOVA with Bonferroni's post-test; $n = 3$ cultures).

3.4. *Comparison of MNP mediated transfection in oligodendrocytes versus OPCs*

Comparison of the numbers of transfected oligodendrocytes compared with our previously published data for OPCs at each field condition[11] shows that the differentiated cells consistently exhibit lower transfection efficiencies than the precursor cells, although this was not found to be significant for the no field condition [Fig. 2(e)]. The difference in transfection levels was most pronounced at the $F = 4$ Hz condition, with OPC transfection levels being almost four-fold higher than for oligodendrocytes [Fig. 2(e)].

4. Discussion

During neural development, the differentiation of OPCs into mature oligodendrocytes is characterized by dramatic alterations in the migratory and proliferative features of these cells. This includes a switch from the bipolar highly migratory and proliferative phenotype characteristic of OPCs, to the complex, highly branched, nonmigratory and nonproliferative phenotype of the differentiated oligodendrocyte; such changes are accompanied by a major changes in antigenic expression by these cells.[2,13] Therefore, the use of oligodendroglial cell cultures allows for the genesis of two cell types that exhibit distinct biological properties but are derived

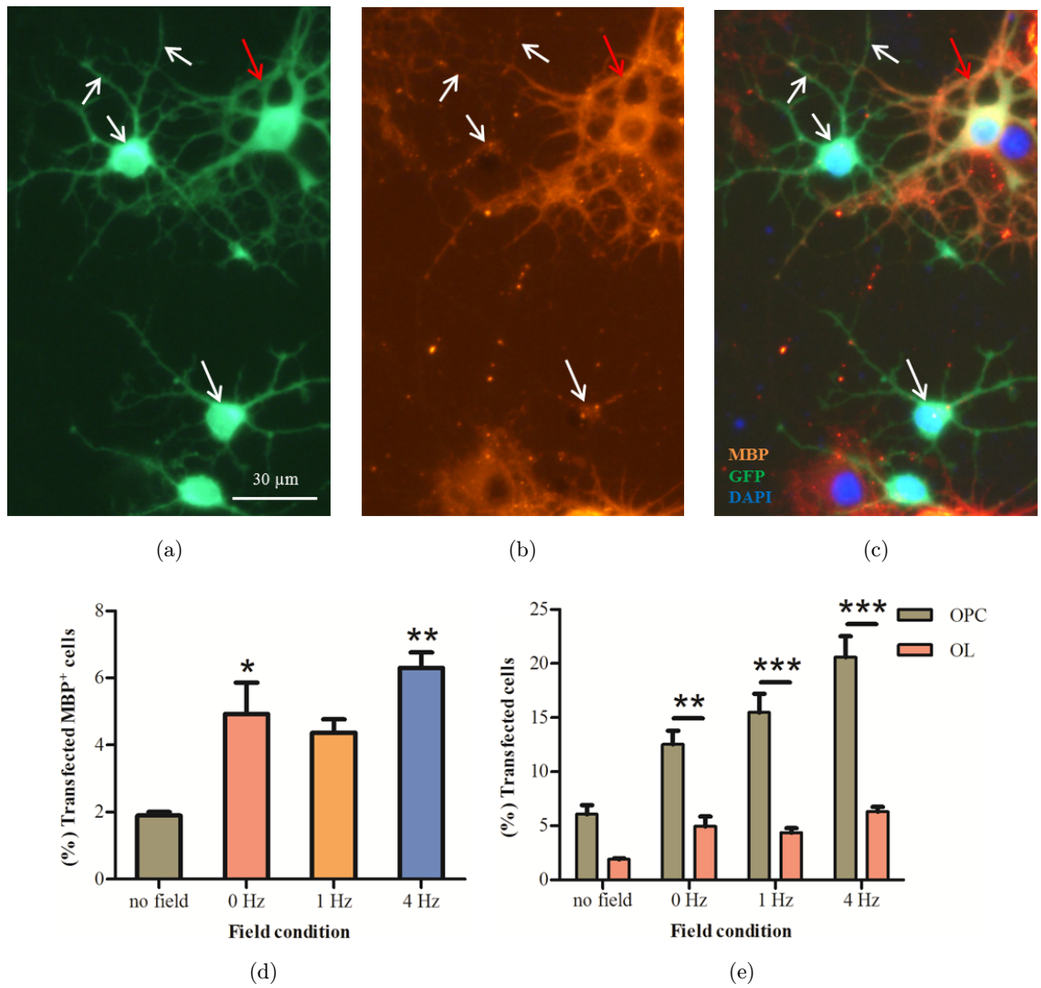

Fig. 2. Application of a static or oscillating magnetic field (magnetofection) enhances MNP-mediated gene delivery to oligodendrocytes. (a) Fluorescence micrograph showing GFP^+ cells in an oligodendrocyte culture magnetofected at $F = 4$ Hz. (b) Counterpart fluorescence micrograph to (a) showing MBP expression. (c) Merged image of (a) and (b) showing one GFP^+ cell with clear expression of the late-stage oligodendrocyte marker MBP throughout the cell (red arrow), two GFP^+ cells with faint MBP expression (white arrows indicate regions of MBP expression), and a GFP^+/MBP^- cell. Note also two GFP^-/MBP^+ cells. (d) Bar graph illustrating transfection efficiencies in oligodendrocyte cultures for all field conditions tested as judged by the percentage of MBP^+ cells expressing GFP. The $F = 0$ Hz and 4 Hz magnetic field conditions significantly enhanced transfection levels compared to the no field condition ($^*p < 0.05$, $^{**}p < 0.01$; one-way ANOVA with Bonferroni's post-test; $n = 3$ cultures). (e) Bar graph indicating comparative transfection efficiencies in OPCs and oligodendrocytes under all field conditions tested (OPC data adapted from Ref. 11). ($^{**}p < 0.01$, $^{***}p < 0.001$; one-way ANOVA with Bonferroni's post-test; $n = 3$ cultures). OL = oligodendrocyte (Color online).

from the same neural cell lineage. This ability offers a relatively simple experimental technique to robustly dissect the influence of biological parameters such as proliferation/differentiation status that may govern neural cell-nanomaterial interactions (and consequently, successful transfection in neural cells), whilst excluding neural lineage related variations. As far as we are aware, this is the first report to address the effect of cellular differentiation state on such interactions in any cell type (either neural or nonneural).

More specifically, our report is the first to prove that oligodendrocytes can be transfected using MNP-plasmid complexes as vectors. Similar to reports in other neural cell types, gene transfer could be significantly enhanced using applied static

Table 1. Comparative *in vitro* transfection efficiencies in rat oligodendrocytes for viral and nonviral vectors.

Method	Gene	Source of cells	Efficiency	Related toxicity	Ref
Viral					
Retrovirus	β-Gal	P15−20	< 0.1%	No data supplied	15
Retrovirus (MoMuLV)	β-Gal	P28−42	0%	No data supplied	16
Nonviral					
Particle bombardment	β-Gal	P15−20	20%	No data supplied	15
Lipofection	β-Gal	P15−20	10%	No data supplied	15
Lipofection	β-Gal	P28−42	0%	No data supplied	16
Magnetic nanoparticles	GFP	P1−3	6%	Not significant	*
Calcium phosphate precipitation	β-Gal	P28−42	< 3%	90% cell death	16
Calcium phosphate precipitation	β-Gal	P15−20	< 2%	"*most cells died*"	15
Electroporation	β-Gal	P28−42	No data supplied	"*drastic*" cell death	16

Note: MoMuLV = Moloney murine leukaemia virus; β-Gal = β-Galactosidase; P = postnatal day; GFP = green fluorescent protein; *current study.

and oscillating magnetic fields.[8,10,11] Transfection levels in oligodendrocytes were dramatically lower than those achieved in OPCs and it is noteworthy that transduction levels for oligodendrocytes using viral systems, such as retroviruses, are also typically low (Table 1). Indeed, one *in vivo* study comparing adeno-, retro- and lentiviral systems found no evidence of oligodendrocyte transduction even at high viral titres.[14] By contrast, another report found evidence that oligodendrocytes can be transduced *in vivo* using adenoviruses, but that gene delivery is complicated by immunogenic and cytopathic effects on oligodendrocytes, limiting the translational potential of the approach.[6] Nonviral transfection methods such as calcium phosphate precipitation and electroporation yield no/low transfection in oligodendrocytes and are associated with high levels of cell loss.[15,16] Delivery methods such as the gene gun approach and lipofection yield higher transfection levels than MNPs (up to 20%, Table 1) and have been described to be relatively safe, so these approaches should still represent the methods of choice for oligodendrocyte transfection applications.[16]

In every case, the methodologies above have yielded significantly higher transfection in OPCs than in oligodendrocytes. Together, these data clearly indicate that differentiated oligodendrocytes are intrinsically far less amenable to gene delivery than are their precursor forms; the underlying causes for this intercellular difference are not clear. The issue is complicated by the diversity of approaches used for genetic modification of cells of the oligodendrocyte lineage, each of which utilizes different mechanisms to achieve gene transfer.[11,15−19] This highlights a major current need to systematically evaluate the biological and physicochemical parameters governing successful transfection of neural cells using nonviral vectors, an area where little or no information currently exists.

Uptake of MNP−DNA complexes by mammalian cells is widely accepted to be via endocytosis of these complexes. Magnetofection approaches are considered to enhance gene transfer by simple sedimentation of particle plasmid complexes over cells,[9,20,21] or potentially by stimulation of endocytosis in the case of oscillating field strategies.[10,11,22] Bearing this in mind, we can speculate that the differences in OPC versus oligodendrocyte transfection levels could be related to a number of parameters (Fig. 3). The first is the extent of membrane that participates in the endocytotic uptake of MNPs into cells. Although oligodendrocytes have a high branch order per cell and generate elaborate sheets of myelin membrane, for both OPCs and oligodendrocytes we observe that particle uptake is restricted to the cell body, and uptake in cellular processes is never seen. This suggests that the total amount of membrane elaborated by the cell (and hence the total cell surface area) is not necessarily reflective of the capacity for particle uptake. In general there is little information currently regarding which specific modes of endocytosis are utilized by OPCs versus oligodendrocytes, and what the level of activity for each of these mechanisms is. Such information will be a pre-requisite to understanding the relationship between particle uptake and transfection. In recent studies,

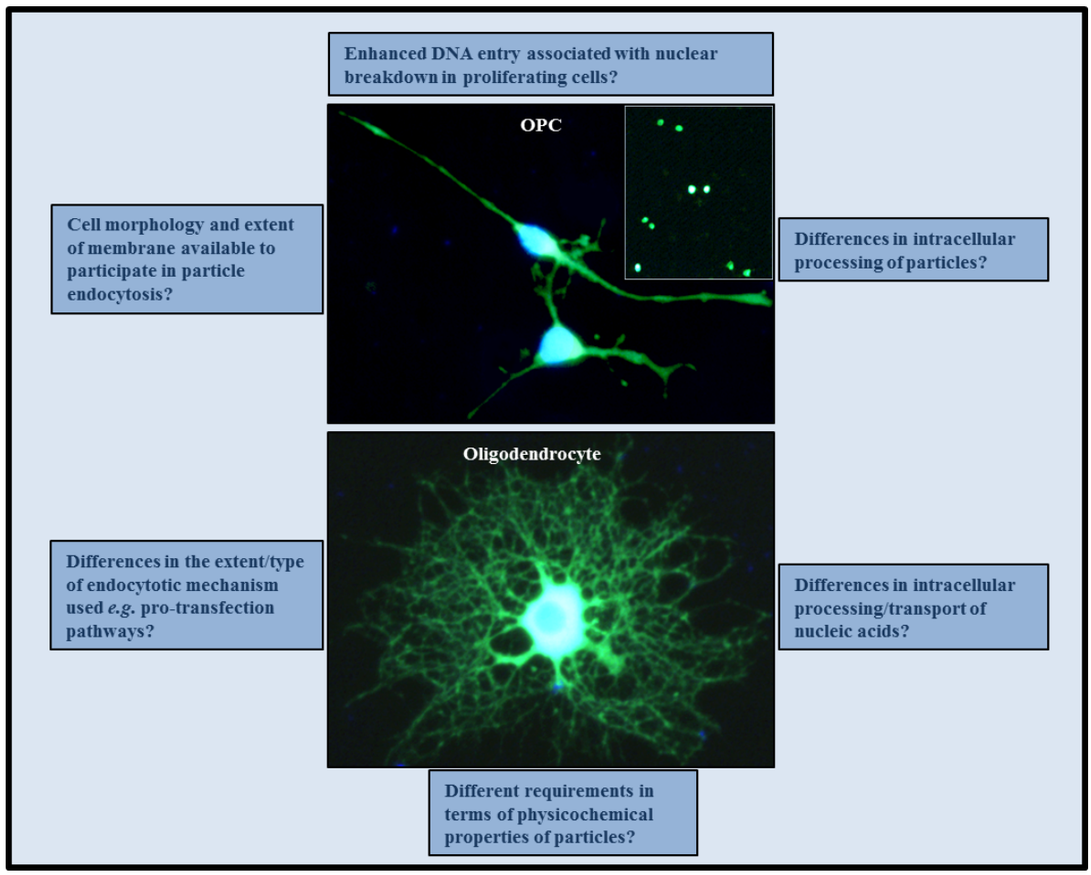

Fig. 3. Schematic summary of the potential factors underlying the difference in amenability to transfection in OPCs versus oligodendrocytes. Representative fluorescence micrographs are included of GFP^+ OPCs and a GFP^+ oligodendrocyte to highlight the morphological differences between the two cell types. The OPCs typically display bipolar morphologies with limited branching and a nucleus occupying a large proportion of the soma. GFP^+ OPCs were frequently observed in pairs, indicative of recent mitosis (inset). Although less amenable to transfection than OPCs, even mature oligodendrocytes could be transfected, as indicated by the complex highly-branched morphology of the transfected cell shown here.

we applied a test magnetic particle [specifically, Sphero^{TM} from Spherotech Inc, USA (particles with a polystyrene core incorporating a Nile Red fluorophore, surrounded by a polystyrene and magnetite layer bound to carboxyl groups with *ca.*1.63×10^6 carboxyl groups per particle), 15−20% iron content, average diameter (SEM) = 360 nm, average hydrodynamic diameter (dynamic light scattering) = 850 nm, zeta potential −14.3 mV (in Sato medium)], to cultures of OPCs and oligodendrocytes (using identical cell densities, particle concentrations and incubation times). Here, we have consistently found that the proportion of OPCs incorporating MNPs is significantly higher than oligodendrocytes, with particle accumulations within OPCs also being typically larger (Jenkins *et al.*, 2012, manuscript in preparation). Further, cells at more advanced stages of oligodendrocyte differentiation (judged by the number/complexity of processes) contained smaller particle accumulations than oligodendrocytes with relatively immature, less branching morphologies. These observations suggest an inverse relationship between cellular maturity and the capacity for particle uptake, which could provide a basis for the lower transfection levels observed here.

The second parameter could be the proliferative status of the target cell population and related nuclear breakdown, facilitating DNA entry into the nucleus, a mechanism similar to that utilized by some viral vectors,[23,24] with the consequence that oligodendrocytes, a major post-mitotic population,

may be relatively refractory to transfection. However, contradicting this idea, an earlier study in primary human fibroblasts has suggested that for virus-independent transfection methods, a round of cell division (with dissolution of the nuclear membrane) is *not* a pre-requisite for DNA to enter the nucleus.[25] Our own experiments provide contradictory data in this regard. In support of the nuclear breakdown hypothesis, we observe consistently that GFP expression is often found in cells that appear to have recently undergone mitosis (see Ref. 11 and Fig. 3 inset for an example). However, using cultures of differentiated oligodendrocytes, we have also shown that complex, highly processed, post-mitotic cells can be transfected using MNPs (Figs. 2 and 3). Therefore the relationship between cell proliferation, nuclear breakdown and the extent of transfection in oligodendroglial cells, is currently unresolved.

Third, it is not apparent whether there are differences in the mechanisms of intracellular processing of MNPs and nucleic acids within OPCs versus oligodendrocytes, in respect of rates of intracellular particle trafficking (especially to the nucleus), the extent of vacuolar localization, potential breakdown of particles and so on. Ideally, studies should use particles with well characterized physicochemical properties, in conjunction with high resolution electron/time lapse microscopy and inhibitors of various endocytotic pathways, to resolve these issues. Such work will aid nanotechnology research in the identification of MNPs with appropriate properties for optimal use in a range of biological applications involving oligodendroglial cells, a major target population in regenerative medicine.

References

1. M. R. Kotter, C. Stadelmann and H. P. Hartung, *Brain* **134**, 1882 (2011).
2. V. E. Miron, T. Kuhlmann and J. P. Antel, *Biochim. Biophys. Acta* **1812**, 184 (2011).
3. J. Zhang *et al.*, *FEBS Lett.* **585**, 3813 (2011).
4. A. P. Byrnes, R. E. MacLaren and H. M. Charlton, *J. Neurosci.* **16**, 3045 (1996).
5. M. J. Wood, H. M. Charlton, K. J. Wood, K. Kajiwara and A. P. Byrnes, *Trends Neurosci.* **19**, 497 (1996).
6. R. M. Franklin, M. M. Quick and G. Haase, *Gene Ther.* **6**, 1360 (1999).
7. M. T. O'Leary and H. M. Charlton, *Gene Ther.* **6**, 1351 (1999).
8. C. Fallini, G. J. Bassell and W. Rossoll, *Mol. Neurodegener.* **5**, 17 (2010).
9. C. Sapet *et al. Biotechniques* **50**, 187 (2011).
10. M. R. Pickard and D. M. Chari, *Nanomedicine (London)* **5**, 217 (2010).
11. S. I. Jenkins, M. R. Pickard, N. Granger and D. M. Chari, *ACS Nano* **5**, 6527 (2011).
12. K. D. McCarthy, and J. de Vellis, *J. Cell Biol.* **85**, 890 (1980).
13. J. C. Dugas, Y. C. Tai, T. P. Speed, J. Ngai and B. Barres, *J. Neurosci.* **26**, 10967 (2006).
14. A. A. Abdellatif *et al.*, *J. Neurosci. Res.* **567**, 553 (2006).
15. C. Lubetzki *et al.*, *Ann. N Y Acad. Sci.* **605**, 66 (1990).
16. Z. Guo *et al.*, *J. Neurosci. Res.* **43**, 32 (1996).
17. H. Chen, D. M. McCarty, A. T. Bruce, K. Suzuki and K. Suzuki, *Gene Ther.* **5**, 50 (1998).
18. N. Rubio, R. Rodriguez and M. A. Arevalo, *Glia* **47**, 78 (2004).
19. W. H. H. Krueger, D. L. Madison and S. E. Pfeiffer, *Neurochem. Res.* **23**, 421 (1998).
20. F. Scherer *et al.*, *Gene Ther.* **9**, 102 (2002).
21. D. Luo and W. M. Saltzman, *Nat. Biotechnol.* **18**, 893 (2000).
22. C. Plank, O. Zelphati and O. Mykhaylyk, *Adv. Drug Deliv. Rev.* **63**, 1300 (2011).
23. S. Brunner *et al.*, *Gene Ther.* **7**, 401 (2000).
24. J. L. Anderson and T. J. Hope, *Gene Ther.* **12**, 1667 (2005).
25. A. Coonrod, F.-Q. Li and M. Horwitz, *Gene Ther.* **4**, 1313 (1997).

Appendix 6: Article published by Tissue Engineering: Part C.

The astrocyte uptake data (Sphero MPs) used for the cross-cellular comparison (Chapter 5) was published previously, and the article is included here as appendix 6.

Magnetic nanoparticle labeling of astrocytes derived for neural transplantation

Mark R Pickard, Stuart I Jenkins, Chris J. Koller, David N Furness, Divya M Chari

Tissue Engineering: Part C vol. 17, no. 1, 2011

TISSUE ENGINEERING: Part C
Volume 17, Number 1, 2011

DOI: 10.1089/ten.tec.2010.0170

Magnetic Nanoparticle Labeling of Astrocytes Derived for Neural Transplantation

Mark R. Pickard, Ph.D.,[1] Stuart I. Jenkins, B.Sc.,[1] Chris J. Koller, M.Sc.,[2]
David N. Furness, Ph.D.,[1] and Divya M. Chari, D.Phil.[1]

Astrocytes are a major transplant cell population to promote neural repair in a range of pathological conditions. In this context, the development of robust methods to label neural transplant populations (for subsequent detection and cell tracking *in vivo*) is key for translational applications. Magnetic iron oxide nanoparticles (MNP)-based vector systems offer a range of advantages for neural cell transplantation, notably, as contrast agents for magnetic resonance imaging, which allows for MNP-labeled cells to be detected using minimally invasive methods. Additionally, MNPs have other key features such as safety, the potential for linking with genetic material/drugs, and magnetic cell targeting. Therefore, MNPs can potentially be developed as a multipurpose nanoplatform for neural cell transplantation. The feasibility of labeling astrocytes derived for transplantation with MNPs has not been assessed to date. Here, we have established simple protocols to safely label astrocytes with MNPs; the survival and differentiation of labeled cells was assessed in three dimensional neural tissue arrays. Additionally, we have established the major mechanisms of MNP uptake by astrocytes.

Introduction

Astrocytes are a major neuroglial subclass, ie., non-neuronal support cells of the central nervous system (CNS), that outnumber neurons by about 10-fold.[1] These cells play key roles in the maintenance of normal CNS homeostatic mechanisms, including synaptic glutamate uptake, regulation of extracellular calcium, and provision of nutrients for neurons[1–4]; indeed, a range of neuropathological conditions are associated with astrocytic dysfunction.[5–7] Importantly, these cells have been proven to be major candidates for *ex vivo* gene delivery and neural tissue engineering/transplantation strategies in several experimental models of neural injury/disease, given the significant capacity of these cells to migrate, survive, and integrate after introduction into the normal or injured CNS parenchyma.[8–11] When evaluating the translational potential of astrocyte transplantation (to promote neural regeneration) into viable clinical therapies, a major (but often overlooked) consideration is the development of robust methodologies to non-invasively detect transplant populations in host tissue to monitor transplant cell survival and fate; this is critical to evaluating the comparative benefits and limitations of various cell therapies to promote neural regeneration. Experimental studies in transplantation neurobiology generally employ a wide range of methods to label neural cell transplant populations for identification in host tissue. Examples of these are labeling with lipophilic carbocyanine dyes, Y chromosome detection (after transplantation of male cells into female hosts), and genetic labeling with subsequent detection of enzymes or fluorescent protein (e.g., LacZ or GFP) and chemical markers such as bisbenzamide.[12–16] Many of these labeling methods have significant disadvantages associated with them such as technical complexity, toxicity, unreliability due to diffusion of label, and the lack of ability to detect transplanted cells by noninvasive methods.

Recent advances in nanotechnology have highlighted the significant potential offered by delivery systems employing magnetic iron oxide nanoparticles (MNPs) for imaging applications in tissue engineering. Such particles have emerged as a major class of contrast agent for magnetic resonance imaging (MRI) with advances in chemical methods to control particle properties such as size, coatings, biodegradability, and toxicity. The ability to label cells with MNPs *ex vivo* therefore provides a technique to detect transplant cell populations *in vivo* using MRI[17] allowing for

[1]Cellular and Neural Engineering Group, Institute for Science and Technology in Medicine, Keele University, Staffordshire, United Kingdom.
[2]MR Suite, Main X-ray Department, City General Hospital, University Hospital of North Staffordshire NHS Trust, Staffordshire, United Kingdom.

the noninvasive monitoring of the biodistribution, integration, and survival of transplanted cells. In this context, it has been demonstrated that neural progenitor/stem cells, including glial-restricted precursors, can be safely labeled with magnetic particles and tracked using MRI after transplantation into areas of pathology (with no demonstrable loss of functional capacity and limited effects on cell survival/differentiation).[18–21] To date, however, the feasibility of using MNPs for cell labeling in astrocyte transplantation therapies has not been assessed. In addition to cell tracking, MNPs have applications in magnetic targeting (including magnetic cell targeting) and—because they can be readily functionalized with drugs/genetic material—they have the potential to serve as a multifunctional nanoplatform for cell transplantation applications.[22] We recently demonstrated, for the first time, that astrocytes derived from primary cultures can be transfected using MNPs in the presence of applied static/oscillating magnetic fields (the so-called magnetofection approaches), achieving efficiencies close to that of some viral vector systems. We further proved in this study that transfected cells could survive and integrate into host neural circuitry after transplantation into three-dimensional neural tissue arrays (organotypic cerebellar slice cultures).[22] These findings taken in conjunction with the multiple benefits of MNP vector systems led us to suggest that MNPs could represent the multifunctional vector system of choice for astrocyte transplantation therapies.

Here, we have established protocols to safely label astrocyte transplant populations with MNPs *ex vivo* for cell tracking applications. To achieve this, we have employed fluorescently labeled MNPs and astrocyte cultures to examine a range of parameters related to particle uptake and toxicity. We also demonstrate the survival and differentiation potential of astrocytes post-MNP labeling after transplantation into organotypic slice cultures derived from the rat cerebellum.

Materials and Methods

Astrocyte cell culture

Mixed glial cultures were established from cerebral cortices of neonatal Sprague-Dawley rats and astrocytes were purified using a published procedure.[23] The adherent astrocyte cell layer was trypsinized, and subcultured once in D-10 medium (Dulbecco's modified Eagle's medium plus 2 mM glutaMAX-I, 1 mM sodium pyruvate, 50 U/mL penicillin, 50 μg/mL streptomycin, and 10% fetal bovine serum) in poly-D-lysine (PDL)-coated T75 flasks. All cultures were incubated at 37°C in 5% CO_2/95% air, with medium changes every 2–3 days, unless otherwise specified. Subconfluent astrocyte cultures were trypsinized, resuspended in D-10 medium, and used for MNP uptake, transplantation, and toxicity studies, as described below.

Cerebellar slice cultures

Brains of Sprague-Dawley rat pups at 10 postnatal days were collected into ice-cold slicing medium (Earle's balanced salts solution buffered with 25 mM HEPES). Cerebella were dissected, meninges removed, and 400 μm parasagittal slices prepared using a McIlwain tissue chopper. Slices were transferred to slicing medium at 4°C for 30 min, and then individual slices were transferred to pieces of Omnipore membrane on Millicell culture inserts (Millipore) in six-well plates containing the culture medium (50% minimum essential medium, 25% Earle's balanced salts solution, and 25% horse serum; supplemented with 1 mM glutaMAX-I, 36 mM D-glucose, 50 U/mL penicillin, and 50 μg/mL streptomycin). Slices were cultured at 37°C in 5% CO_2/95% air, with medium changes every 2–3 days. All experiments involving animals were conducted in strict accordance with United Kingdom Home Office guidelines.

Uptake experiments

Paramagnetic, carboxyl-modified SPHERO Nile Red fluorescent magnetic particles (0.20–0.39 μm diameter, iron content 15%–20%) were obtained from Spherotech, Inc. These comprise a polystyrene core, stained with the fluorophore Nile Red, coated with a magnetite layer, and then overcoated with a functionalized monomer. For all incubations, unless specified otherwise, astrocytes were seeded into PDL-coated chamber slides (0.4×10^5 cells/cm^2) and allowed to attach for 24 h before MNP addition in fresh D-10 medium. (A) For time course experiments, cells were incubated with 2–50 μg/mL MNPs for 1–24 h. (B) To determine the temperature dependence of uptake, cells were incubated with 20 μg/mL MNPs for 1 h at 4°C or 37°C (in 100% air); uptake at 37°C under these conditions was similar to that in incubations conducted in 5% CO_2/95% air. (C) To determine mechanisms of MNP uptake, selective endocytosis inhibitors[24] (Sigma) were used at concentrations routinely employed for other cell types.[24–26] Inhibitors comprised dynasore (80 μM) and tyrphostin 23 (350 μM) (inhibitors of clathrin-dependent endocytosis); filipin III (5 μg/mL) (inhibitor of caveolin-dependent endocytosis); and amiloride (1 mM) and 5-(N-ethyl-N-isopropyl) amiloride (EIPA; 100 μM) (macropinocytosis inhibitors); all stock solutions (×1000) were dissolved in dimethyl sulfoxide (DMSO) vehicle. Cells were preincubated for 20 min with inhibitor, and then with the same inhibitor plus MNPs (20 μg/mL) for 1 h. Controls included cells incubated with vehicle or medium alone ("no addition" control). The latter was included to verify that the vehicle (DMSO) was without effect on cells. (D) To determine the intracellular fate of MNPs by transmission electron microscopy (TEM), cells were seeded onto PDL-coated Aclar sheeting (0.6×10^5 cells/cm^2). After 24 h, cells were incubated with 20 μg/mL MNPs for 24 h. (E) To determine the long-term disposition of particles (up to 3 weeks), cells were seeded onto PDL-coated glass coverslips or 12-well plates (0.1×10^5 cells/cm^2). After 24 h, cells were incubated with either 0 or 20 μg/mL Spherofluor MNPs for 24 h. The medium was replaced with fresh D-10 minus MNPs and cells were cultured for up to a further 21 days. Cells were split (1 in 3) by trypsinization at weekly intervals. To terminate incubations, cells were washed three times with phosphate-buffered saline (PBS) then fixed, as described below.

Transplantation of labeled astrocytes into slice cultures

Astrocytes were seeded into PDL-coated plates (0.2×10^5 cells/cm^2) and, after 24 h, incubated with fresh D-10 medium containing 20 μg/mL MNPs for 4 h. Medium was then

replaced with fresh D-10 medium alone for 20 h. Nuclei were labeled by subsequent incubation of cells in medium containing 50 μg/mL 4,6-diamidino-2-phenylindole (DAPI) for 30 min, and then washed with PBS; this dual labeling procedure was used to robustly differentiate the transplant population from host astrocytes. Cells were trypsinized and resuspended at 4×10^7 cells/mL D-10 medium. Then, 0.25 μL of medium containing 10,000 cells was pipetted onto cerebellar slices that had been cultured for 9 days *in vitro*. To observe the passive spread of transplanted astrocytes due to the force of injection, immediately after application of cells ($t = 0$ h), slices were transferred to a slide, cells applied, and live slices observed using fluorescence microscopy. To monitor the survival and morphology of the trypsinized cells after transplantation and to confirm intracellular MNP localization, astrocyte transplant populations were additionally plated onto PDL-coated chamber slides. A total of 12 slices were examined.

Immunocytochemistry and histochemistry

Samples were fixed with 4% (w/v) paraformaldehyde (in PBS) for 20 min and then washed three times with PBS. For identification of astrocytes, polyclonal rabbit anti-glial fibrillary acidic protein (GFAP) antibody (DakoCytomation) was used. Fixed samples were incubated with blocking solution (5% normal donkey serum in PBS–0.3% Triton X-100) (room temperature [RT], 30 min), and then with primary antibody to GFAP (1:500 dilution in blocking solution; 4°C, overnight). After washing, samples were incubated with blocking solution (RT, 30 min), and then with fluorescein isothiocyanate-labeled donkey anti-rabbit IgG (Jackson ImmunoResearch Laboratoratories, Inc.; diluted 1:200 in blocking solution; RT for 2 h). Samples were then washed and usually mounted with Vectashield mounting medium containing DAPI (Vector Laboratories); for the slice cultures experiments, mounting medium without DAPI was used for cells and slices. For Perl's Prussian Blue staining to observe intracellular iron, fixed cells were incubated with 2% potassium ferricyanide in 2% HCl for 30 min, washed three times with distilled water, and mounted without DAPI.

Fluorescence microscopy and image analysis

Fluorescence microscopy was performed using an Axio Scope A1 microscope equipped with an Axio Cam ICc1 digital camera and AxioVision software (release 4.7.1; Carl Zeiss MicroImaging GmbH). Images were merged in Adobe Photoshop CS3 (version 10.0.1), and used for semiquantitative analysis, as described previously.[27] Purity of astrocyte cultures was assessed from merged images of GFAP and DAPI-stained cells (≥100 cells were scored per culture). To assess the effects of particles or endocytosis inhibitors on cell viability, counts of DAPI-positive nuclei were compared between control and treated wells with assessment of nuclear morphology; a minimum of three microscopic fields at ×400 magnification (≥100 nuclei in total) were assessed. Particle uptake by astrocytes (including endocytosis inhibitor experiments) was assessed from triple merges (×400 magnification) of DAPI, Nile Red, and GFAP fluorescent images, and the proportion of astrocytes (GFAP-positive cells) demonstrating particle uptake (termed % labeled cells) was calculated. To determine the extent of particle accumulation, labeled astrocytes were categorized based on the area of the cell occupied by the accumulated nanoparticles relative to the area of the cell nucleus; categories were low (≤10%), moderate (11%–50%), and high (≥51%). Labeled astrocytes were also classified with respect to the subcellular localization of nanoparticles; the proportion of labeled cells with a perinuclear particle localization either exclusively or combined with a cytoplasmic particle distribution is reported here. For all uptake calculations, a minimum of 100 GFAP-positive cells per treatment were evaluated. Confocal laser scanning microscopy, using a BioRad MRC1024 confocal microscope, was employed to determine if cell-associated particles had been internalized rather than simply adsorbed onto the cell surface.

Electron microscopy (scanning and transmission)

To assess particle size and shape, Spherofluor particles were placed in pure water, air-dried onto aluminum stubs, and observed uncoated using a high-resolution field emission scanning electron microscope (Hitachi S4500) operated at an accelerating voltage of 5 kV. To assess the intracellular localization of MNPs, samples were fixed with 2.5% (w/v) glutaraldehyde (in 0.1 M sodium cacodylate buffer containing 2 mM $CaCl_2$; SCB) for 2 h, and then washed three times with SCB. Samples were postfixed with 1% osmium tetroxide in SCB for 1 h, washed, and then dehydrated in a graded series of ethanol, before infiltration in Spurr resin. After polymerization of the resin at 60°C for 16 h, ultrathin sections were cut on a Reichert Ultracut E microtome, and placed on 200 mesh thin bar copper grids and stained with 2% uranyl acetate in 70% ethanol and 2% Reynold's lead citrate. Sections were examined in a JEOL 1230 TEM operated at 100 kV.

MRI of agar-embedded MNPs

An initial proof of principle study was undertaken using a 1.5 T Philips Intera-Achivea MRI Scanner (Best) and a medium sense flex coil, to provide an assessment of the clinical feasibility of detecting MNP labeled astrocytes using clinical scanning methods. Spherofluor particle concentrations of 5, 20, and 50 μg/mL were embedded in agar gel; a test transfection-grade MNP with low iron content (0.5%, Neuromag; Oz Biosciences) was also included and a gradient echo sequence undertaken to qualitatively assess visibility.

Toxicity assays

Astrocytes were plated into PDL-coated 96-well plates (1×10^4 cells/cm^2; 0.2 mL medium/well). After 24 h, the medium was replaced with fresh D-10 containing 0–50 μg/mL concentrations of Spherofluor MNPs, and cells were incubated at 37°C in a humidified atmosphere of 5% CO_2/95% air for 24 h. The medium was then replaced with fresh D-10 alone, and the medium was changed every 2–3 days. MTS assays (CellTiter 96 AQueous One Solution Cell Proliferation Assay; Promega) were performed at 0–96 h postmedium change according to the supplier's instructions. Blank incubations, comprising medium plus MNPs but no cells, were run with each assay and the corresponding absorbance readings at 490 nm (A490) were subtracted from the appropriate test readings. Values were expressed as percentage cellular viability relative to control incubations minus MNPs.

Statistical analysis

Data are expressed as mean ± standard error of the mean. To assess the effects of MNP concentration and time of exposure on proportion of cells showing particle uptake, extent of particle accumulation, and degree of perinuclear localization, data were analyzed by a two-way analysis of variance followed by Bonferroni's post-tests; for clarity, comparisons versus the 2 μg/mL MNP group at a given time point (in the case of concentration dependence) and comparisons versus the same MNP concentration at 1 h (in the case of time dependence) only are displayed on bar charts. For temperature dependence of uptake, data were analyzed by Student's *t*-test (two-tailed). One-way analysis of variance, with either Bonferroni's multiple comparison test or Dunnett's multiple comparison test, was used to analyze data for the endocytosis inhibitor and cytotoxicity experiments, respectively. GraphPad Prism 4 for Windows software (version 4.03) was used for statistical analyses.

Results

Culture characteristics

Astrocyte cultures were of consistently high purity, as judged by GFAP immunostaining (97.8% ± 0.3%; $n = 8$ cultures). The majority of cells exhibited a flattened, polygonal appearance, characteristic of type 1 astrocytes, while cells with the complex, branching morphology of type 2 astrocytes accounted for <1% of the astrocyte population.

MNP uptake by astrocytes

Cell-associated fluorescent MNPs were clearly visible within both type 1 and type 2 astrocytes. Confocal microscopy revealed that fluorescence associated with MNPs and cytoskeletal GFAP was coincident; the former was only clearly visible in internal slices of cells (Fig. 1A and Supplementary Fig. S1, available online at www.liebertonline.com/ten); therefore, cell-associated fluorescence was inferred to represent internalized MNPs. Importantly, Perl's staining of cells prelabeled with MNPs for 24 h revealed colocalization of iron-containing material (Fig. 1B) and Nile Red fluorescence (Fig. 1C), indicating that ingested MNPs remained chemically stable. Blue deposits, characteristic of precipitated iron, were not seen in control cells (data not shown). Scanning electron microscopy analyses revealed that particles were of regular shape and size (Fig. 1D), consistent with the size range (200–390 nm diameter; mean = 360 nm) reported by the manufacturer.

Astrocytes demonstrated clear heterogeneity in particle uptake (Fig. 1E); both the proportions of cells exhibiting MNP uptake and the extent of particle accumulation within cells showed time and concentration dependence (Fig. 1 F, G). Importantly, near-complete labeling of cells (>95%) was observed in incubations with ≥20 μg/mL MNPs for 24 h (Fig. 1F).

MRI of agar-embedded MNPs

Spherofluor particles embedded in agar gel at the higher concentrations studied (20 and 50 μg/mL) were readily observed using MRI. The lowest particle concentration and particles with low iron content yielded limited contrast. Preliminary findings indicate that the different concentrations resulted in ~25%–75% reduction in T2* relaxation times compared with agar gel alone.

Perinuclear targeting of MNPs

Perinuclear clustering was a prominent feature after incubation of astrocytes with MNPs (Fig. 1E); presence of cytoplasmic and perinuclear collections of MNPs were confirmed by TEM (Fig. 2A). Perinuclear particles were never observed fusing with the nuclear membrane, localized within membrane bound structures or in obvious association with the endoplasmic reticulum or Golgi apparatus.

Analysis of the subcellular location of MNPs revealed that in incubations with 2 μg/mL MNPs for 1 h, ingested particles were localized to the cytoplasm in most cells with a minor proportion showing perinuclear/nuclear distribution. The proportion of labeled cells containing particles with a perinuclear localization showed both time and concentration dependence (Fig. 2B). Astrocytes prelabeled with MNPs for 24 h, then cultured for a further 6 days retained large collections of particles (Fig. 2C). There was clear evidence of cellular heterogeneity of astrocytes with respect to the subcellular localization of MNPs at this time. Thus, although the majority (~85%) of labeled cells contained particles in close proximity to the nucleus; the remainder contained MNPs with a predominantly cytoplasmic localization (Fig. 2C). Particles showed progressive dilution of label with time, with ~82% of cells labeled at 14 days and 63% at 21 days.

Mechanism of MNP uptake and intracellular trafficking

MNP uptake was temperature dependant, as reducing the incubation temperature to 4°C markedly inhibited (by 84%) the proportion of cells showing uptake (Fig. 3A), indicating the energy dependence of uptake mechanisms. In endocytosis blocker studies, the proportions of astrocytes that accumulated MNPs were similar to that under both control conditions (Fig. 3B). Macropinocytosis inhibitors markedly inhibited MNP uptake by astrocytes (Fig. 3B) compared with DMSO alone (reduced by 66% [amiloride] and 70% [EIPA]). Inhibitors of clathrin-dependent endocytosis reduced the proportion of astrocytes displaying particle uptake to a lesser extent than macropinocytosis blockers (Fig. 3B); (reduced by 31% [tyrphostin 23] and 28% [dynasore]). A blocker of caveolin-mediated uptake (filipin) did not inhibit particle uptake (data not shown). In experiments where both inhibitors of clathrin mediated uptake and macropinocytosis were applied to cultures, significant cellular toxicity was observed; therefore, it was difficult to draw conclusions from these experiments. Cell densities, as judged by counts of DAPI-stained nuclei per field, were similar for astrocytes treated with and without inhibitors (Table 1), indicating the absence of associated short-term toxic effects of inhibitors alone.

TEM analyses supported findings from the inhibitor studies. Cells displayed extensive projections of the plasma membrane that appeared to be engulfing collections of MNPs (Fig. 3C), consistent with a role for macropinocytosis in particle uptake. Further, coated pit-like structures in the astrocytic plasma membrane were also observed (Fig. 3D; inset) and, occasionally, particles were seen externally, in close apposition to such structures (Fig. 3D), consistent with a role for clathrin-mediated endocytosis.

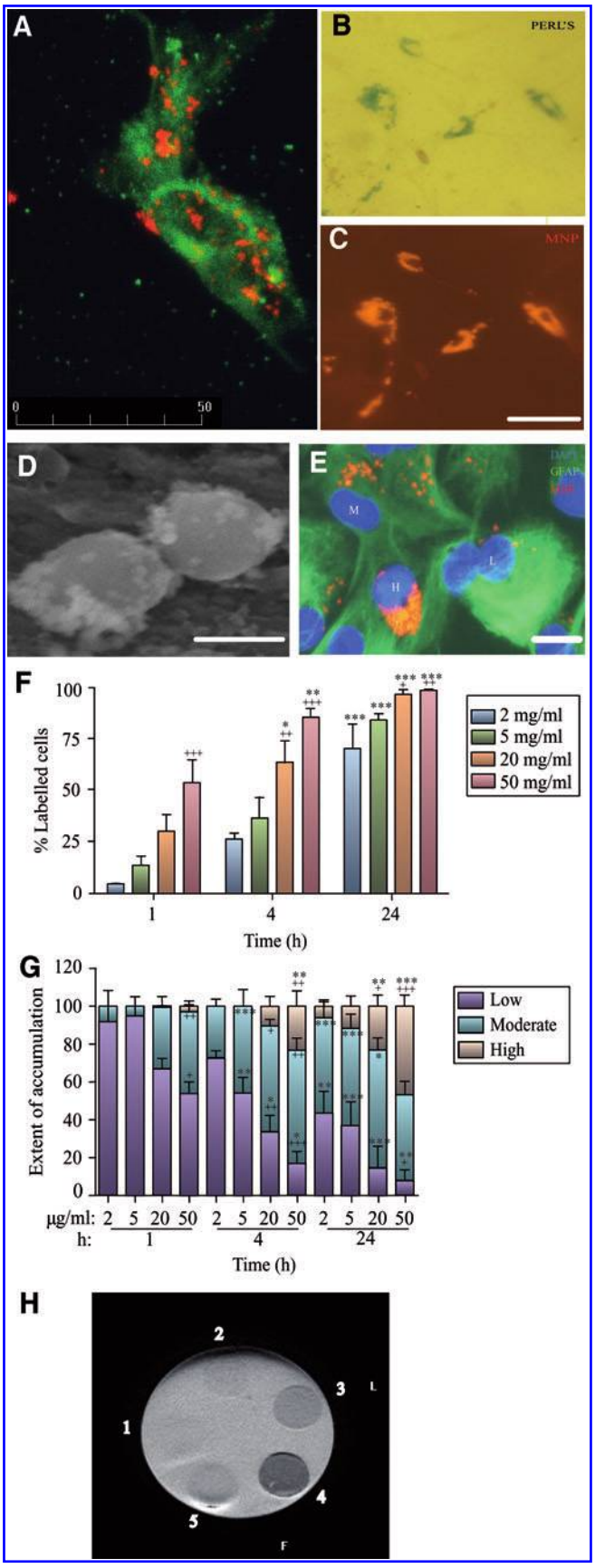

Toxicity

Incubation of astrocytes with 2–50 µg/mL MNPs for 24 h had no statistically significant cytotoxic effects as judged by a MTS assay, immediately after incubation with particles or after a further 24–96 h in medium alone (Table 2). Indeed, in the experiment to determine the time course and concentration dependence of MNP uptake, visual examination revealed that incubation of astrocytes with increasing concentrations of MNPs had no effect on counts of DAPI-stained nuclei per microscopic field, nuclear morphology (Supplementary Fig. S2, available online at www.liebertonline.com/ten), and cell morphology (data not shown).

Transplantation of labeled astrocytes into slice cultures

To assess if MNP-labeled astrocytes could survive and integrate within host tissue after transplantation, experiments were conducted using organotypic cerebellar slice cultures as the recipient tissue. Immediately after delivery of trypsinized cells, colocalization of DAPI and Nile Red (MNP) fluorescence could be observed (Fig. 4) in a highly localized focus within the slice (Fig. 4A; inset); cells typically

FIG. 1. Uptake of magnetic iron oxide nanoparticles (MNPs) by rat astrocytes varies with particle concentration and length of incubation. **(A)** Confocal image through the center of an astrocyte incubated with MNPs (50 µg/mL, 24 h). MNP-linked fluorescence and glial fibrillary acidic protein (GFAP) staining is coincident, demonstrating an intracellular localization for MNPs. Please see Supplemental Figure S1 for the full montage of images taken through the cell. **(B)** Iron (Perl's stain) of astrocytes at 7 days postlabeling with MNPs. **(C)** Nile Red fluorescence in the same field shown in **(B)**. Note the colocalization of iron and Nile Red fluorescence in these cells. **(D)** Scanning electron microscopy image of Spherofluor MNPs demonstrating uniformity of size of particles. **(E)** Example triple-merged image of cells demonstrating classification of cells showing low (L), moderate (M), and high (H) levels of particle accumulation. **(F)** Bar graph demonstrating variation in proportions of cells showing particle uptake with length of incubation and MNP concentration. The proportion of labeled cells is significantly related to each factor ($p < 0.001$; $n = 3$ cultures; two-way analysis of variance [ANOVA]); $^{*}p < 0.05$, $^{**}p < 0.01$, and $^{***}p < 0.001$ versus the same MNP concentration at 1 h; $^{+}p < 0.05$, $^{++}p < 0.01$, and $^{+++}p < 0.001$ versus 2 µg/mL MNPs at the same time point (Bonferroni's post-tests). **(G)** Bar graph showing variations in extent of MNP accumulation in cells with length of incubation and MNP concentration. The proportion of labeled cells classified as having low, moderate, or high levels of particle accumulation varies with length of incubation and MNP concentration ($p < 0.001$ for each factor for each category; $n = 3$ cultures; two-way ANOVA); $^{*}p < 0.05$, $^{**}p < 0.01$, and $^{***}p < 0.001$ versus the same MNP concentration at 1 h; $^{+}p < 0.05$, $^{++}p < 0.01$, and $^{+++}p < 0.001$ versus 2 µg/mL MNPs at the same time point (Bonferroni's post-tests). **(H)** Magnetic resonance imaging (1.5 T clinical scanner) image of MNP embedded in agar gel showing contrast is proportional to MNP concentration: well 1, 0 µg/mL; well 2, 5 µg/mL; well 3, 20 µg/mL; and well 4, 50 µg/mL Spherofluor MNPs. Commercial transfection-grade MNPs with low iron content were embedded in well 5. Scale bar = 50 µm in **(A)**, 100 µm in **(C)**, 250 nm in **(D)**, and 25 µm in **(E)**. Color images available online at www.liebertonline.com/ten.

display a rounded morphology at this stage with withdrawal of cellular processes, consequent upon trypsinization. At 10 days post-transplantation, a restricted area of DAPI fluorescence was detected within the slice (Fig. 4A); robust GFAP labeling was present throughout the slice that can be attributed to both host and transplanted astrocytes (Fig. 4B). A focus of Nile Red fluorescence associated with the injection site could also still be clearly observed (Fig. 4C) with colocalization of DAPI and red fluorescence detected against a background of host tissue (Fig. 4D). Importantly, Nile Red and DAPI-labeled cells appeared to be radiating outward from the central application point, suggesting cell migration; the majority of cells appeared to remain at the application site. Further, high-power images of slices revealed the presence of multiple, well-differentiated DAPI/Nile Red/GFAP triple-positive cells (Fig. 4E), indicating that MNP label was retained by astrocytes and did not impair the ability of astrocytes to re-acquire their normal cellular morphologies after transplantation. When labeled astrocyte transplant populations were replated in culture wells, retention of particles was apparent (Fig. 4F), although a slight decline in the proportion of labeled cells with time observed (from ~93% at 72 h to 70% at 10 days; this suggests that the majority of fluorescent signal detected in transplanted slices at 10 days is due to the transplant population). This was associated with a gradual decrease in the proportion of labeled cells showing MNPs in a perinuclear localization (from ~80% at 72 h to 50% at 10 days), with particles showing a tendency to progressively accumulate near the cell membrane. Importantly, labeled cells were able to reacquire their normal morphological characteristics after trypsinization and transplantation (Fig. 4F), and cultures exhibited similar confluence and cell morphology to cultures that had been treated in a similar manner but incubated without either MNPs or DAPI (data not shown). The dominant morphology observed in both transplanted and plated astrocytes was that of type 1 cells (similar to the distributions observed before cell labeling), indicating that MNP labeling did not alter the phenotypic distributions of astrocytes.

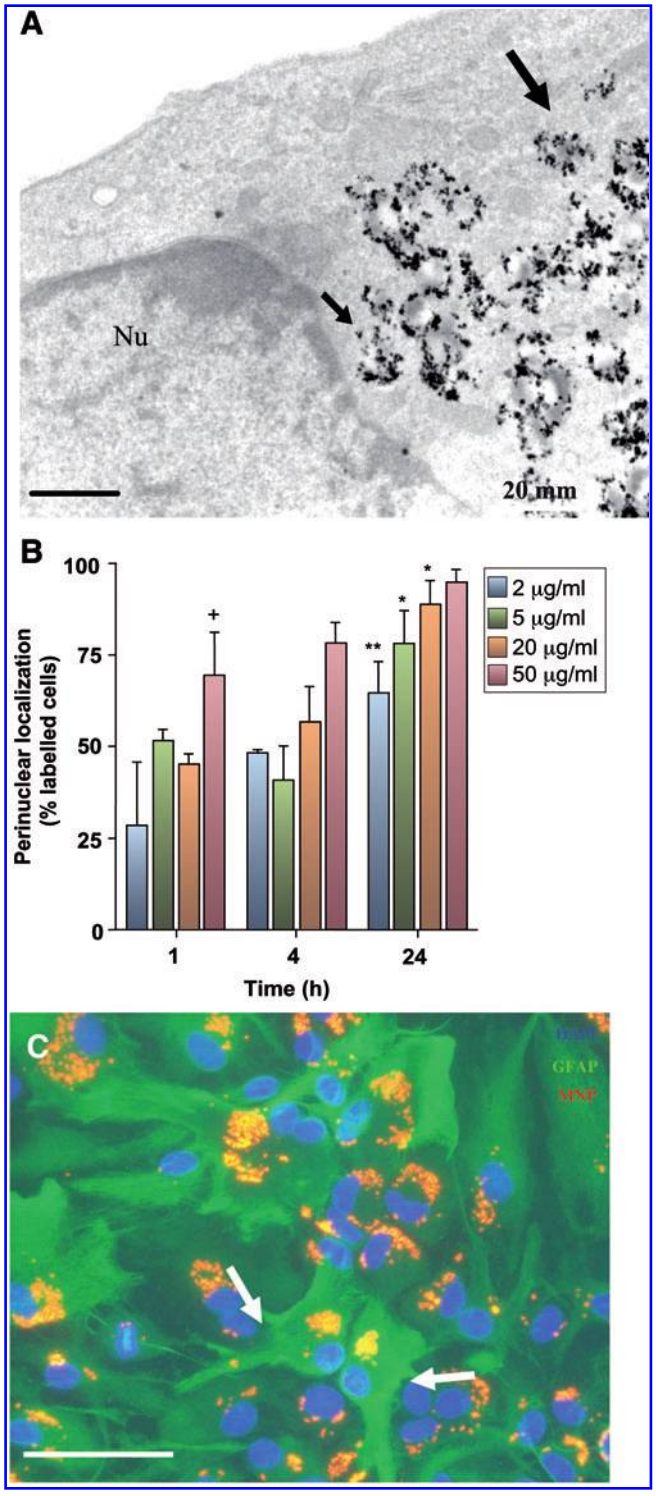

Discussion

Here, we provide proof of principle (using cells obtained from primary cultures) that astrocytes derived for neural tissue engineering applications can be rapidly and efficiently labeled with MNPs. We employed relatively large (0.20–0.39 µm) particles for cell labeling in these studies; we have considered elsewhere the advantages of using particles with these dimensions.[27] We consider that the combination of methods used in this study is valid for several reasons. Experiments using cell lines have provided valuable information on the cellular dynamics of nanoparticle uptake;

FIG. 2. Perinuclear localization of MNPs in astrocytes. **(A)** Electron micrograph of an astrocyte showing perinuclear accumulation of MNPs (small arrow). Other particles show a more distal cytoplasmic localization (large arrow). Nu, nucleus. **(B)** Bar graph showing proportions of cells with a perinuclear/nuclear particle localization (either exclusively or with a cytoplasmic distribution) after incubation with MNPs for up to 24 h. This parameter is significantly related to MNP concentration and length of MNP exposure ($p < 0.001$ for each factor; $n = 3$ cultures; two-way ANOVA); $^{*}p < 0.05$ and $^{**}p < 0.01$ versus the same MNP concentration at 1 h; $^{+}p < 0.05$ versus 2 µg/mL MNPs at the same time point (Bonferroni's post-tests). **(C)** Triple-merged fluorescent images of astrocytes prelabeled with MNPs taken at 7 days. Labeled cells show heterogeneity with respect to the subcellular localization of MNPs; most show perinuclear accumulations, whereas a minor proportion (arrows) show cytoplasmic accumulations. Scale bar = 1 µm in **(A)** and 50 µm in **(C)**. Color images available online at www.liebertonline.com/ten.

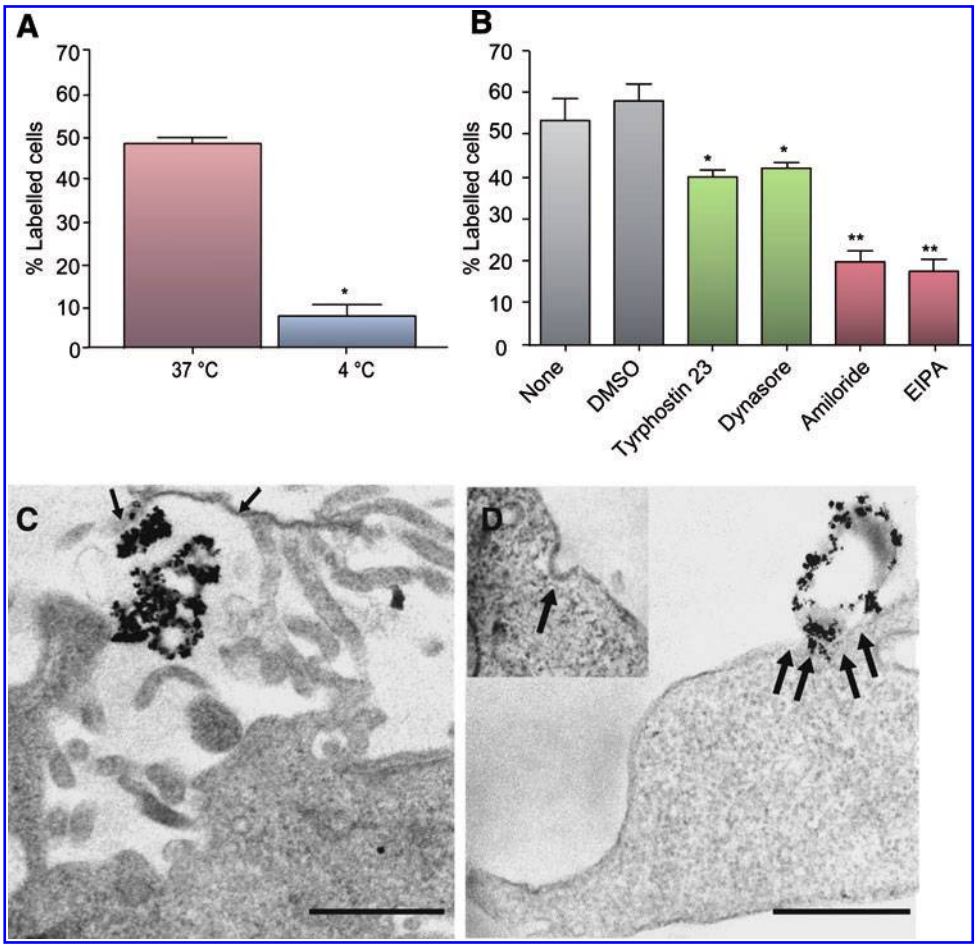

FIG. 3. Mechanism of MNP uptake in rat primary astrocytes. **(A)** Bar chart showing temperature dependence of particle uptake. The proportions of cells demonstrating particle uptake is reduced at 4°C versus 37°C incubation (*$p < 0.05$; Student's *t*-test). **(B)** Bar chart showing effects of endocytosis inhibitors on particle uptake (*$p < 0.05$ and **$p < 0.01$ vs. dimethyl sulfoxide [DMSO] control; Bonferroni's multiple comparison test). **(C)** Electron micrograph showing extensive projections of the plasma membrane (arrows) enveloping collections of MNPs suggestive of macropinocytosis-mediated uptake. **(D)** Electron micrograph showing MNPs in association with a coated pit-like structure (arrows); inset shows the presence of a coated pit at the cell surface (arrow), suggesting clathrin-mediated uptake. Scale bar = 1 μm in **(C)** and 500 nm in **(D)**. Color images available online at www.liebertonline.com/ten.

however, the use of untransformed cells can overcome a range of disadvantages that are inherent to the use of cell lines (such as microbial contamination, aneuploidy, the need for cellular karyotyping to establish cell identity, and altered cell physiology secondary to transformation). In cells that had been pulse-labeled with MNPs, close overlap was found between particle-associated fluorescence and iron-containing material, excluding possible experimental artifacts due to chemical instability of the particles or their intracellular

Table 1. Short-Term Exposure of Astrocytes to Endocytosis Inhibitors Has No Effect on Cell Density as Estimated from Counts of 4,6-Diamidino-2-Phenylindole-Stained Nuclei

Inhibitor	*DAPI counts*
None	54.0 ± 11.3
DMSO	50.1 ± 10.4
Tyrphostin A23	44.8 ± 6.6
Dynasore	52.2 ± 11.3
Amiloride	51.2 ± 15.1
EIPA	50.3 ± 2.7

Data are from three different cultures.
DAPI, 4,6-diamidino-2-phenylindole; DMSO, dimethyl sulfoxide; EIPA, 5-(N-ethyl-N-isopropyl) amiloride.

Table 2. Exposure of Astrocytes to a Range of Particle Concentrations Does Not Result in Significant Cytotoxicity at 24–120 h Postincubation

Concentration (μg/mL)	*Viability (% control)*		
	24 h	*48 h*	*120 h*
0	100.0 ± 15.6	100.0 ± 14.9	100.0 ± 7.8
2	90.1 ± 15.6	101.5 ± 14.7	92.7 ± 12.0
5	93.2 ± 15.8	95.7 ± 12.8	93.9 ± 11.7
20	88.2 ± 14.1	83.8 ± 13.5	82.5 ± 13.9
50	81.9 ± 12.1	68.8 ± 14.5	75.1 ± 14.4

Data are from five different cultures.

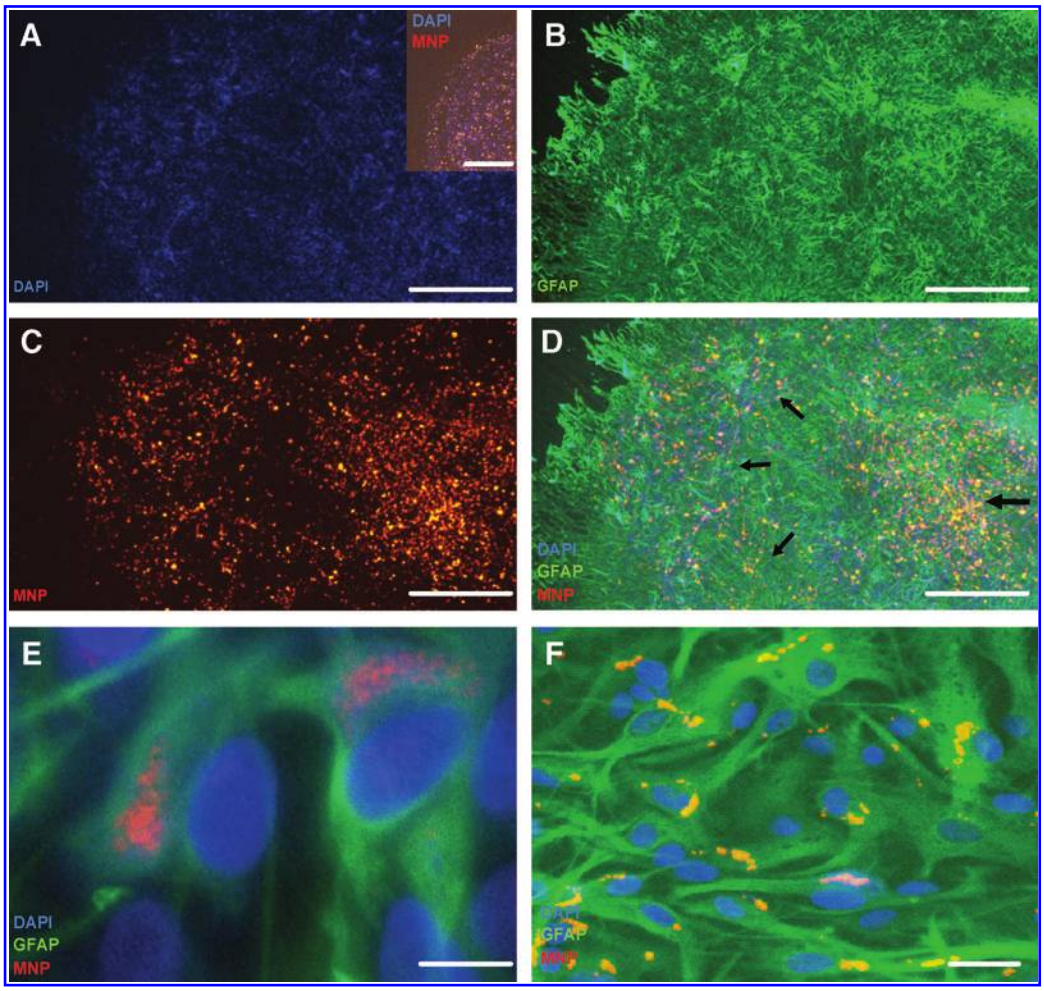

FIG. 4. Survival and differentiation of astrocytes prelabeled with MNPs and 4,6-diamidino-2-phenylindole (DAPI) after transplantation into organotypic slice cultures of cerebellum. **(A)** DAPI image of slice at 10 days after transplantation with DAPI/Spherofluor-labeled astrocytes; inset shows a Nile Red (MNP) and DAPI double-merged image of a live slice immediately after transplantation of cells. **(B)** GFAP image of the same slice shown in **(A)**. **(C)** Nile Red (MNP) image of the same slice shown in **(A)**. **(D)** Triple-merged image of the transplanted slice; arrows indicate central application point of the labeled astrocyte population. **(E)** High-magnification image of slice demonstrating the presence of DAPI/Nile Red/GFAP triple-positive cells. **(F)** Image of the transplant population after plating on tissue culture plastic also demonstrating the presence of DAPI/Nile Red/GFAP triple-positive cells at 10 days. Scale bar = 400 μm in **(A–D)**, 200 μm in **(A,** inset), 10 μm in **(E)**, and 50 μm in **(F)**. Color images available online at www.liebertonline.com/ten.

degradation; this stability was further confirmed in electron microscopy analyses and may account for the limited particle toxicity observed for astrocytes. Confocal microscopy confirmed that cells had internalized particles rather than the latter adhering to the astrocyte surface. This observation, in conjunction with the marked reduction in MNP uptake at 4°C or in the presence of endocytosis inhibitors, suggests that the contribution of particles adherent to the astrocyte surface (to cell counts) was negligible and that cellular labeling is a true reflection of intracellular particle localization, which will be important for imaging applications involving transplanted astrocytes.

The extent and time course of particle uptake was found to be dependant on both extracellular MNP concentrations and the length of exposure to particles. These observations suggest that MNP loading of astrocyte transplant populations can be varied to suit the required downstream application by simply manipulating particle concentrations at the initial incubation step. Combined with the ease of detection of the particles using standard fluorescence techniques, these observations make the particles employed a desirable choice for studies related to cell tracking and intracellular MNP processing in astrocytes. Notably, we found that after embedding in gels, the particles can be readily observed using a 1.5 T MRI scanner that is used routinely in human clinical testing. Particle detection *in vitro* does not necessarily indicate that cells containing MNPs can be detected *in vivo* (as the sample itself will impact on image signal to noise ratio and contrast to noise ratio particularly in neural injury sites). However, our preliminary findings do suggest that MNP labeling of transplant populations may have considerable translational potential for clinical tracking of transplanted astrocytes *in vivo*, an issue that that warrants further investigation.

In pulse-labeling experiments, particles were retained in high numbers in astrocytes for up to 21 days. Indeed, recent

preliminary data from our laboratory indicate significant particle retention for up to 28 days (the latest time point examined so far) although we observed a gradual dilution of MNP label with time. We can predict that such dilution may be due to cell division and/or cellular excretion (likely via exocytosis); the gradual reduction in perinuclear MNPs with time, in conjunction with progressive accumulation of particles near the cell membrane, would be consistent with a process of cellular excretion. During this period, cultures became confluent and exhibited normal morphologies, suggesting limited MNP effects on cell survival and differentiation—observations that were further supported by the MTS assays. Others have reported significant short-term toxicity of MNPs (of undisclosed formulation and size) on primary rat astrocytes, as evidenced by markedly reduced cell adherence, when nanoparticles were added to cells before attachment to the substratum.[28] We noted no effects on astrocyte adherence, possibly because cells were allowed to attach and mature before MNP addition. Our findings agree with a recent report that MNP addition (10 nm diameter particles) to astrocytes results in no acute loss of cell viability.[29]

Importantly, astrocytes prelabeled with MNPs could survive and differentiate after transplantation into organotypic slice cultures of the rat cerebellum; the latter model provides a three-dimensional network of neural cells and has been widely employed in studies on neural regeneration, providing an ideal bridge between experiments on isolated cells and the intact CNS *in vivo*, while allowing for high-throughput assays. Although we cannot rule out that excreted particles and/or particles that are released from dying transplanted astrocytes are taken up by cells such as microglia and host astrocytes, the majority of the astrocyte transplant population (~70%) was noted to be both MNP and DAPI positive at 10 days after plating on tissue culture plastic, suggesting that the majority of signal in host tissue is due to the transplant population. Our findings therefore indicate that this major neural cell population is highly amenable to labeling with MNPs and can provide the basis for the development of a technically simple and efficient method to safely label astrocytes derived for transplantation (which can be further adapted for long-term tracking of transplanted cells in host tissue). This method would be adaptable for either noninvasive imaging of transplant populations by MRI or for simple histological staining of tissue (to detect iron in transplant populations), and fluorescence/electron microscopy, making this a highly versatile labeling approach.

Findings from various mammalian cell types indicate that the intracellular accumulation of iron oxide-particles is mediated by endocytosis.[30,31] With regard to the specific endocytotic pathways that mediate MNP uptake, there is

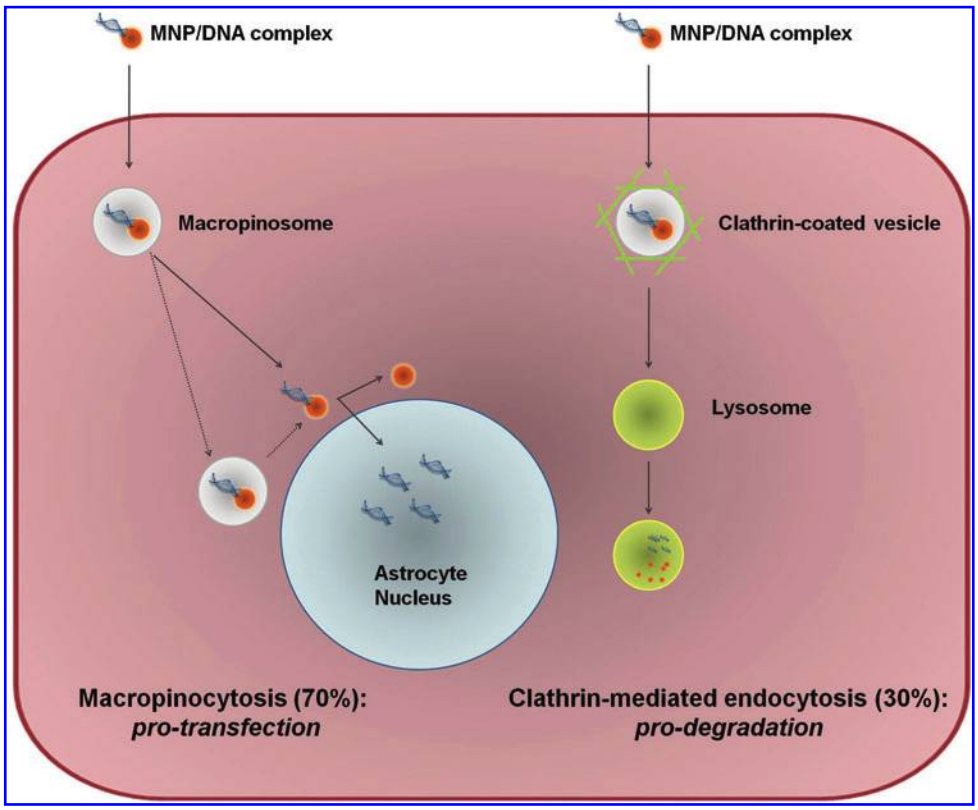

FIG. 5. Schematic diagram illustrating the primary modes of MNP uptake by astrocytes, subsequent intracellular processing and implications for gene delivery. Macropinocytosis, the major mechanism of astrocytic MNP uptake, can be considered a protransfection mechanism of uptake, as macropinosomes fuse with lysosomes at a low rate. Consequently, successful gene delivery to the nucleus is likely by this route. In contrast, clathrin-mediated endocytosis, a minor mechanism of astrocytic MNP uptake, can be considered a prodegradative mechanism of uptake, since clathrin-coated vesicles fuse with lysosomes at a high rate, resulting in degradation of cargo and particles. Color images available online at www.liebertonline.com/ten.

limited information in relation to primary neural cells and no information with regard to primary astrocytes. In our experiments, the dramatic decrease in particle uptake by astrocytes after incubation at 4°C strongly suggests that the process is mediated by active transport; MNP uptake by primary astrocytes has been recently reported to exhibit a similar temperature dependence, although the actual uptake mechanisms were not addressed further.[29] Our endocytosis blocker analyses reveal that MNP uptake is mediated by two primary mechanisms: macropinocytosis (~70%) and clathrin mediated uptake (~30%); these findings are supported by our TEM analyses. Caveolin-dependent endocytosis, by contrast, does not appear to contribute to MNP uptake. In support of our findings, macropinocytosis is suggested to play a major role in the uptake of a range of nanoparticles (of a similar size to the MNPs employed in our study) in various cell types.[32–35]

We consider our observations on the mechanisms of MNP uptake to be significant from the point of view of developing high efficiency vectors to transfect astrocytes. The rapid perinuclear targeting of MNPs in astrocytes can clearly provide the basis for rapid delivery of genetic material to the nucleus for transfection applications (rapid trafficking of nanoparticles resulting in perinuclear accumulation has been reported previously for other cell types)[36–38] but not, as far as we are aware, for astrocytes. However, a further point to consider with regard to transfection is the mode of particle uptake by astrocytes. Some studies argue that particle uptake via clathrin-dependent mechanisms is not advantageous for transfection, as endolyososomal trafficking is a predictable consequence of clathrin-mediated endocytosis representing a critical rate-limiting step.[39] By contrast, cellular uptake mediated by macropinocytosis may confer significant advantages for drug/gene delivery, since macropinosomes fuse with lysosomes at lower rates than clathrin-coated vesicles,[39] thereby minimizing lysosomal degradation of nanoparticles and/or their cargo (Fig. 5).[32–34] As macropinocytosis accounts for 70% of MNP uptake in astrocytes, we can predict that without further manipulation, it will only be possible to transfect an upper limit of ~70% of astrocytes. This is strongly supported by our recent report that particles (of similar dimensions to those used in this study and with perinuclear targeting properties) can be used to transfect between 43% and 75% of rat astrocytes.

Our findings that MNPs can be used effectively for labeling/imaging of astrocytes derived for transplantation (coupled with earlier findings that MNPs can be used for astrocyte transfection applications) lend support to the idea that MNPs are a versatile platform that can be employed for cell tracking and magnetic cell targeting, transfection, and noninvasive imaging applications for neural cell transplantation therapies. To develop the clinical translational potential of this approach, future challenges will involve collaboration between materials scientists and transplantation neurobiologists to develop multimodal iron oxide nanoparticles that can safely mediate the above combinatorial functions in neural cell transplant populations.

Acknowledgments

This work is supported by research grants from the British Biotechnology and Biological Sciences Research Council (New Investigator Award) and the Royal Society, UK. We would like to thank Ms. Karen Walker for expert assistance with TEM.

Disclosure Statement

No competing financial interests exist.

References

1. Magistretti, P.J., and Ransom, B.R. Astrocytes. In: Davis, K.L., Charney, D., Coyle, J.T., and Nemeroff, C., eds. Neuropharmacology: The Fifth Generation of Progress. Philadelphia: Lippincott Williams and Wilkins, 2002, pp. 181–208.
2. Anderson, C.M., and Swanson, R.A. Astrocyte glutamate transport: review of properties, regulation, and physiological functions. Glia **32,** 1, 2000.
3. Pekny, M., and Nilsson, M. Astrocyte activation and reactive gliosis. Glia **50,** 427, 2005.
4. Abbott, N.J., Ronnback, L., and Hansson, E. Astrocyte-endothelial interactions at the blood-brain barrier. Nat Rev Neurosci **7,** 41, 2006.
5. Liedtke, W., Edelmann, W., Bieri, P.L., Chiu, F.C., Cowan, N.J., and Kucherlapati, R. GFAP is necessary for the integrity of CNS white matter architecture and long-term maintenance of myelination. Neuron **17,** 607, 1996.
6. Quinlan, R.A., Brenner, M., Goldman, J.E., and Messing, A. GFAP and its role in Alexander disease. Exp Cell Res **313,** 2077, 2007.
7. Maragakis, N.J., and Rothstein, J.D. Mechanisms of disease: astrocytes in neurodegenerative disease. Nat Clin Pract Neurol **2,** 679, 2006.
8. Lepore, A.C., Rauck, B., Dejea, C., Pardo, A.C., Rao, M.S., Rothstein, J.D., and Maragakis, N.J. Focal transplantation-based astrocyte replacement is neuroprotective in a model of motor neuron disease. Nat Neurosci **11,** 1294, 2008.
9. White, R.E., and Jakeman, L.B. Don't fence me in: harnessing the beneficial roles of astrocytes for spinal cord repair. Restor Neurol Neurosci **26,** 197, 2008.
10. Ericson, C., Georgievska, B., and Lundberg, C. *Ex vivo* gene delivery of GDNF using primary astrocytes transduced with a lentiviral vector provides neuroprotection in a rat model of Parkinson's disease. Eur J Neurosci **22,** 2755, 2005.
11. Lin, Q., Cunningham, L.A., Epstein, L.G., Pechan, P.A., Short, M.P., Fleet, C., and Bohn, M.C. Human fetal astrocytes as an *ex vivo* gene therapy vehicle for delivering biologically active nerve growth factor. Hum Gene Ther **8,** 331, 1997.
12. Sechrist, J., Coulombe, J.N., and Bronner-Fraser, M. Combined vital dye labeling and catecholamine histofluorescence of transplanted ciliary ganglion cells. J Neural Transplant **1,** 113, 1989.
13. O'Leary, M.T., and Blakemore, W.F. Use of a rat Y chromosome probe to determine the long-term survival of glial cells transplanted into areas of CNS demyelination. J Neurocytol **26,** 191, 1997.
14. Othman, M.M., Klueber, K.M., and Roisen, F.J. Identification and culture of olfactory neural progenitors from GFP mice. Biotech Histochem **78,** 57, 2003.
15. Lee, J.P., McKercher, S., Muller, F.J., and Snyder, E.Y. Neural stem cell transplantation in mouse brain. Curr Protoc Neurosci Chapter 3, Unit 3.10, 2008.
16. Aleksandrova, M.A., Poltavtseva, R.A., Revishchin, A.V., Korochkin, L.I., and Sukhikh, G.T. Development of neural stem/progenitor cells from human brain by transplantation

into the brains of adult rats. Neurosci Behav Physiol **34,** 659, 2004.
17. Bulte, J.W., and Kraitchman, D.L. Monitoring cell therapy using iron oxide MR contrast agents. Curr Pharm Biotechnol **5,** 567, 2004.
18. Song, M., Kim, Y., Kim, Y., Ryu, S., Song, I., Kim, S.U., and Yoon, B.W. MRI tracking of intravenously transplanted human neural stem cells in rat focal ischemia model. Neurosci Res **64,** 235, 2009.
19. Guzman, R., Uchida, N., Bliss, T.M., He, D., Christopherson, K.K., Stellwagen, D., Capela, A., Greve, J., Malenka, R.C., Moseley, M.E., Palmer, T.D., and Steinberg, G.K. Long-term monitoring of transplanted human neural stem cells in developmental and pathological contexts with MRI. Proc Natl Acad Sci USA **104,** 10211, 2007.
20. Dunning, M.D., Lakatos, A., Loizou, L., Kettunen, M., ffrench-Constant, C., Brindle, K.M., and Franklin, R.J. Superparamagnetic iron oxide-labeled Schwann cells and olfactory ensheathing cells can be traced *in vivo* by magnetic resonance imaging and retain functional properties after transplantation into the CNS. J Neurosci **24,** 9799, 2004.
21. Lepore, A.C., Walczak, P., Rao, M.S., Fischer, I., and Bulte, J.W. MR imaging of lineage-restricted neural precursors following transplantation into the adult spinal cord. Exp Neurol **201,** 49, 2006.
22. Pickard M., and Chari, D. Enhancement of magnetic nanoparticle-mediated gene transfer to astrocytes by "magnetofection": effects of static and oscillating fields. Nanomedicine (Lond) **5,** 217, 2010.
23. Cole, R., and de Vellis, J. Preparation of astrocyte, oligodendrocyte, and microglia cultures from primary rat cerebral cultures. In: Fedoroff, S., and Richardson, A., eds. Protocols for Neural Cell Culture. Totowa, NJ: Humana Press, 2001, pp. 117–127.
24. Ivanov, A.I. Pharmacological inhibition of endocytic pathways: is it specific enough to be useful? Methods Mol Biol **440,** 15, 2008.
25. Macia, E., Ehrlich, M., Massol, R., Boucrot, E., Brunner, C., and Kirkhausen, T. Dynasore, a cell-permeable inhibitor of dynamin. Dev Cell **10,** 839, 2006.
26. Banbury, D.N., Oakley, J.D., Sessions, R.B., and Banting, G. Tyrphostin A23 inhibits internalization of the transferring receptor by perturbing the interaction between tyrosine motifs and the medium chain subunit of the AP-2 adaptor complex. J Biol Chem **278,** 12022, 2003.
27. Pickard, M.R., and Chari, D.M. Robust uptake of magnetic nanoparticles (MNPs) by central nervous system (CNS) microglia: implications for particle uptake in mixed neural cell populations. Int J Mol Sci **11,** 967, 2010.
28. Au, C., Mutkus, L., Dobson, A., Riffle, J., Lalli, J., and Aschner, M. Effects of nanoparticles on the adhesion and cell viability on astrocytes. Biol Trace Elem Res **120,** 248, 2007.
29. Geppert, M., Hohnholt, M., Gaetjen, L., Grunwald, I., Bäumer, M., and Dringen, R. Accumulation of iron oxide nanoparticles by cultured brain astrocytes. J Biomed Nanotechnol **5,** 285, 2009.
30. Bulte, J.W.M., Duncan, I.D., and Frank, J.A. *In vivo* magnetic resonance tracking of magnetically labeled cells after transplantation. J Cereb Blood Flow Metab **22,** 899, 2002.
31. Rogers, W.J., Meyer, C.H., and Kramer, C.M. Technology insight: *in vivo* cell tracking by use of MRI. Nat Clin Pract Cardiovasc Med **3,** 554, 2006.
32. Walsh, M., Tangney, M., O'Neill, M.J., Larkin, J.O., Soden, D.M., McKenna, S.L., Darcy, R., O'Sullivan, G.C., and O'Driscoll, C.M. Evaluation of cellular uptake and gene transfer efficiency of pegylated poly-L-lysine compacted DNA: implications for cancer gene therapy. Mol Pharm **3,** 644, 2006.
33. Khalil, I.A., Kogure, K., Futaki, S., and Harashima, H. High density of octaarginine stimulates macropinocytosis leading to efficient intracellular trafficking for gene expression. J Biol Chem **281,** 3544, 2006.
34. Khalil, I.A., Kogure, K., Futaki, S., Hama, S., Akita, H., Ueno, M., Kishida, H., Kudoh, M., Mishina, Y., Kataoka, K., Yamada, M., and Harashima, H. Octaarginine-modified multifunctional envelope-type nanoparticles for gene delivery. Gene Ther **14,** 682, 2007.
35. Nam, H.Y., Kwon, S.M., Chung, H., Lee, S.Y., Kwon, S.H., Jeon, H., Kim, Y., Park, J.H., Kim, J., Her, S., Oh, Y.K., Kwon, I.C., Kim, K., and Jeong, S.Y. Cellular uptake mechanism and intracellular fate of hydrophobically modified glycol chitosan nanoparticles. J Control Release **135,** 259, 2009.
36. Lai, S.K., Hida, K., Chen, C., and Hanes, J. Characterization of the intracellular dynamics of a non-degradative pathway accessed by polymer nanoparticles. J Control Release **125,** 107, 2008.
37. Shenoy, D., Little, S., Langer, R., and Amiji, M. Poly (ethylene oxide)-modified poly(beta-amino ester) nanoparticles as a pH-sensitive system for tumor-targeted delivery of hydrophobic drugs: part 2. *In vivo* distribution and tumor localization studies. Pharm Res **22,** 2107, 2005.
38. Suh, J., Wirtz, D., and Hanes, J. Efficient active transport of gene nanocarriers to the cell nucleus. Proc Natl Acad Sci USA **100,** 3878, 2003.
39. Khalil, I.A., Kogure, K., Akita, H., and Harashima, H. Uptake pathways and subsequent intracellular trafficking in nonviral gene delivery. Pharmacol Rev **58,** 32, 2006.

Address correspondence to:
Mark R. Pickard, Ph.D.
Cellular and Neural Engineering Group
Institute for Science and Technology in Medicine
Keele University
Staffordshire ST5 5BG
United Kingdom

E-mail: m.r.pickard@biol.keele.ac.uk

Received: March 19, 2010
Accepted: July 19, 2010
Online Publication Date: September 21, 2010

References

1. Chari, D. M. Remyelination in Multiple Sclerosis. *Int. Rev. Neurobiol.* **79**, 589–620 (2007).

2. Keegan, B. M. & Noseworthy, J. H. Multiple Sclerosis. *Annu. Rev. Med.* **53**, 285–302 (2002).

3. Waxman, S. G. Demyelination in spinal cord injury and multiple sclerosis: what can we do to enhance functional recovery? *J. Neurotrauma* **9 Suppl 1**, S105–S117 (1992).

4. Zhang, H., Jarjour, A. A., Boyd, A. & Williams, A. Central nervous system remyelination in culture - A tool for multiple sclerosis research. *Exp. Neurol.* **230**, 138–148 (2011).

5. Kim, B. G., Hwang, D. H., Lee, S. I., Kim, E. J. & Kim, S. U. Stem cell-based cell therapy for spinal cord injury. *Cell Transplant.* **16**, 355–364 (2007).

6. Franklin, R. J. M. & ffrench-Constant, C. Remyelination in the CNS: from biology to therapy. *Nat. Rev. Neurosci.* **9**, 839–855 (2008).

7. Bradl, M. & Lassmann, H. Oligodendrocytes: biology and pathology. *Acta Neuropath.* **119**, 37–53 (2010).

8. Hartline, D. K. What is myelin? *Neuron Glia Biol.* **4**, 153–163 (2008).

9. Baumann, N. & Pham-Dinh, D. Biology of oligodendrocyte and myelin in the mammalian central nervous system. *Physiol. Rev.* **81**, 871–927 (2001).

10. Potter, G. B., Rowitch, D. H. & Petryniak, M. A. Myelin restoration: progress and prospects for human cell replacement therapies. *Arch. Immunol. Ther. Exp. (Warsz)* **59**, 179–193 (2011).

11. Chandran, S. & Compston, A. Neural stem cells as a potential source of oligodendrocytes for myelin repair. *J. Neurol. Sci.* **233**, 179 – 181 (2005).

12. Felts, P. A., Baker, T. A. & Smith, K. J. Conduction in segmentally demyelinated mammalian central axons. *J. Neurosci.* **17**, 7267–77 (1997).

13. Constantinou, S. & Fern, R. Conduction block and glial injury induced in developing central white matter by glycine, GABA, noradrenalin, or nicotine, studied in isolated neonatal rat optic nerve. *Glia* **57**, 1168–1177 (2009).

14. Rodriguez, M. A function of myelin is to protect axons from subsequent injury: implications for deficits in multiple sclerosis. *Brain* **126**, 751–752 (2003).

15. Nave, K.-A. Myelination and the trophic support of long axons. *Nat. Rev. Neurosci.* **11**, 275–283 (2010).

16. Griffiths, I. *et al.* Axonal swellings and degeneration in mice lacking the major proteolipid of myelin. *Science* **280**, 1610–1613 (1998).

17. Lappe-Siefke, C. *et al.* Disruption of Cnp1 uncouples oligodendroglial functions in axonal support and myelination. *Nat. Genet.* **33**, 366–374 (2003).

18. Lee, Y. *et al.* Oligodendroglia metabolically support axons and contribute to neurodegeneration. *Nature* **487**, 443–448 (2012).

19. Bunge, M. B., Bunge, R. P. & Ris, H. Ultrastructural study of remyelination in an experimental lesion in adult cat spinal cord. *J. Biophys. Biochem. Cytol.* **10**, 67–94 (1961).

20. Bunge, R. P., Bunge, M. B. & Ris, H. Electron microscopic study of demyelination in an experimentally induced lesion in adult cat spinal cord. *J. Biophys. Biochem. Cytol.* **7**, 685–696 (1960).

21. Blakemore, W. F. Pattern of remyelination in the CNS. *Nature* **249**, 577–578 (1974).

22. Gledhill, R. F., Harrison, B. M. & McDonald, W. I. Pattern of remyelination in the CNS. *Nature* **244**, 443–444 (1973).

23. Smith, K. J., Blakemore, W. F. & McDonald, W. I. Central remyelination restores secure conduction. *Nature* **280**, 395–396 (1979).

24. Smith, K. J., Blakemore, W. F. & McDonald, W. I. The restoration of conduction by central remyelination. *Brain* **104**, 383–404 (1981).

25. Mekhail, M., Almazan, G. & Tabrizian, M. Oligodendrocyte-protection and remyelination post-spinal cord injuries: a review. *Prog. Neurobiol.* **96**, 322–339 (2012).

26. Richardson, W. D., Kessaris, N. & Pringle, N. Oligodendrocyte wars. *Nat. Rev. Neurosci.* **7**, 11–18 (2006).

27. Kessaris, N. *et al.* Competing waves of oligodendrocytes in the forebrain and postnatal elimination of an embryonic lineage. *Nat. Neurosci.* **9**, 173–179 (2006).

28. Chari, D. M. & Blakemore, W. New insights into remyelination failure in multiple sclerosis: implications for glial cell transplantation. *Mult. Scler.* **8**, 271–277 (2002).

29. De Castro, F. & Bribián, A. The molecular orchestra of the migration of oligodendrocyte precursors during development. *Brain Res. Brain Res. Rev.* **49**, 227–241 (2005).

30. Watkins, T. A., Emery, B., Mulinyawe, S. & Barres, B. A. Distinct stages of myelination regulated by gamma-secretase and astrocytes in a rapidly myelinating CNS coculture system. *Neuron* **60**, 555–569 (2008).

31. Huang, J. K. *et al.* Glial membranes at the node of Ranvier prevent neurite outgrowth. *Science* **310**, 1813–1817 (2005).

32. LeBaron, F. N., Sanyal, S. & Jungalwala, F. B. Turnover rate of molecular species of sphingomyelin in rat brain. *Neurochem. Res.* **6**, 1081–1089 (1981).

33. Lajtha, A., Toth, J., Fujimoto, K. & Agrawal, H. C. Turnover of myelin proteins in mouse brain in vivo. *Biochem. J.* **164**, 323–329 (1977).

34. Buchet, D. & Baron-Van Evercooren, A. In search of human oligodendroglia for myelin repair. *Neurosci. Lett.* **456**, 112–119 (2009).

35. Butts, B. D., Houde, C. & Mehmet, H. Maturation-dependent sensitivity of oligodendrocyte lineage cells to apoptosis: implications for normal development and disease. *Cell Death Differ.* **15**, 1178–1186 (2008).

36. Yakovlev, A. Y., Boucher, K., Mayer-Pröschel, M. & Noble, M. Quantitative insight into proliferation and differentiation of oligodendrocyte type 2 astrocyte progenitor cells in vitro. *Proc. Natl. Acad. Sci. USA* **95**, 14164–14167 (1998).

37. Jakovcevski, I., Filipovic, R., Mo, Z., Rakic, S. & Zecevic, N. Oligodendrocyte development and the onset of myelination in the human fetal brain. *Front. Neuroanat.* **3**, 1–15 (2009).

38. Miron, V. E. *et al.* Fingolimod (FTY720) enhances remyelination following demyelination of organotypic cerebellar slices. *Am. J. Pathol.* **176**, 2682–2694 (2010).

39. Zawadzka, M. *et al.* CNS-resident glial progenitor/stem cells produce Schwann cells as well as oligodendrocytes during repair of CNS demyelination. *Cell Stem Cell* **6**, 578–90 (2010).

40. Franklin, R. J. M. & Hinks, G. L. Understanding CNS remyelination : clues from developmental and regeneration biology. *J. Neurosci. Res.* **58**, 207–213 (1999).

41. Hinks, G. L. & Franklin, R. J. Distinctive patterns of PDGF-A, FGF-2, IGF-I, and TGF-beta1 gene expression during remyelination of experimentally-induced spinal cord demyelination. *Mol. Cell Neurosci.* **14**, 153–168 (1999).

42. Miron, V., Cuo, Q., Wegner, C., Antel, J. & Brück, W. Differentiation block of oligodendroglial progenitor cells as a cause for remyelination failure in chronic multiple sclerosis. *Brain* **131**, 1749–1758 (2008).

43. Stangel, M. & Trebst, C. Remyelination strategies: new advancements toward a regenerative treatment in multiple sclerosis. *Curr. Neurol. Neurosci. Rep.* **6**, 229–235 (2006).

44. Webber, D. J., Compston, A. & Chandran, S. Minimally manipulated oligodendrocyte precursor cells retain exclusive commitment to the oligodendrocyte lineage following transplantation into intact and injured hippocampus. *Eur. J. Neurosci.* **26**, 1791–1800 (2007).

45. Franklin, R. J. M. Remyelination of the demyelinated CNS: the case for and against transplantation of central, peripheral and olfactory glia. *Brain Res. Bull.* **57**, 827–832 (2002).

46. Groves, A. K. *et al.* Repair of demyelinated lesions by transplantation of purified 0-2A progenitor cells. *Nature* **362**, 453–455 (1993).

47. Gumpel, M. *et al.* Transplantation of human embryonic oligodendrocytes into shiverer brain. *Ann. N. Y. Acad. Sci.* **495**, 71–85 (1987).

48. Windrem, M. S. *et al.* Neonatal chimerization with human glial progenitor cells can both remyelinate and rescue the otherwise lethally hypomyelinated shiverer mouse. *Cell Stem Cell* **2**, 553–565 (2008).

49. Vignais, L. *et al.* Transplantation of oligodendrocyte precursors in the adult demyelinated spinal cord: migration and remyelination. *Int. J. Dev. Neurosci.* **11**, 603–612 (1993).

50. Givogri, M. I. *et al.* Oligodendroglial progenitor cell therapy limits central neurological deficits in mice with metachromatic leukodystrophy. *J. Neurosci.* **26**, 3109 –3119 (2006).

51. Keirstead, H. S. *et al.* Human embryonic stem cell-derived oligodendrocyte progenitor cell transplants remyelinate and restore locomotion after spinal cord injury. *J. Neurosci.* **25**, 4694–705 (2005).

52. Hinks, G. L. *et al.* Depletion of endogenous oligodendrocyte progenitors rather than increased availability of survival factors is a likely explanation for enhanced survival of transplanted oligodendrocyte progenitors in X-irradiated compared to normal CNS. *Neuropathol. Appl. Neurobiol.* **27**, 59–67 (2001).

53. Franklin, R. J. M., Bayley, S. A. & Blakemore, W. F. Transplanted CG4 cells (an oligodendrocyte progenitor cell line) survive, migrate, and contribute to repair of areas of demyelination in X-irradiated and damaged spinal cord but not in normal spinal cord. *Exp. Neurol.* **137**, 263–276 (1996).

54. Brüstle, O. *et al.* Embryonic stem cell-derived glial precursors: a source of myelinating transplants. *Science* **285**, 754–756 (1999).

55. Sypecka, J. Searching for oligodendrocyte precursors for cell replacement therapies. *Acta Neurobiol. Exp. (Wars)* **71**, 94–102 (2011).

56. Watson, R. A. & Yeung, T. M. What is the potential of oligodendrocyte progenitor cells to successfully treat human spinal cord injury? *BMC Neurol.* **11**, 113 (2011).

57. Lebkowski, J. GRNOPC1: the world's first embryonic stem cell-derived therapy. Interview with Jane Lebkowski. *Regen. Med.* **6**, 11–13 (2011).

58. Frantz, S. Embryonic stem cell pioneer Geron exits field, cuts losses. *Nat. Biotechnol.* **30**, 12–13 (2012).

59. Karimi-Abdolrezaee, S., Eftekharpour, E., Wang, J., Schut, D. & Fehlings, M. G. Synergistic effects of transplanted adult neural stem/progenitor cells, chondroitinase, and growth factors promote functional repair and plasticity of the chronically injured spinal cord. *J. Neurosci.* **30**, 1657–1676 (2010).

60. Cao, Q. *et al.* Transplantation of ciliary neurotrophic factor-expressing adult oligodendrocyte precursor cells promotes remyelination and functional recovery after spinal cord injury. *J. Neurosci.* **30**, 2989–3001 (2010).

61. Milward, E. A. *et al.* Enhanced proliferation and directed migration of oligodendroglial progenitors co-grafted with growth factor-secreting cells. *Glia* **32**, 264–270 (2000).

62. Rose, L. C., Kucharski, C. & Uludağ, H. Protein expression following non-viral delivery of plasmid DNA coding for basic FGF and BMP-2 in a rat ectopic model. *Biomaterials* **33**, 3363–3674 (2012).

63. Magy, L. *et al.* Inducible expression of FGF2 by a rat oligodendrocyte precursor cell line promotes CNS myelination in vitro. *Exp. Neurol.* **184**, 912 – 922 (2003).

64. Cao, Q. *et al.* Functional recovery in traumatic spinal cord injury after transplantation of multineurotrophin-expressing glial-restricted precursor cells. *J. Neurosci.* **25**, 6947– 6957 (2005).

65. Russell, W. M. S. & Burch, R. L. *The principles of humane experimental technique*. xiv + 238 pp. (Methuen & Co. Ltd., London: 1959).

66. Liebsch, M. *et al.* Alternatives to animal testing: current status and future perspectives. *Arch. Toxicol.* **85**, 841–858 (2011).

67. Baker, D. & Jackson, S. J. Models of Multiple Sclerosis. *ACNR* **6**, 10–12 (2007).

68. Baker, D., Gerritsen, W., Rundle, J. & Amor, S. Critical appraisal of animal models of multiple sclerosis. *Mult. Scler.* **17**, 647–657 (2011).

69. Stoppini, L., Buchs, P. A. & Muller, D. A simple method for organotypic cultures of nervous tissue. *J. Neurosci. Methods* **37**, 173–182 (1991).

70. Gähwiler, B. H., Capogna, M., Debanne, D., McKinney, R. A. & Thompson, S. M. Organotypic slice cultures: a technique has come of age. *Trends Neurosci.* **20**, 471–477 (1997).

71. Kessler, M., Kiliman, B., Humes, C. & Arai, A. C. Spontaneous activity in Purkinje cells: multi-electrode recording from organotypic cerebellar slice cultures. *Brain Res.* **1218**, 54–69 (2008).

72. De Simoni, A. & Yu, L. M. Y. Preparation of organotypic hippocampal slice cultures: interface method. *Nat. Protoc.* **1**, 1439–1445 (2006).

73. Sundstrom, L., Morrison, B. 3rd, Bradley, M. & Pringle, A. Organotypic cultures as tools for functional screening in the CNS. *Drug Discov. Today* **10**, 993–1000 (2005).

74. Morrison, B. 3rd, Saatman, K. E., Meaney, D. F. & McIntosh, T. K. In vitro central nervous system models of mechanically induced trauma: a review. *J Neurotrauma* **15**, 911–928 (1998).

75. Gähwiler, B. H. Organotypic monolayer cultures of nervous tissue. *J. Neurosci. Methods* **4**, 329–342 (1981).

76. Xiang, Z. *et al.* Long-term maintenance of mature hippocampal slices in vitro. *J. Neurosci. Methods* **98**, 145–154 (2000).

77. Adamchik, Y. & Frantseva, M. Methods to induce primary and secondary traumatic damage in organotypic hippocampal slice cultures. *Brain Res. Brain Res. Protoc.* **5**, 153–158 (2000).

78. Dean, J. M. *et al.* An organotypic slice culture model of chronic white matter injury with maturation arrest of oligodendrocyte progenitors. *Mol. Neurodegener.* **5**, 46 (2011).

79. Cho, S., Wood, A. & Bowlby, M. R. Brain slices as models for neurodegenerative disease and screening platforms to identify novel therapeutics. *Curr. Neuropharmacol.* **5**, 19–33 (2007).

80. Lu, H.-X., Levis, H., Liu, Y. & Parker, T. Organotypic slices culture model for cerebellar ataxia: potential use to study Purkinje cell induction from neural stem cells. *Brain Res. Bull.* **84**, 169–173 (2011).

81. Berger, T. & Frotscher, M. Distribution and morphological characteristics of oligodendrocytes in the rat hippocampus in situ and in vitro: an immunocytochemical study with the monoclonal Rip antibody. *J. Neurocytol.* **23**, 61–74 (1994).

82. Bahr, B. A. Long-term hippocampal slices: a model system for investigating synaptic mechanisms and pathologic processes. *J. Neurosci. Res.* **42**, 294–305 (1995).

83. Jaeger, C., Kapoor, R. & Llinás, R. Cytology and organization of rat cerebellar organ cultures. *Neuroscience* **26**, 509–538 (1988).

84. Reeves, S. A. & Xiang, Z. Simvastatin induces cell death in a mouse cerebellar slice culture (CSC) model of developmental myelination. *Exp. Neurol.* **215**, 41–47 (2009).

85. Kapfhammer, J. P. Cellular and molecular control of dendritic growth and development of cerebellar Purkinje cells. *Prog. Histochem. Cytochem.* **39**, 131–182 (2004).

86. Davids, E. *et al.* Organotypic rat cerebellar slice culture as a model to analyze the molecular pharmacology of GABAA receptors. *Eur. Neuropsychopharmacol.* **12**, 201–208 (2002).

87. Ohnishi, T., Matsumura, H., Izumoto, S., Hiraga, S. & Hayakawa, T. A novel model of glioma cell invasion using organotypic brain slice culture. *Cancer Res.* **58**, 2935–2940 (1998).

88. Harrer, M. D. *et al.* Live imaging of remyelination after antibody-mediated demyelination in an ex-vivo model for immune mediated CNS damage. *Exp. Neurol.* **216**, 431–438 (2009).

89. Seil, F. J. & Blank, N. K. Myelination of central nervous system axons in tissue culture by transplanted oligodendrocytes. *Science* **212**, 1407–1408 (1981).

90. Nishimura, R. N., Blank, N. K., Tiekotter, K. L., Cole, R. & De Vellis, J. Myelination of mouse cerebellar explants by rat cultured oligodendrocytes. *Brain Res.* **337**, 159–162 (1985).

91. Franklin, R. J. M. & Blakemore, W. F. Transplanting myelin-forming cells into the central nervous system: principles and practice. *Methods* **16**, 311–9 (1998).

92. Muja, N. & Bulte, J. W. M. M. Magnetic resonance imaging of cells in experimental disease models. *Prog. Nucl. Magn. Reson. Spectrosc.* **55**, 61–77 (2009).

93. Bulte, J. W. M. *et al.* Magnetic labeling and tracking of cells using magnetodendrimers as MR contrast agent. *Eur. Cells Mater.* **3**, 7–8 (2002).

94. Franklin, R. J. M. *et al.* Magnetic resonance imaging of transplanted oligodendrocyte precursors in the rat brain. *Neuroreport* **10**, 3961–3965 (1999).

95. Lepore, A. C., Walczak, P., Rao, M. S., Fischer, I. & Bulte, J. W. M. MR imaging of lineage-restricted neural precursors following transplantation into the adult spinal cord. *Exp. Neurol.* **201**, 49–59 (2006).

96. Bulte, J. W. *et al.* Magnetodendrimers allow endosomal magnetic labeling and in vivo tracking of stem cells. *Nat. Biotechnol.* **19**, 1141–1147 (2001).

97. Bulte, J. W. M., Duncan, I. D. & Frank, J. A. In vivo magnetic resonance tracking of magnetically labeled cells after transplantation. *J. Cereb. Blood Flow Metab.* **22**, 899–907 (2002).

98. Dunning, M. D. *et al.* Superparamagnetic iron oxide-labeled Schwann cells and olfactory ensheathing cells can be traced in vivo by magnetic resonance imaging and retain functional properties after transplantation into the CNS. *J. Neurosci.* **24**, 9799–9810 (2004).

99. Taylor, A., Wilson, K. M., Murray, P., Fernig, D. G. & Lévy, R. Long-term tracking of cells using inorganic nanoparticles as contrast agents: are we there yet? *Chem. Soc. Rev.* **41**, 2707–2717 (2012).

100. Hinds, K. A. *et al.* Highly efficient endosomal labeling of progenitor and stem cells with large magnetic particles allows magnetic resonance imaging of single cells. *Blood* **102**, 867–872 (2003).

101. Stroh, A. *et al.* In vivo detection limits of magnetically labeled embryonic stem cells in the rat brain using high-field (17.6 T) magnetic resonance imaging. *Neuroimage* **24**, 635–645 (2005).

102. Yiu, H. H. P. *et al.* Fe3O4-PEI-RITC magnetic nanoparticles with imaging and gene transfer capability: development of a tool for neural cell transplantation therapies. *Pharm. Res.* **29**, 1328–1343 (2012).

103. Kulbatski, I. *et al.* Glial precursor cell transplantation therapy for neurotrauma and multiple sclerosis. *Prog. Histochem. Cytochem.* **43**, 123–176 (2008).

104. Mothe, A. J. & Tator, C. H. Transplanted neural stem/progenitor cells generate myelinating oligodendrocytes and Schwann cells in spinal cord demyelination and dysmyelination. *Exp. Neurol.* **213**, 176–190 (2008).

105. Willerth, S. M. & Sakiyama-Elbert, S. E. Cell therapy for spinal cord regeneration. *Adv. Drug Deliv. Rev.* **60**, 263–276 (2008).

106. Boddington, S. E. *et al.* Labeling human mesenchymal stem cells with fluorescent contrast agents: the biological impact. *Mol. Imaging Biol.* **13**, 3–9 (2011).

107. Bulte, J. W. M. In vivo MRI cell tracking: clinical studies. *Am. J. Roentgenol.* **193**, 314–325 (2009).

108. Lubetzki, C. *et al.* Gene transfer of rat mature oligodendrocytes and glial progenitor cells with the LacZ gene. *Ann. N. Y. Acad. Sci.* **605**, 66–70 (1990).

109. Mintzer, M. A. & Simanek, E. E. Nonviral vectors for gene delivery. *Chem. Rev.* **109**, 259–302 (2009).

110. Krueger, W. H. H., Madison, D. L. & Pfeiffer, S. E. Transient transfection of oligodendrocyte progenitors by electroporation. *Neurochem. Res.* **23**, 421–426 (1998).

111. Guo, Z. *et al.* Efficient and sustained transgene expression in mature rat oligodendrocytes in primary culture. *J. Neurosci. Res.* **43**, 32–41 (1996).

112. Blits, B. & Bunge, M. B. Direct gene therapy for repair of the spinal cord. *J. Neurotraum.* **23**, 508–520 (2006).

113. Jiang, S., Seng, S., Avraham, H. K., Fu, Y. & Avraham, S. Process elongation of oligodendrocytes is promoted by the Kelch-related protein MRP2/KLHL1. *J. Biol. Chem.* **282**, 12319–12329 (2007).

114. Franklin, R. J. M., Quick, M. M. & Haase, G. Adenoviral vectors for in vivo gene delivery to oligodendrocytes: transgene expression and cytopathic consequences. *Gene Ther.* **6**, 1360–1367 (1999).

115. Hermens, W. T. J. M. C. & Verhaagen, J. Viral vectors, tools for gene transfer in the nervous system. *Prog. Neurobiol.* **55**, 399–432 (1998).

116. Pichon, C., Billiet, L. & Midoux, P. Chemical vectors for gene delivery: uptake and intracellular trafficking. *Curr. Opin. Biotech.* **21**, 640–645 (2010).

117. Ryan, D. A. & Federoff, H. J. Translational considerations for CNS gene therapy. *Expert Opin. Biol. Ther.* **7**, 305–318 (2007).

118. Chen, D., Sung, R. & Bromberg, J. S. Gene therapy in transplantation. *Transpl. Immunol.* **9**, 301–314 (2002).

119. O'Leary, M. T. & Charlton, H. M. A model for long-term transgene expression in spinal cord regeneration studies. *Gene Ther.* **6**, 1351–9 (1999).

120. Lentz, T. B., Gray, S. J. & Samulski, R. J. Viral vectors for gene delivery to the central nervous system. *Neurobiol. Dis.* **48**, 179–188 (2011).

121. Maxwell, D. J. *et al.* Fluorophore-conjugated iron oxide nanoparticle labeling and analysis of engrafting human hematopoietic stem cells. *Stem Cells* **26**, 517–524 (2008).

122. Neve, R. L. & Carlezon, W. A. J. Gene delivery into the brain using viral vectors. *Neuropsychopharmacology: The fifth generation of progress* pp253–262 (2002).

123. Pritchard, C. D. *et al.* Establishing a model spinal cord injury in the African green monkey for the preclinical evaluation of biodegradable polymer scaffolds seeded with human neural stem cells. *J. Neurosci. Methods* **188**, 258–69 (2010).

124. Wang, M. *et al.* Bioengineered scaffolds for spinal cord repair. *Tissue Eng. Part B Rev.* **17**, 177–194 (2011).

125. Teng, Y. D. *et al.* Functional recovery following traumatic spinal cord injury mediated by a unique polymer scaffold seeded with neural stem cells. *Proc. Natl. Acad. Sci. USA* **99**, 3024–3029 (2002).

126. Bliss, T. M., Andres, R. H. & Steinberg, G. K. Optimizing the success of cell transplantation therapy for stroke. *Stroke* **37**, 275–294 (2011).

127. Li, J.-Y., Christophersen, N. S., Hall, V., Soulet, D. & Brundin, P. Critical issues of clinical human embryonic stem cell therapy for brain repair. *Trends Neurosci.* **31**, 146–153 (2008).

128. Okamura, R. M. *et al.* Immunological properties of human embryonic stem cell-derived oligodendrocyte progenitor cells. *J. Neuroimmunol.* **192**, 134–144 (2007).

129. Srinivas, M. *et al.* Imaging of cellular therapies. *Adv. Drug Deliv. Rev.* **62**, 1080–1093 (2010).

130. Berman, S. C., Galpoththawela, C., Gilad, A. A., Bulte, J. W. M. & Walczak, P. Long-term MR cell tracking of neural stem cells grafted in immunocompetent versus immunodeficient mice reveals distinct differences in contrast between live and dead cells. *Magn. Reson. Med.* **65**, 564–574 (2011).

131. Soenen, S. J. H., Himmelreich, U., Nuytten, N. & De Cuyper, M. Cytotoxic effects of iron oxide nanoparticles and implications for safety in cell labelling. *Biomaterials* **32**, 195–205 (2011).

132. Marszałł, M. P. Application of magnetic nanoparticles in pharmaceutical sciences. *Pharm. Res.* **28**, 480–3 (2011).

133. Yiu, H. H. P. Engineering the multifunctional surface on magnetic nanoparticles for targeted biomedical applications: a chemical approach. *Nanomedicine (Lond.)* **6**, 1429–1446 (2011).

134. Hofmann-Amtenbrink, M., Hofmann, H. & Montet, X. Superparamagnetic nanoparticles - a tool for early diagnostics. *Swiss Med. Weekly* **140**, w13081 (2010).

135. Berry, C. C. Progress in functionalization of magnetic nanoparticles for applications in biomedicine. *J. Phys. D: Appl. Phys.* **42**, 224003 (2009).

136. Aliaga, M. E., Carrasco-Pozo, C., López-Alarcón, C., Olea-Azar, C. & Speisky, H. Superoxide-dependent reduction of free Fe(3+) and release of Fe(2+) from ferritin by the physiologically-occurring Cu(I)-glutathione complex. *Bioorg. Med. Chem.* **19**, 534–541 (2011).

137. Kress, G. J., Dineley, K. E. & Reynolds, I. J. The relationship between intracellular free iron and cell injury in cultured neurons, astrocytes, and oligodendrocytes. *J. Neurosci.* **22**, 5848–55 (2002).

138. Mornet, S., Vasseur, S., Grasset, F. & Duguet, E. Magnetic nanoparticle design for medical diagnosis and therapy. *J. Mater. Chem.* **14**, 2161 (2004).

139. Olariu, C. I. *et al.* Multifunctional Fe3O4 nanoparticles for targeted bi-modal imaging of pancreatic cancer. *J. Mater. Chem.* **21**, 12650 (2011).

140. Pankhurst, Q. A., Thanh, N. K. T., Jones, S. K. & Dobson, J. Progress in applications of magnetic nanoparticles in biomedicine. *J. Phys. D: Appl. Phys.* **42**, 224001 (2009).

141. Dobson, J. Magnetic micro- and nano-particle-based targeting for drug and gene delivery. *Nanomedicine (Lond.)* **1**, 31–37 (2006).

142. McBain, S. C., Yiu, H. H. P. & Dobson, J. Magnetic nanoparticles for gene and drug delivery. *Int. J. Nanomed.* **3**, 169–180 (2008).

143. Frank, J. A. *et al.* Clinically applicable labeling of Mammalian and Stem Cells by Combining Superparamagnetic Iron Oxides and Transfection Agents. *Radiology* (2003).

144. Sasaki, H. *et al.* Therapeutic effects with magnetic targeting of bone marrow stromal cells in a rat spinal cord injury model. *Spine (Phila Pa 1976)* **36**, 933–938 (2011).

145. Vaněček, V. *et al.* Highly efficient magnetic targeting of mesenchymal stem cells in spinal cord injury. *Int. J. Nanomedicine* **7**, 3719–3730 (2012).

146. Shubayev, V. I., Pisanic, T. R. 2nd & Jin, S. Magnetic nanoparticles for theragnostics. *Adv. Drug Delivery Rev.* **61**, 467–477 (2009).

147. Debbage, P. & Jaschke, W. Molecular imaging with nanoparticles: giant roles for dwarf actors. *Histochem. Cell Biol.* **130**, 845–875 (2008).

148. Tartaj, P., Del Puerto Morales, M., Veintemillas-Verdaguer, S., Gonzalez-Carreno, T. & Serna, C. J. The preparation of magnetic nanoparticles for applications in biomedicine. *J. Phys. D: Appl. Phys.* **36**, R182–R197 (2003).

149. Fang, C. & Zhang, M. Multifunctional magnetic nanoparticles for medical imaging applications. *J. Mater. Chem.* **19**, 6258–6266 (2009).

150. Wang, Y. X., Hussain, S. M. & Krestin, G. P. Superparamagnetic iron oxide contrast agents: physicochemical characteristics and applications in MR imaging. *Eur. Radiol.* **11**, 2319–2331 (2001).

151. Nitin, N., LaConte, L. E. W., Zurkiya, O., Hu, X. & Bao, G. Functionalization and peptide-based delivery of magnetic nanoparticles as an intracellular MRI contrast agent. *J. Biol. Inorg. Chem.* **9**, 706–712 (2004).

152. Ben-Hur, T. *et al.* Serial in vivo MR tracking of magnetically labeled neural spheres transplanted in chronic EAE mice. *Magn. Reson. Med.* **57**, 164–71 (2007).

153. Zhu, J., Wu, X. & Zhang, H. L. Adult neural stem cell therapy: expansion in vitro, tracking in vivo and clinical transplantation. *Curr. Drug. Targets* **6**, 97–110 (2005).

154. Focke, A. *et al.* Labeling of human neural precursor cells using ferromagnetic nanoparticles. *Magn. Reson. Med.* **60**, 1321–1328 (2008).

155. Bulte, J. W. M. *et al.* Neurotransplantation of magnetically labeled oligodendrocyte progenitors: Magnetic resonance tracking of cell migration and myelination. *Proc. Natl. Acad. Sci. U. S. A.* **96**, 15256–15261 (1999).

156. Shapiro, E. M., Skrtic, S. & Koretsky, A. P. Sizing it up: cellular MRI using micron-sized iron oxide particles. *Magn. Reson. Med.* **53**, 329–338 (2005).

157. Modo, M. *et al.* Tracking transplanted stem cell migration using bifunctional, contrast agent-enhanced, magnetic resonance imaging. *Neuroimage* **17**, 803–811 (2002).

158. Kircher, M. F., Mahmood, U., King, R. S., Weissleder, R. & Josephson, L. A multimodal nanoparticle for preoperative magnetic resonance imaging and intraoperative optical brain tumor delineation. *Cancer Res.* **63**, 8122–8125 (2003).

159. Ben-Hur, T., Einstein, O. & Bulte, J. W. Stem cell therapy for myelin diseases. *Curr. Drug Targets* **6**, 3–19 (2005).

160. Kim, J., Kim, P.-H., Kim, S. W. & Yun, C.-O. Enhancing the therapeutic efficacy of adenovirus in combination with biomaterials. *Biomaterials* **33**, 1838–50 (2012).

161. Plank, C., Zelphati, O. & Mykhaylyk, O. Magnetically enhanced nucleic acid delivery. Ten years of magnetofection - Progress and prospects. *Adv. Drug Deliv. Rev.* **63**, 1300–1331 (2011).

162. Buerli, T. *et al.* Efficient transfection of DNA or shRNA vectors into neurons using magnetofection. *Nat. Protoc.* **2**, 3090–3101 (2007).

163. Pickard, M. R., Barraud, P. & Chari, D. M. The transfection of multipotent neural precursor/stem cell transplant populations with magnetic nanoparticles. *Biomaterials* **32**, 2274–84 (2011).

164. Pickard, M. R. & Chari, D. M. Enhancement of magnetic nanoparticle-mediated gene transfer to astrocytes by "magnetofection": effects of static and oscillating fields. *Nanomedicine (Lond.)* **5**, 217–232 (2010).

165. Godbey, W. T. & Mikos, A. G. Recent progress in gene delivery using non-viral transfer complexes. *J. Control. Release* **72**, 115–125 (2001).

166. Bergen, J. M., Park, I.-K., Horner, P. J. & Pun, S. H. Nonviral approaches for neuronal delivery of nucleic acids. *Pharm. Res.* **25**, 983–998 (2008).

167. Luo, D. & Saltzman, W. M. Enhancement of transfection by physical concentration of DNA at the cell surface. *Nat. Biotechnol.* **18**, 893–895 (2000).

168. Bunnell, B. A., Muul, L. M., Donahue, R. E., Blaese, R. M. & Morgan, R. A. High-efficiency retroviral-mediated gene transfer into human and nonhuman primate peripheral blood lymphocytes. *Proc. Natl. Acad. Sci. USA* **92**, 7739–7743 (1995).

169. Plank, C. *et al.* The magnetofection method: using magnetic force to enhance gene delivery. *Biol. Chem.* **384**, 737–747 (2003).

170. Mah, C. *et al.* Microsphere-mediated delivery of recombinant AAV vectors in vitro and in vivo. *Mol. Ther.* **1**, S239 (2000).

171. Plank, C., Scherer, F., Schillinger, U. & Anton, M. Magnetofection: enhancement and localization of gene delivery with magnetic particles under the influence of a magnetic field. *J. Gene. Med.* **2**, 24 (2000).

172. McBain, S. C. *et al.* Magnetic nanoparticles as gene delivery agents: enhanced transfection in the presence of oscillating magnet arrays. *Nanotechnology* **19**, 405102 (2008).

173. Fouriki, A., Farrow, N., Clements, M. A. & Dobson, J. Evaluation of the magnetic field requirements for nanomagnetic gene transfection. *Nano Rev.* **1**, 1–5 (2010).

174. Creusat, G. *et al.* Proton sponge trick for pH-sensitive disassembly of polyethylenimine-based siRNA delivery systems. *Bioconjug. Chem.* **21**, 994–1002 (2010).

175. Suh, J., Wirtz, D. & Hanes, J. Efficient active transport of gene nanocarriers to the cell nucleus. *Proc. Natl. Acad. Sci. USA* **100**, 3878–3882 (2003).

176. Van der Aa, M. A. E. M. *et al.* The nuclear pore complex: the gateway to successful nonviral gene delivery. *Pharm. Res.* **23**, 447–459 (2006).

177. Brunner, S. *et al.* Cell cycle dependence of gene transfer by lipoplex, polyplex and recombinant adenovirus. *Gene Ther.* **7**, 401–407 (2000).

178. Kim, J.-B. *et al.* Enhanced transfection of primary cortical cultures using arginine-grafted PAMAM dendrimer, PAMAM-Arg. *J. Control. Release* **114**, 110–117 (2006).

179. Bettinger, T., Carlisle, R. C., Read, M. L., Ogris, M. & Seymour, L. W. Peptide-mediated RNA delivery: a novel approach for enhanced transfection of primary and post-mitotic cells. *Nucleic Acids Res.* **29**, 3882–3891 (2001).

180. Zanta, M. A., Belguise-Valladier, P. & Behr, J.-P. Gene delivery: A single nuclear localization signal peptide is sufficient to carry DNA to the cell nucleus. *Proc. Natl. Acad. Sci. USA* **96**, 91–96 (1999).

181. Kyrtatos, P. G. *et al.* Magnetic tagging increases delivery of circulating progenitors in vascular injury. *JACC. Cardiovasc. Interv.* **2**, 794–802 (2009).

182. Yanai, A. *et al.* Focused magnetic stem cell targeting to the retina using superparamagnetic iron oxide nanoparticles. *Cell Transplant.* **21**, 1137–1148 (2012).

183. Schäfer, R. *et al.* Functional investigations on human mesenchymal stem cells exposed to magnetic fields and labeled with clinically approved iron nanoparticles. *BMC Cell Biol.* **11**, 22 (2010).

184. MacDougall, I. C. Evolution of IV iron compounds over the last century. *J. Ren. Care* **35**, 8–13 (2009).

185. Laurent, N., Sapet, C., Le Gourrierec, L., Bertosio, E. & Zelphati, O. Nucleic acid delivery using magnetic nanoparticles: the Magnetofection technology. *Ther. Deliv.* **2**, 471–482 (2011).

186. Scherer, F. *et al.* Magnetofection: enhancing and targeting gene delivery by magnetic force in vitro and in vivo. *Gene Ther.* **9**, 102–109 (2002).

187. Baryshev, M., Vainauska, D., Kozireva, S. & Karpovs, A. New device for enhancement of liposomal magnetofection efficiency of cancer cells. *World Acad. Sci. Eng. Tech.* **58**, 306–309 (2011).

188. Yiu, H. H. P., McBain, S. C., Lethbridge, Z. A. D., Lees, M. R. & Dobson, J. Preparation and characterization of polyethylenimine-coated Fe3O4-MCM-48 nanocomposite particles as a novel agent for magnet-assisted transfection. *J. Biomed. Mater. Res. A* **92**, 386–392 (2010).

189. Petri-Fink, A., Chastellain, M., Juillerat-Jeanneret, L., Ferrari, A. & Hofmann, H. Development of functionalized superparamagnetic iron oxide nanoparticles for interaction with human cancer cells. *Biomaterials* **26**, 2685–2694 (2005).

190. Musyanovych, A. *et al.* Criteria impacting the cellular uptake of nanoparticles: A study emphasizing polymer type and surfactant effects. *Acta Biomater.* **7**, 4160–4168 (2011).

191. Al-Ali, S. Y. & Al-Hussain, S. M. An ultrastructural study of the phagocytic activity of astrocytes in adult rat brain. *J. Anat.* **188**, 257–262 (1996).

192. Nguyen, K. B. & Pender, M. P. Phagocytosis of apoptotic lymphocytes by oligodendrocytes in experimental autoimmune encephalomyelitis. *Acta Neuropathol.* **95**, 40–46 (1998).

193. Noske, W., Lentzen, H., Lange, K. & Keller, K. Phagocytotic activity of glial cells in culture. *Exp. Cell Res.* **142**, 437–445 (1982).

194. Triarhou, L. C., Cerro, M. D. E. L. & Herndon, R. M. Ultrastructural evidence for phagocytosis by oligodendroglia. *Neurosci. Lett.* **53**, 185–189 (1985).

195. Walczak, P., Kedziorek, D. a, Gilad, a a, Lin, S. & Bulte, J. W. M. Instant MR labeling of stem cells using magnetoelectroporation. *Magn. Reson. Med.* **54**, 769–774 (2005).

196. Gratton, S. E. A. *et al.* The effect of particle design on cellular internalization pathways. *Proc. Natl. Acad. Sci. USA* **105**, 11613–11618 (2008).

197. Cannon, G. J. & Swanson, J. A. The macrophage capacity for phagocytosis. *J. Cell Sci.* **101**, 907–913 (1992).

198. Canton, I. & Battaglia, G. Endocytosis at the nanoscale. *Chem. Soc. Rev.* **41**, 2718–2739 (2012).

199. Conner, S. D. & Schmid, S. L. Regulated portals of entry into the cell. *Nature* **422**, 37–44 (2003).

200. Swanson, J. A. & Watts, C. Macropinocytosis. *Trends Cell Biol.* **5**, 424–428 (1995).

201. Mercer, J. & Helenius, A. Gulping rather than sipping: macropinocytosis as a way of virus entry. *Curr. Opin. Microbiol.* **15**, 490–499 (2012).

202. Kumari, S., Mg, S. & Mayor, S. Endocytosis unplugged: multiple ways to enter the cell. *Cell Res.* **20**, 256–275 (2010).

203. Chithrani, B. D. & Chan, W. C. W. Elucidating the mechanism of cellular uptake and removal of protein-coated gold nanoparticles of different sizes and shapes. *Nano Lett.* **7**, 1542–1550 (2007).

204. Thorek, D. L. J. & Tsourkas, A. Size, charge and concentration dependent uptake of iron oxide particles by non-phagocytic cells. *Biomaterials* **29**, 3583–3590 (2008).

205. Hutter, E. *et al.* Microglial response to gold nanoparticles. *ACS Nano* **4**, 2595–2606 (2010).

206. Qiu, Y. *et al.* Surface chemistry and aspect ratio mediated cellular uptake of Au nanorods. *Biomaterials* **31**, 7606–19 (2010).

207. Weill, C. O., Biri, S. & Erbacher, P. Cationic lipid-mediated intracellular delivery of antibodies into live cells. *Biotechniques* **44**, Pvii–Pxi (2008).

208. Xia, T., Kovochich, M., Liong, M., Zink, J. I. & Nel, A. E. Cationic polystyrene nanosphere toxicity depends on cell-specific endocytic and mitochondrial injury pathways. *ACS Nano* **2**, 85–96 (2008).

209. Xu, M., Zhao, Y. & Feng, M. Polyaspartamide derivative nanoparticles with tunable surface charge achieve highly efficient cellular uptake and low cytotoxicity. *Langmuir* **28**, 11310–11318 (2012).

210. Lin, J., Zhang, H., Chen, Z. & Zheng, Y. Penetration of lipid membranes by gold nanoparticles: insights into cellular uptake, cytotoxicity, and their relationship. *ACS Nano* **4**, 5421–5429 (2010).

211. Wilhelm, C. *et al.* Intracellular uptake of anionic superparamagnetic nanoparticles as a function of their surface coating. *Biomaterials* **24**, 1001–11 (2003).

212. Verma, A. & Stellacci, F. Effect of surface properties on nanoparticle-cell interactions. *Small* **6**, 12–21 (2010).

213. Safi, M., Courtois, J., Seigneuret, M., Conjeaud, H. & Berret, J.-F. The effects of aggregation and protein corona on the cellular internalization of iron oxide nanoparticles. *Biomaterials* **32**, 9353–63 (2011).

214. Monopoli, M. P. *et al.* Physical-chemical aspects of protein corona: relevance to in vitro and in vivo biological impacts of nanoparticles. *J. Am. Chem. Soc.* **133**, 2525–2534 (2011).

215. Walczyk, D., Bombelli, F. B., Monopoli, M. P., Lynch, I. & Dawson, K. A. What the cell "sees" in bionanoscience. *J. Am. Chem. Soc.* **132**, 5761–5768 (2010).

216. Jing, Y. *et al.* Quantitative intracellular magnetic nanoparticle uptake measured by live cell magnetophoresis. *FASEB J.* **22**, 4239–4247 (2008).

217. Prijic, S. *et al.* Increased cellular uptake of biocompatible superparamagnetic iron oxide nanoparticles into malignant cells by an external magnetic field. *J. Membr. Biol.* **236**, 167–179 (2010).

218. Chaudhari, K. R. *et al.* Opsonization, biodistribution, cellular uptake and apoptosis study of PEGylated PBCA nanoparticle as potential drug delivery carrier. *Pharm. Res.* **29**, 53–68 (2011).

219. Soenen, S. J. H. *et al.* Intracellular nanoparticle coating stability determines nanoparticle diagnostics efficacy and cell functionality. *Small* **6**, 2136–2145 (2010).

220. Dos Santos, T., Varela, J., Lynch, I., Salvati, A. & Dawson, K. A. Quantitative assessment of the comparative nanoparticle-uptake efficiency of a range of cell lines. *Small* **7**, 3341–3349 (2011).

221. Kim, J.-S. & Yoon, T.-J. Cellular uptake of magnetic nanoparticle is mediated through energy-dependent endocytosis in A549 cells. *J. Vet. Sci.* **7**, 321–326 (2006).

222. Pinkernelle, J., Calatayud, P., Goya, G. F., Fansa, H. & Keilhoff, G. Magnetic nanoparticles in primary neural cell cultures are mainly taken up by microglia. *BMC Neurosci.* **13**, 32 (2012).

223. Greene, L. A. & Tischler, A. S. Establishment of a noradrenergic clonal line of rat adrenal pheochromocytoma cells which respond to nerve growth factor. *Proc. Natl. Acad. Sci. USA* **73**, 2424–2428 (1976).

224. Connolly, J. L., Green, S. A. & Greene, L. A. Comparison of rapid changes in surface morphology and coated pit formation of PC12 cells in response to nerve growth factor, epidermal growth factor, and dibutyryl cyclic AMP. *J. Cell Biol.* **98**, 457–465 (1984).

225. Pisanic, T. R. 2nd, Blackwell, J. D., Shubayev, V. I., Fiñones, R. R. & Jin, S. Nanotoxicity of iron oxide nanoparticle internalization in growing neurons. *Biomaterials* **28**, 2572–2581 (2007).

226. American Type Culture Collection Standards Development Organization Workgroup ASN-0002 Cell line misidentification: the beginning of the end. *Nat. Rev. Cancer* **10**, 441–448 (2010).

227. Nardone, R. M. Curbing rampant cross-contamination and misidentification of cell lines. *Biotechniques* **45**, 221–227 (2008).

228. Buehring, G. C., Eby, E. A. & Eby, M. J. Cell line cross-contamination: how aware are Mammalian cell culturists of the problem and how to monitor it? *In Vitro Cell. Dev. Biol. Anim.* **40**, 211–5 (2004).

229. Bubeník, J. Cross-contamination of cell lines in culture. *Folia Bio. (Praha)* **46**, 163–164 (2000).

230. Rojas, A. Cell line cross-contamination: who wins? *J. Biol. Chem.* **286**, le20 (2011).

231. MacLeod, R. A. F. *et al.* Widespread intraspecies cross-contamination of human tumor cell lines arising at source. *Int. J. Cancer* **83**, 555–563 (1999).

232. Freshney, R. I. Cell line provenance. *Cytotechnology* **39**, 55–67 (2002).

233. Parks, G. Manual of Animal Technology. *The Canadian Veterinary Journal* pp374 (2009).

234. Freshney, R. I. *Culture of Animal Cells: A Manual of Basic Technique*. (John Wiley & Sons, Inc.: 2005).doi:10.1002/cii.8

235. Hughes, P., Marshall, D., Reid, Y., Parkes, H. & Gelber, C. The costs of using unauthenticated, over-passaged cell lines: how much more data do we need? *BioTechniques* **43**, 575–586 (2007).

236. Nel, A., Xia, T., Mädler, L. & Li, N. Toxic potential of materials at the nanolevel. *Science* **311**, 622–627 (2006).

237. Hansmann, F. *et al.* Highly malignant behavior of a murine oligodendrocyte precursor cell line following transplantation into the demyelinated and non-demyelinated central nervous system. *Cell Transplant.* **21**, 1161–1175 (2012).

238. Kitada, M. & Rowitch, D. H. Transcription factor co-expression patterns indicate heterogeneity of oligodendroglial subpopulations in adult spinal cord. *Glia* **54**, 35–46 (2006).

239. Abrajano, J. J. *et al.* Differential deployment of REST and CoREST promotes glial subtype specification and oligodendrocyte lineage maturation. *PLoS One* **4**, e7665 (2009).

240. Pickard, M. R., Jenkins, S. I., Koller, C., Furness, D. N. & Chari, D. M. Magnetic nanoparticle labelling of astrocytes derived for neural transplantation. *Tissue Eng., Part C* **17**, 89–99 (2011).

241. Pickard, M. R. & Chari, D. M. Robust uptake of magnetic nanoparticles (MNPs) by central nervous system (CNS) microglia: implications for particle uptake in mixed neural cell populations. *Int. J. Mol. Sci.* **11**, 967–981 (2010).

242. Sharp, J., Frame, J., Siegenthaler, M., Nistor, G. & Keirstead, H. S. Human embryonic stem cell-derived oligodendrocyte progenitor cell transplants improve recovery after cervical spinal cord injury. *Stem Cells* **28**, 152–163 (2010).

243. Lachapelle, F. *et al.* Transplanted transgenically marked oligodendrocytes survive, migrate and myelinate in the normal mouse brain as they do in the shiverer mouse brain. *Eur. J. Neurosci.* **6**, 814–824 (1994).

244. Richter-Landsberg, C. & Heinrich, M. OLN-93: a new permanent oligodendroglia cell line derived from primary rat brain glial cultures. *J. Neurosci. Res.* **45**, 161–173 (1996).

245. Jain, T. *et al.* Magnetic nanoparticles with dual functional properties: drug delivery and magnetic resonance imaging. *Biomaterials* **29**, 4012–4021 (2008).

246. Jasmin *et al.* Optimized labeling of bone marrow mesenchymal cells with superparamagnetic iron oxide nanoparticles and in vivo visualization by magnetic resonance imaging. *J. Nanobiotechnology* **9**, 4 (2011).

247. Ståhlberg, A. *et al.* Defining cell populations with single-cell gene expression profiling: correlations and identification of astrocyte subpopulations. *Nucleic Acids Res.* **39**, 1–12 (2011).

248. Bouslama-Oueghlani, L., Wehrle, R., Sotelo, C. & Dusart, I. Heterogeneity of NG2-expressing cells in the newborn mouse cerebellum. *Dev. Biol.* **285**, 409–421 (2005).

249. Geppert, M. *et al.* Uptake of dimercaptosuccinate-coated magnetic iron oxide nanoparticles by cultured brain astrocytes. *Nanotechnology* **22**, 145101 (2011).

250. Yang, Z. *et al.* A review of nanoparticle functionality and toxicity on the central nervous system. *J. R. Soc. Interface* **7**, S411–422 (2010).

251. Busch, W. *et al.* Internalisation of engineered nanoparticles into mammalian cells in vitro: influence of cell type and particle properties. *J. Nanopart. Res.* **13**, 293–310 (2010).

252. Chissoe, W. F., Vezey, E. L. & Skvarla, J. J. The use of osmium-thiocarbohydrazide for structural stabilization and enhancement of secondary electron images in scanning electron microscopy of pollen. *Grana* **34**, 317–324 (1995).

253. Jongebloed, W. L., Stokroos, I., Kalicharan, D. & Van der Want, J. J. L. Is cryopreservation superior over tannic acid/arginine/osmium tetroxide non-coating preparation in field emission scanning electron microscopy? *Scanning Microsc.* **13**, 93–109 (1999).

254. Friedman, P. L. & Ellisman, M. H. Enhanced visualization of peripheral nerve and sensory receptors in the scanning electron microscope using cryofracture and osmium-thiocarbohydrazide-osmium impregnation. *J. Neurocytol.* **10**, 111–131 (1981).

255. Grandfield, K. Focused ion beam in the study of biomaterials and biological matter. *Adv. Mater. Sci. Eng.* **2012**, 1–6 (2011).

256. Dunnebier, E., Segenhout, J. & Kalicharan, D. Low-voltage field-emission scanning electron microscopy of non-coated guinea-pig hair cell stereocilia. *Hear. Res.* **90**, 139–148 (1995).

257. McGregor, J. E., Wang, Z., Ffrench-Constant, C. & Donald, A. M. Microscopy of myelination. *Microscopy: Science, technology, applications and education* pp1185–1195 (2010).

258. Forge, A., Nevill, G., Zajic, G. & Wright, A. Scanning electron microscopy of the mammalian organ of corti: assessment of preparative procedures. *Scanning Microsc.* **6**, 521–534 (1992).

259. Furness, D. N., Mahendrasingam, S., Ohashi, M., Fettiplace, R. & Hackney, C. M. The dimensions and composition of stereociliary rootlets in mammalian cochlear hair cells: comparison between high- and low-frequency cells and evidence for a connection to the lateral membrane. *J. Neurosci.* **28**, 6342–6353 (2008).

260. De la Fuente, J. M., Berry, C. C., Riehle, M. O. & Curtis, A. S. G. Nanoparticle targeting at cells. *Langmuir* **22**, 3286–93 (2006).

261. Gupta, A. K., Berry, C. C., Gupta, M. & Curtis, A. Receptor-mediated targeting of magnetic nanoparticles using insulin as a surface ligand to prevent endocytosis. *IEEE Trans. Nanobioscience* **2**, 255–261 (2003).

262. Berry, C. C., Wells, S., Charles, S., Aitchison, G. & Curtis, A. S. G. Cell response to dextran-derivatised iron oxide nanoparticles post internalisation. *Biomaterials* **25**, 5405–5413 (2004).

263. McCarthy, K. D. & De Vellis, J. Preparation of separate astroglial and oligodendroglial cell cultures from rat cerebral tissue. *J. Cell Biol.* **85**, 890–902 (1980).

264. Florez, L. *et al.* How shape influences uptake: interactions of anisotropic polymer nanoparticles and human mesenchymal stem cells. *Small* **8**, 2222–2230 (2012).

265. Ang, D. *et al.* Insights into the mechanism of magnetic particle assisted gene delivery. *Acta Biomater.* **7**, 1319–1326 (2011).

266. Borchert, H. *et al.* Determination of nanocrystal sizes: a comparison of TEM, SAXS, and XRD studies of highly monodisperse CoPt3 particles. *Langmuir* **21**, 1931–1936 (2005).

267. Rubio, N., Rodriguez, R. & Arevalo, M. A. In vitro myelination by oligodendrocyte precursor cells transfected with the neurotrophin-3 gene. *Glia* **47**, 78–87 (2004).

268. Zhang, S., Li, J., Lykotrafitis, G., Bao, G. & Suresh, S. Size-dependent endocytosis of nanoparticles. *Adv. Mater.* **21**, 419–424 (2009).

269. Tenzer, S. *et al.* Nanoparticle size is a critical physicochemical determinant of the human blood plasma corona: a comprehensive quantitative proteomic analysis. *ACS Nano* **5**, 7155–7167 (2011).

270. Jiang, W., Kim, B. Y. S., Rutka, J. T. & Chan, W. C. W. Nanoparticle-mediated cellular response is size-dependent. *Nat. Nanotechnol.* **3**, 145–150 (2008).

271. Sanchez-Antequera, Y. *et al.* Magselectofection: an integrated method of nanomagnetic separation and genetic modification of target cells. *Blood* **117**, e171–181 (2011).

272. Summers, H. D. *et al.* Statistical analysis of nanoparticle dosing in a dynamic cellular system. *Nat. Nanotech.* **6**, 170–174 (2011).

273. Hohnholt, M. C., Geppert, M. & Dringen, R. Treatment with iron oxide nanoparticles induces ferritin synthesis but not oxidative stress in oligodendroglial cells. *Acta Biomater.* **7**, 3946–3954 (2011).

274. Hirrlinger, J., Resch, A., Gutterer, J. M. & Dringen, R. Oligodendroglial cells in culture effectively dispose of exogenous hydrogen peroxide: comparison with cultured neurones, astroglial and microglial cells. *J. Neurochem.* **82**, 635–644 (2002).

275. Fisichella, M. *et al.* Mesoporous silica nanoparticles enhance MTT formazan exocytosis in HeLa cells and astrocytes. *Toxicol. In Vitro* **23**, 697–703 (2009).

276. Berry, C. C., Wells, S., Charles, S. & Curtis, A. S. G. Dextran and albumin derivatised iron oxide nanoparticles: influence on fibroblasts in vitro. *Biomaterials* **24**, 4551–4557 (2003).

277. Cengelli, F. *et al.* Interaction of functionalized superparamagnetic iron oxide nanoparticles with brain structures. *J. Pharmacol. Exp. Ther.* **318**, 108–116 (2006).

278. Marquis, B. J., Love, S. A., Braun, K. L. & Haynes, C. L. Analytical methods to assess nanoparticle toxicity. *Analyst* **134**, 425–439 (2009).

279. Allen, T. *Introduction to electron microscopy for biologists*. (Elsevier Inc.: Burlington, MA, USA, 2008).

280. Dhawan, A. & Sharma, V. Toxicity assessment of nanomaterials: methods and challenges. *Anal. Bioanal. Chem.* **398**, 589–605 (2010).

281. Bjørnerud, A. & Johansson, L. The utility of superparamagnetic contrast agents in MRI: theoretical consideration and applications in the cardiovascular system. *NMR Biomed.* **17**, 465–477 (2004).

282. Murray, M. & Fischer, I. Transplantation and gene therapy: combined approaches for repair of spinal cord injury. *Neuroscientist* **7**, 28–41 (2001).

283. Filbin, M. T. Recapitulate development to promote axonal regeneration: good or bad approach? *Philos. Trans. R. Soc. Lond. B. Biol. Sci.* **361**, 1565–1574 (2006).

284. Duncan, I. D. Replacing cells in multiple sclerosis. *J. Neurol. Sci.* **265**, 89–92 (2008).

285. Madhavan, L. & Collier, T. J. A synergistic approach for neural repair: cell transplantation and induction of endogenous precursor cell activity. *Neuropharmacology* **58**, 835–44 (2010).

286. Huang, J. K. *et al.* Myelin regeneration in multiple sclerosis: targeting endogenous stem cells. *Neurotherapeutics* **8**, 650–658 (2011).

287. Wolswijk, G. Chronic stage multiple sclerosis lesions contain a relatively quiescent population of oligodendrocyte precursor cells. *J. Neurosci.* **18**, 601–609 (1998).

288. GIBCO Neon™ Transfection Protocol for GIBCO® Rat Glial Precursor Cells (GPCs). *http://protocolexchange.community.invitrogen.com/protocol/1036/protocol-1036.pdf*

289. www.lonzabio.com Amaxa Nucleofector Protocol for Rat Oligodendrocytes. *Lonzabio protocol*

290. Anitei, M. *et al.* A role for Sec8 in oligodendrocyte morphological differentiation. *J. Cell Sci.* **119**, 807–818 (2006).

291. Fallini, C., Bassell, G. J. & Rossoll, W. High-efficiency transfection of cultured primary motor neurons to study protein localization, trafficking, and function. *Mol. Neurodegener.* **5**, 17 (2010).

292. Sapet, C. *et al.* High transfection efficiency of neural stem cells with magnetofection. *BioTechniques* **50**, 187–189 (2011).

293. Regenberg, A. *et al.* The role of animal models in evaluating reasonable safety and efficacy for human trials of cell-based interventions for neurologic conditions. *J. Cereb. Blood Flow Metab.* **29**, 1–9 (2009).

294. Seil, F. J. Tissue culture models of myelination after oligodendrocyte transplantation. *J. Neural Transplant.* **1**, 49–55 (1989).

295. Seil, F. J., Johnson, M. L., Saneto, R. P., Herndon, R. M. & Mass, M. K. Myelination of axons within cytosine arabinoside treated mouse cerebellar explants by cultured rat oligodendrocytes. *Brain Res.* **503**, 111–117 (1989).

296. Davidson, S. *et al.* Differential activity by polymorphic variants of a remote enhancer that supports galanin expression in the hypothalamus and amygdala: implications for obesity, depression and alcoholism. *Neuropsychopharmacology* **36**, 2211–2221 (2011).

297. Pickard, M. R. & Chari, D. M. Magnetic nanoparticle applications for neural stem cell transplantation therapies. *Programme of the Fourth Annual Scientific Conference of the UK National Stem Cell Network, University of York* (2011).

298. Furlani, E. P. & Ng, K. C. Nanoscale magnetic biotransport with application to magnetofection. *Phys. Rev.* **77**, 061094 (2008).

299. Verwer, R. W. H. *et al.* Cells in human postmortem brain tissue slices remain alive for several weeks in culture. *FASEB J.* **16**, 54–60 (2002).

300. Choi, J. Y. *et al.* In vitro cytotoxicity screening of water-dispersible metal oxide nanoparticles in human cell lines. *Bioprocess Biosyst. Eng.* **33**, 21–30 (2010).

301. Gómez-Pinilla, F., Vu, L. & Cotman, C. W. Regulation of astrocyte proliferation by FGF-2 and heparan sulfate in vivo. *J. Neurosci.* **15**, 2021–2029 (1995).

302. Forget, C., Stewart, J. & Trudeau, L.-E. Impact of basic FGF expression in astrocytes on dopamine neuron synaptic function and development. *Eur. J. Neurosci.* **23**, 608–616 (2006).

303. Leclere, P. G. *et al.* Effective gene delivery to adult neurons by a modified form of electroporation. *J. Neurosci. Meth.* **142**, 137–143 (2005).

304. Chen, C.-J. *et al.* Identification of a key pathway required for the sterile inflammatory response triggered by dying cells. *Nat. Med.* **13**, 851–856 (2007).

305. Tokumoto, Y. M., Apperly, J. A., Gao, F.-B. & Raff, M. C. Posttranscriptional regulation of p18 and p27 Cdk inhibitor proteins and the timing of oligodendrocyte differentiation. *Dev. Biol.* **245**, 224 – 234 (2002).

306. Hermens, W. T. J. M. C. *et al.* Transient gene transfer to neurons and glia: analysis of adenoviral vector performance in the CNS and PNS. *J. Neursoci. Methods* **71**, 85–98 (1997).

307. Tang, X. M. *et al.* Cell cycle arrest induced by ectopic expression of p27 is not sufficient to promote oligodendrocyte differentiation. *J. Cell Biochem.* **76**, 270–279 (1999).

308. Blakemore, W. F. Regeneration and repair in multiple sclerosis: the view of experimental pathology. *J. Neurol. Sci.* **265**, 1–4 (2008).

309. Baron, W. *et al.* PDGF and FGF-2 signaling in oligodendrocyte progenitor cells: regulation of proliferation and differentiation by multiple intracellular signaling pathways. *Mol. Cell Neurosci.* **15**, 314–329 (2000).

310. Fan, R. *et al.* Minocycline reduces microglial activation and improves behavioral deficits in a transgenic model of cerebral microvascular amyloid. *J. Neurosci.* **27**, 3057–3063 (2007).

311. Dobson, J. Remote control of cellular behaviour with magnetic nanoparticles. *Nat. Nanotechnol.* **3**, 139–143 (2008).

312. Kamau, S. W. *et al.* Enhancement of the efficiency of non-viral gene delivery by application of pulsed magnetic field. *Nucleic Acids Res.* **34**, e40 (2006).

313. Smith, C.-A. M. *et al.* The effect of static magnetic fields and tat peptides on cellular and nuclear uptake of magnetic nanoparticles. *Biomaterials* **31**, 4392–4400 (2010).

314. Birgbauer, E., Rao, T. S. & Webb, M. Lysolecithin induces demyelination in vitro in a cerebellar slice culture system. *J. Neurosci. Res.* **78**, 157–166 (2004).

315. Jarjour, A. A., Zhang, H., Bauer, N., Ffrench-Constant, C. & Williams, A. In vitro modeling of central nervous system myelination and remyelination. *Glia* **60**, 1–12 (2012).

316. Johnson, S. L. *et al.* Synaptotagmin IV determines the linear Ca2+ dependence of vesicle fusion at auditory ribbon synapses. *Nat. Neurosci.* **13**, 45–52 (2010).

317. Jasinska, M. *et al.* Rapid, learning-induced inhibitory synaptogenesis in murine barrel field. *J. Neurosci.* **30**, 1176–1184 (2010).

318. Bonnici, B. & Kapfhammer, J. P. Spontaneous regeneration of intrinsic spinal cord axons in a novel spinal cord slice culture model. *Eur. J. Neurosci.* **27**, 2483–2492 (2008).

319. Sun, Y.-Y. *et al.* Glucocorticoid protection of oligodendrocytes against excitotoxin involving hypoxia-inducible factor-1alpha in a cell-type-specific manner. *J. Neurosci.* **30**, 9621–9630 (2010).

320. Abdellatif, A. A. *et al.* Gene delivery to the spinal cord: comparison between lentiviral, adenoviral, and retroviral vector delivery systems. *J. Neurosci. Res.* **84**, 553–567 (2006).

321. Halfpenny, C. A. Remyelination biology: The neurobiology of oligodendrocyte progenitor cells and their potential for myelin repair in Multiple Sclerosis. *PhD Thesis* (2003).

322. Kippert, A., Trajkovic, K., Rajendran, L., Ries, J. & Simons, M. Rho regulates membrane transport in the endocytic pathway to control plasma membrane specialization in oligodendroglial cells. *J. Neurosci.* **27**, 3560–3570 (2007).

323. Dugas, J. C., Tai, Y. C., Speed, T. P., Ngai, J. & Barres, B. A. Functional genomic analysis of oligodendrocyte differentiation. *J. Neurosci.* **26**, 10967–10983 (2006).

324. Tang, D. G., Tokumoto, Y. M. & Raff, M. C. Long-term culture of purified postnatal oligodendrocyte precursor cells. Evidence for an intrinsic maturation program that plays out over months. *J. Cell Biol.* **148**, 971–984 (2000).

325. Simons, M. & Trajkovic, K. Neuron-glia communication in the control of oligodendrocyte function and myelin biogenesis. *J. Cell Sci.* **119**, 4381–4389 (2006).

326. Broughton, S. K. *et al.* Large-scale generation of highly enriched neural stem-cell-derived oligodendroglial cultures: maturation-dependent differences in insulin-like growth factor-mediated signal transduction. *J. Neurochem.* **100**, 628–638 (2007).

327. Zauner, W., Brunner, S., Buschle, M., Ogris, M. & Wagner, E. Differential behaviour of lipid based and polycation based gene transfer systems in transfecting primary human fibroblasts: a potential role of polylysine in nuclear transport. *Biochim. Biophys. Acta* **1428**, 57–67 (1999).

328. Barres, B. A. The mystery and magic of glia: a perspective on their roles in health and disease. *Neuron* **60**, 430–40 (2008).

329. Park, J.-Y. *et al.* On the mechanism of internalization of alpha-synuclein into microglia: roles of ganglioside GM1 and lipid raft. *J. Neurochem.* **110**, 400–411 (2009).

330. Pocock, J. M. & Liddle, A. C. Microglial signalling cascades in neurodegenerative disease. *Prog. Brain Res.* **132**, 555–565 (2001).

331. Nair, A., Frederick, T. J. & Miller, S. D. Astrocytes in multiple sclerosis: a product of their environment. *Cell Mol. Life Sci.* **65**, 2702–2720 (2008).

332. Magistretti, P. J. & Ransom, B. R. Astrocytes. *Neuropharmacology: The fifth generation of progress* pp181–208 (2002).

333. Iacono, R. F. & Berria, M. I. Cell differentiation increases astrocyte phagocytic activity. A quantitative analysis of both GFAP labeling and PAS-stained yeast cells. *Medicina (B. Aires)* **59**, 171–175 (1999).

334. Sherwood, C. C. *et al.* Evolution of increased glia-neuron ratios in the human frontal cortex. *Proc. Natl. Acad. Sci. USA* **103**, 13606–13611 (2006).

335. Jehee, J. F. M. & Murre, J. M. J. The scalable mammalian brain: emergent distributions of glia and neurons. *Biol. Cybern.* **98**, 439–445 (2008).

336. Zhu, X., Bergles, D. E. & Nishiyama, A. NG2 cells generate both oligodendrocytes and gray matter astrocytes. *Development* **135**, 145–157 (2008).

337. De Palma, R. *et al.* Silane ligand exchange to make hydrophobic superparamagnetic nanoparticles water-dispersible. *Chem. Mater.* **19**, 1821–1831 (2007).

338. Chen, Z. *et al.* Dual enzyme-like activities of iron oxide nanoparticles and their implication for diminishing cytotoxicity. *ACS Nano* **6**, 4001–4012 (2012).

339. Fleige, G. *et al.* Magnetic labeling of activated microglia in experimental gliomas. *Neoplasia* **3**, 489–99 (2001).

340. Schädlich, A. *et al.* How stealthy are PEG-PLA nanoparticles? An NIR in vivo study combined with detailed size measurements. *Pharm. Res.* **28**, 1995–2007 (2011).

341. Bouzier-Sore, A.-K. *et al.* Nanoparticle phagocytosis and cellular stress: involvement in cellular imaging and in gene therapy against glioma. *NMR Biomed.* **23**, 88–96 (2010).

342. Hillaireau, H. & Couvreur, P. Nanocarriers' entry into the cell: relevance to drug delivery. *Cell Mol. Life Sci.* **66**, 2873–2896 (2009).

343. Kumar, A. *et al.* Multifunctional magnetic nanoparticles for targeted delivery. *Nanomedicine* **6**, 64–69 (2010).

344. Liu, J. Scanning transmission electron microscopy and its application to the study of nanoparticles and nanoparticle systems. *J. Electron Microsc. (Tokyo)* **54**, 251–278 (2005).

345. Chen, T. *et al.* Smart multifunctional nanostructure for targeted cancer chemotherapy and magnetic resonance imaging. *ACS Nano* **5**, 7866–7873 (2011).

346. Guilhon, E. *et al.* Spatial and temporal control of transgene expression in vivo using a heat-sensitive promoter and MRI-guided focused ultrasound. *J. Gene Med.* **5**, 333–342 (2003).

347. Johannsen, M., Thiesen, B., Wust, P. & Jordan, A. Magnetic nanoparticle hyperthermia for prostate cancer. *Int. J. Hyperthermia* **26**, 790–795 (2010).

348. Clancy, B., Darlington, R. B. & Finlay, B. L. Translating developmental time across mammalian species. *Science* **105**, 7–17 (2001).

349. Clancy, B., Finlay, B. L., Darlington, R. B. & Anand, K. J. S. Extrapolating brain development from experimental species to humans. *Neurotoxicology* **28**, 931–937 (2007).

350. Jeong, D.-K., Taghavi, C. E., Song, K.-J., Lee, K.-B. & Kang, H.-W. Organotypic human spinal cord slice culture as an alternative to direct transplantation of human bone marrow precursor cells for treating spinal cord injury. *World Neurosurg.* **75**, 533–539 (2011).

351. Fukushima, T., Tezuka, T., Shimomura, T., Nakano, S. & Kataoka, H. Silencing of insulin-like growth factor-binding protein-2 in human glioblastoma cells reduces both invasiveness and expression of progression-associated gene CD24. *J. Biol. Chem.* **282**, 18634–18644 (2007).

352. Dinkel, K., Ogle, W. O. & Sapolsky, R. M. Glucocorticoids and central nervous system inflammation. *J. Neurovirol.* **8**, 513–528 (2002).

353. Havrdova, E., Horakova, D., Kovarova, I. & Krasulova, E. Future directions in the treatment of Multiple Sclerosis. *Casopis Lekaru Ceskych* **144**, 663–665 (2005).

354. Jain, T. K., Reddy, M. K., Morales, M. A., Leslie-Pelecky, D. L. & Labhasetwar, V. Biodistribution, clearance, and biocompatibility of iron oxide magnetic nanoparticles in rats. *Molec. Pharm.* **5**, 316–327 (2008).

355. Tandon, P. & Nordstrom, R. J. Next-generation imaging development for nanoparticle biodistribution measurements. *Wiley Interdiscip. Rev. Nanomed. Nanobiotechnol.* **3**, 5–10 (2011).

356. Rosner, M. H. & Auerbach, M. Ferumoxytol for the treatment of iron deficiency. *Expert Rev. Hematol.* **4**, 399–406 (2011).

357. Schwenk, M. H. Ferumoxytol: a new intravenous iron preparation for the treatment of iron deficiency anemia in patients with chronic kidney disease. *Pharmacotherapy* **30**, 70–79 (2010).